NUREG/CR–5331
SAND89–0072

MELCOR Analyses for Accident Progression Issues

Prepared by S. E. Dingman, C. J. Shaffer, A. C. Payne, M. K. Carmel

Sandia National Laboratories
Operated by
Sandia Corporation

Prepared for
U.S. Nuclear Regulatory Commission

NUREG/CR--5331

TI91 007247

MELCOR Analyses for Accident Progression Issues

Manuscript Completed: December 1990
Date Published: January 1991

Prepared by
S. E. Dingman, C. J. Shaffer, A. C. Payne, M. K. Carmel

Sandia National Laboratories
Albuquerque, NM 87185

Prepared for
Division of Systems Research
Office of Nuclear Regulatory Research
U.S. Nuclear Regulatory Commission
Washington, DC 20555
NRC FIN A1392

ABSTRACT

Results of calculations performed with MELCOR and HECTR in support of the NUREG-1150 study are presented in this report. The analyses examined a wide range of issues. The analyses included integral calculations covering an entire accident sequence, as well as calculations that addressed specific issues that could affect several accident sequences. The results of the analyses for Grand Gulf, Peach Bottom, LaSalle, and Sequoyah are described, and the major conclusions are summarized.

CONTENTS

Page

Acknowledgements.....xiii

Executive Summary.....1

1. Introduction.....1-1

2. Grand Gulf Analyses.....2-1

2.1 Brief Grand Gulf Description.....2-1

2.2 Integral Station Blackout Calculation.....2-3

2.2.1 In-Vessel Melt Progression.....2-4
2.2.2 Early Containment Response.....2-13
2.2.3 Late Containment Response.....2-13
2.2.4 Radionuclide Behavior.....2-16
2.2.5 Effect of Early Burn.....2-21

2.3 Drywell Flammability.....2-25

2.3.1 Results of Integral Calculations.....2-25
2.3.2 Results of Containment-Only Calculations.....2-29

2.4 Drywell Flooding.....2-29

2.4.1 Results of Integral Calculations.....2-32
2.4.2 Results of Analyses Using STCP Releases.....2-32

2.5 Containment Loads from Burns and Subsequent Cooldown.....2-35

2.6 Steam De-Inerting Following Spray Recovery.....2-40

2.7 Stuck-Open Tailpipe Vacuum Breaker.....2-45

2.8 Containment Response and Release Rates Following Containment Failure.....2-45

2.9 Pressure Relief During Burn in Failed Containment.....2-50

2.10 RPV Repressurization Following SRV Closure.....2-50

3. Peach Bottom Analyses.....3-1

3.1 Brief Peach Bottom Description.....3-1

3.2 MELCOR Model Description.....3-1

3.3 Results of the Base Calculations.....3-5

CONTENTS (Continued)

Page

3.4 Station Blackout Sensitivity Studies.....3-9

3.4.1 Vent Downcomer Model Sensitivity Study.....3-9
3.4.2 Containment Heat Transfer Sensitivity Studies.....3-10
3.4.3 Flashing of Residual Downcomer Water Sensitivity Study.....3-13
3.4.4 Lower Head Break Area Sensitivity Study.....3-13
3.4.5 Reactor Vessel Gas Temperature Sensitivity Study.....3-18
3.4.6 Suppression Pool Temperature Sensitivity Study.....3-18
3.4.7 Bubble Relative Humidity Sensitivity Study.....3-27
3.4.8 Suppression Pool Bypass Sensitivity Study.....3-27
3.4.9 In-Vessel Hydrogen Content Sensitivity Study.....3-27
3.4.10 Melt Progression Sensitivity Study.....3-30

4. LaSalle Analyses.....4-1

4.1 Brief LaSalle Description.....4-1

4.2 Steam Flooding of Reactor Building.....4-4

4.3 Preliminary Station Blackout Analysis.....4-14

4.3.1 Nodalization.....4-14
4.3.2 In-Vessel Response.....4-16
4.3.3 Ex-Vessel Response.....4-18
4.3.4 Summary of Insights.....4-18

5. Sequoyah Analyses.....5-1

5.1 Brief Sequoyah Description.....5-1

5.2 Sump Boiloff Timing.....5-1

5.3 Ice Condenser Bypass Following Detonation.....5-3

6. References.....6-1

APPENDIX A - MELCOR NODALIZATIONS.....A-1

LIST OF FIGURES

Figure		Page
2-1	Grand Gulf Schematic	2-2
2-2	Grand Gulf Nodalization	2-5
2-3	Core State at 67 Minutes	2-7
2-4	Core State at 108 Minutes	2-9
2-5	Core State at 212 Minutes	2-10
2-6	Vessel Liquid Level	2-11
2-7	Base Case Hydrogen Production	2-12
2-8	Base Case Concrete Degassing	2-14
2-9	Base Case Containment Hydrogen Mole Fraction	2-15
2-10	Base Case Flow Split through Leakage and Suppression Pool	2-17
2-11	Base Case Radionuclide Release in Vessel	2-18
2-12	Base Case Radionuclide Deposition in Vessel	2-19
2-13	Base Case Radionuclide Distribution	2-20
2-14	Base Case Sr and Ba Release during Core-Concrete Attack	2-22
2-15	Base Case Ru, Ce and La Release during Core-Concrete Attack	2-23
2-16	Flow Split through Drywell Wall Leakage and Suppression Pool with Large Drywell Hole	2-26
2-17	Effect of Burn on Containment Pressure during Station Blackout	2-27
2-18	Base Case Drywell Mole Fractions	2-28
2-19	Drywell Mole Fractions for Station Blackout with Containment Burns	2-30
2-20	Drywell Hydrogen Mole Fractions for Various Containment Burn Assumptions	2-31
2-21	Suppression Pool Water Level	2-33
2-22	Pedestal Water Mass	2-34

LIST OF FIGURES (Continued)

Figure		Page
2-23	Mass of Water Overflowing Onto Drywell Floor	2-36
2-24	Wetwell Pressure Rise vs. Hydrogen Mole Fraction	2-38
2-25	Wetwell Temperature Rise vs. Hydrogen Mole Fraction	2-39
2-26	Containment Depressurization Following Burns	2-41
2-27	Containment Steam Mole Fractions During Spray Injection	2-42
2-28	Containment Steam Mole Fractions During Spray Injection with Increased Evaporation Rate	2-43
2-29	HECTR Containment Steam Mole Fractions During Spray Injection	2-44
2-30	Containment Pressure vs. Failure Area	2-47
2-31	Energy Release vs. Containment Failure Area	2-48
2-32	Drywell Wall Differential Pressure vs. Containment Failure Area	2-49
2-33	Effect of Suppression Pool Subcooling on Depressurization	2-51
3-1	Peach Bottom Schematic	3-2
3-2	Peach Bottom Nodalization	3-3
3-3	Station Blackout Drywell Pressure	3-6
3-4	Station Blackout Drywell Atmosphere Temperature	3-7
3-5	Sensitivity of Drywell Pressure to Model Changes	3-11
3-6	Sensitivity of Drywell Temperature to Model Changes	3-12
3-7	Drywell Pressure Sensitivity to Breach Area	3-14
3-8	Drywell Temperature Sensitivity to Breach Area	3-15
3-9	Drywell Peak Pressure Sensitivity to Breach Area	3-16
3-10	Drywell Peak Temperature Sensitivity to Breach Area	3-17
3-11	Event Timing Sensitivity to Breach Area	3-19

LIST OF FIGURES (Continued)

Figure		Page
3-12	Drywell Pressure Sensitivity to RV Gas Temperature	3-20
3-13	Drywell Temperature Sensitivity to RV Gas Temperature	3-21
3-14	Drywell Peak Pressure Sensitivity to RV Gas Temperature	3-22
3-15	Drywell Peak Temperature Sensitivity to RV Gas Temperature	3-23
3-16	Drywell Pressure Sensitivity to Suppression Pool Temperature	3-24
3-17	Drywell Peak Pressure Sensitivity to Pool Temperature	3-25
3-18	Drywell Peak Temperature Sensitivity to Pool Temperature	3-26
3-19	Drywell Peak Pressure Sensitivity to Bubble Relative Humidity	3-28
3-20	Drywell Pressure Sensitivity to Suppression Pool Bypass	3-29
3-21	Short Term Drywell Pressure Sensitivity to Core Melt Models	3-31
3-22	Short Term Drywell Temperature Sensitivity to Core Melt Models	3-32
4-1	LaSalle Containment Schematic	4-2
4-2	LaSalle Reactor Building Schematic	4-3
4-3	MELCOR Nodalization for LaSalle Reactor Building	4-6
4-4	Reactor Building Pressures for 4" Drywell Leak	4-7
4-5	Reactor Building Temperatures for 4" Drywell Leak	4-8
4-6	Reactor Building Pressures for 7 ft^2 Drywell Rupture	4-10
4-7	Reactor Building Temperatures for 7 ft^2 Drywell Rupture	4-11
4-8	Reactor Building Temperatures for 18" Wetwell Vent Case	4-13
4-9	MELCOR Nodalization for LaSalle Integral Calculation	4-15
4-10	Comparison of Hydrogen Production from MELCOR Calculations	4-19

LIST OF FIGURES (Continued)

Figure		Page
4-11	Vessel Structure Temperatures for Station Blackout	4-20
4-12	Containment Pressures for Station Blackout	4-21
4-13	Steam and Carbon Dioxide Generation from Degassing and Core-Concrete Attack	4-22
5-1	Schematic of Sequoyah Containment	5-2

LIST OF TABLES

Table		Page
2-1	Event Summary for Grand Gulf Station Blackout Calculation	2-6
2-2	Fractional Distribution of Radioactive Fission Products	2-24
2-3	Grand Gulf Outer Containment Burns	2-37
2-4	Pressure Relief from Containment Failure	2-52
3-1	MELCOR Station Blackout Results	3-8
3-2	Summary of Sensitivity Study Cases	3-10
4-1	Reactor Building Temperatures	4-9
4-2	Event Summary for LaSalle Station Blackout Calculation	4-17

ACKNOWLEDGEMENTS

The authors would like to acknowledge several individuals who contributed significantly to this report. Chris Ryder and John Kelly provided valuable technical and editorial input through their reviews. F. Eric Haskin contributed significantly to the Peach Bottom evaluations. George Crane, the Commonwealth Edison Company representative, provided information for constructing the LaSalle input decks. We would also like to thank Josephine Graf, who prepared the document.

EXECUTIVE SUMMARY

Results of calculations performed with MELCOR and HECTR in support of the NUREG-1150 study (Ref. 1) are presented in this report. The analyses examined a wide range of issues. The analyses included integral calculations covering an entire accident sequence, as well as calculations that addressed specific issues that could affect several accident sequences. The results of the analyses for Grand Gulf, Peach Bottom, LaSalle, and Sequoyah are described, and the major conclusions are summarized. This report is intended for persons with a general familiarity of MELCOR capabilities and severe accident phenomena. Additional information on MELCOR capabilities and limitations is available in Reference 2.

Grand Gulf

Base Case Integral Calculation

Two integral MELCOR calculations were performed for a station blackout scenario at Grand Gulf. The base case was a station blackout with nominal leakage between the drywell and outer containment, and no outer-containment burns. The results provided information for quantification of the Grand Gulf accident progression event tree used in the NUREG-1150 study.

Suppression Pool Bypass

A variation of the base case calculation was performed in which a large outer-containment burn was assumed to occur before vessel breach, creating a large hole in the drywell wall. This calculation was performed to examine the effects of suppression pool bypass on the results calculated before and during vessel breach, particularly the effects on suppression pool bypass and containment pressure rise. It was found that, even with this large bypass, about 70% of the blowdown from the vessel passed through the suppression pool at vessel breach. Also, the hole did not significantly affect the size of the pressure rise at vessel breach.

Containment Flammability

Additional MELCOR calculations were performed using a simplified deck to examine the flammability in various regions of containment. This is a large concern at Grand Gulf because the unavailability of igniters during station blackout accidents causes these sequences to dominate risk. The MELCOR calculations showed that, although the outer containment would reach detonable levels, the drywell would be at most marginally flammable for most of the station blackout scenarios. The calculations predicted that insufficient hydrogen would accumulate in the drywell before vessel breach, and that lack of oxygen would prevent burning after vessel

breach. Outer-containment burns and large holes in the drywell wall did not affect these conclusions. The only exception was a case in which a vacuum breaker on an SRV tailpipe was postulated to stick open during the period of peak in-vessel hydrogen production.

Containment Response to Burns

Numerous calculations were performed to characterize containment response to burns initiated over a wide range of containment conditions. Of interest were peak outer-containment pressures, peak outer-containment temperatures, peak differential pressure across the drywell wall, and the rate of containment depressurization after the burn terminated. The numerical values are reported in Section 2.5. In addition, bounding calculations were performed to determine if containment failure during a large burn would provide sufficient pressure relief to prevent the additional failure of the drywell wall. The MELCOR results showed that, for the large burns necessary to threaten the drywell wall, even a .65 m^2 (7 ft^2) hole in the containment wall could not sufficiently mitigate the pressure rise in the outer-containment to prevent drywell wall failure.

Steam Inerting

MELCOR and HECTR calculations were performed to examine the effect of spray injection into a steam-filled containment. The results indicate that when sprays inject water into a containment that is saturated with steam by evaporation from a hot suppression pool, significant amounts of steam are removed. The calculations predicted that the steam would be removed relatively rapidly by the sprays, such that hydrogen burns in the outer containment would be likely. This implies that there is a potential for igniting hydrogen-rich mixtures in containment following power recovery when previous burning had been prevented by the high containment steam content.

Suppression Pool Backflow

The potential for pushing water over the weir wall onto the drywell floor was investigated. The amount of water on the drywell floor affects the likelihood of ex-vessel steam explosions and the amount of scrubbing by the overlying water pool during core-concrete attack. It was known from previous unpublished analyses and Reference 3 that suppression pool water backflow would be likely if a deflagration occurred in the outer containment. However, the potential for suppression pool backflow caused by hydrogen pressurization alone in the outer containment had not been well characterized. The MELCOR results showed that this is a highly uncertain phenomenon. It is affected by the rate and integral amount of hydrogen released to containment, the amount of leakage through the drywell wall, and the rate of concrete degassing in the drywell. It was found that varying these parameters within their uncertainty ranges would result in backflow in some cases, but no backflow in other equally valid

cases. A more definitive answer on suppression pool backflow will not be possible until the uncertainty in in-vessel hydrogen generation is reduced.

Source Terms

The mass and energy releases from containment were estimated for the case with containment failure occurring because of a hydrogen burn. The results of these calculations provided guidance in quantifying the source term for Grand Gulf. The responses for both dry and saturated containment atmospheres were characterized and numerical values are reported in Section 2.8.

Peach Bottom

An analysis of the Peach Bottom containment response following vessel breach was performed using MELCOR. The analysis was performed to examine the potential for containment failure at vessel breach from the depressurization alone. Loads from direct heating and steam explosions were not considered because MELCOR did not contain models for these phenomena. Before these calculations were performed, it was not known whether or not depressurization alone was sufficient to fail the Peach Bottom containment at vessel breach. Long-term and short-term station blackout scenarios were examined, and sensitivity studies were performed on vent downcomer clearing, containment heat transfer, flashing of residual water in the vessel downcomer, vessel break area, in-vessel gas temperatures, suppression pool temperature, relative humidity of gas bubbles leaving the suppression pool, suppression pool bypass, and in-vessel hydrogen content. The calculations indicated that containment failure at the time of lower head failure is unlikely for accidents at Peach Bottom in which direct heating and steam explosions do not contribute significantly to the containment response.

LaSalle

Reactor Building Response

The LaSalle reactor building response following wetwell venting or drywell failure was examined using MELCOR. The level of steam predicted in various regions and the environmental temperatures were provided to a NUREG-1150 expert panel for estimating the potential for equipment survival under these severe conditions. A relatively-detailed nodalization was used for these analyses to capture differences among the various regions in the reactor building. The numerical results are reported in Section 4.2.

Station Blackout Calculation

Results of an integral, shakedown calculation for a short term station blackout are discussed in the report. This calculation used a heavily

noded deck which was found to give unsatisfactory results. The calculated results have mainly been used to provide guidance for subsequent analyses for LaSalle and other BWRs, and to identify limitations in MELCOR. A large number of modeling insights were gained through this calculation, and these are discussed in Section 4.3.

Sequoyah

A very limited analysis was performed to estimate the timing for boiling the reactor cavity dry for a case with a coolable debris bed submerged under 1125 m^3 of water. This estimate was used to provide initial conditions for a separate analysis investigating the potential for a delayed core-concrete attack and its consequences. MELCOR calculated that a long time (39 hours) would be required to boil the water away.

Calculations were also performed using HECTR to estimate the response in the ice condenser at vessel breach if a detonation had previously voided the ice columns from a region of the ice bed and had created a hole in the containment wall. It was found that the amount of flow bypassing the ice condenser and escaping to the environment would be relatively low for the postulated level of damage.

1. INTRODUCTION

The MELCOR computer code (Ref. 2) was developed at Sandia National Laboratories for the United States Nuclear Regulatory Commission as a tool for calculating realistic estimates of severe accident progressions and source terms. MELCOR has advanced to a state that it can now treat most major aspects of severe accidents. Models are included for in-vessel and ex-vessel thermal-hydraulics, core degradation and relocation, radionuclide release and transport, core-concrete interactions, engineered safety features, and gas combustion. MELCOR provides an integrated treatment of these phenomena at a level of detail sufficient for source term calculations.

MELCOR was previously used to address specific issues for PRAs, but it has only recently reached the level of development necessary for its acceptance as the primary tool for calculating source terms. Because of this, MELCOR was not used to provide the source terms for the dominant sequences for NUREG-1150. However, MELCOR was used to help address many of the phenomenological questions in the accident progression event trees (APETs) and to provide guidance for the expert opinion panels. Often, these analyses required modeling capabilities that were only available in MELCOR.

The MELCOR analyses examined a range of issues. The analyses included integral calculations covering an entire accident sequence, as well as calculations that addressed specific issues that could affect several accident sequences. Analyses were performed for both the pressurized water reactor (PWR) plants and the boiling water reactor (BWR) plants. The results of the analyses for Grand Gulf, Peach Bottom, LaSalle, and Sequoyah are described in Sections 2 through 5, respectively.

Unknown errors undoubtedly exist in MELCOR, which affect the results to an unknown extent. However, errors in MELCOR do not preclude its use. The MELCOR estimated source terms are not used directly in the PRAs, but rather, judgment is used to account for known code errors and modeling weaknesses, as well as variations in possible plant conditions, and alternate accident progressions. If errors are known to exist when a calculation is performed, either alternate input is devised to correct the error, or the effect of the error on the results is considered when developing the actual input to the PRA. While some errors have been discovered since completing the MELCOR calculations discussed in this report, no errors have been found that would alter the conclusions drawn from the calculations.

At the time these calculations were performed, MELCOR did not include an ice condenser model. Thus, to address an issue related to ice condenser effectiveness, the HECTR computer code was used.

This report is intended for persons with a general familiarity of MELCOR capabilities and severe accident phenomena. Additional information on MELCOR capabilities and limitations is available in Reference 2.

2. GRAND GULF ANALYSES

There were a large number of issues for NUREG-1150 concerning containment thermal-hydraulics in Grand Gulf that could not be adequately addressed with the source term code package (STCP) (Refs. 4,5) because of its limited thermal-hydraulic modeling. Most of the issues involved the likelihood of forming flammable or detonable mixtures in various regions of containment during both the early and late phases of station blackout sequences. A second large concern in the NUREG-1150 analyses was the likelihood of suppression pool water being forced back over the weir wall onto the drywell floor. If this were to occur, it would establish conditions for an ex-vessel steam explosion, which could fail the containment and lead to higher containment releases. However, the water would also provide the potential for beneficial effects by scrubbing releases from the molten pool during core-concrete attack, thus mitigating the fission product release to the drywell.

Both the containment flammability and drywell flooding issues are important for Grand Gulf because they affect the likelihood of breaching the drywell wall and forming a direct flow path between the drywell and outer containment that would bypass the suppression pool. Unless the suppression pool is bypassed, the source terms following containment failure are calculated to be relatively low.

Two integral MELCOR calculations were performed to address these issues. The calculations modeled the accident progression following core uncovering, including radionuclide behavior. In addition, numerous calculations were performed to examine sensitivities and specific containment issues using a simplified deck that modeled only the containment. The results of the Grand Gulf calculations and a brief comparison to STCP fission product releases are presented in the following sections, following a summary description of the plant characteristics that are relevant to the analyses described in this report.

2.1 Brief Grand Gulf Description

The pertinent features of the Grand Gulf plant are described in this section. The significance of the specific features discussed will become obvious as the Grand Gulf issues are addressed in the remainder of Section 2.

Grand Gulf is a BWR/6 reactor with a Mark III containment. The containment, shown in Figure 2-1, is divided into 2 main regions, the drywell and the outer containment. The drywell is a cylindrical region that surrounds the reactor pressure vessel (RPV). The outer containment surrounds the drywell and is separated from it by the drywell wall. The two regions are further isolated by an annular suppression pool which is located at the base of containment. The suppression pool is contained between the outer containment wall and a shorter wall in the drywell called the weir wall. Besides leakage through the drywell wall, the only

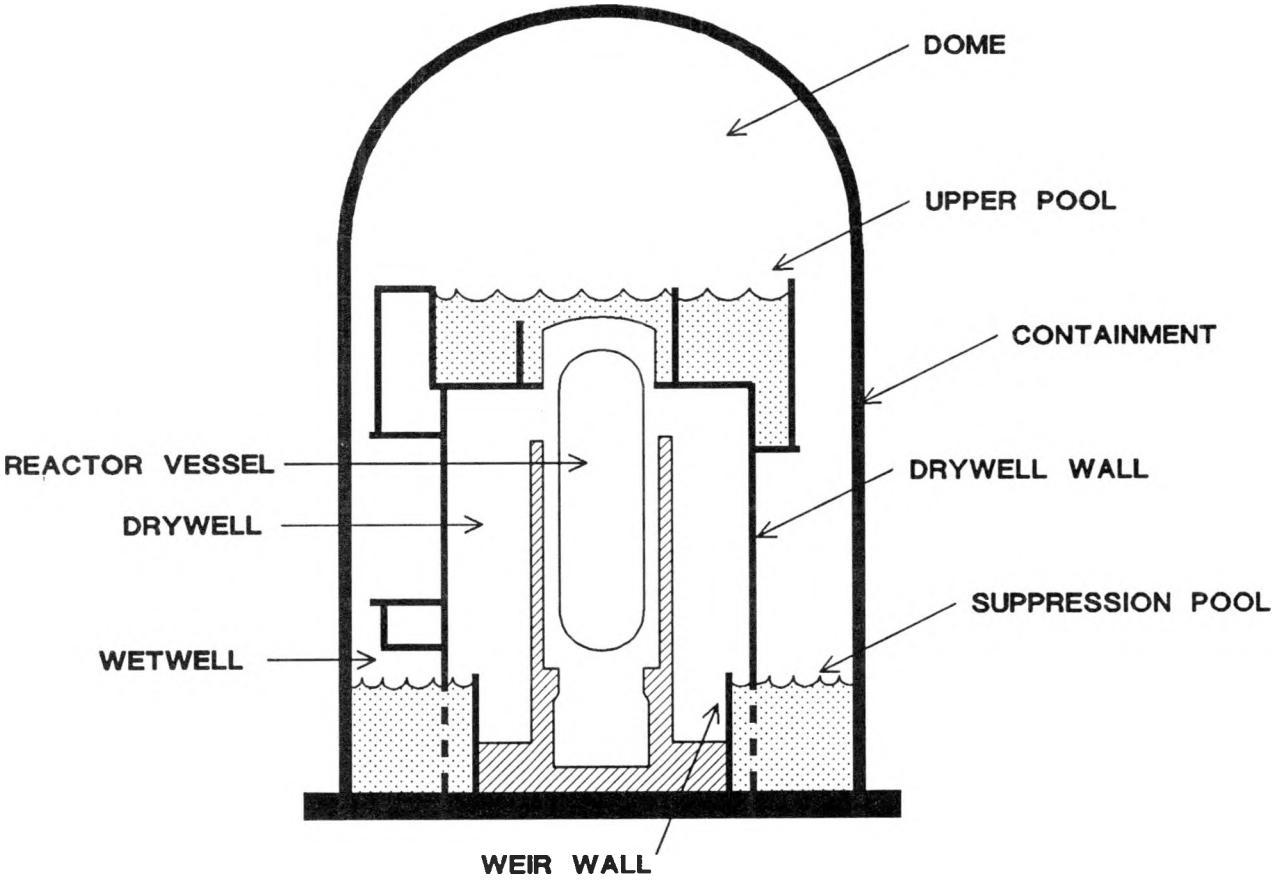

Figure 2-1. Grand Gulf Schematic

flow path between the two containment regions in a station blackout accident is through horizontal vents that are submerged in the suppression pool.

The weir wall containing the suppression pool is not high enough to prevent backflow of suppression pool water onto the drywell floor when the outer containment pressure exceeds the drywell pressure by a large enough margin to overcome the water head in the weir annulus. The water overflowing onto the drywell floor would then drain into the pedestal region beneath the vessel through floor drains.

The RPV vents through safety relief valves (SRVs) into the suppression pool. There are vacuum breakers in the piping between the SRVs and the suppression pool which open to avoid condensation-induced problems in the tailpipes following SRV reclosure. If these vacuum breakers in the SRV tailpipes fail to reclose, a portion of the subsequent flow through the SRVs would enter the drywell directly, and the remainder would continue to be discharged to the suppression pool.

The outer containment can be cooled by a spray system, with injection nozzles located in the upper dome. Because this system is ac-powered, it would not be available during a station blackout. However, if ac power was restored during a station blackout, the sprays would become available.

Grand Gulf is equipped with igniters in both the drywell and outer containment to provide controlled burning of hydrogen and carbon monoxide during accidents. Because of this, threats from containment burning are not important for many sequences. However, these igniters are ac-powered, so they would not be available during station blackout sequences.

2.2 Integral Station Blackout Calculation

Integral calculations were performed for two variations of a short term station blackout scenario. In both variations, ac and dc power were assumed to have failed, so the vessel could not be depressurized before vessel breach. Loss of ac power also prevented igniter operation, upper pool dump, and operation of the vacuum breakers in the drywell wall. In the base calculation, nominal leakage was modeled between the drywell and the outer containment, and containment burns were precluded. In a variation of the base calculation, the effect of containment burning was examined by initiating a large burn in the outer containment before vessel breach. This burn was assumed to create a .093 m^2 (1 ft^2) bypass hole in the drywell wall. The two calculations were performed to:

1. estimate steam and hydrogen release rates that would be used in addressing various containment issues,

2. examine the potential for backflow of suppression pool water onto the drywell floor when hydrogen is released to the containment through the safety relief valves (SRVs),

3. estimate the flow between the drywell and outer containment through the suppression pool relative to the amount flowing through drywell leakage paths (both at vessel breach and during core-concrete attack), and

4. estimate drywell and outer containment conditions (pressure and flammability) throughout the transient to compare with STCP results.

The nodalization used for the calculations is shown in Figure 2-2. The input deck for MELCOR is a combination of a MELCOR containment-only section that will be described in Section 2.3 and a vessel section derived from the LaSalle deck which will be described in Section 4.2. Because of NUREG-1150 schedule constraints, the core input was generated by simply scaling the LaSalle input to Grand Gulf, and simplifying the LaSalle vessel nodalization. That is, core masses and powers were increased by the ratio of the number of fuel assemblies in Grand Gulf and LaSalle. The vessel was represented by six control volumes, the outer containment by five, and the drywell by three. The core was collapsed from the LaSalle nodalization to four radial rings and 13 axial levels. More details of the nodalization are included in Sections 2.3, 4.2, and Appendix A.

The results of the base case (without containment burns) will be discussed first, followed by a discussion of the differences that were predicted for the second case (with containment burns). The in-vessel melt progression is described in considerable detail to allow comparison with STCP results. Containment results are then described, followed by radionuclide results. The conclusions from these calculations regarding drywell flammability and drywell flooding are deferred until Sections 2.3 and 2.4, respectively, because additional containment-only calculations were performed to support the analyses of those issues.

2.2.1 In-Vessel Melt Progression

Table 2-1 summarizes the predicted timing of key events, relative to the start of core uncovering. The initial phase of the sequence was not calculated with MELCOR because code modeling was not sufficient to examine the very early phase of the accident at the time this calculation was performed. Instead, the calculation was initiated when the water level had dropped to the top of active fuel (TAF). The conditions at this time were obtained from an existing calculation that had been performed with the LTAS code (Ref. 6) to provide timing information for the core damage frequency analysis in the NUREG-1150 study.

About 46 minutes after the core uncovered, MELCOR calculated that core material began melting and relocating down to lower elevations. Enough of this material was predicted to refreeze at the lower core elevations to form a complete blockage of the inner ring at about 63 minutes. Complete blockages were formed in rings 2 and 3 at 65 and 67 minutes, respectively.

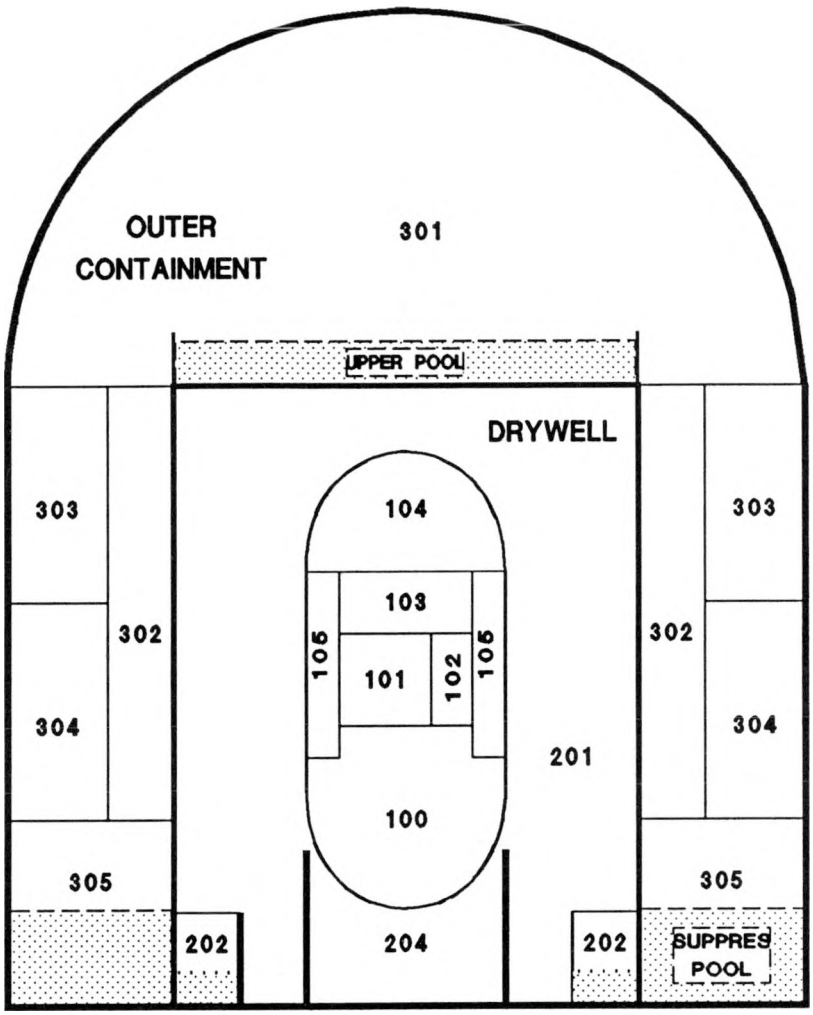

Figure 2-2. Grand Gulf Nodalization

Table 2-1

Event Summary for Grand Gulf Station Blackout Calculations (Relative to Core Uncovering)

EVENT	(min)
Water Reaches TAF	0
Start Oxidizing Zircaloy	27
Start Melting and Material Relocation	46
Complete Blockage of Inner Ring	63
Complete Blockage of Ring 2	65
Complete Blockage of Ring 3	67
Partial Core Plate Failure (Ring 3)	108
Partial Core Plate Failure (Ring 1)	206
Lower Head Failure	212
Begin Debris Ejection	287

A schematic of the core state just prior to blockage formation in ring 3 is shown in Figure 2-3. Although the schematic does not show the morphology predicted by MELCOR, it does indicate the relative location of the core components (fuel, cladding, debris, canisters). Each shaded box in the figure indicates that a particular core component is present for that radial ring and core level. If a particular shaded box is absent from a radial ring / core level, none of that component is present at the noted time in the transient. As indicated on the figure, a blockage had formed in the second fueled node above the core plate for the central two rings. Debris beds existed above the blockages which consisted mostly of fuel pellets, with oxidized and unoxidized zirconium also present. A small amount of debris had also settled down to the core plate for both rings. Debris beds were also predicted on the bottom head, but they contained only steel fragments.

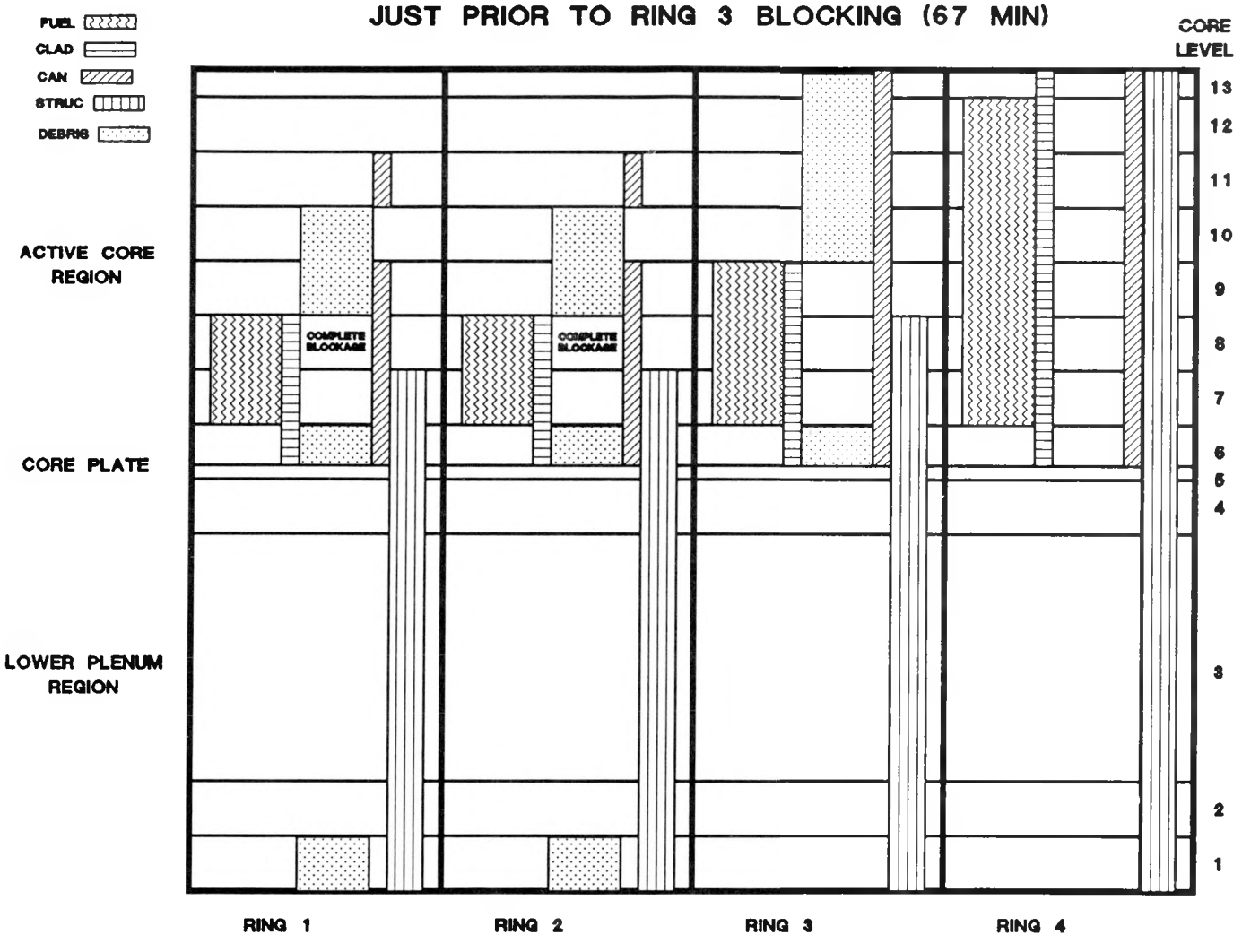

Figure 2-3. Core State at 67 Minutes

The amount of fuel damage became progressively less for the outer rings. In fact, in the outer ring, no fuel relocation had been predicted at this time, but zirconium oxidation had begun.

At about 108 minutes, the core plate temperature for ring 3 exceeded the temperature that had been specified as the failure criterion. This triggered a partial core collapse of that ring, which dumped the core debris that had been held up by the core plate into the lower plenum. The heat transfer from this hot debris rapidly boiled away a large fraction of the water residing in the lower plenum. A schematic of the core state after this collapse is shown in Figure 2-4. Because of the core plate failure, only canister walls and control blades were predicted to remain above the core plate in ring 3. The configuration of the inner two rings had not changed significantly from the configuration that existed when ring 3 initially blocked (shown previously in Figure 2-3), but the material temperatures were much higher. In addition, a larger amount of the zirconium below the blockage had been oxidized. Significant melting and relocation had also been predicted for ring 4 at 108 minutes but only incomplete blockages had been formed.

During the next 100 minutes, the blockage in ring 1 melted, relocated downward, then reformed at lower levels. During this process, the fuel debris bed that had been held up by the blockage relocated downward such that a debris bed was present in the 5 levels immediately above the core plate. At about 206 minutes, the core plate reached an assumed failure temperature, triggering a partial core collapse for this ring. This dumped enough core debris into the lower plenum to rapidly boil away the remaining water. With the water gone, the debris quickly heated up the lower head, and a lower head penetration failure was predicted to occur at about 212 minutes in ring 1. Failure in ring 3 was predicted shortly thereafter. A schematic of the core conditions at this time (vessel breach) is shown in Figure 2-5. Although there was fuel debris on the lower head in rings 1 and 3, the debris was not molten at the time the lower head penetration failed, so it was not ejected to the cavity. Thereafter, the debris continued to heat up in the lower head, and at about 287 minutes it began melting and pouring out onto the pedestal floor.

The collapsed water levels for the channel and lower plenum control volumes of the RPV are shown in Figure 2-6. Initially, the core boiloff rate was relatively rapid, and the core level fell quickly. As the level dropped and less of the core was covered, a smaller fraction of the core energy was transferred to the water, slowing the rate of level decrease. At about 70 minutes, the level crossed from the channel volume to the lower plenum. The two sharp level drops at 108 and 206 minutes were caused by the partial core plate failures in rings 3 and 1, respectively.

Figure 2-7 shows the in-vessel hydrogen generation for this calculation. The figure shows the integral mass of hydrogen generated during the transient as well as the fraction of the total zirconium oxidized. A

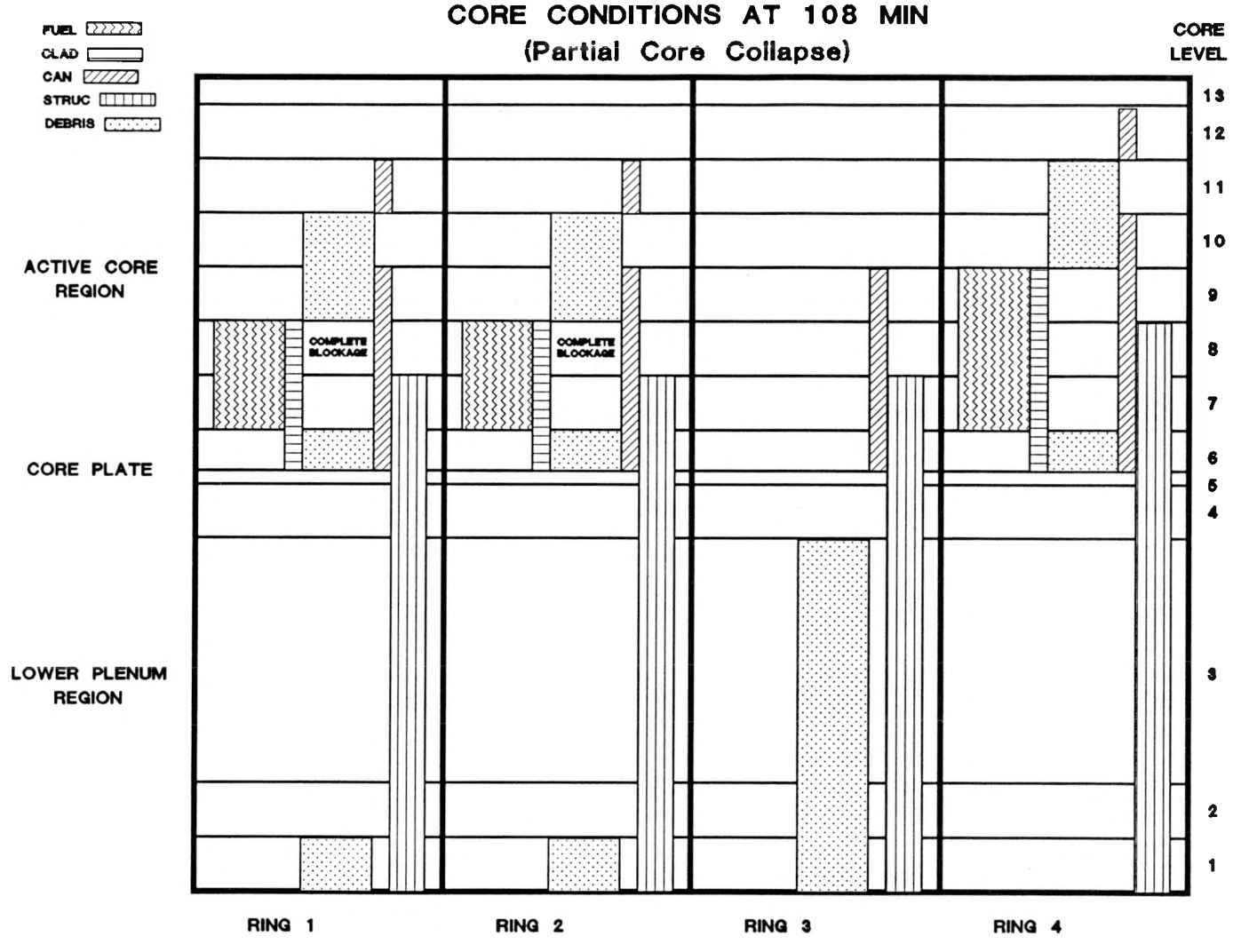

Figure 2-4. Core State at 108 Minutes

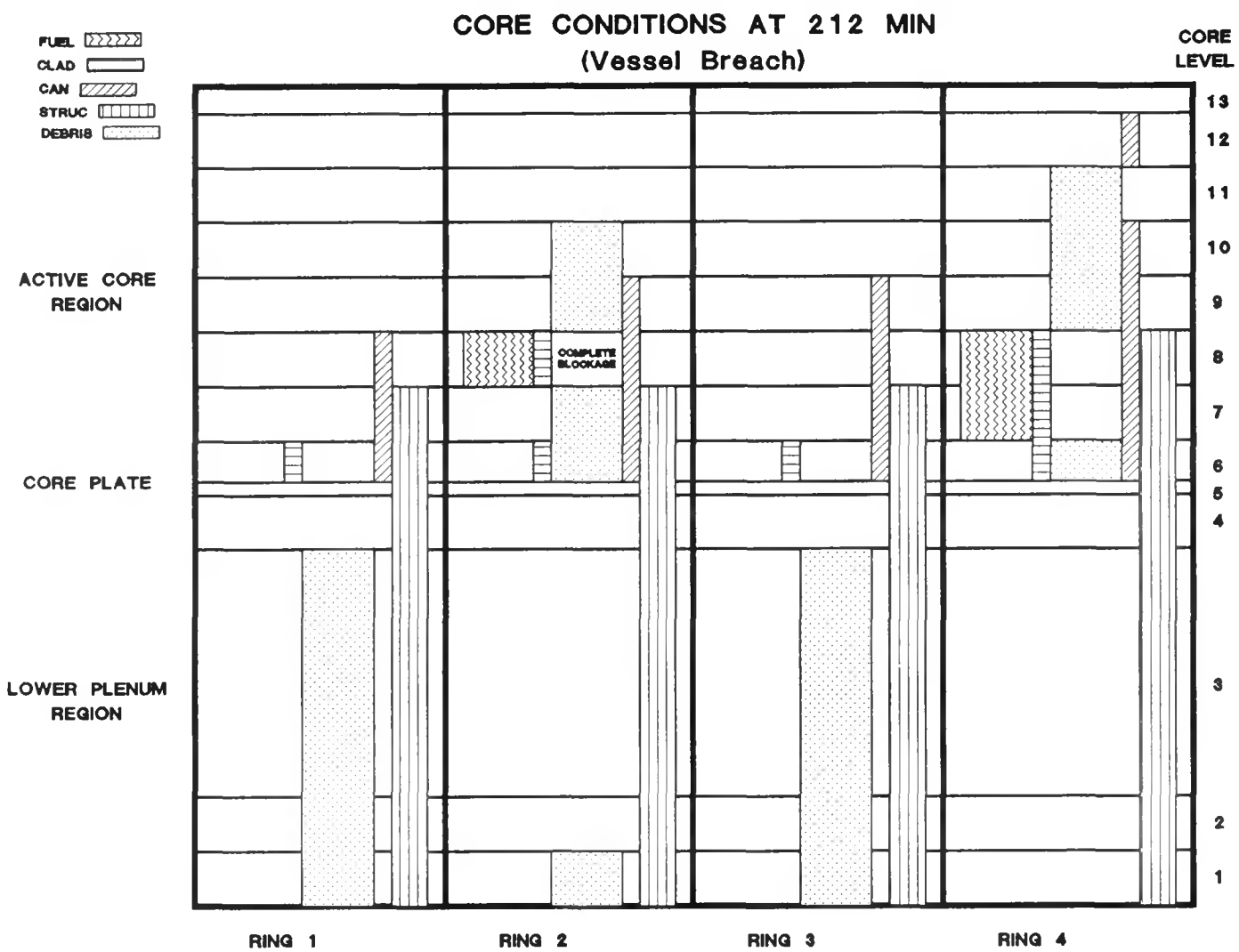

Figure 2-5. Core State at 212 Minutes

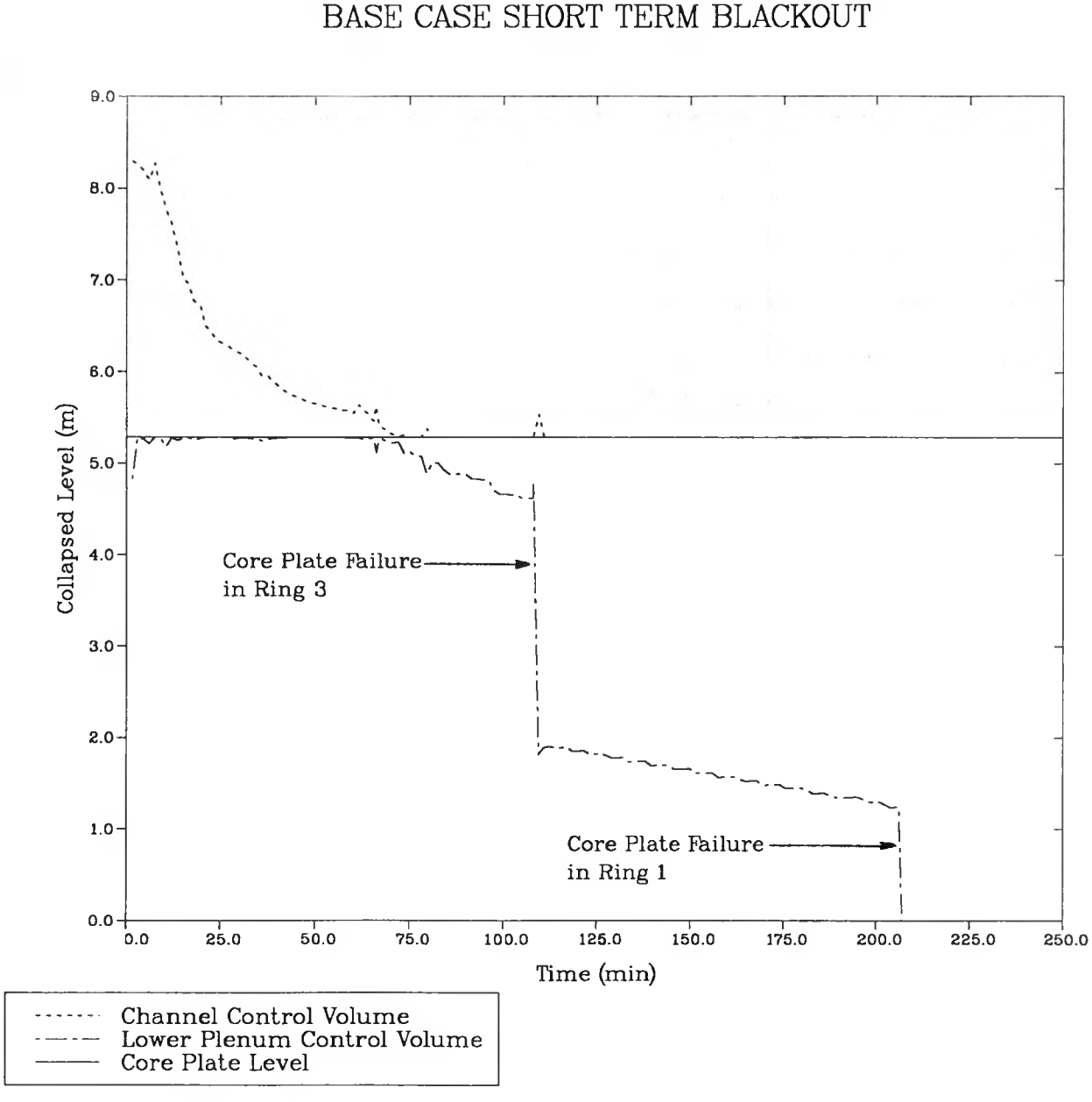

Figure 2-6. Vessel Liquid Level

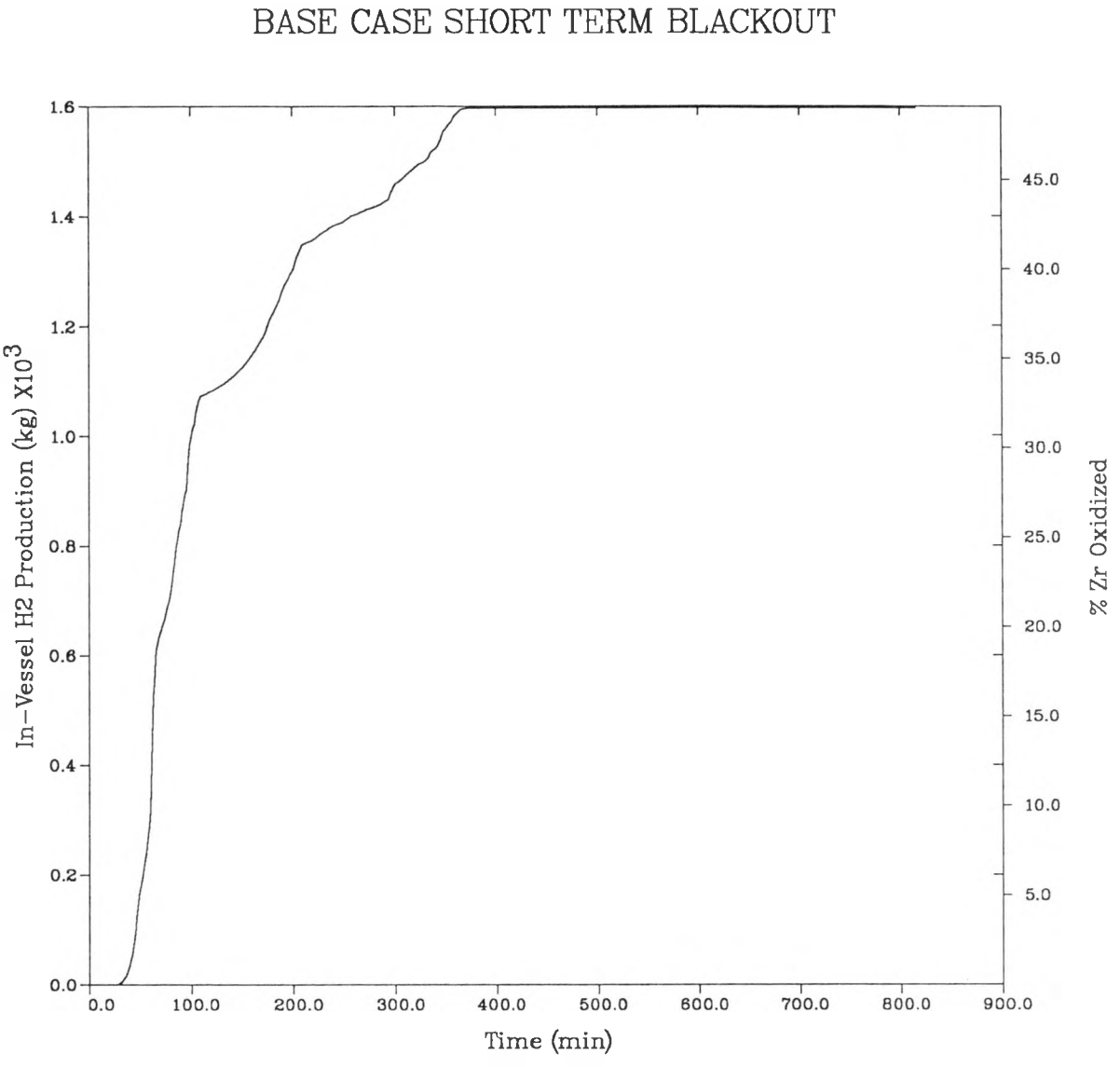

Figure 2-7. Base Case Hydrogen Production

relatively high amount of hydrogen generation was calculated and this resulted in high containment hydrogen concentrations as will be discussed in Section 2.2.2. Most of the hydrogen was generated during about a 60 minute period, starting at about 40 minutes. Thereafter, the hydrogen production continued at a reduced rate until about 360 minutes, at which time most of the zirconium had melted out of the vessel.

2.2.2 Early Containment Response

The temperature rise was not very large in either the drywell or outer containment before vessel breach, but it was sufficiently large in the drywell to initiate concrete degassing by about 85 minutes. The total amount of steam released from the drywell structures by degassing is shown in Figure 2-8. The steam release after vessel breach was larger than the release before vessel breach, but the steam release before vessel breach was sufficiently large to affect the potential for backflow of suppression pool water onto the drywell floor. This will be discussed in Section 2.4.

The containment pressure increases were quite low before vessel breach because the suppression pool remained subcooled and was able to condense most of the steam released from the RPV. The slight pressurization resulted from hydrogen release to containment and from the relocation of some of the air in the drywell to the outer containment when concrete degassing began. At vessel breach, the remaining air was purged from the drywell, causing a rapid, but relatively small pressure increase (about 35 kPa).

The large amount of in-vessel hydrogen generation resulted in high hydrogen concentrations in the outer containment as shown in Figure 2-9. These concentrations are well within the detonability range. The concentration was highest near the suppression pool where the hydrogen was released, and lowest in the dome. Small spikes in hydrogen concentration were generally predicted near the suppression pool as the SRVs opened, yielding short time periods with slight hydrogen concentration gradients in containment. However, the hydrogen rapidly mixed after the SRVs cycled closed, yielding a uniform hydrogen mixture in the outer containment. The large drop in hydrogen concentrations shown in Figure 2-9 for the lower containment levels at about 200 minutes occurred because a large steam release to containment, resulting from core plate failure and vessel breach, diluted the lower containment regions with steam. Hydrogen levels in containment were again well-mixed by about 260 minutes.

2.2.3 Late Containment Response

A core-concrete attack proceeded at a relatively low rate because of the large amount of in-vessel zirconium oxidation shown in Figure 2-7. With a reduced amount of zirconium remaining in the debris, the chemical reactions occurring during core-concrete attack were not as aggressive,

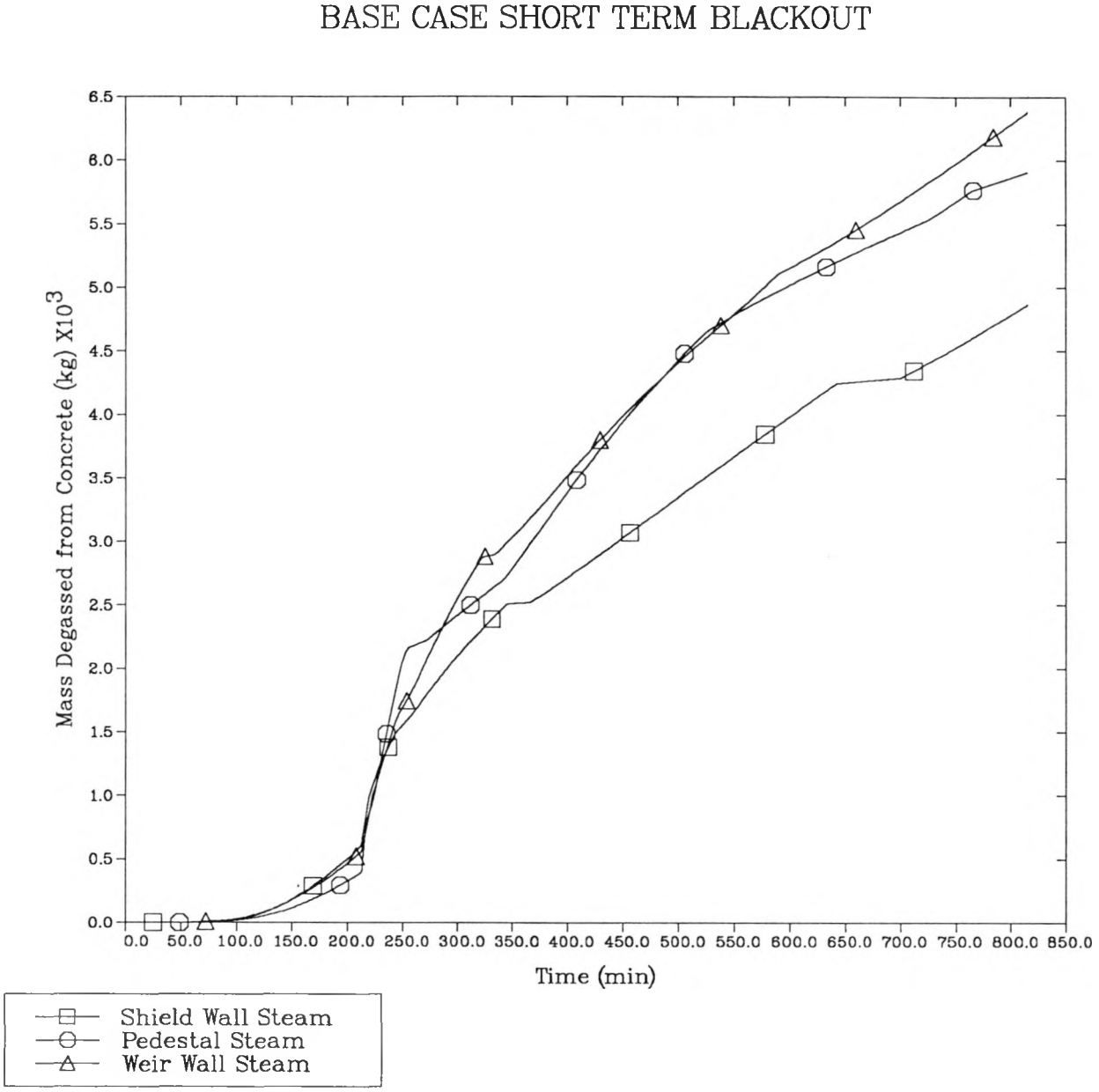

Figure 2-8. Base Case Concrete Degassing

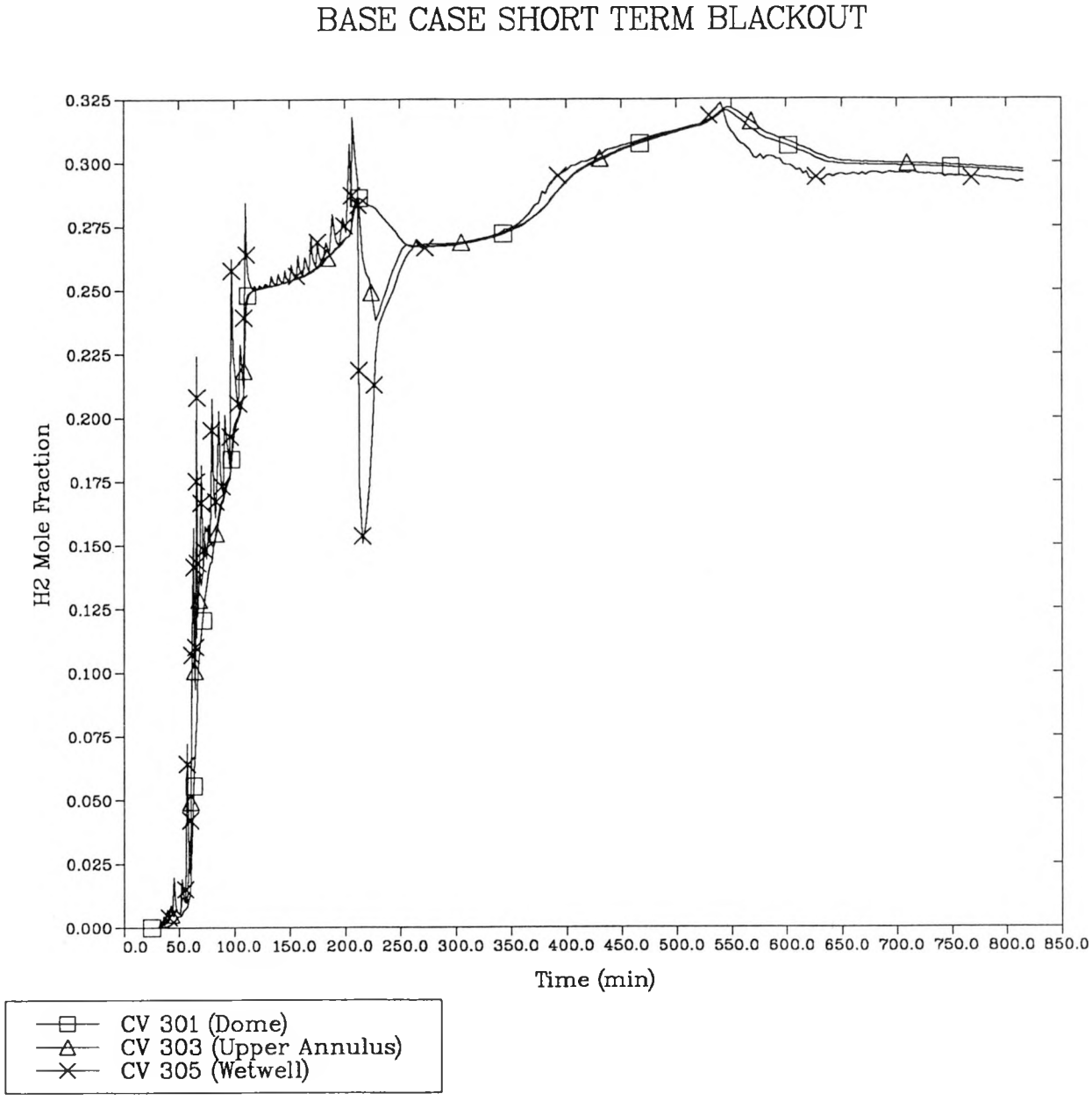

Figure 2-9. Base Case Containment Hydrogen Mole Fraction

so a smaller amount of gases were predicted than in previous, undocumented, MELCOR calculations. As a result, the containment pressurized relatively slowly. When the calculation was terminated at about 815 min, the containment pressure was only about 285 kPa.

The MELCOR results also provide estimates of containment flammability during core-concrete attack. During core-concrete attack, a large amount of carbon dioxide can be generated. If sufficient quantities are released to the drywell and carried to the outer containment, the outer containment could become inerted. This then would eliminate the threat from late containment burns. However, the slow containment pressurization calculated by MELCOR during core-concrete attack was accompanied by a low rate of carbon dioxide generation. Thus, the containment remained flammable throughout the calculation, rather than becoming inert by carbon dioxide addition.

Figure 2-10 shows the flow rates through the suppression pool and the leakage paths in the drywell wall. Early in this calculation, much of the suppression pool inventory had been pushed back onto the drywell floor. As a result, little pressure differential between drywell and outer containment was required to depress the suppression pool level below the top row of vents in the weir annulus. This in turn caused almost all of the flow to pass through the suppression pool. When the core-concrete attack was most active, about 40 times as much flow passed through the suppression pool vents as through leaks in the drywell wall, and by the end of the calculation, the relative flow through the vents had been reduced to about ten times the amount flowing through the drywell wall. This result is greatly affected by the suppression pool level. According to a previous, undocumented, MELCOR calculation, conditions were sufficiently different that none of the suppression pool water was pushed over the weir wall onto the drywell floor. In that calculation, the relative flow through the drywell leakage path was much larger; 7 times as much flow passed through the suppression pool vents as through the drywell wall leaks during active core-concrete attack and the ratio was reduced to about 2 by the end of that calculation.

2.2.4 Radionuclide Behavior

The masses of Cs, I, and Te released from the fuel while it was in the RPV are shown in Figure 2-11. The total mass of CsOH, Te, and CsI deposited on in-vessel structures is shown in Figure 2-12. The in-vessel retention was predicted to be quite high for all 3 classes, with most of the deposition occurring on the separators. Some revaporization was predicted for each class, but the in-vessel retention was still quite high at the end of the calculation.

The noble gases were predicted to be released early from the fuel and rapidly transported to the outer containment. There was little mixing between the outer containment and drywell, so most of the gases remained in the outer containment throughout the transient as shown in Figure 2-13.

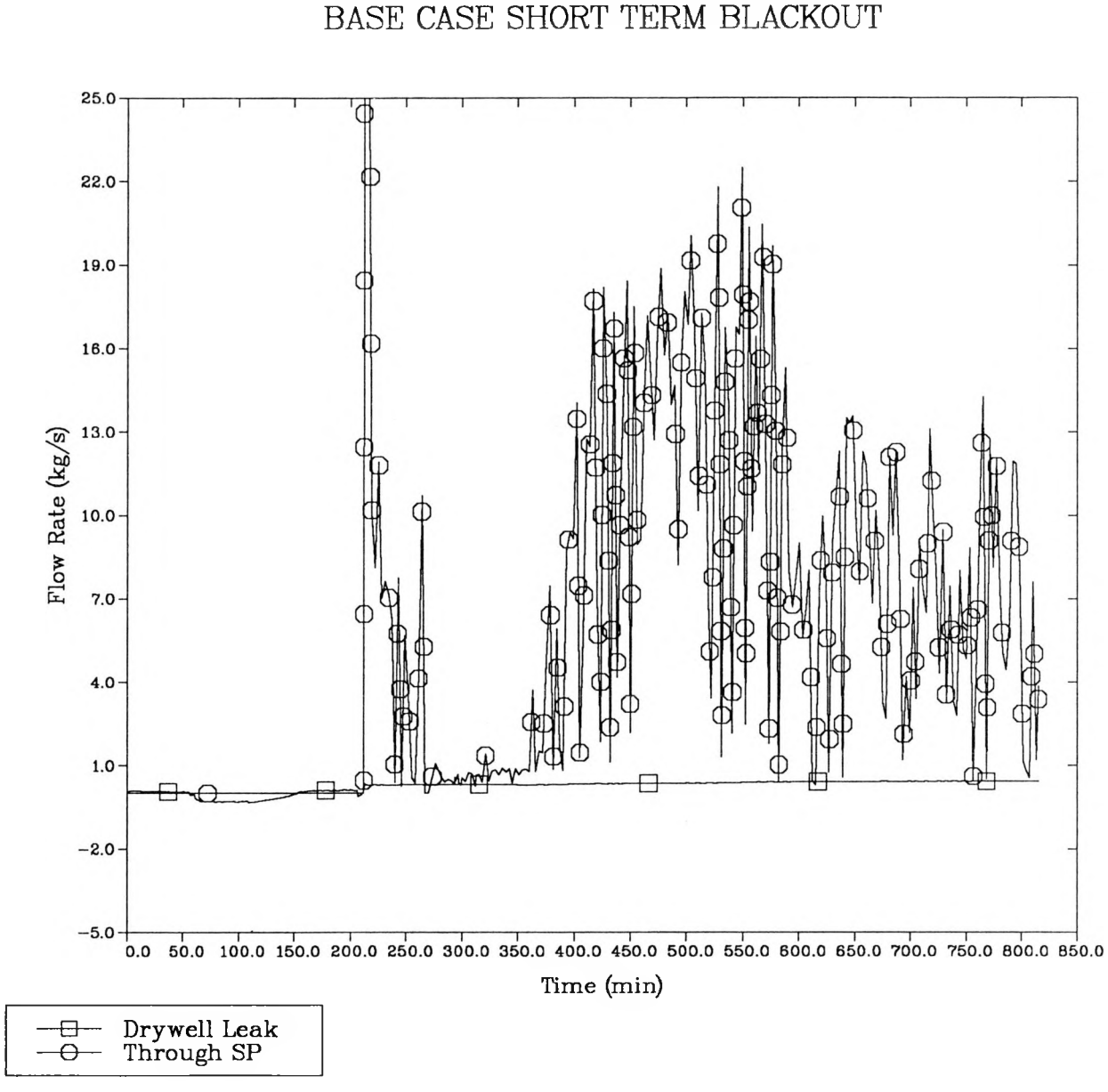

Figure 2-10. Base Case Flow Split through Leakage and Suppression Pool

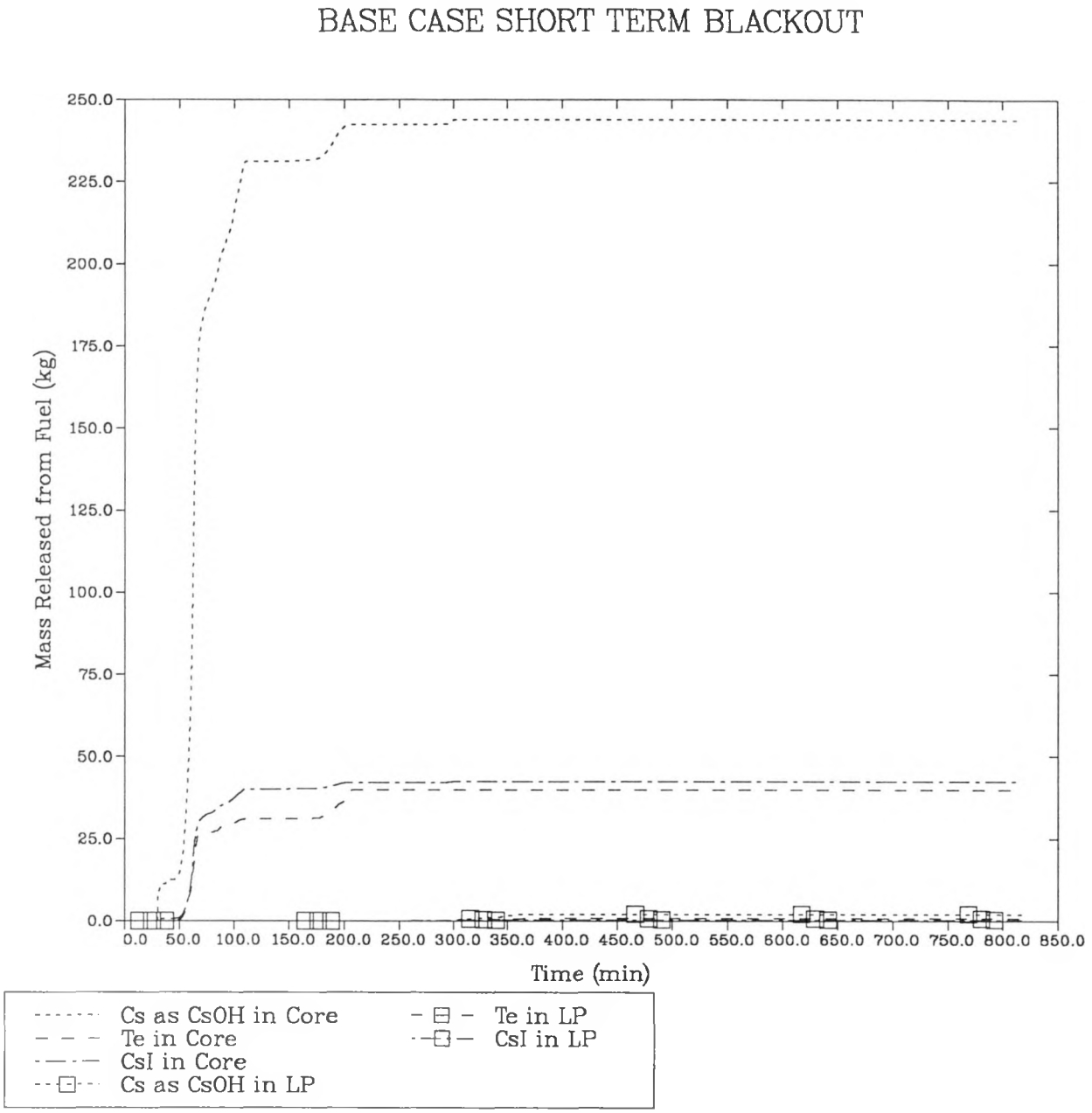

Figure 2-11. Base Case Radionuclide Release in Vessel

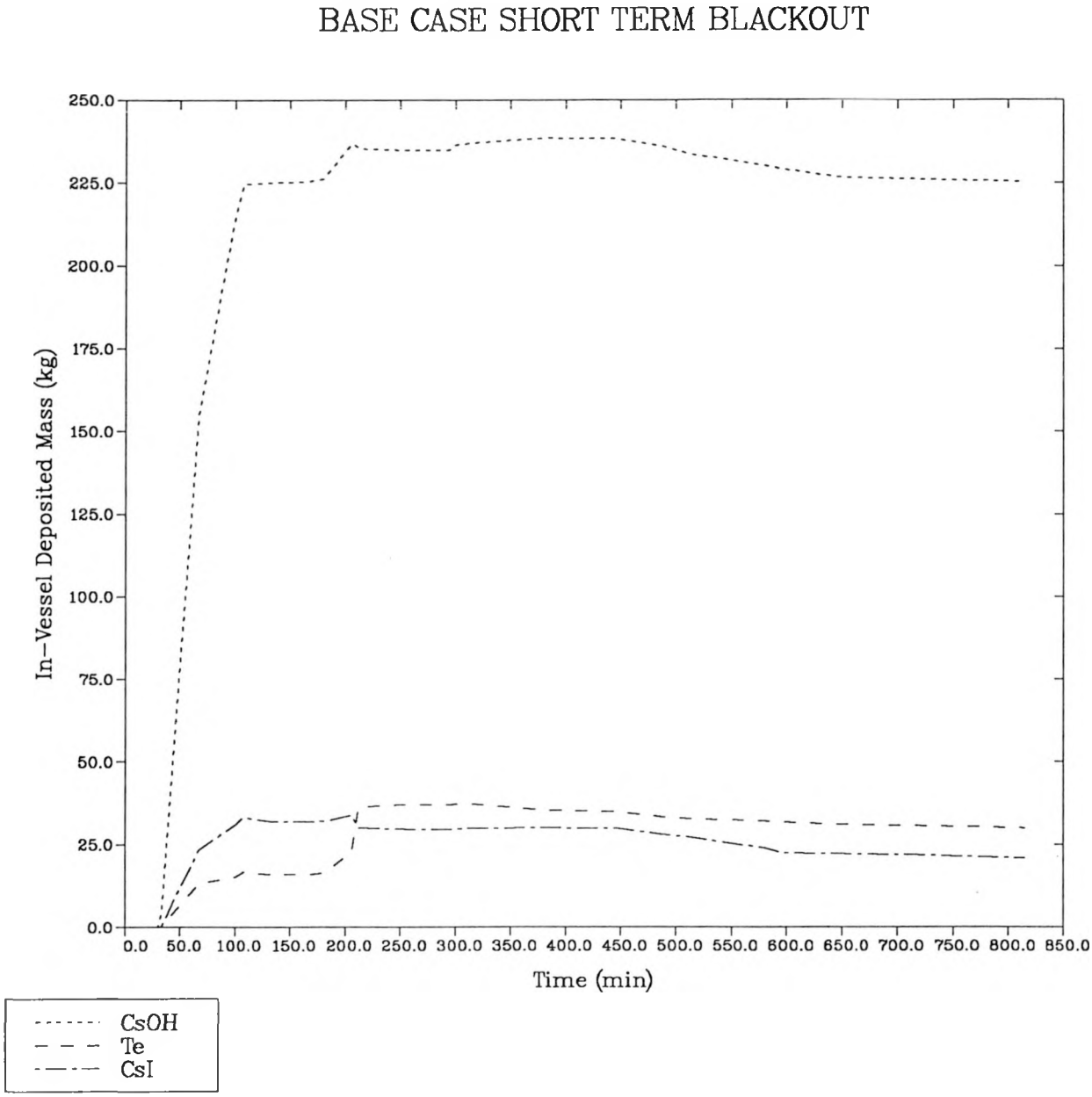

Figure 2-12. Base Case Radionuclide Deposition in Vessel

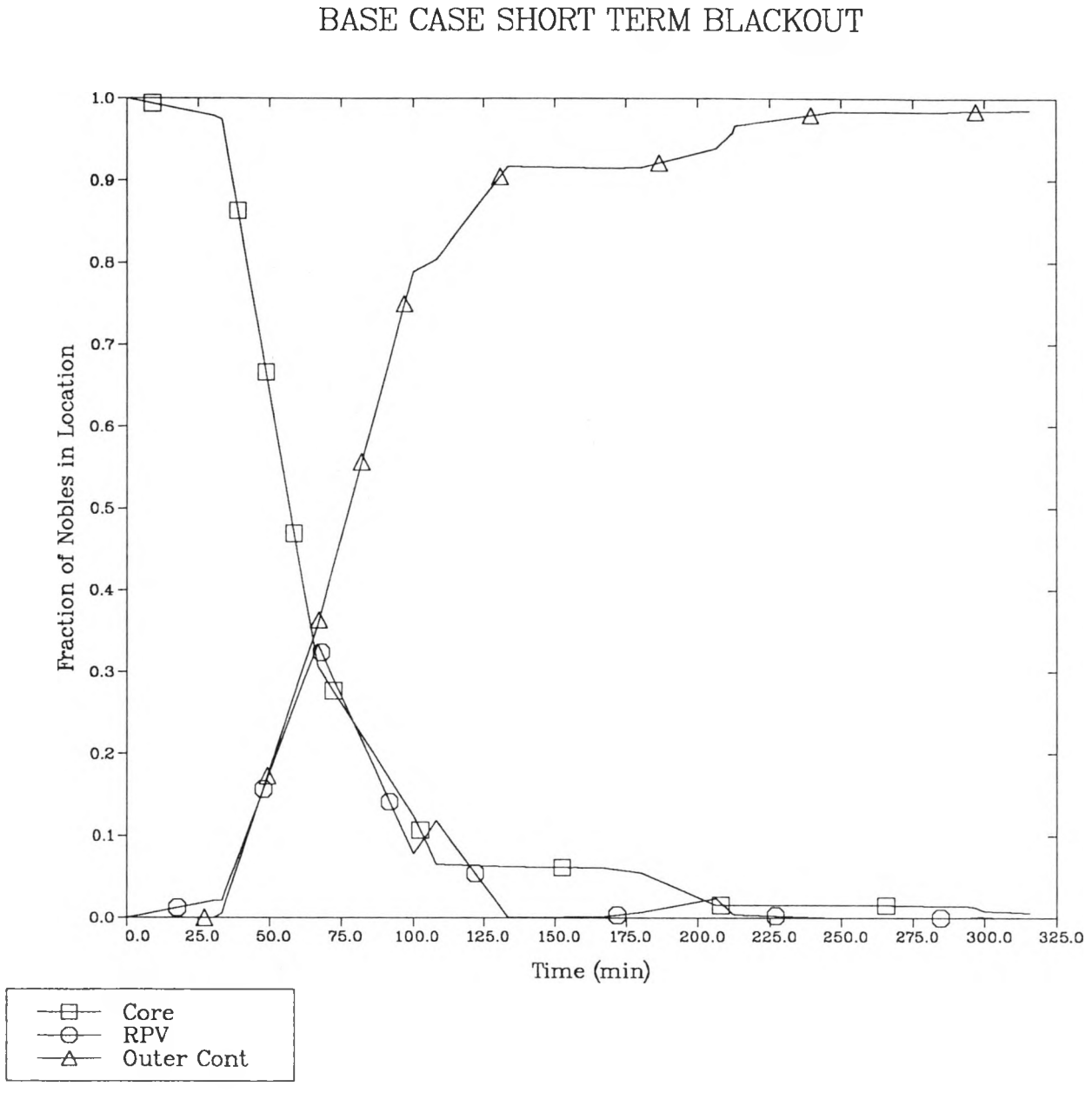

Figure 2-13. Base Case Radionuclide Distribution

The total mass (radioactive plus non-radioactive) of Sr and Ba released during core-concrete attack is shown in Figure 2-14, and the masses of Ru, La, and Ce are shown in Figure 2-15. The releases of all of these classes are quite low because of the slow rate of core-concrete attack. In addition, the releases are scrubbed by the overlying water pool in the pedestal, causing even smaller releases to the drywell.

The Te release is much higher than predicted by STCP (Refs. 4,5) for similar scenarios. This difference results from modeling of core melting phenomena. In both MELCOR and STCP, the Te release from the fuel is suppressed when the fuel is surrounded by unoxidized zirconium in the clad, so early releases of Te are low. However, as the accident proceeds, MELCOR melts and relocates the clad, leaving a fuel debris bed which can then release Te (because intact cladding is no longer present). STCP does not model clad relocation, so STCP predicts a much lower Te release than predicted by MELCOR.

As a summary, Table 2-2 lists the radioactive fractions of the fission product classes present in the RPV, and in the major containment regions both at the time of vessel breach and at the end of the calculation. Also listed are the radioactive fractions of each class still residing in the fuel. The fractions presented in the table are only for the radioactive portion of the classes; the fractional distribution of total mass for classes with large non-radioactive release during core-concrete attack is quite different than the radioactive fractions shown in Table 2-2.

After these calculations were performed, it was discovered that large errors in mass conservation of aerosols were possible under certain conditions because of MELCOR coding errors. However, for the Grand Gulf calculations, we found that these errors resulted in a maximum mass conservation error of about 5%. In addition, a misunderstanding of code input led to a radionuclide inventory which was about 7% lower than the desired value. These errors are not expected to have a significant effect on the Grand Gulf calculations. The source of error has been located and will be corrected in release 1.8.1.

2.2.5 Effect of Early Burn

To examine the effect of an early deflagration in the outer containment on the results of the integral station blackout calculation, the base calculation was restarted after a large quantity of hydrogen had been released to the containment, and the hydrogen was allowed to burn. The containment was assumed to survive the burn, but the drywell wall was assumed to be damaged (a .093 m^2 (1 ft^2) hole). This calculation was performed to determine the fraction of the flow that would bypass the suppression pool through such a hole and to investigate the effect of leakage through the hole on drywell flammability, outer containment conditions, and containment loads at vessel breach. The containment was assumed to remain intact to give a bounding case for the amount of hydrogen that could enter the drywell for such scenarios. If the containment had been assumed to fail, much of the hydrogen would have been released to the environment. The results regarding drywell

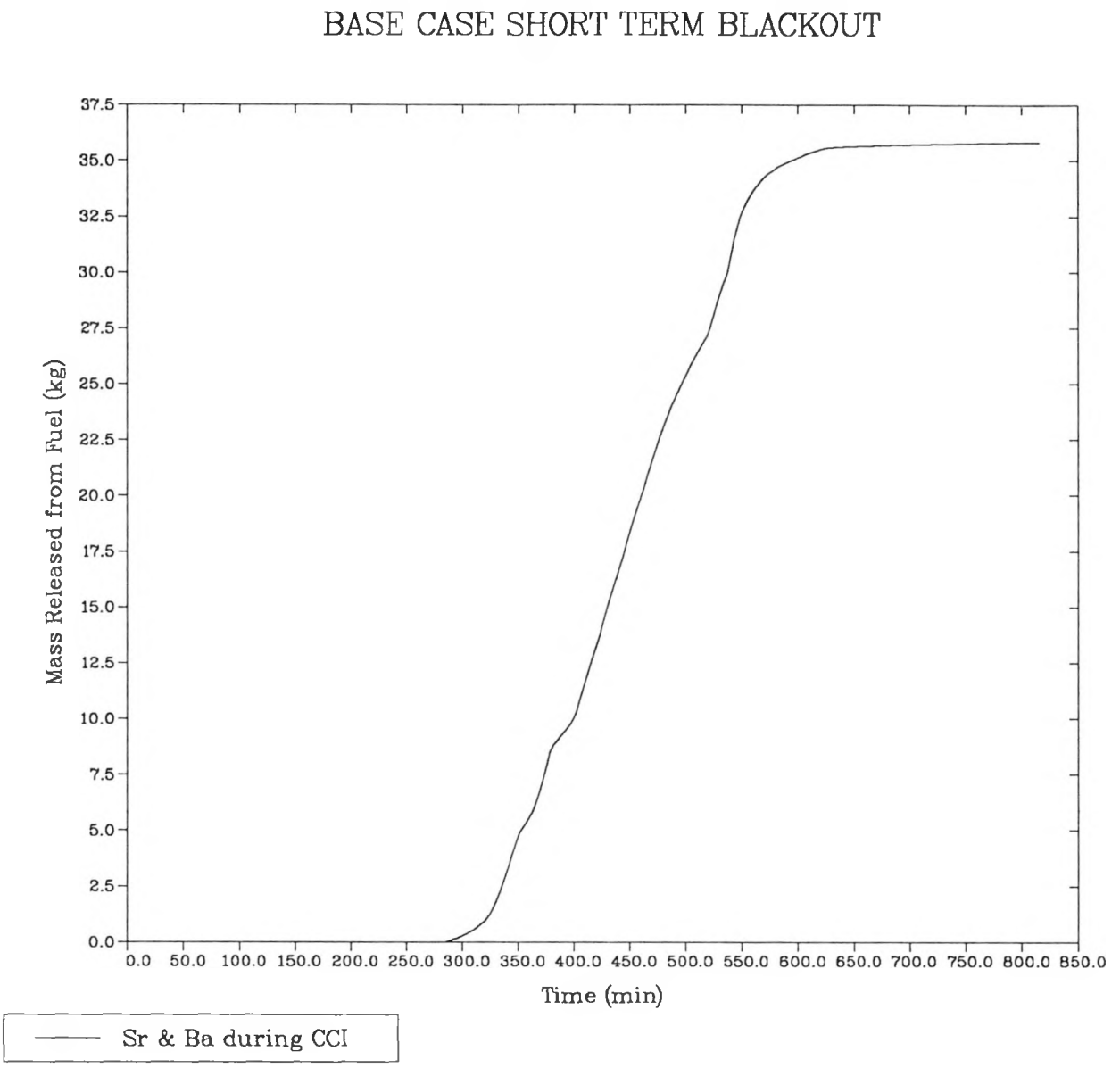

Figure 2-14. Base Case Sr and Ba Release during Core-Concrete Attack

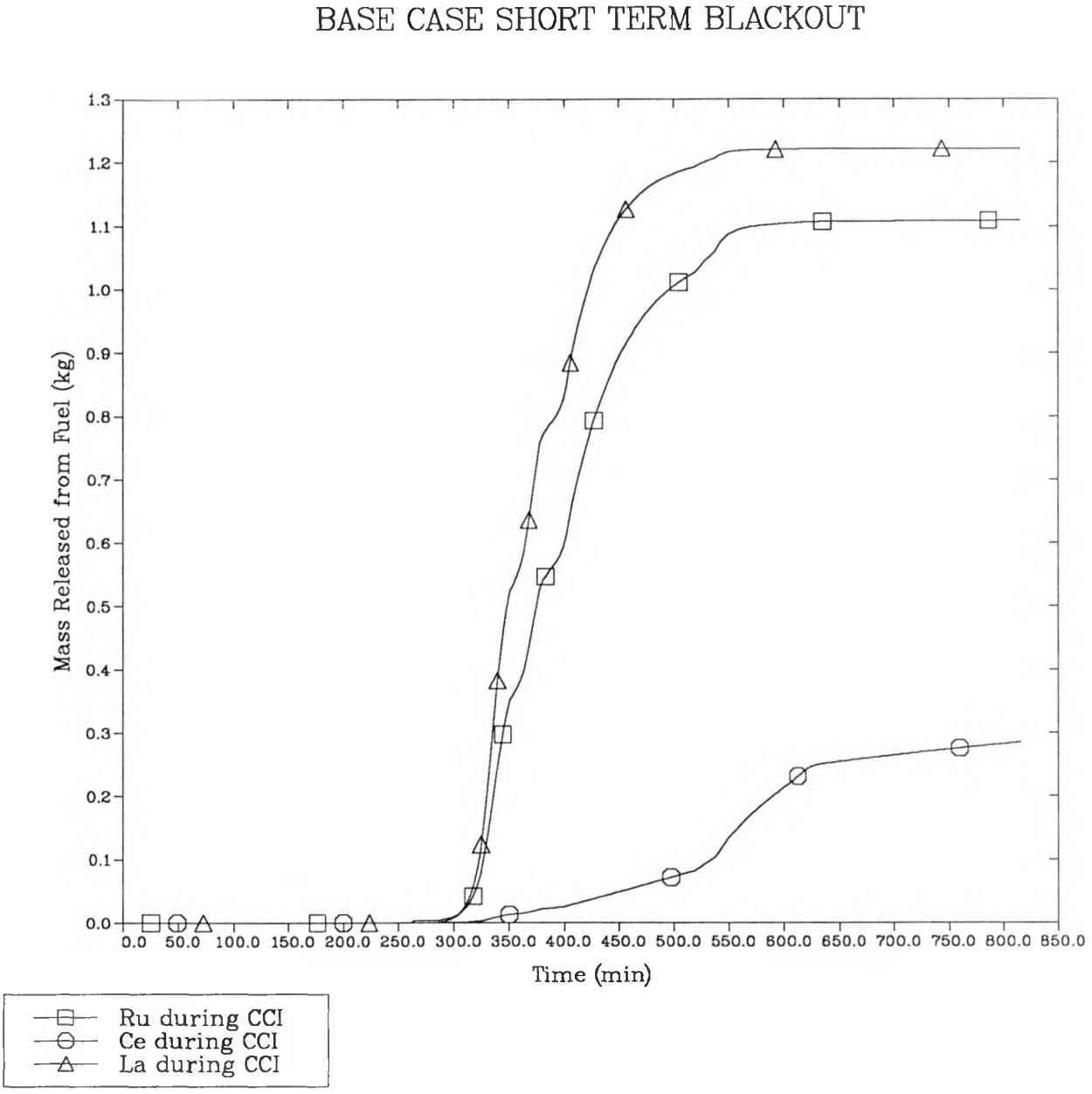

Figure 2-15. Base Case Ru, Ce and La Release during Core-Concrete Attack

Table 2-2

Fractional Distribution of Radioactive Fission Products

At Vessel Breach

Class	Fuel in Core	Fuel in Cavity	RPV	Pedestal Water Pool	Drywell	Suppress Pool	Outer Cont.
Xe	.0154	0.	.0044	0.	.0224	0.	.9580
Cs	.0166	0.	.8590	.0153	.0004	.0741	.0339
Ba	.8590	0.	.1290	.0013	0.	.0105	0.
Te	.0217	0.	.9150	.0171	.0002	.0245	.0213
Ru	1.	0.	0.	0.	0.	0.	0.
Mo	1.	0.	0.	0.	0.	0.	0.
Ce	1.	0.	0.	0.	0.	0.	0.
La	1.	0.	0.	0.	0.	0.	0.
U	.9980	0.	.0018	0.	0.	.0002	0.
Cd	1.	0.	0.	0.	0.	0.	0.
Sn	.4910	0.	.4740	.0040	0.	.0310	0.
CsI	0.	0.	.8640	.0149	.0006	.0616	.0584

At End of Calculation

Class	Fuel in Core	Fuel in Cavity	RPV	Pedestal Water Pool	Drywell	Suppress Pool	Outer Cont.
Xe	0.	0.	0.	0.	0.	0.	1.
Cs	0.	0.	.8140	.0166	.0115	.1300	.0280
Ba	0.	.6860	.1300	.1612	.0008	.0219	.0004
Te	0.	.0023	.7460	.0273	.0234	.1772	.0238
Ru	0.	1.	0.	0.	0.	0.	0.
Mo	0.	.9900	0.	.0094	.0001	.0006	0.
Ce	0.	1.	0.	0.	0.	0.	0.
La	0.	.9980	0.	.0021	0.	.0001	0.
U	0.	.9980	.0018	0.	0.	.0002	0.
Cd	0.	1.	0.	0.	0.	0.	0.
Sn	0.	.4810	.4750	.0046	.0021	.0366	.0007
CsI	0.	0.	.5070	.0299	.1001	.3074	.0556

flammability will be discussed in Section 2.3, and the results for the other issues will be discussed in this section.

The amount of flow that bypassed the suppression pool for this case is shown in Figure 2-16. During most of the calculation, all of the flow bypassed the suppression pool, because there was not sufficient drywell pressurization to depress the suppression pool level below the top row of vents. However, the vessel blowdown loads were sufficiently large to force about 70% of the flow through the suppression pool for about a 3 minute period following vessel breach.

The pressure in the outer containment is compared to the base case pressure in Figure 2-17. The peak pressure during the burn was very high (above the predicted failure threshold) because of the large amount of hydrogen burned. As seen in Figure 2-17, the additional leakage through the drywell wall for the case with a containment burn did not significantly affect the size of the pressure rise at vessel breach. The pressure rise was about the same as for the base case because of two factors. First, the containment had fewer moles after the burn, since one mole of hydrogen and 1/2 mole of oxygen combine to give only one mole of steam. Second, more noncondensibles had been pushed from the drywell to the outer containment during the burn cooldown, so the pressurization from addition of drywell gases to outer containment gases at vessel breach was lower than in the base calculation.

2.3 Drywell Flammability

An important issue in Grand Gulf is hydrogen burning within various containment regions because the burning can cause the drywell wall to fail, leading to a bypass of the suppression pool. In addition, the hydrogen content in the drywell at vessel breach can greatly affect the pressurization for scenarios with direct containment heating (Ref. 7). The results of the integral station blackout calculations (discussed in Section 2.2) were combined with additional containment-only calculations to examine the potential for forming flammable mixtures in the drywell during a station blackout. The effects of drywell leakage area and burning in the outer containment on the amount of hydrogen in the drywell before vessel breach were examined.

2.3.1 Results of Integral Calculations

The results of the integral MELCOR station blackout calculations support previous conclusions from undocumented calculations that were performed with the HECTR code (Ref. 8) which indicate that the amount of hydrogen flowing from the outer containment to the drywell was small enough to yield at most a marginally flammable mixture (4% hydrogen) before vessel breach. At vessel breach, the oxygen was predicted to be swept from the drywell, leaving an inert steam/hydrogen mixture. Gas generation during core-concrete attack kept the drywell pressurized, preventing the oxygen from reentering the drywell. Thus the drywell was never more than marginally flammable in either the MELCOR or HECTR calculations. The drywell concentrations calculated by MELCOR are shown in Figure 2-18.

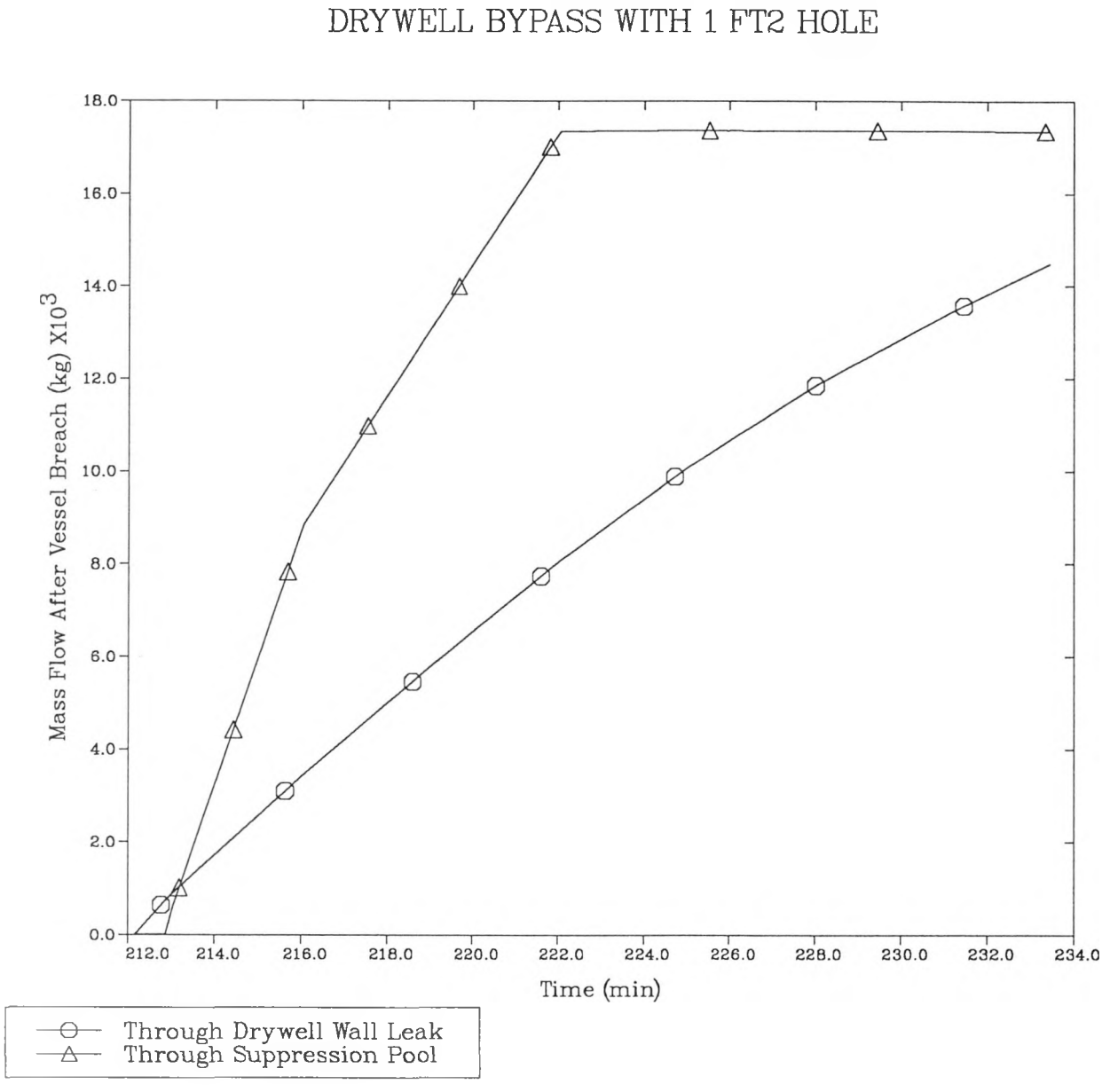

Figure 2-16. Flow Split through Drywell Wall Leakage and Suppression Pool with Large Drywell Hole

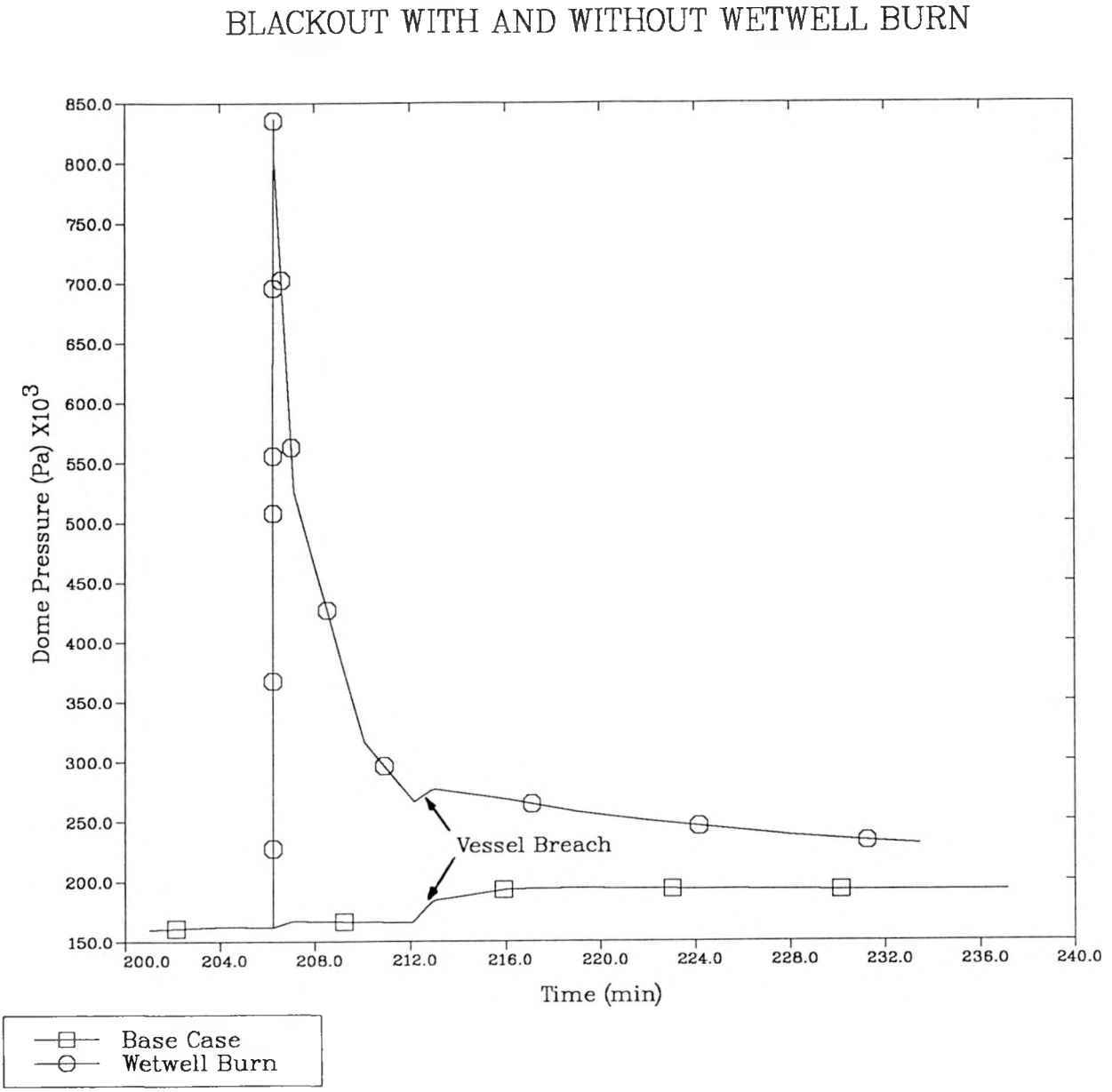

Figure 2-17. Effect of Burn on Containment Pressure during Station Blackout

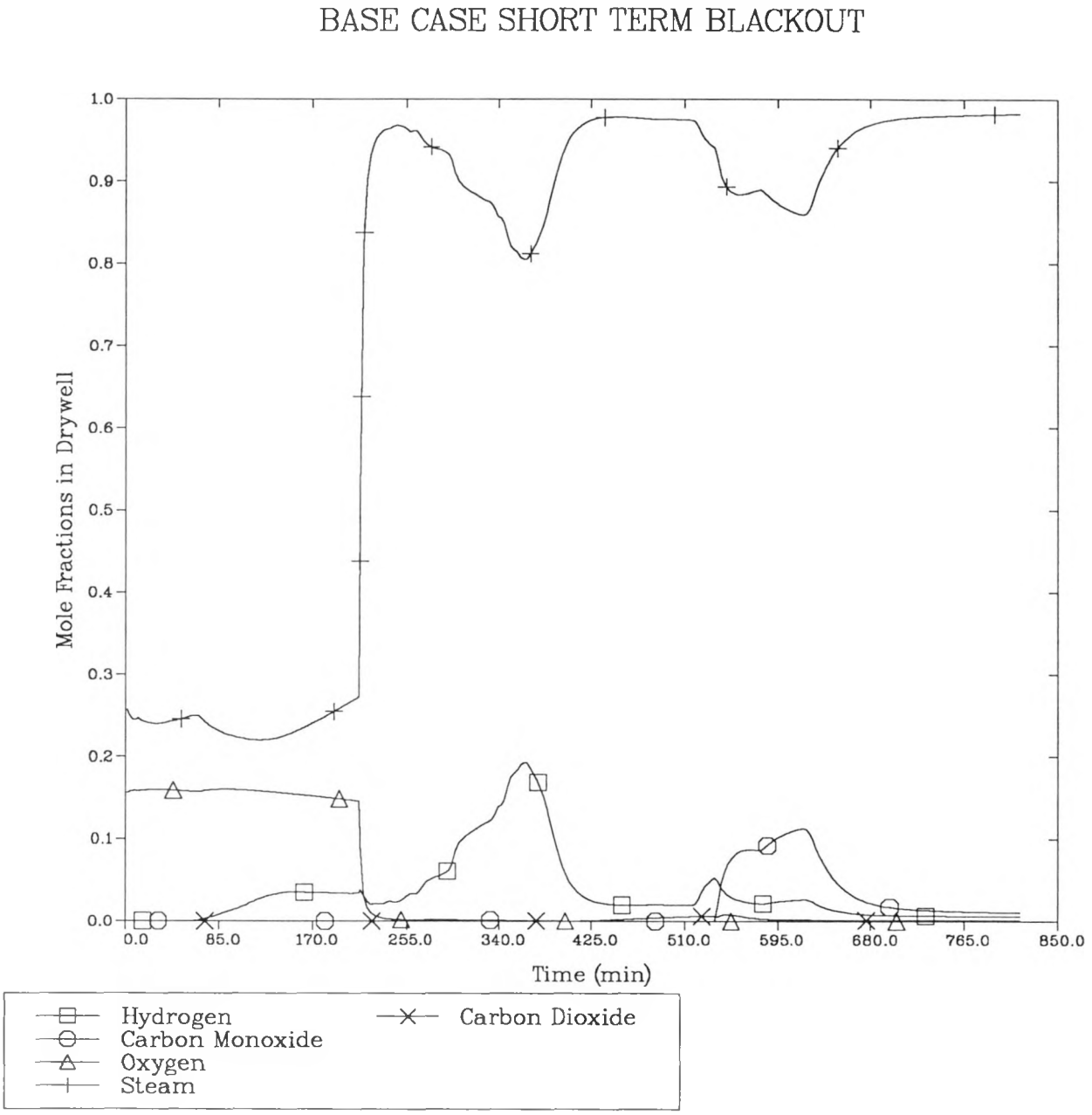

Figure 2-18. Base Case Drywell Mole Fractions

The second integral MELCOR calculation (with burns allowed in the outer containment) also showed inflammable conditions in the drywell before vessel breach. Neither the larger hole created by the burn nor the larger flows from containment to drywell during the burns caused a flammable mixture to form. The drywell concentrations for this second case are shown in Figure 2-19.

2.3.2 Results of Containment-Only Calculations

The containment-only deck described in Appendix A was used to perform additional studies of drywell flammability. The model was driven by RPV steam and hydrogen releases from the integral MELCOR calculation discussed in Section 2.2. The containment deck was modified for these calculations to include concrete degassing in the drywell as well as heat sources that modeled RPV heat losses and fission product heating of the drywell and outer containment atmosphere.

A base case was run to insure the containment-only deck would give equivalent results to the integral calculation. Two cases were run to examine the effect of containment burning and drywell wall leakage on the drywell conditions. In the first case, burns were allowed in the containment based on an ignition limit of 10% hydrogen and assuming the burns created a large (.093 m^2 (1 ft^2)) breach of the drywell. The second case was similar, but only a single burn was allowed. These two variations on ignition timing were examined because the igniters do not operate in station blackouts, so a reliable ignition source is not available, and ignition is thus random. As expected, the case with multiple burns had more depletion of the oxygen in the drywell and containment and a lower containment pressure at vessel breach because of condensation of the steam produced during the burns. The case with only a single burn had drywell conditions similar to those in the base case, where there were no burns and nominal drywell wall leakage. In both cases, the large drywell wall leakage did not allow enough hydrogen to enter the drywell to exceed marginally flammable limits. The drywell hydrogen concentrations for these calculations are shown in Figure 2-20.

2.4 Drywell Flooding

Water on the drywell floor creates the conditions for ex-vessel steam explosions, the potential for debris coolability, and the potential for scrubbing gas and aerosol releases to containment during core-concrete attack. Water can be present on the drywell floor if the outer containment pressure exceeds the drywell pressure by a large enough margin to push the water in the suppression pool over the weir wall and onto the drywell floor. In fact, this backflow would begin well before the suppression pool level was pushed down below the top row of vents. Previous unpublished analyses and Reference 3 have shown that relatively small deflagrations in the outer containment would sufficiently pressurize the outer containment to cause such a backflow. The potential

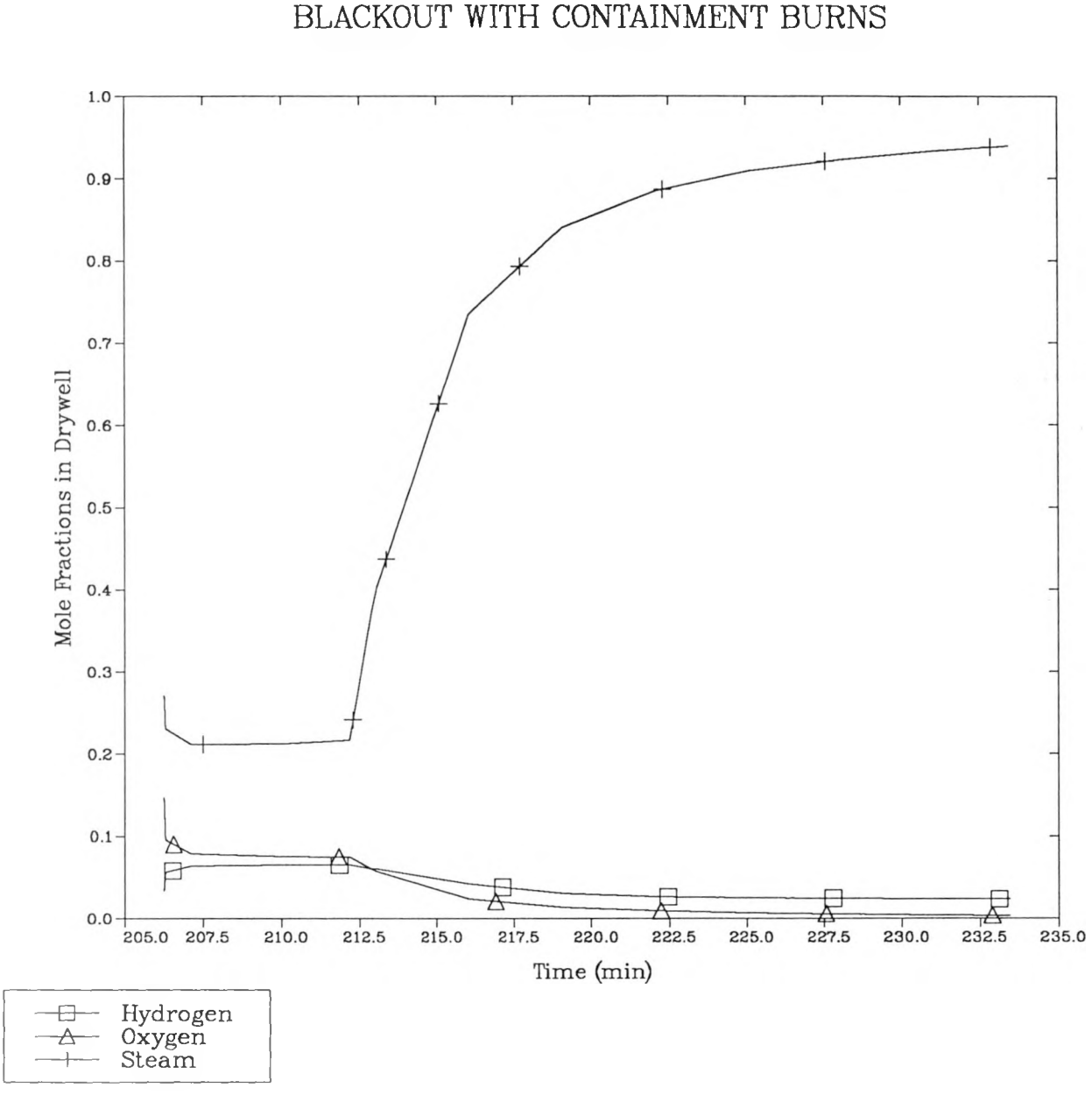

Figure 2-19. Drywell Mole Fractions for Station Blackout with Containment Burns

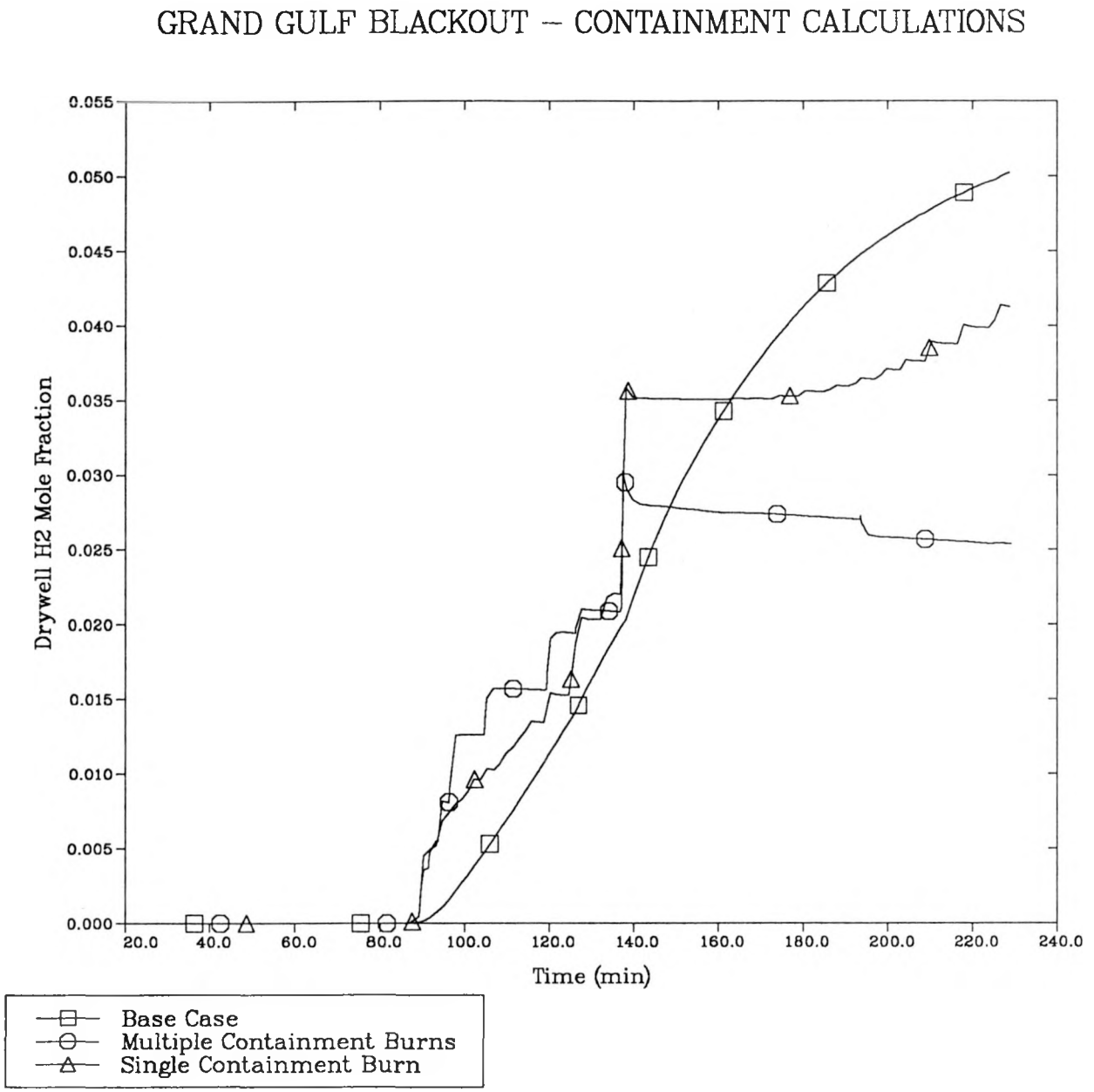

Figure 2-20. Drywell Hydrogen Mole Fractions for Various Containment Burn Assumptions

also exists for drywell flooding early in station blackout scenarios, even without burning. Calculations performed to examine this potential are discussed in this section.

During a station blackout scenario, the vacuum breakers in the drywell wall would be closed at Grand Gulf, so pressurization of the outer containment (relative to the drywell) could only be relieved through drywell wall leakage or flow through the suppression pool vents. The suppression pool water would be pushed over the weir wall before the suppression pool level on the wetwell side fell below the vents, so the outer containment pressurization would have to be relieved through drywell wall leakage to prevent suppression pool backflow. Before vessel breach, the drywell and outer containment would each be pressurized, but at different rates and by different phenomena. The drywell would be pressurized by concrete degassing and vessel heat losses; the outer containment would be pressurized by hydrogen addition and pool evaporation. The potential for drywell flooding during this time was examined using the integral MELCOR station blackout calculation and additional containment-only calculations. The containment-only calculations were driven by steam and hydrogen releases to the suppression pool that had been predicted by STCP (Ref. 4).

2.4.1 Results of Integral Calculations

The integral MELCOR calculations showed that the potential for drywell flooding is very sensitive to competing phenomena. The suppression pool was always pushed to near the top of the weir wall, but in some cases, concrete degassing in the drywell would increase sufficiently to prevent water from spilling into the drywell. Figures 2-21 and 2-22 show the suppression pool level and the mass of water on the drywell floor for the station blackout calculation described in Section 2.2 and for a preliminary calculation, in which somewhat less hydrogen generation had been predicted. The differences in timing and rate of hydrogen release relative to the onset of significant concrete degassing determined whether or not overflow occurred.

2.4.2 Results of Analyses Using STCP Releases

Two cases that had previously been analyzed in the NUREG-1150 study using the HECTR code (Ref. 8) to examine the potential for drywell flooding were re-examined using MELCOR because a coding error in HECTR that was discovered after that analysis was completed made the previous conclusions questionable. MELCOR calculations were performed using the containment-only deck described in Appendix A and were driven by hydrogen and steam sources predicted by STCP for the TQUV sequence reported in Reference 4. The first case used a .00642 m^2 leak area between the drywell and outer containment, and the second case used a reduced area of .0013 m^2 as well as a reduced hydrogen injection rate. The leakage area had been varied in the HECTR calculations to bound the potential leakage range. Currently, the best estimate of leakage area is .001579 m^2.

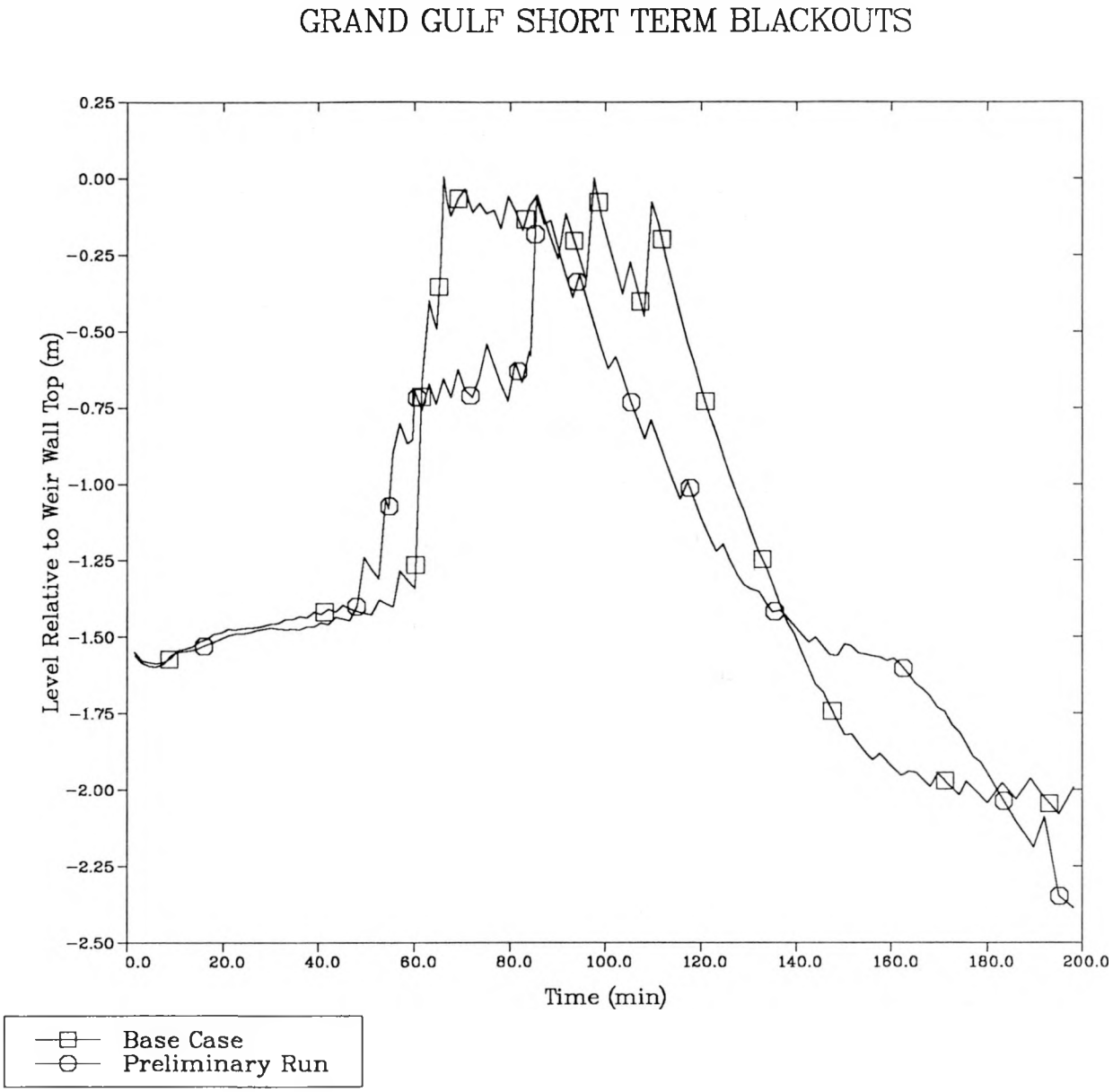

Figure 2-21. Suppression Pool Water Level

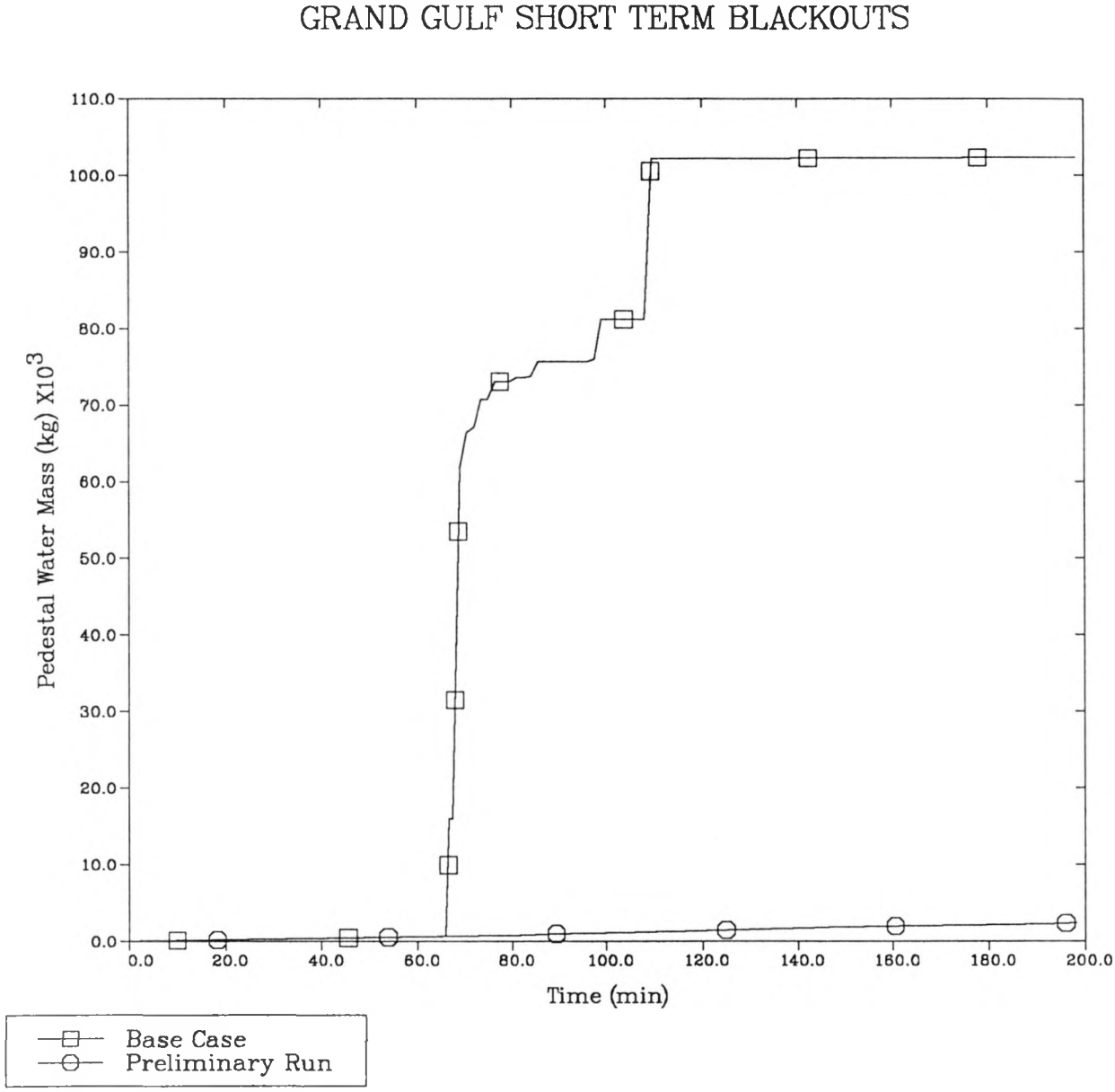

Figure 2-22. Pedestal Water Mass

MELCOR predicted that water would flow from the suppression pool onto the drywell floor for both cases, but that only a small amount would be pushed over for the first case. In both cases, the water was only pushed over during the peak hydrogen release, and the amount of water pushed over the weir wall was found to be very sensitive to modeling assumptions. This sensitivity is consistent with the previous conclusions from the HECTR calculations. The water masses on the drywell floor for the two MELCOR calculations are shown in Figure 2-23.

2.5 Containment Loads from Burns and Subsequent Cooldown

Calculations of containment loads from outer containment hydrogen burns were performed to address the possible loadings during a station blackout. Since ignition is not predictable in a station blackout, a wide range of conditions was examined to estimate the possible loads. The hydrogen concentration was varied from 5% (near the lower flammability limit) to 12% (near detonability and high enough that containment failure pressure is exceeded). The steam concentration was varied from 50% relative humidity (relatively dry) to 55% on a molar basis (steam inerting limit). The flame speed and completeness were varied over the ranges observed in experiments at VGES (Ref. 9), FITS (Ref. 10), and NTS (Ref. 11).

Experiments at the Quarter Scale Test Facility (Ref. 12) indicated that good mixing of hydrogen will occur in the outer containment region. Therefore, the 5 volumes used to model the outer containment in the MELCOR containment-only deck were collapsed into a single volume, and no attempt was made to estimate the effect of stratified mixtures. The drywell and suppression pool were retained in the model to account for their pressure suppression capability. Leakage between the drywell and containment was included, but the vacuum breakers were assumed to be closed because the scenario was station blackout where power is unavailable to operate the vacuum breakers. All of the containment heat sinks from the containment-only deck were included in the model. Both containment sprays and upper pool dump were assumed unavailable because of the station blackout.

Table 2-3 summarizes the cases run and the resulting loads. The results are also presented graphically in Figures 2-24 and 2-25. The results characterize the containment response during deflagrations.

A set of MELCOR calculations was also run to estimate the rate of containment depressurization during the cooldown from outer containment burns. These runs provided estimates for new baseline pressures after burn effects subside for the Grand Gulf accident progression event tree. Bounding calculations were performed with high hydrogen concentration (18% hydrogen and 18 m/s flame speed) and low hydrogen concentration (6% hydrogen, 60% complete burn, 5 m/s flame speed). Two sets of calculations were done, one set without radiative heat transfer modeled,

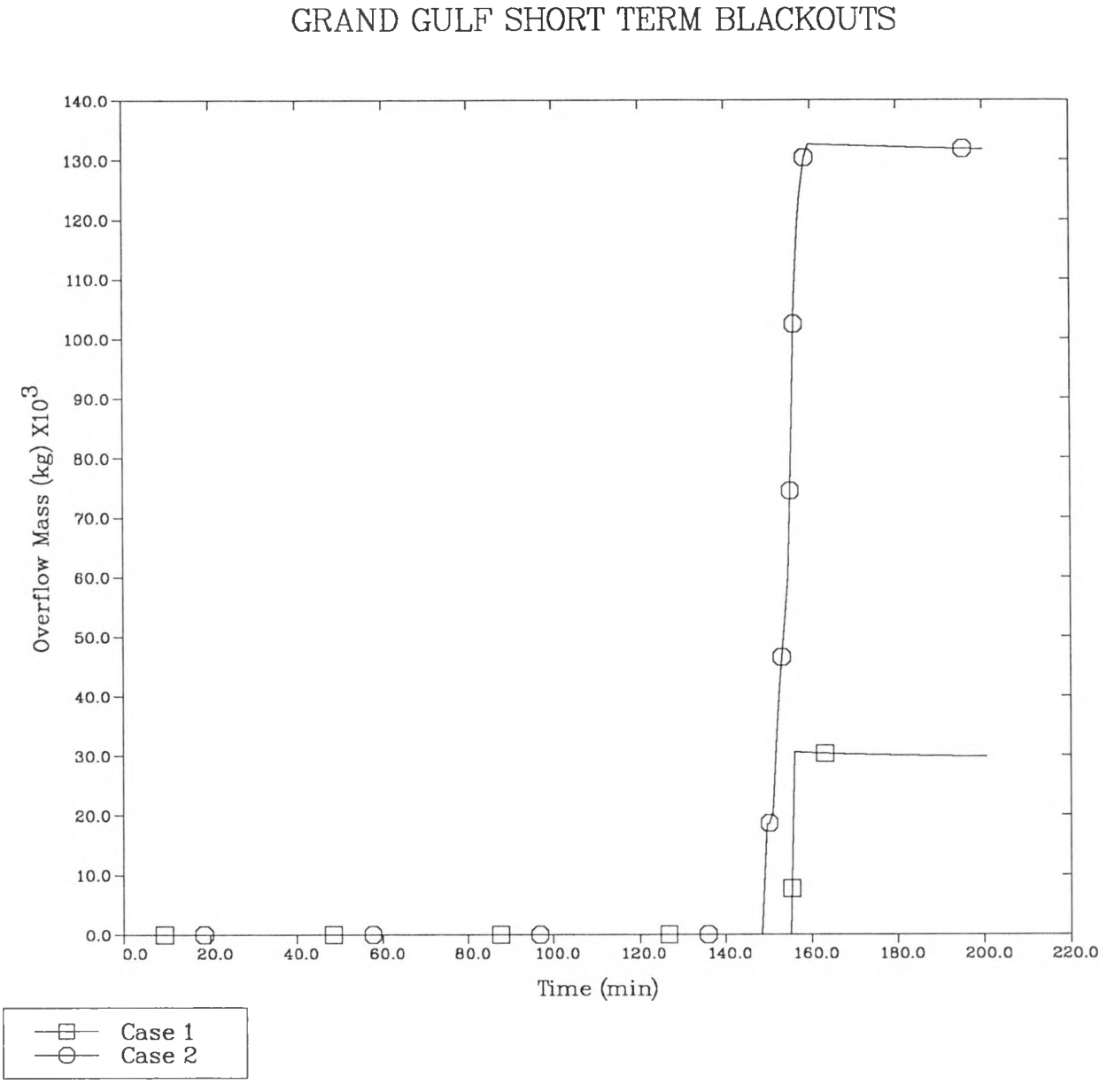

Figure 2-23. Mass of Water Overflowing Onto Drywell Floor

Table 2-3

Grand Gulf Outer Containment Burns

Initial Conditions						Maximum after Burn			
P kPa	T K	XH2	XH2O	Flame* Speed m/s	% Com-plete	WW P kPa	WW T K	WW/DW DP kPa	Pmax/ Pinit
Low Steam Cases:									
101	300	0.05	50% RH	0.5	30	148	451	31	1.46
				1.5	40	166	514	44	1.64
				6.5	40	171	521	61	1.69
		0.06		0.5	30	157	481	35	1.55
				1.5	70	213	720	63	2.10
				7.5	70	240	748	122	2.37
		0.08		1.0	100	270	1033	70	2.66
				3.5	100	286	1074	143	2.82
				9.0	100	343	1120	220	3.39
		0.10		1.0	100	293	1190	80	2.89
				4.0	100	319	1253	175	3.15
				10.0	100	393	1308	269	3.88
		0.12		2.0	100	334	1403	129	3.30
				4.5	100	353	1433	230	3.48
				11.0	100	439	1490	317	4.33
High Steam Cases:									
187	373.6	0.05	0.55	0.5	30	246	515	32	1.32
				1.5	40	269	565	44	1.44
				6.5	40	276	568	68	1.48
190	374.1	0.08		1.0	100	392	1041	71	2.06
				3.5	100	415	1060	159	2.18
				9.0	100	501	1090	269	2.63
192	374.4	0.10		1.0	100	420	1183	81	2.18
				4.0	100	458	1214	196	2.38
				10.0	100	574	1248	340	2.98
194	374.7	0.12		2.0	100	473	1352	143	2.43
				4.5	100	501	1367	243	2.58
				11.0	100	637	1406	401	3.28

* Burn duration = Burn length / Flame speed. A 25 m burn length was used in all of these calculations

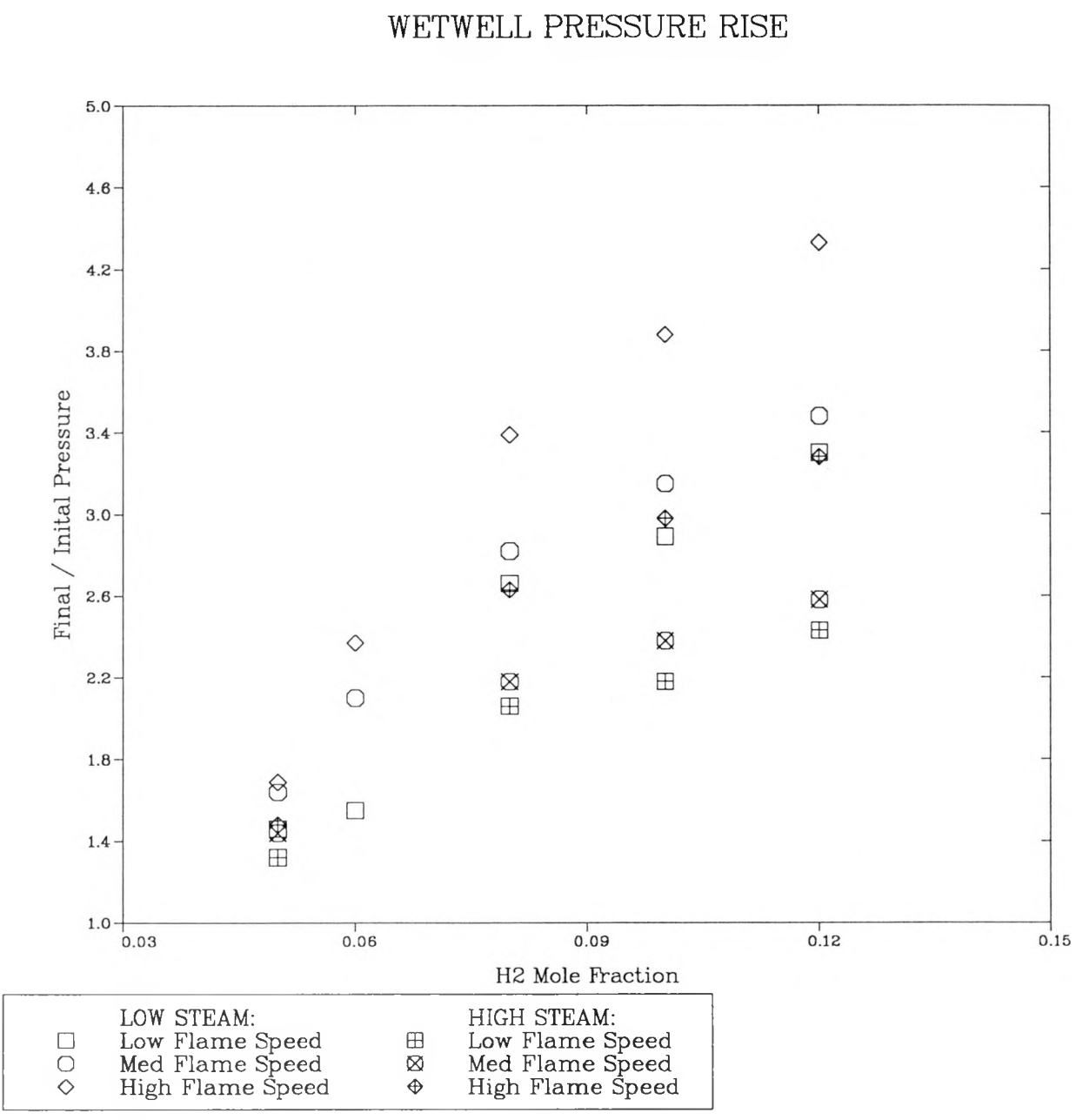

Figure 2-24. Wetwell Pressure Rise vs. Hydrogen Mole Fraction

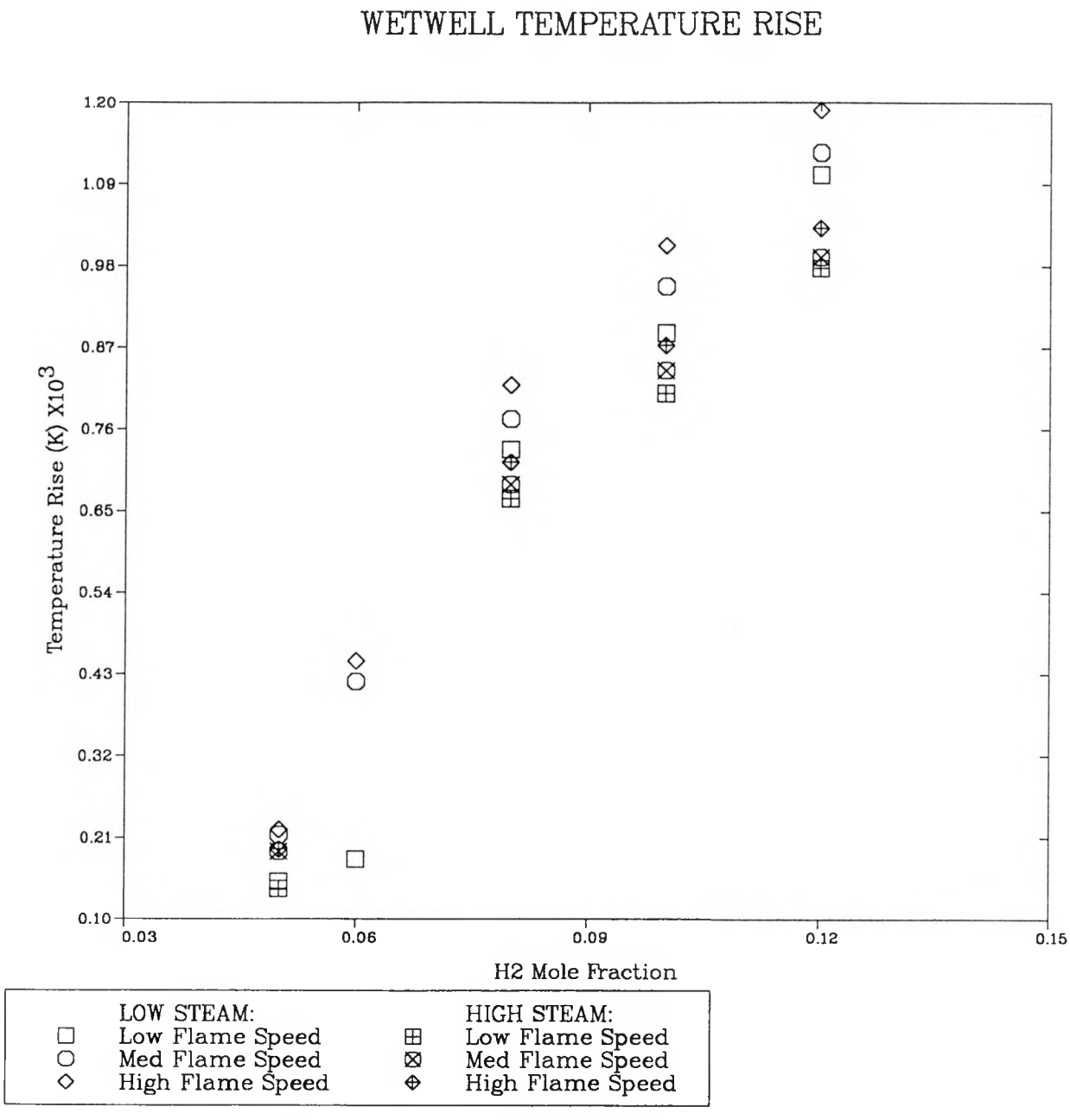

Figure 2-25. Wetwell Temperature Rise vs. Hydrogen Mole Fraction

and the other set with radiative heat transfer. The containment pressures during the tail of the burn for the 4 calculations are plotted in Figure 2-26.

2.6 Steam De-Inerting Following Spray Recovery

Following power recovery late in a station blackout sequence, the containment may contain a rich hydrogen mixture that avoided burning because of a high steam concentration. If containment sprays are initiated following power recovery, the steam might condense, leaving a flammable mixture with high hydrogen and carbon monoxide content. Alternatively, it is possible that the containment would remain at high steam concentration even if sprays are activated because of steaming from the hot suppression pool. To provide insight into this issue, MELCOR calculations were performed.

The MELCOR containment-only deck described in Appendix A was used for this analysis. The containment atmosphere was assumed to be at saturation corresponding to 55% steam mole fraction, giving an initial pressure of about 273 kPa and temperature of 383 K. The suppression pool was assumed to be in equilibrium with the atmosphere such that its temperature was also 383 K; thus, it was subcooled. A single train of sprays was assumed to draw from the suppression pool and pass through the heat exchangers. The temperature drop in the heat exchangers was estimated using rated conditions from the Grand Gulf FSAR and assuming the service water temperature was 305 K (90 F). This gave a spray injection temperature of 344 K (160 F). These assumptions give a lower bound on the amount of steam condensation from the atmosphere.

Figure 2-27 shows the calculated steam concentrations in the wetwell and dome control volumes. Although there is stratification predicted, the steam concentrations drop nearly 10% in all of the control volumes in about 10 minutes. This supports the contention that spray injection will act to de-inert the containment.

The results are affected by the rate of evaporation of suppression pool water. Therefore, a sensitivity calculation was run with the evaporation rate multiplied by 10. The results, shown in Figure 2-28, still indicate relatively rapid steam condensation.

To confirm the findings, the base case was again examined, this time using the HECTR code. The pool evaporation model in HECTR is somewhat different from MELCOR's, but the steam concentrations predicted by the two codes are very similar, giving further support to MELCOR's prediction of de-inerting. The HECTR steam concentrations are shown in Figure 2-29.

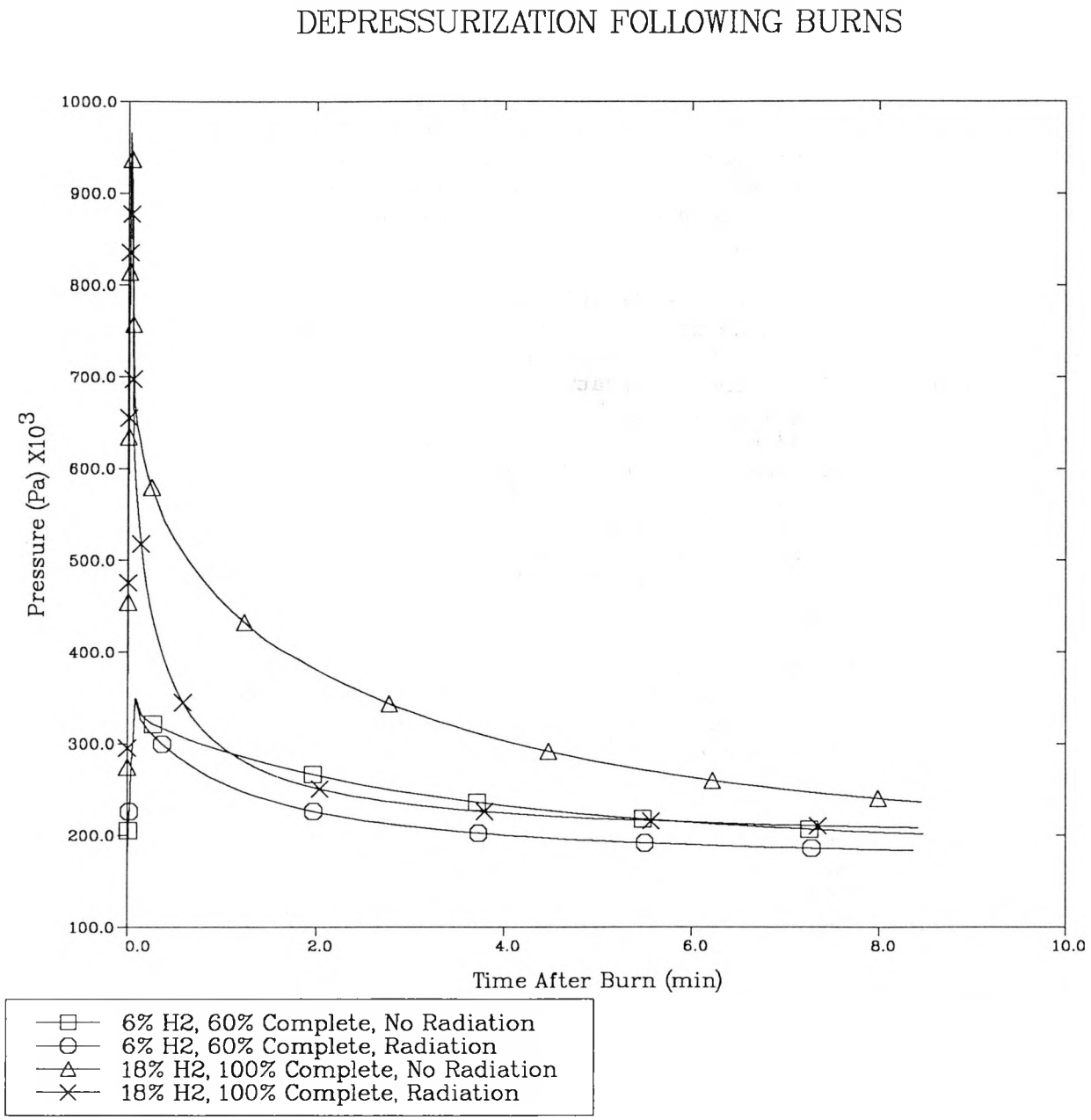

Figure 2-26. Containment Depressurization Following Burns

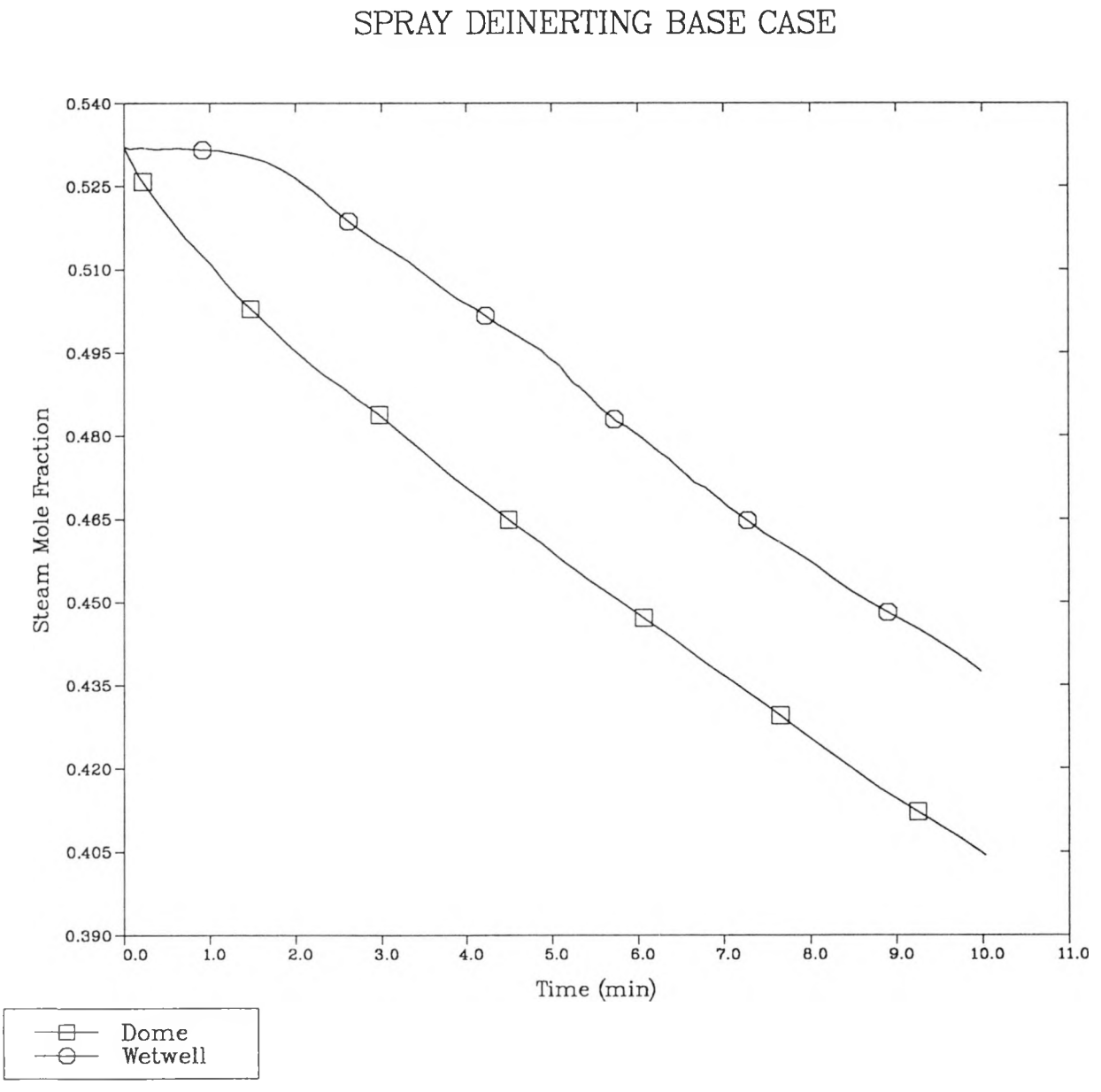

Figure 2-27. Containment Steam Mole Fractions During Spray Injection

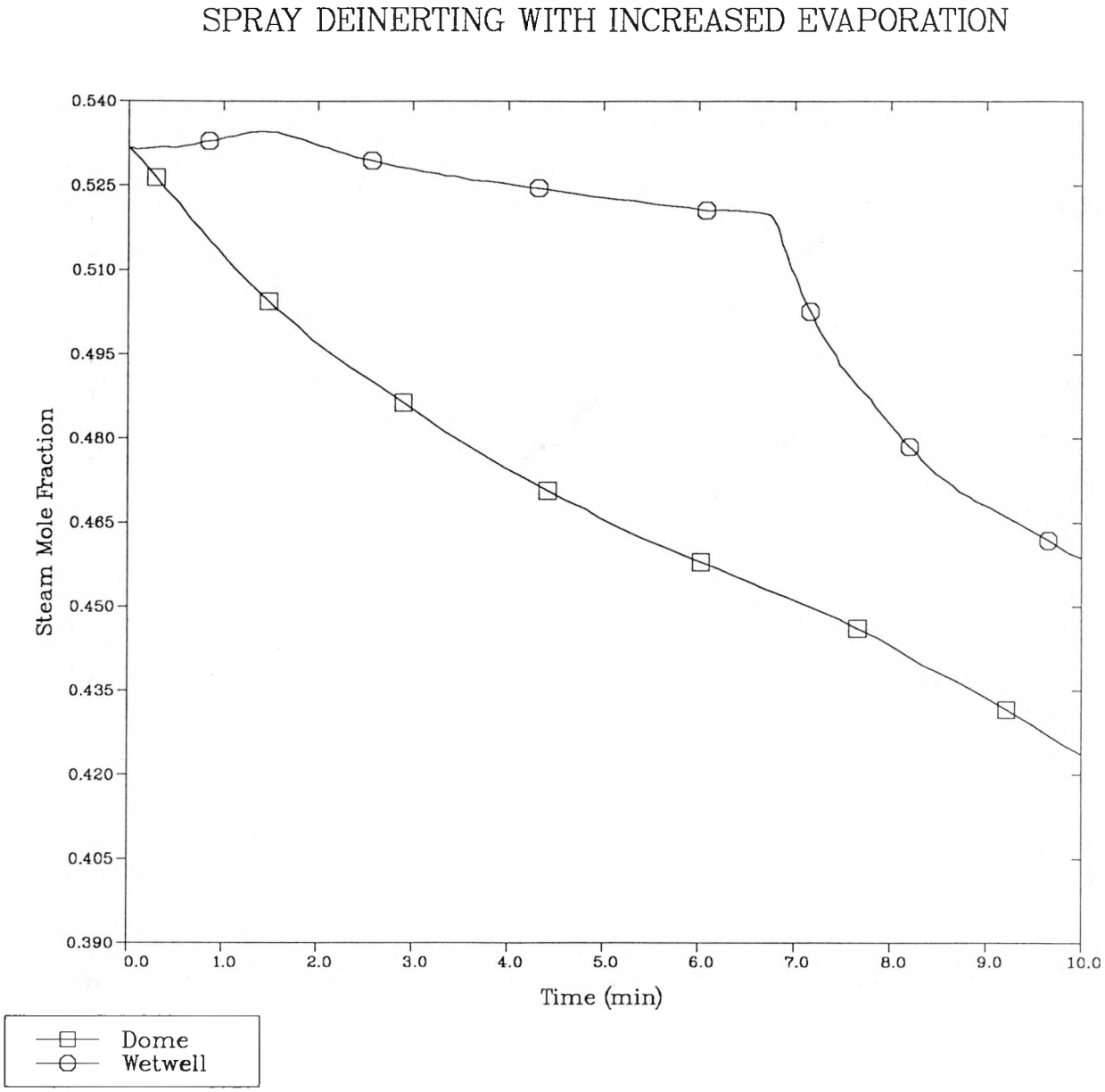

Figure 2-28. Containment Steam Mole Fractions During Spray Injection with Increased Evaporation Rate

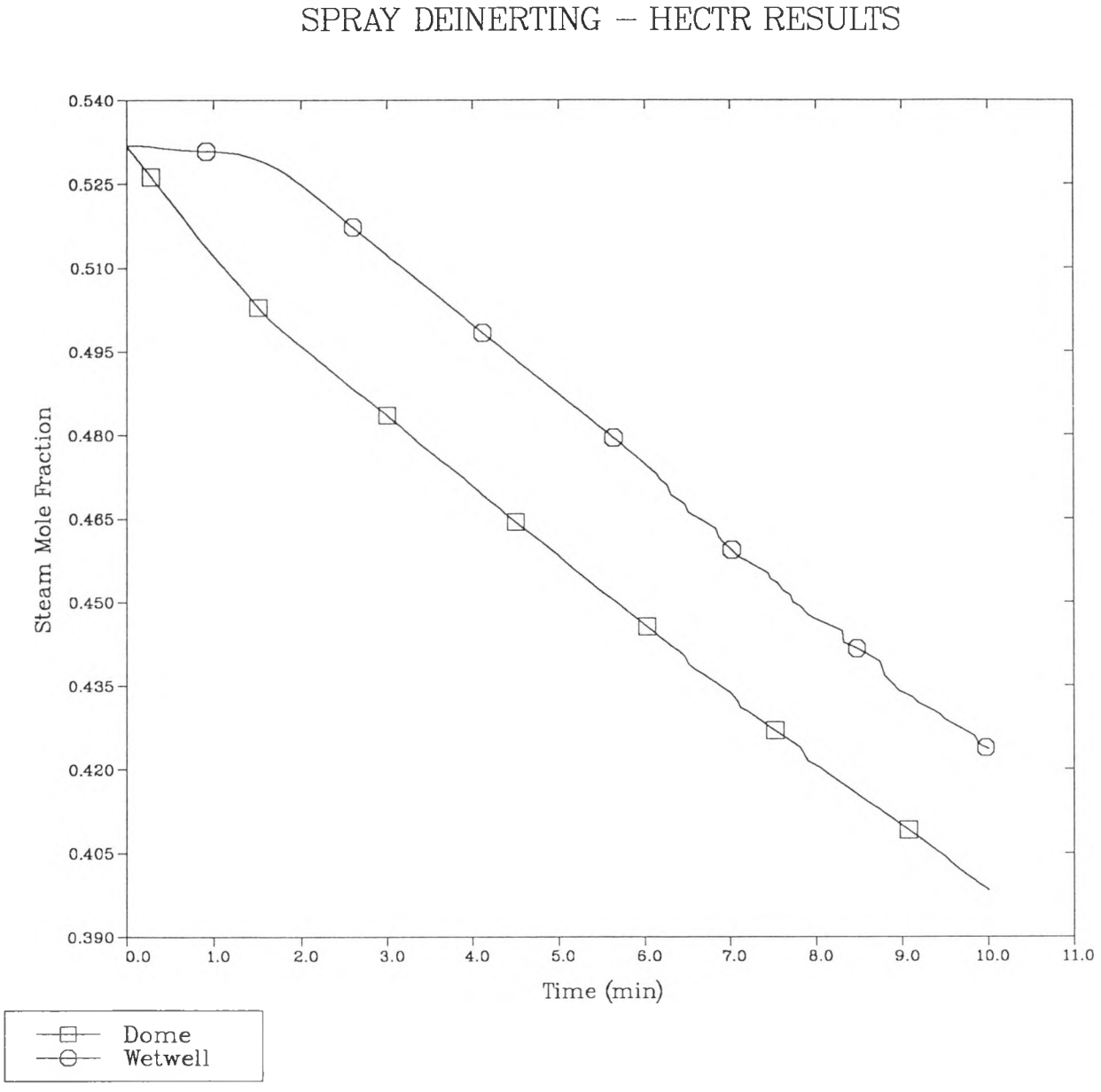

Figure 2-29. HECTR Containment Steam Mole Fractions During Spray Injection

2.7 Stuck-Open Tailpipe Vacuum Breaker

A flammable mixture might form in the drywell if an SRV tailpipe vacuum breaker were to stick open during a transient. The tailpipe vacuum breakers open to relieve the vacuum created by condensation of steam in the tailpipe after the SRVs cycle. If a vacuum breaker sticks open during this process, some of the hydrogen being vented from the vessel will be discharged directly into the drywell. This can then create the potential for high drywell hydrogen concentrations.

To determine the conditions in the drywell with a stuck-open tailpipe vacuum breaker, MELCOR calculations were performed using the containment-only deck and the RPV steam and hydrogen releases calculated for the TQUV sequence in Reference 4. The MELCOR calculations examined the drywell response when the vacuum breakers were assumed to stick open at three different times during the accident: 1) at the beginning of the transient, 2) when hydrogen release from the vessel began, and 3) near the peak hydrogen release rate. MELCOR indicated that the drywell would quickly become steam inerted for Cases 1 and 2. For Case 3, the drywell was predicted to be flammable for about 20 minutes before becoming steam inert.

A fourth calculation was run to examine the effect of burning during the time that the drywell atmosphere was flammable in Case 3. Since the hydrogen would be entering containment at a high temperature, it would likely burn continuously as a jet anchored to the vacuum breaker, rather than accumulating and then burning as a deflagration. To model jet burning, a case was run with the vacuum breaker assumed to stick open near the time that the hydrogen release rate peaked (same time as Case 3), and MELCOR input parameters were chosen such that the hydrogen was effectively allowed to burn continuously as it entered the drywell. The hydrogen began burning immediately after the vacuum breaker stuck open. However, the oxygen was depleted about 8 minutes later, and the burning ceased. The drywell pressure and temperature increases were both relatively low. The peak drywell gas temperature during this burning was only about 470 K. Although local temperatures near the flame would be much higher, there does not appear to be a global drywell threat to equipment from such burning. The peak outer containment pressure was actually less with drywell burning than without burning. This occurred because the greatest outer containment pressure rise for both cases was caused by hydrogen pressurization, so burning the hydrogen in the drywell and allowing the resultant steam to condense in the suppression pool yielded a lower pressure rise.

2.8 Containment Response and Release Rates Following Containment Failure

Mass and energy releases from containment following containment failure caused by a hydrogen burn were predicted. This information was needed to guide input for the Grand Gulf consequence calculations. The Grand Gulf

containment-only deck was used for this analysis, using steam and hydrogen sources calculated for the short term blackout discussed in Section 2.2. Calculations were performed for three break sizes: .0093, .093, and .65 m^2 (.1, 1, and 7 ft^2). For each calculation, the containment was assumed to fail during a burn that initiated when the dome reached 12% hydrogen. The results provide timing information for consequence calculations and information on peak differential pressures across the drywell wall during a containment burn.

The containment pressure for the 3 break sizes is shown in Figure 2-30. The integral energy release, relative to the energy at ambient conditions, is shown in Figure 2-31 and the peak differential pressure across the drywell is shown in Figure 2-32. The results predict a differential pressure that is below the failure value for all of the cases that were considered. However, higher drywell wall differential pressures would be calculated for burns with higher hydrogen content.

An unexpected result of the calculations was that outside air was drawn back into containment as the containment cooled down following the completion of the burns (even though hydrogen injection was continuing). This occurred for the small hole size as well as the larger sizes. The result could be affected by the modeling of burns. It is possible that the initial burn in containment would yield enough ignition sources that subsequent burns would occur more frequently and at a lower hydrogen concentration than the initial burn. This could result in a continuous outflow of gases instead of the periodic outflow/inflow calculated for the multiple deflagration cases. To examine this possibility, two additional calculations were performed. In these, a single large burn was modeled to fail the containment, then the hydrogen ignition limit was reset to a very low value to approximate "continuous burning." The pressurization from the continuous burning was not large enough to prevent the inflow for the large break size. For the small break size, continuous burning resulted in sustained outflow from the containment until the oxygen in containment was consumed. Thereafter, the containment cooled down and outside air was drawn back into containment.

This phenomenon probably does not pose any additional threat to containment. It mainly affects the amount of oxygen available for burning, and could delay containment inerting. It could also allow burning of additional hydrogen after the original oxygen content is depleted, but this would probably occur at a relatively slow rate as an "inverted diffusion flame". Since containment surfaces would be hot from previous burns, oxygen would probably not be able to accumulate to levels that would support detonations, because it would be burning as it entered containment.

During the consequence analyses performed for the NUREG-1150 study it was noted that the depressurization times predicted by MELCOR were significantly shorter than those predicted by STCP (Ref. 5) for a long-term station blackout for the same containment break size (2 vs 10 min).

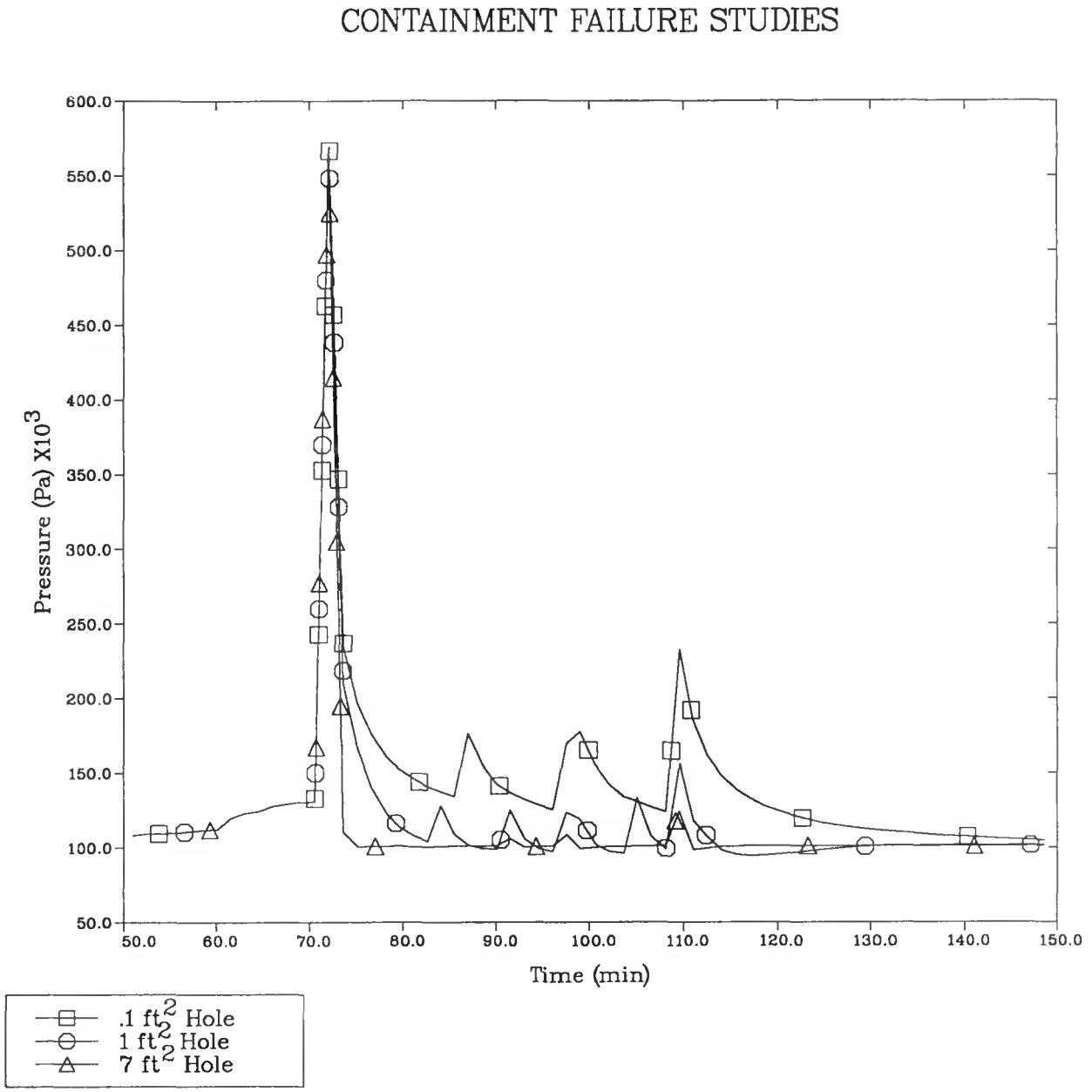

Figure 2-30. Containment Pressure vs. Failure Area

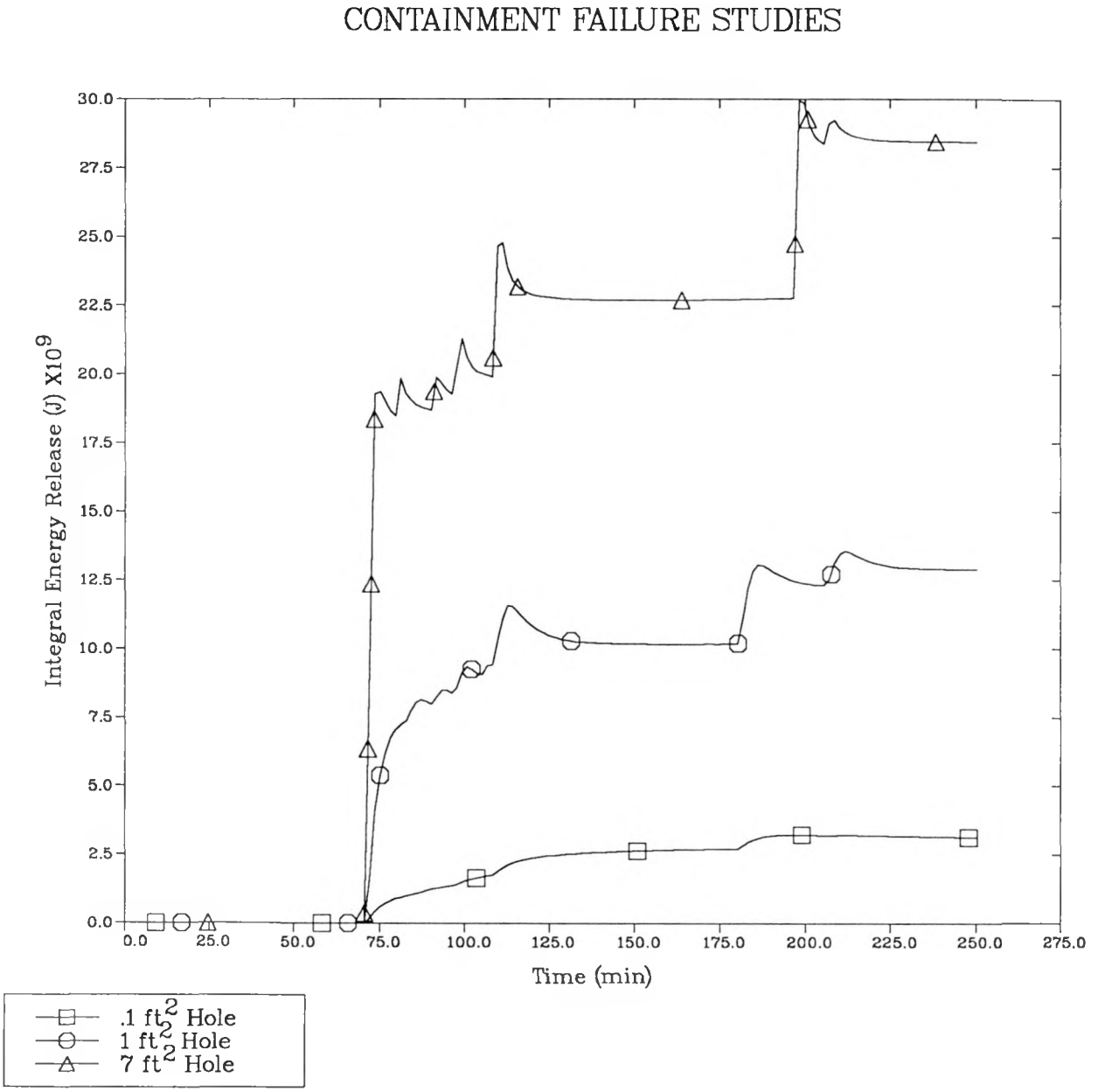

Figure 2-31. Energy Release vs. Containment Failure Area

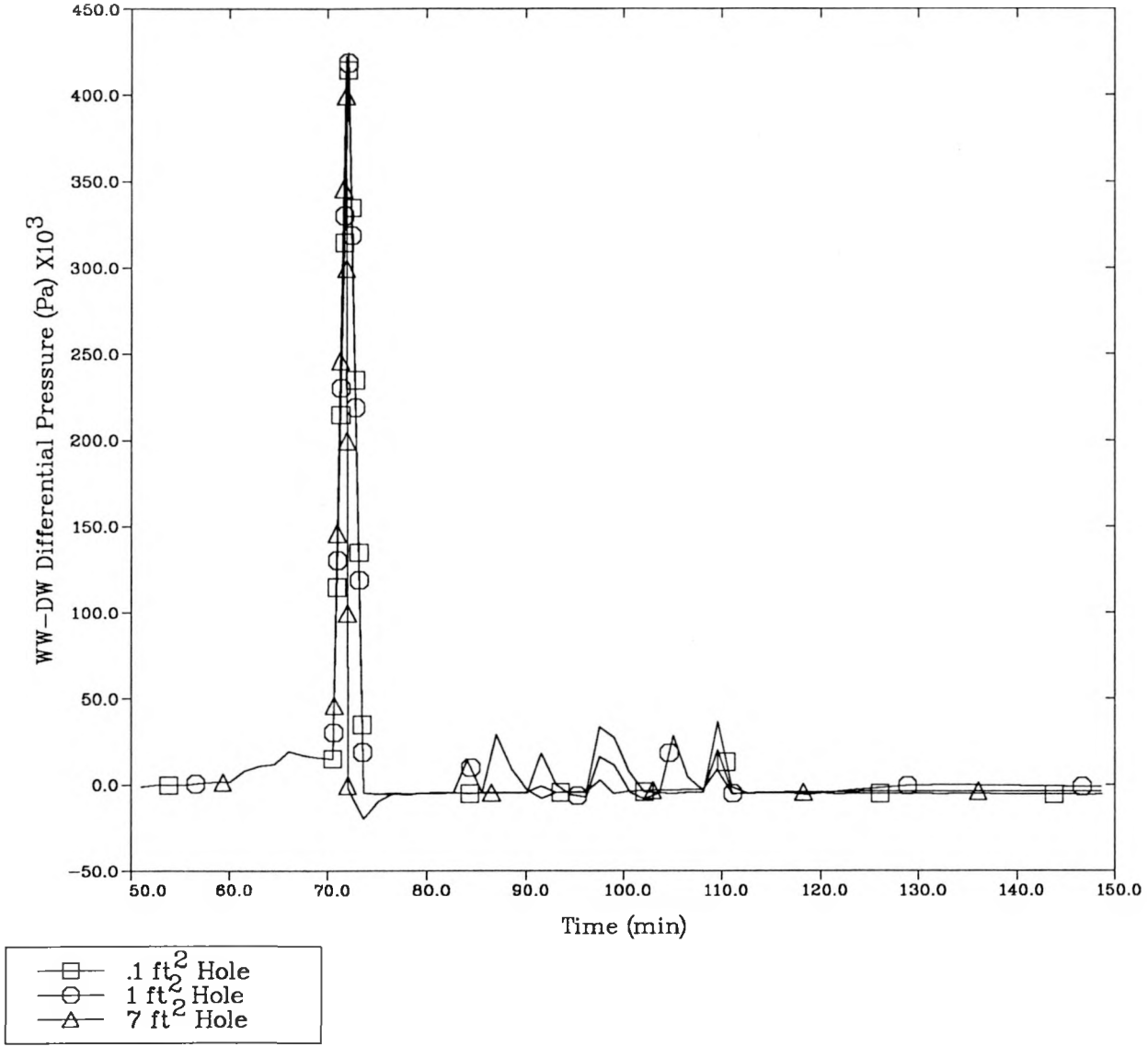

Figure 2-32. Drywell Wall Differential Pressure vs. Containment Failure Area

It was felt that this difference was caused by the different suppression pool conditions (subcooled vs saturated), and to confirm this, an additional MELCOR calculation was performed with a saturated pool. The containment took much longer to depressurize for this case as shown in Figure 2-33.

2.9 Pressure Relief During Burn in Failed Containment

In the Grand Gulf accident progression analysis for the NUREG-1150 work, it was assumed that containment failure during a burn would not significantly affect the pressure rise resulting from the burn. As a result, containment failure did not preclude drywell wall failure for burns occurring at high hydrogen concentrations. MELCOR calculations were performed to determine if this approximation was reasonable.

Five calculations were performed to estimate the pressure relief that would occur through a hole in containment during a hydrogen burn at 18% mole fraction. Calculations were performed both with and without containment failure modeled, so that the amount of pressure relief from flow through the containment hole could be determined. To determine the maximum effect of the containment hole, a large (.65 m^2 (7 ft^2)) hole was modeled, and it was opened at the beginning of the burn (rather than waiting until the pressure had reached failure levels). The effects of radiative heat transfer and burn duration on the results were also examined. Most of the calculations were of a relatively long burn duration for the particular hydrogen mole fraction being examined.

The cases examined and results of each are summarized in Table 2-4. The containment pressurization was not significantly affected by the .65 m^2 (7 ft^2) hole for the large burns examined. In fact, including radiative heat transfer effects had a larger impact on the results than including the containment hole. These results indicate that the assumptions made for the Grand Gulf accident progression are reasonable.

2.10 RPV Repressurization Following SRV Closure

In a long-term station blackout with early ADS followed by reclosure of the valves after battery depletion, the vessel could repressurize. In such a scenario, the vessel would initially be at low pressure, but could then be repressurized (after SRV reclosure) to a level that would cause a greater containment load at vessel breach. The vessel would repressurize because of vaporization of any water remaining in the vessel, heating gases by heat transfer from hot structures in the vessel, and from zirconium oxidation. If the SRVs were to reclose early in the accident, the vessel water inventory would be larger than if the SRVs were to reclose late. Thus, early reclosure would give a greater potential for repressurizing the vessel. The precise timing of SRV reclosure because of battery depletion was not available from the front-end analysis, but it appeared unlikely to us that a long enough time would exist to prevent the vessel from repressurizing. Thus, rather than performing a detailed

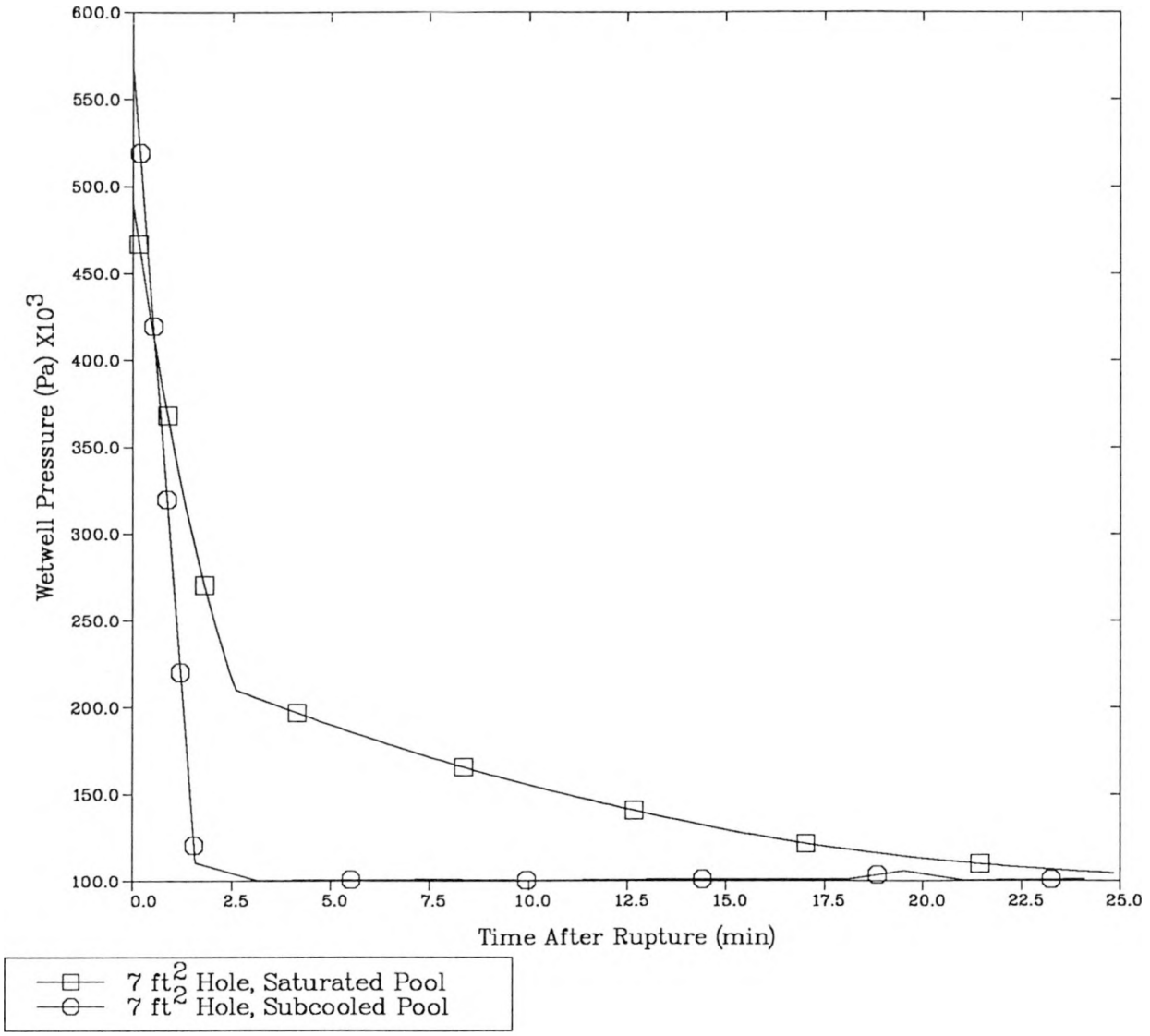

Figure 2-33. Effect of Suppression Pool Subcooling on Depressurization

analysis, a bounding calculation was performed to investigate the potential for repressurization. In this calculation, only the pressurization from vaporizing water in the lower head was considered; all other sources of pressurization were neglected.

The results showed that the pressure could be increased from 1.4 to 8 MPa if about 30 m^3 of liquid water were boiled. This is less than one-third of the volume of the lower plenum. If the SRVs were to reclose with at least this much water present, the vessel would repressurize from steam generation alone. This indicates that power recovery would have to occur within a fairly short time, between the times that the lower plenum inventory dropped below 30 m^3 and vessel breach, to prevent the vessel from repressurizing. If the other pressurization mechanisms which had been neglected in this estimate were included, the results would indicate an even greater likelihood of the vessel being repressurized by the time vessel breach occurred.

Table 2-4

Pressure Relief from Containment Failure

Initial Conditions

	Drywell	Wetwell
Pressure (kPa)	125	125
Temperature (K)	310	310
H2 Mole Fraction	0.	.18
Steam Mole Fraction	.04	.04

Results of Calculations

Wetwell Failure	Radiation	Burn Duration (s)	Peak Wetwell P Rise (kPa)	Peak Drywell Wall DP (kPa)
no	no	2	618	561
yes	no	2	606	552
no	yes	2	590	535
yes	yes	2	575	520
no	yes	.1	649	625

3. PEACH BOTTOM ANALYSES

In the NUREG-1150 study a spectrum of containment failure mechanisms were considered for the Peach Bottom Mark I containment, including over-pressure following vessel depressurization at vessel breach. Previous studies (Refs 13-19) indicated that loads sufficient to fail the Peach Bottom Mark I containment could arise for station blackout accidents in which the vessel is not depressurized before vessel breach, even without considering direct containment heating or steam explosions.

To investigate the response of the containment following vessel depressurization and to examine the potential for containment failure because of vessel depressurization, the MELCOR computer code was used to perform a detailed study of this issue. Both long-term and short-term station blackout scenarios were analyzed and a series of sensitivity studies was performed to investigate modeling uncertainties.

3.1 Brief Peach Bottom Description

Peach Bottom is a BWR/4 reactor with a Mark I containment. The containment, shown in Figure 3-1, consists of 2 main regions, a light-bulb-shaped drywell and a torroidal-shaped wetwell. The wetwell region contains a suppression pool designed to limit containment pressurization by condensing steam from reactor pressure vessel (RPV) releases. The RPV is housed in the drywell, but vents to the suppression pool through the safety relief valves (SRVs). Releases through RPV breaks enter the drywell first, then pass through downcomers into the suppression pool. Vacuum breakers allow gas flow from the wetwell to the drywell to relieve any pressure differential that may develop.

The Peach Bottom Mark I containment failure is expected to occur in the upper portion of the torus shell. This conclusion is based on a Chicago Bridge and Iron (CBI) study (Ref. 20). It was estimated that a breach of containment is not likely until the internal pressure reaches or exceeds 1.2 MPa (174 psia). The CBI study also estimated that leakage through the drywell head seals for Peach Bottom will be initiated at an internal pressure of 0.97 MPa (140 psia).

3.2 MELCOR Model Description

The MELCOR nodalization shown in Figure 3-2 was used for the long-term and short-term station blackout analyses. The reactor vessel was modeled with six control volumes representing the lower plenum, the core fuel rod flow channels, the core bypass flow channels, the downcomer annulus, the shroud dome, and steam dome. The core and lower plenum were nodalized into three radial rings; five axial segments were used in the core region and six segments were used in the lower plenum. The containment was modeled with three control volumes representing the drywell, the vent downcomers, and the wetwell. To perform more economical sensitivity studies, the core and radionuclide input were replaced with energy

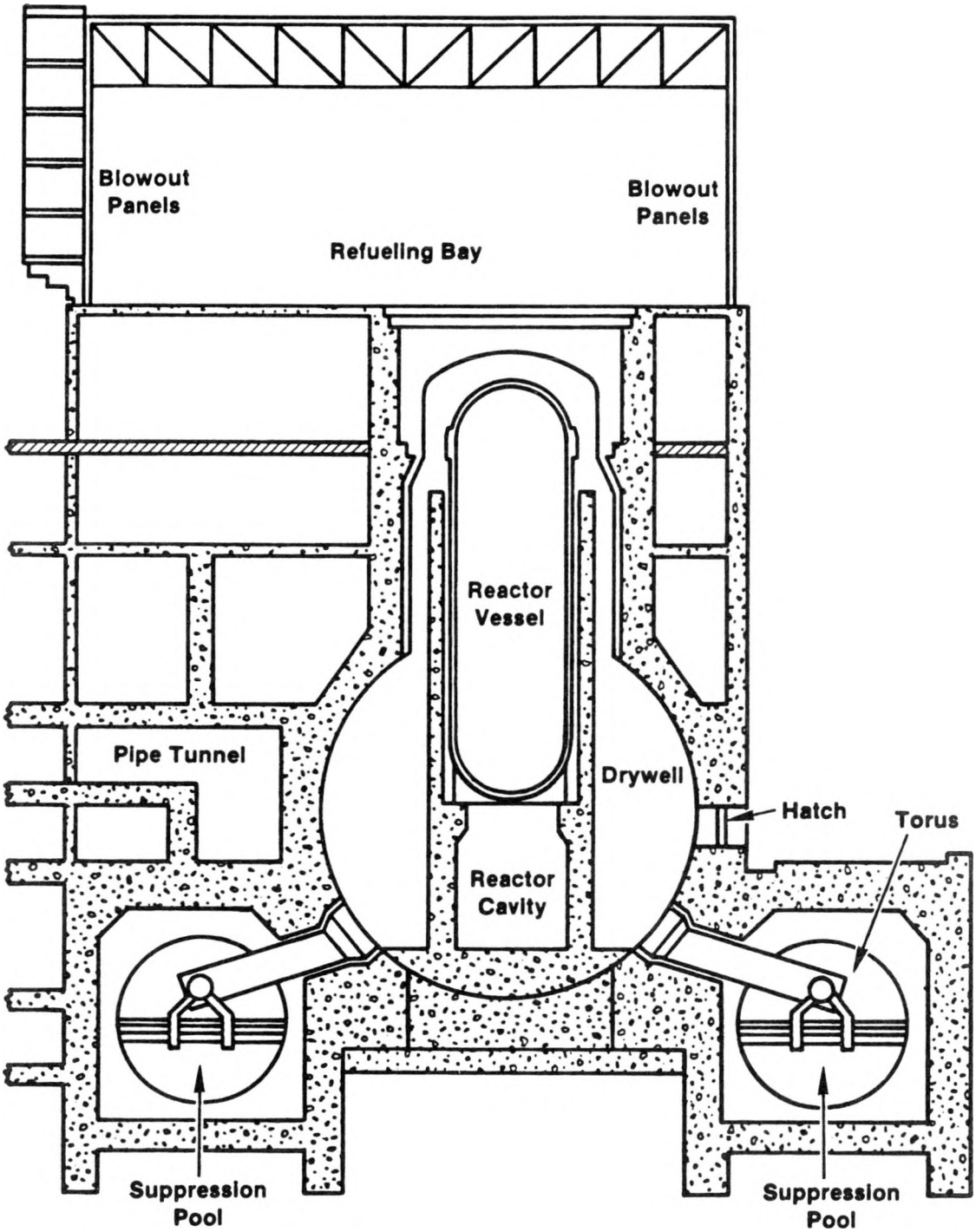

Figure 3-1. Peach Bottom Schematic

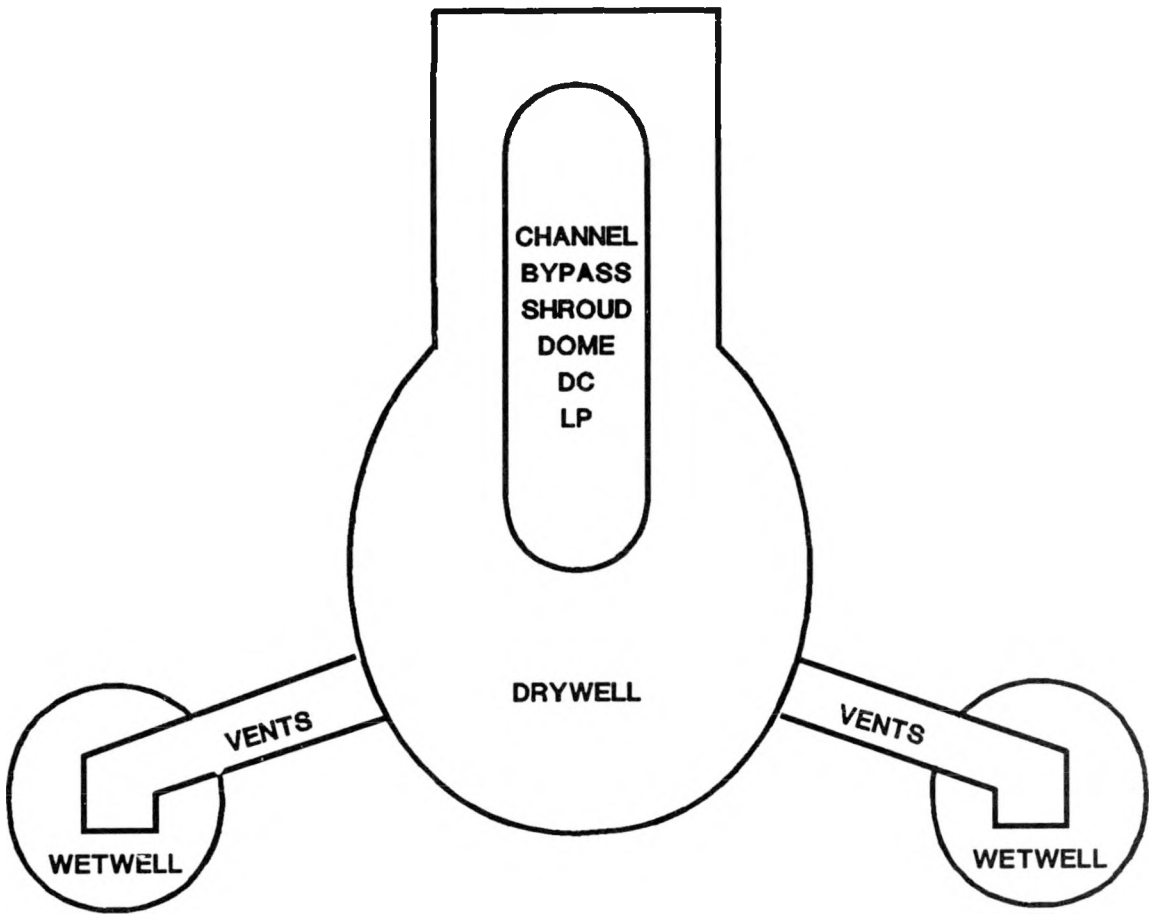

Figure 3-2. Peach Bottom Nodalization

sources to the channel, bypass and lower plenum control volumes that matched the energy transferred in the base case. More details on the model are provided in Appendix A.

The MELCOR calculations were initialized at the time of uncovering of the active fuel (based on the collapsed liquid level) using results of calculations that were performed with the BWR-LTAS code (Ref. 5) to obtain timing information for the core damage frequency analysis for the NUREG-1150 effort. Then, based on the particular scenario being investigated, MELCOR calculated the subsequent boil-off and melt progression to a point well beyond vessel failure. In the base calculations the vessel failure is assumed to be through a penetration with a diameter of 0.1 m. It was assumed that the drywell floor was dry at the time of vessel failure, and hence there was no ex-vessel fuel quenching. Direct heating of the containment by the ejected debris and suppression pool bypass were not modeled.

Since the analyses were focused on the containment response following vessel depressurization at vessel breach, all cases assumed that the ADS had failed. This assumption resulted in the vessel remaining at high pressure until vessel failure occurred. The other key assumption in the analyses was related to the availability of the dc power which directly affects the timing of the accident sequence. For the long-term station blackout scenario, the loss of all off-site and on-site ac power leads to the loss of all active engineered safety features except the steam powered emergency core cooling systems. Loss of dc power because of battery depletion at six hours after accident initiation is assumed to result in the loss of controls for the turbine-driven Reactor Core Isolation Cooling (RCIC) system and a total loss of injection to the primary system. In the short-term station blackout scenario, the dc power and all injection systems are lost at the beginning of the accident.

Both a long-term and short-term station blackout scenario were simulated. These two calculations are referred to as the base calculations. To investigate areas of uncertainty in the base calculations, sensitivity studies were performed, principally for the long-term station blackout scenario. The sensitivity studies for the long-term station blackout scenario investigated the effects of the following parameters and models:

- vent downcomer clearing,
- containment heat transfer,
- flashing of residual water in the vessel downcomer,
- vessel break area,
- in-vessel gas temperatures,

- suppression pool temperature,
- relative humidity of gas bubbles leaving the suppression pool,
- suppression pool bypass, and
- in-vessel hydrogen content.

For the short-term station blackout case, the sensitivity of the results to the core melt progression modeling was investigated by running a case with an increased core relocation temperature relative to the base case.

3.3 Results of the Base Calculations

The principal parameters of interest in this study were the peak pressure and temperature in the drywell following vessel depressurization. The drywell pressure and temperature histories for the station blackout base calculations are shown in Figures 3-3 and 3-4, respectively. The peak drywell pressure in the short-term station blackout case is 0.59 MPa and in the long-term station blackout case it is 0.89 MPa. In both cases these values are significantly below the estimated containment failure pressure of 1.2 MPa. The peak drywell temperatures are 726 K in the short-term station blackout case and 710 K in the long-term station blackout case.

Table 3-1 provides additional information regarding the timing of key events and the containment response. The MELCOR calculations were initiated at the time when the collapsed liquid level reached the top of the active fuel, which occurred at 28 minutes in the short-term station blackout case and at 470 minutes in the long-term station blackout case. The timing of key events in Table 3-1 includes the time at which core relocation begins (indicated by the movement of the center uppermost core node), the time at which the center of the core plate fails, the time at which the lower plenum water dries out (some water still exists in the downcomer annulus), and the time at which a penetration in the lower head fails causing vessel depressurization. The failure of the reactor vessel occurred at 278 minutes for the short-term station blackout case and at 807 minutes for the long-term station blackout case.

The blowdown gases flowing from the drywell to the wetwell pass through the downcomer volume and exit under water in the suppression pool. At the time of vessel failure, the water level in the downcomers was nearly the same as that in the wetwell. The increased drywell pressure from the reactor vessel depressurization pushed the water from the downcomers into the wetwell. The blowdown gases then passed through the downcomer and exited into the pool. In the long-term scenario the downcomers were cleared of water 8 seconds after lower head failure. For this case, the peak drywell pressure occurred at 210 seconds, the downcomers started to refill with water at 358 seconds, and the reactor vessel depressurization was complete at about 700 seconds after vessel head failure.

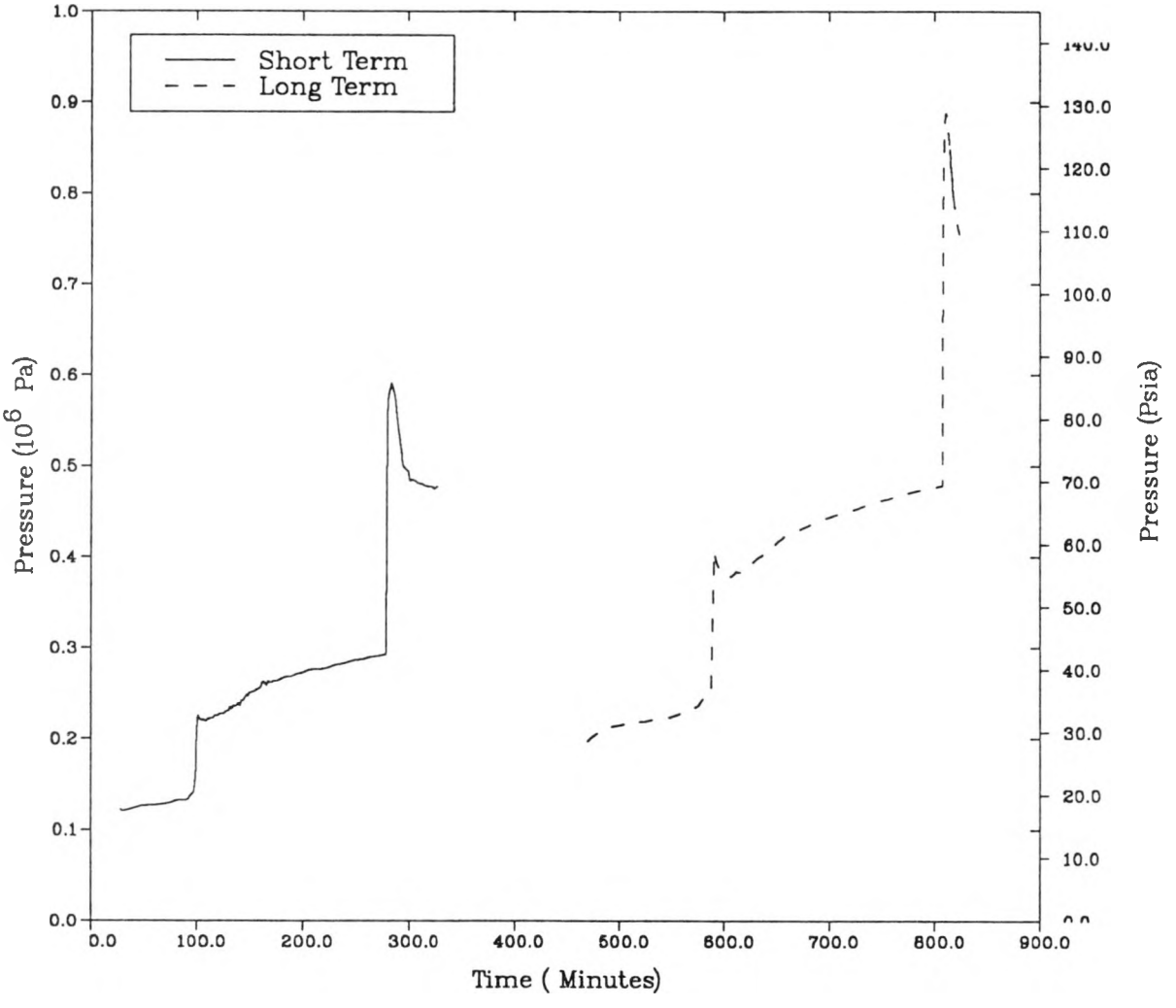

Figure 3-3. Station Blackout Drywell Pressure

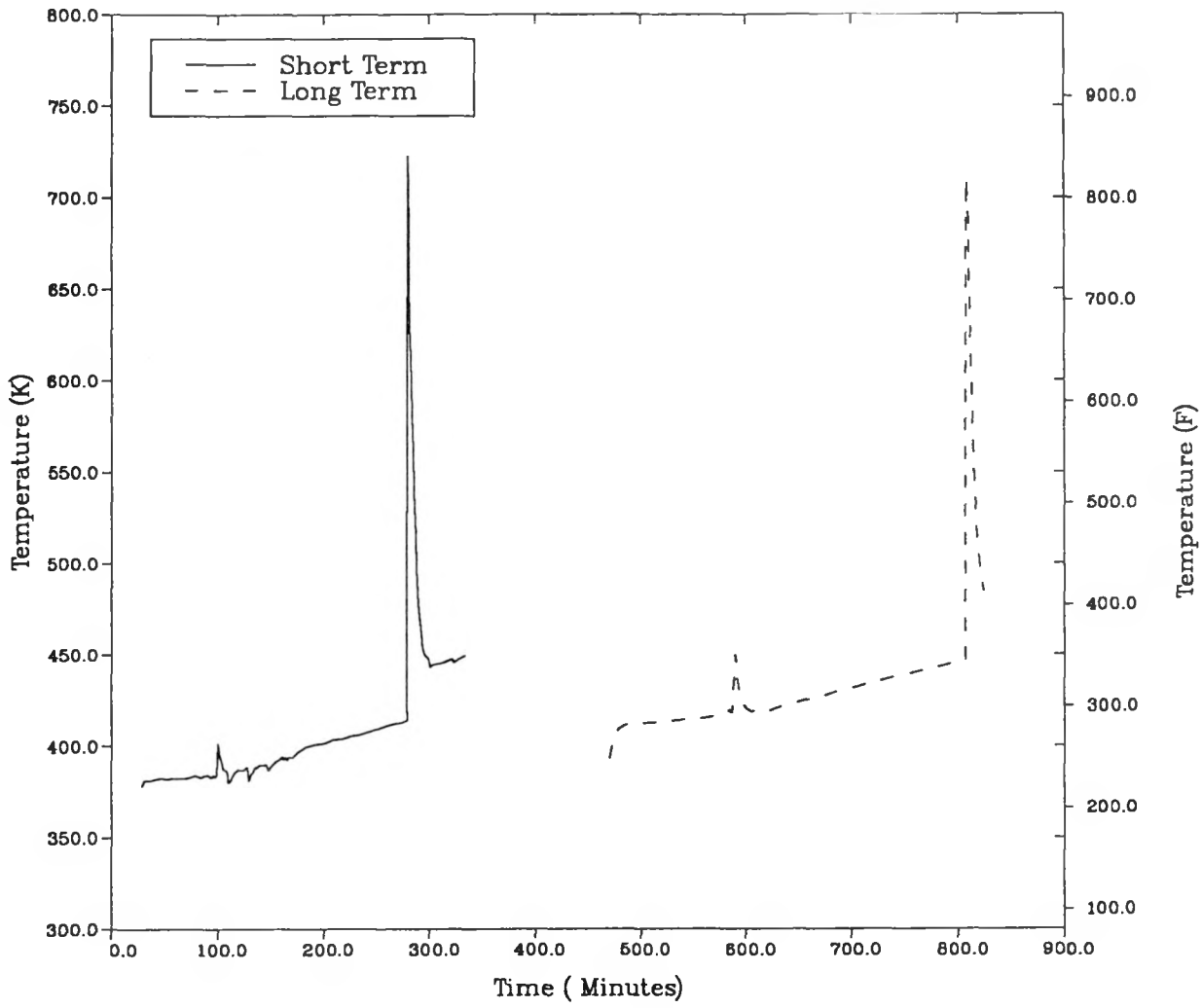

Figure 3-4. Station Blackout Drywell Atmosphere Temperature

In the long-term scenario, a higher peak pressure and a higher pressure increase were calculated than in the short-term scenario for two basic reasons. First, the drywell pressure was higher at lower head failure for the long-term scenario because more steam had been released to the containment. Second, the suppression pool temperature was higher and, hence, the suppression pool was less effective for condensing steam. The suppression pool condensed 2700 kg of steam for the long-term scenario compared to 4100 kg for the short-term scenario. An additional difference concerned leakages from the RPV. Between the times that the long-term and short-term station blackout calculations were performed, it was learned that leakage from the pump and control rod drive seals could be important. Leakage of about 4 gpm was thus added for the short-term station blackout calculation. If this leakage had been included in the long-term station blackout calculation, the containment pressures would have been slightly higher.

Table 3-1

MELCOR Station Blackout Results

	Short-Term	Long-Term
Event Timing (minutes)		
Core Uncovering	28	470
Core Uncovering to First Relocation	72	108
First Relocation to Core Plate Failure	1	12
Core Plate Failure to Lower Plenum Dryout	147	179
Lower Plenum Dryout to Lower Head Failure	30	38
Lower Head Failure	278	807
Conditions at Lower Head Failure		
Volume Averaged In-Vessel		
Gas Temperature (K)	1140	1070
Total Hydrogen Produced (kg)	609	569
DW Pressure (MPa)	0.297	0.478
DW Temperature (K)	415	447
Suppression Pool Temperature (K)	352	399
Containment Response to Depressurization		
DW Peak Pressure (MPa)	0.594	0.888
DW Pressure Increase (MPa)	0.297	0.410
DW Peak Temperature (K)	726	710
DW Temperature Increase (K)	312	263
S.P. Temperature Increase (K)	0.69	0.59
S.P. Mass Increase (kg)	4100	2700

In the short-term station blackout scenario, a higher peak temperature and a higher temperature increase were calculated than in the long-term station blackout scenario. This difference was due to the difference in the in-vessel gas temperatures at the time of lower head failure. The volume averaged in-vessel gas temperatures at head failure were 1144 K and 1073 K for the short-term station blackout and long-term station blackout scenarios, respectively.

3.4 Station Blackout Sensitivity Studies

The sensitivity of the station blackout calculations to variations in some of the modeling assumptions was investigated. As shown in Table 3-2, a variety of geometrical and phenomenological changes were examined. Cases 1 through 9 were all performed using the long-term station blackout case as the base case. Case 10 used the short-term station blackout case as the base case.

3.4.1 Vent Downcomer Model Sensitivity Study

As the drywell pressurizes, the gases in the drywell are forced through the vent downcomer into the suppression pool. Since there will be water in the vent downcomer, the water must be cleared from it before the gases can be relieved into the suppression pool. Hence, modeling of the downcomer clearing could have a direct effect on pressure response. In many previous MELCOR calculations, the downcomer clearing was not modeled, and in some calculations performed with other codes the hydrostatic head associated with injecting these gas flows under water was not treated.

To investigate the sensitivity of the results to downcomer clearing, a calculation was performed in which the vent downcomer was removed. In that case, the gases simply flowed into the suppression pool and the effects of vent clearing were ignored. Note, however, that the gases entered the suppression pool at the correct depth so that the effect of the hydrostatic head was properly treated.

As shown in Figure 3-5, realistic modeling of the vent downcomer has the effect of increasing the peak pressure from 0.83 to 0.89 MPa (6.6%). The peak temperature increased only slightly, as shown in Figure 3-6. With the vent downcomer modeled, the flow of gases from the drywell to the wetwell was delayed at the time when the flow rate from the vessel was highest. The calculated time required to clear the vent downcomers in the base case was 8 s. In the case without the vent downcomer modeled, only 2 s were required to overcome the pool hydrostatic head and begin flowing gases through the vents. The mass of steam condensed by the suppression pool was 2700 kg when the vent downcomer was modeled and 3700 kg when it was not modeled.

Table 3-2

Summary of Sensitivity Study Cases

CASE	DESCRIPTION
1. Vent Downcomer Clearing	Cases with and without the vent downcomer modeled.
2. Containment Heat Transfer	Cases with and without radiation heat transfer and cases with and without structures modeled.
3. Flashing of Residual Water In the Vessel Downcomer	Cases with and without flashing of the residual water modeled.
4. Vessel Break Area	Cases with break areas of .005, .0079, .01, .02, .05, .10, .25, and 1.0 m^2.
5. In-Vessel Gas Temperatures	Cases with gas temperatures of -200, -400, 200, 400, and 600 K relative to the base case.
6. Suppression Pool Temperature	Cases with suppression pool temperatures of 310, 335, 360, 380, 399, and 410 K.
7. Relative Humidity of Gas Bubbles Leaving the Suppression Pool	Cases with bubble relative humidities of 0., .25, .5, .75, and 1.
8. Suppression Pool Bypass	Case in which suppression pool bypass occurred.
9. In-Vessel Hydrogen Content	Cases with in-vessel hydrogen content of 0 and twice the base case value.
10. Core Melt Progression Modeling	Case with an increased core relocation temperature relative to the base case.

3.4.2 Containment Heat Transfer Sensitivity Studies

The effect of containment heat transfer on the containment response during a high pressure reactor vessel depressurization is an area of uncertainty in the base calculation. While a complete assessment of the influence of heat transfer is not practical, its influence was examined in part through two sensitivity study cases. In the first case the containment radiative heat transfer input was removed and in the second case the containment heat structure input was entirely removed.

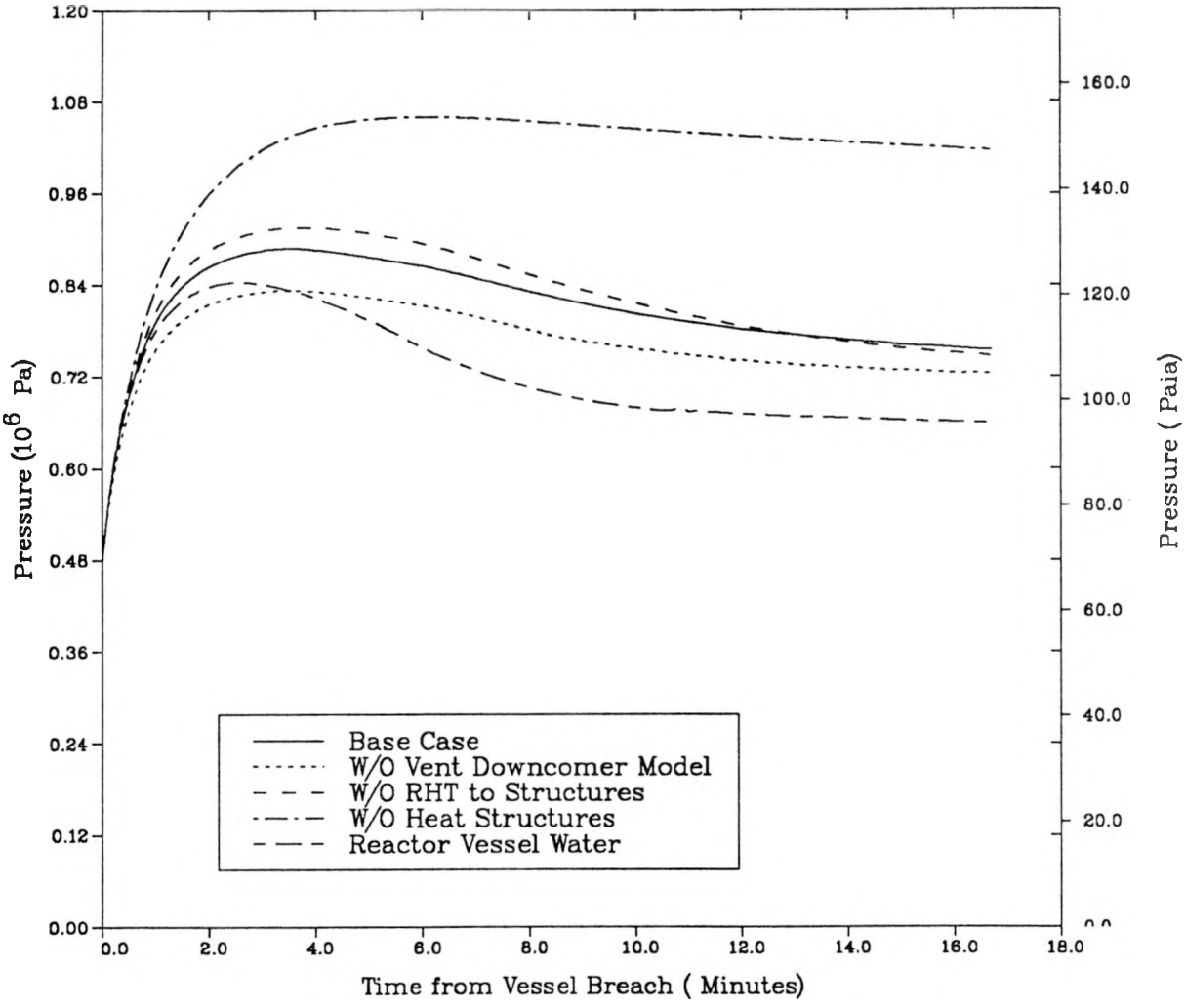

Figure 3-5. Sensitivity of Drywell Pressure to Model Changes

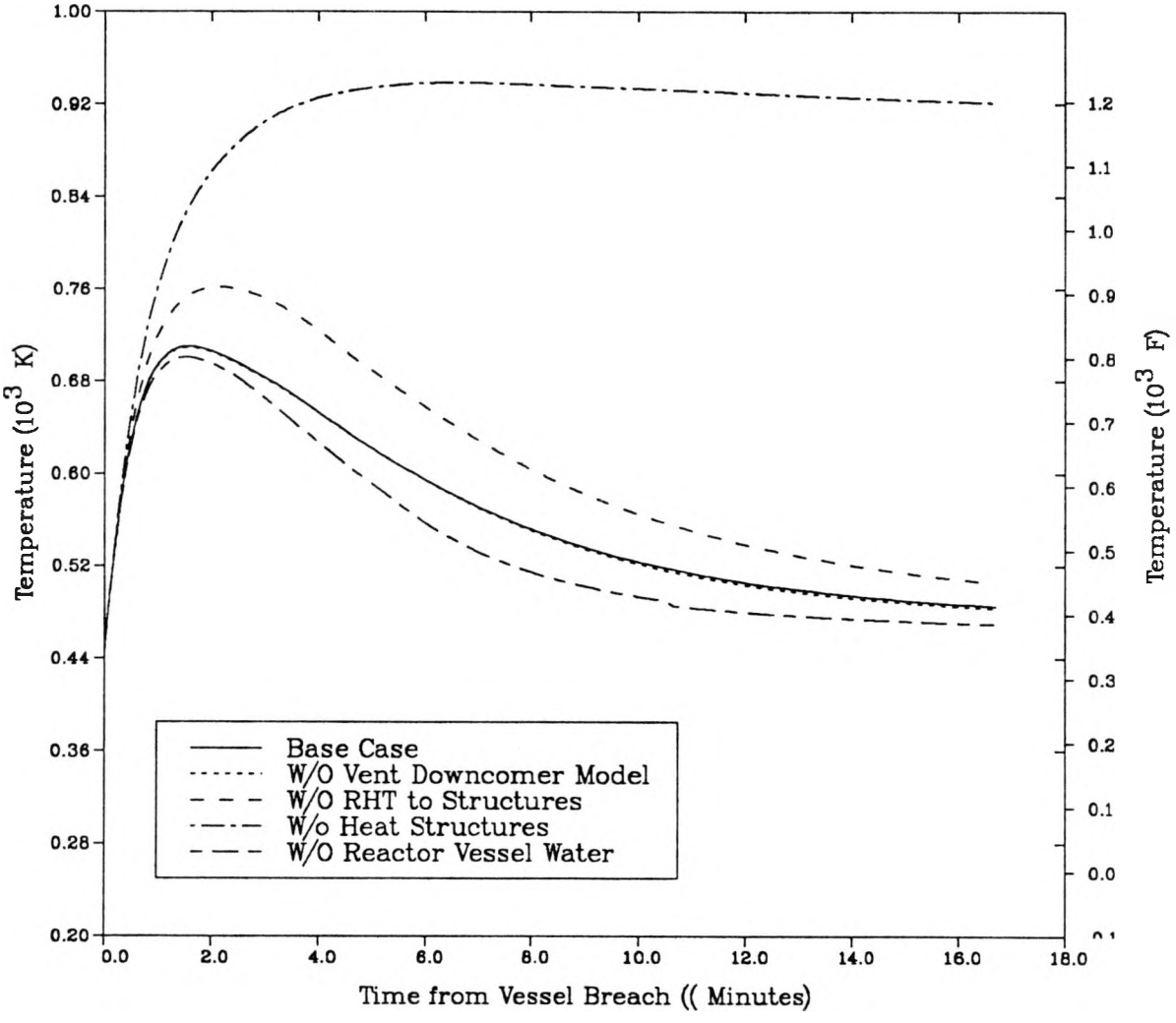

Figure 3-6. Sensitivity of Drywell Temperature to Model Changes

The results from these cases are also shown in Figures 3-5 and 3-6. Radiative heat transfer modeling reduced the peak pressure spike by 0.03 MPa (6.7%) and reduced the peak temperature spike by 51 K. These changes are significant and show that the radiative heat transfer within the containment should be included in severe accident calculations.

In the calculation in which the heat structures were not modeled, the containment response was markedly different from any of the other cases, as shown in Figures 3-5 and 3-6. This comparison clearly demonstrates the importance of heat transfer to both the peak pressure and long-term pressure response.

3.4.3 Flashing of Residual Downcomer Water Sensitivity Study

The effect of water remaining in the reactor vessel downcomer annulus flashing to steam was examined by removing that water and the volume occupied by that water from the base case at the time of lower head failure. Many previous calculations (Refs. 4, 5) lacked the models to calculate heat transfer to the water trapped in the downcomer annulus. Hence, the water remained subcooled and did not contribute to the depressurization. The removal of this water reduced the peak pressure spike by 0.044 MPa (5%) and the peak temperature spike by 9 K as shown in Figures 3-5 and 3-6.

3.4.4 Lower Head Break Area Sensitivity Study

The sensitivity of the pressure response following a high pressure blowdown to the break area in the lower head was investigated by performing calculations with break areas of 0.005, 0.0079, 0.01, 0.02, 0.05, 0.10, 0.25, and 1.0 m^2. The base case used an area of 0.0079 m^2, which corresponds to an effective hole diameter of 0.1 m. The drywell pressures and temperatures for these calculations are shown in Figures 3-7 and 3-8. The peak pressures and peak temperatures are shown as a function of the break area in Figures 3-9 and 3-10.

The peak pressure increased with the break area up to break areas of approximately 0.1 m^2. For break areas larger than this value, the peak pressure was nearly independent of break size. For the case with an area of 1 m^2, the peak pressure occurred before the vent downcomers cleared of water and increased the peak pressure about 10% over that of the base case. The highest peak pressure calculated for this sensitivity study was 0.98 MPa for the 1.0 m^2 case.

The peak temperatures increase with area up to about 755 K at an area of 0.1 m^2 can then decrease slightly. The highest peak temperature was about 45 K higher than the base case. This occurred because more heat can be transferred to the containment heat structures for the smaller break areas during the longer depressurization times. For the largest break areas, the peak temperature decreases sightly because of reduced time for fluid heating in the vessel until the time of peak temperature. The long-term temperature is an increasing function of break size.

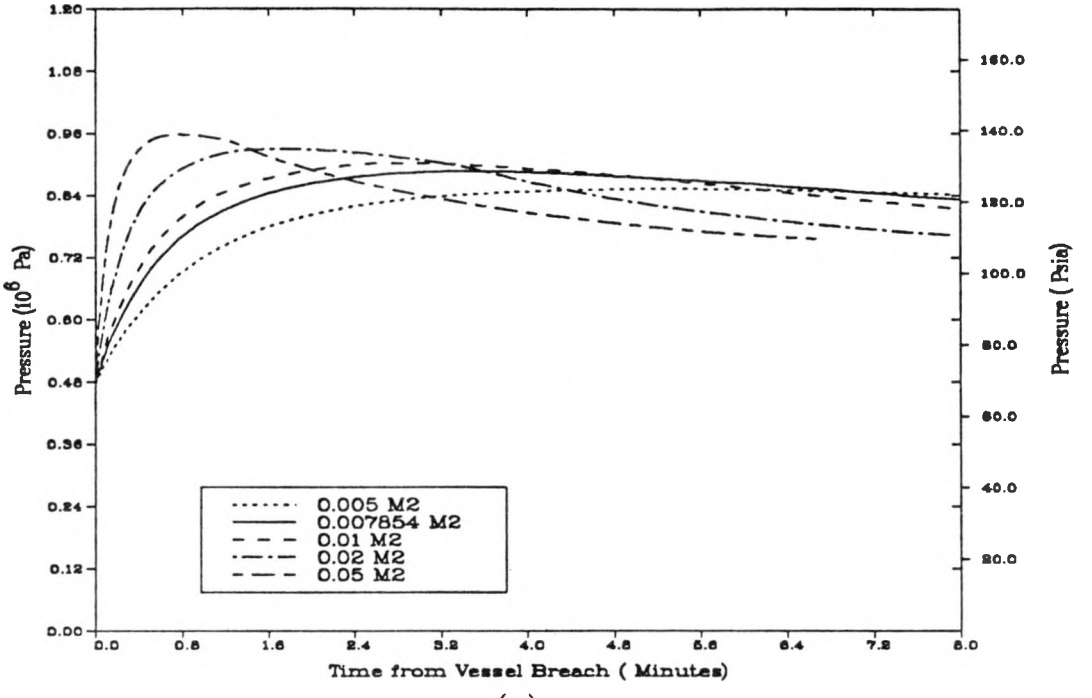

(a)

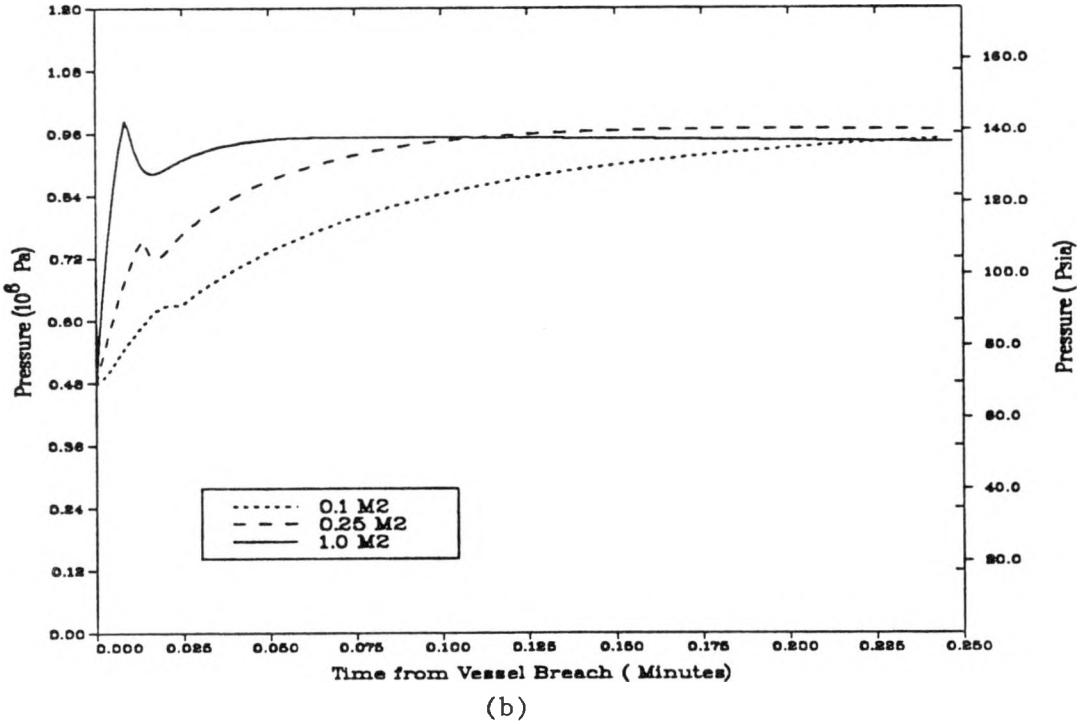

(b)

Figure 3-7. Drywell Pressure Sensitivity to Breach Area

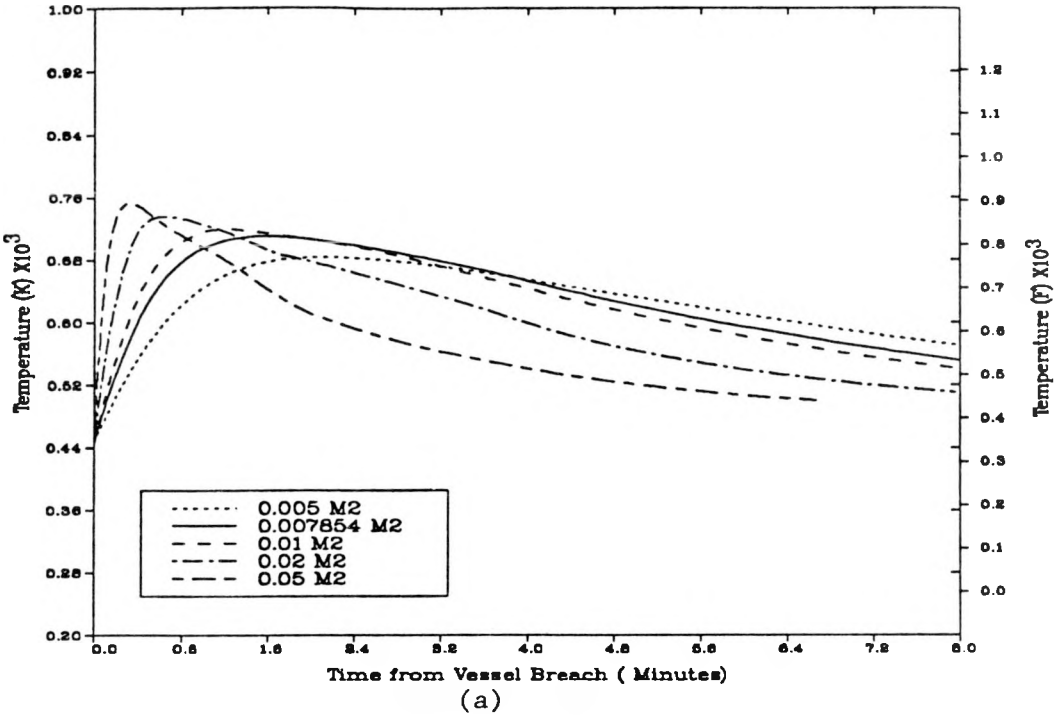

(a)

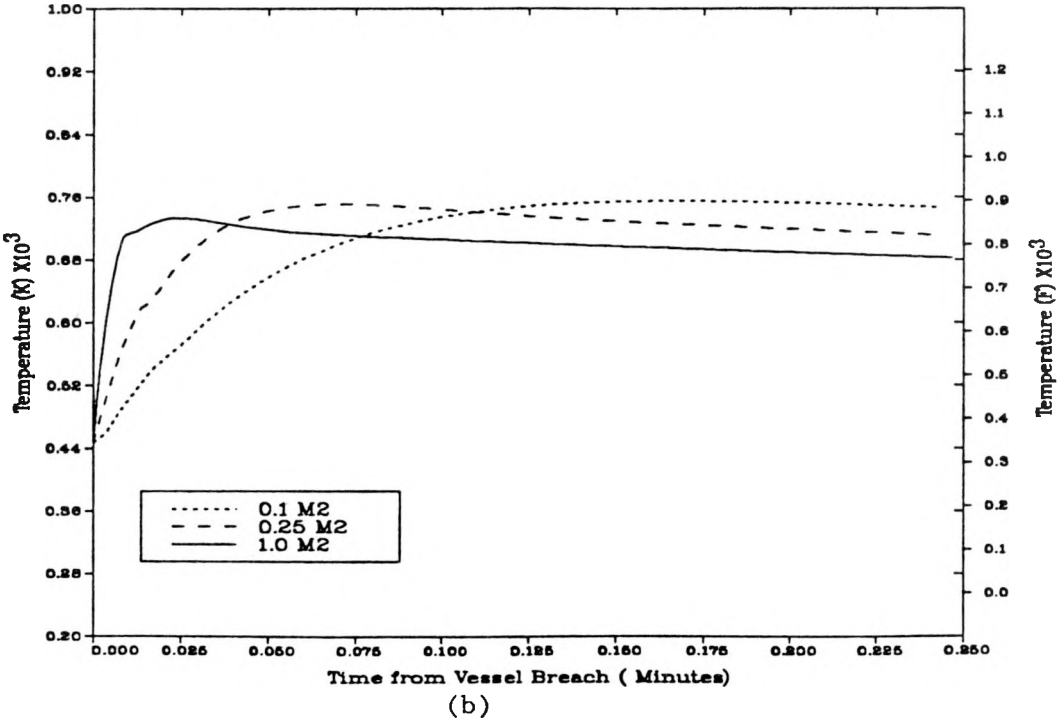

(b)

Figure 3-8. Drywell Temperature Sensitivity to Breach Area

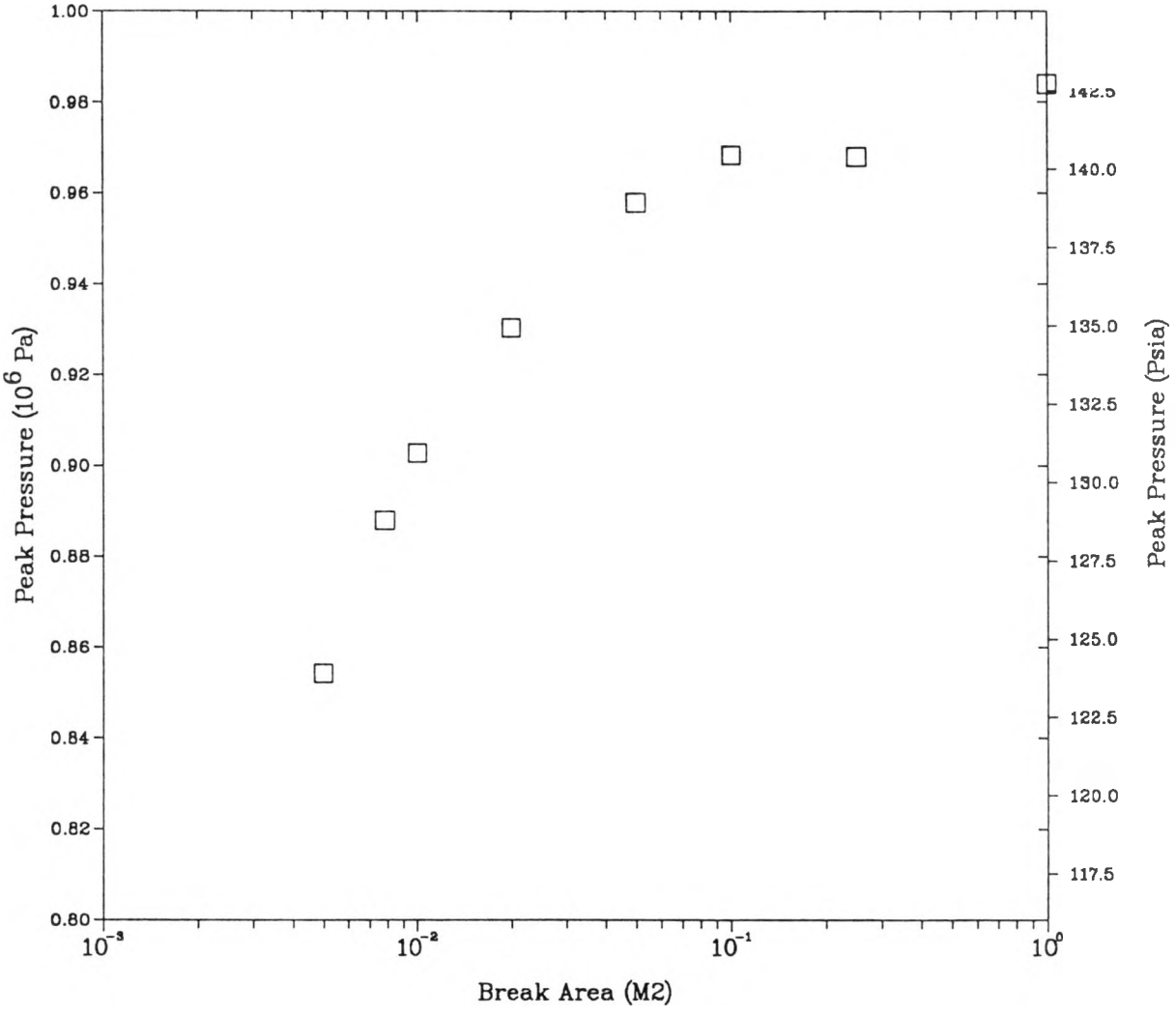

Figure 3-9. Drywell Peak Pressure Sensitivity to Breach Area

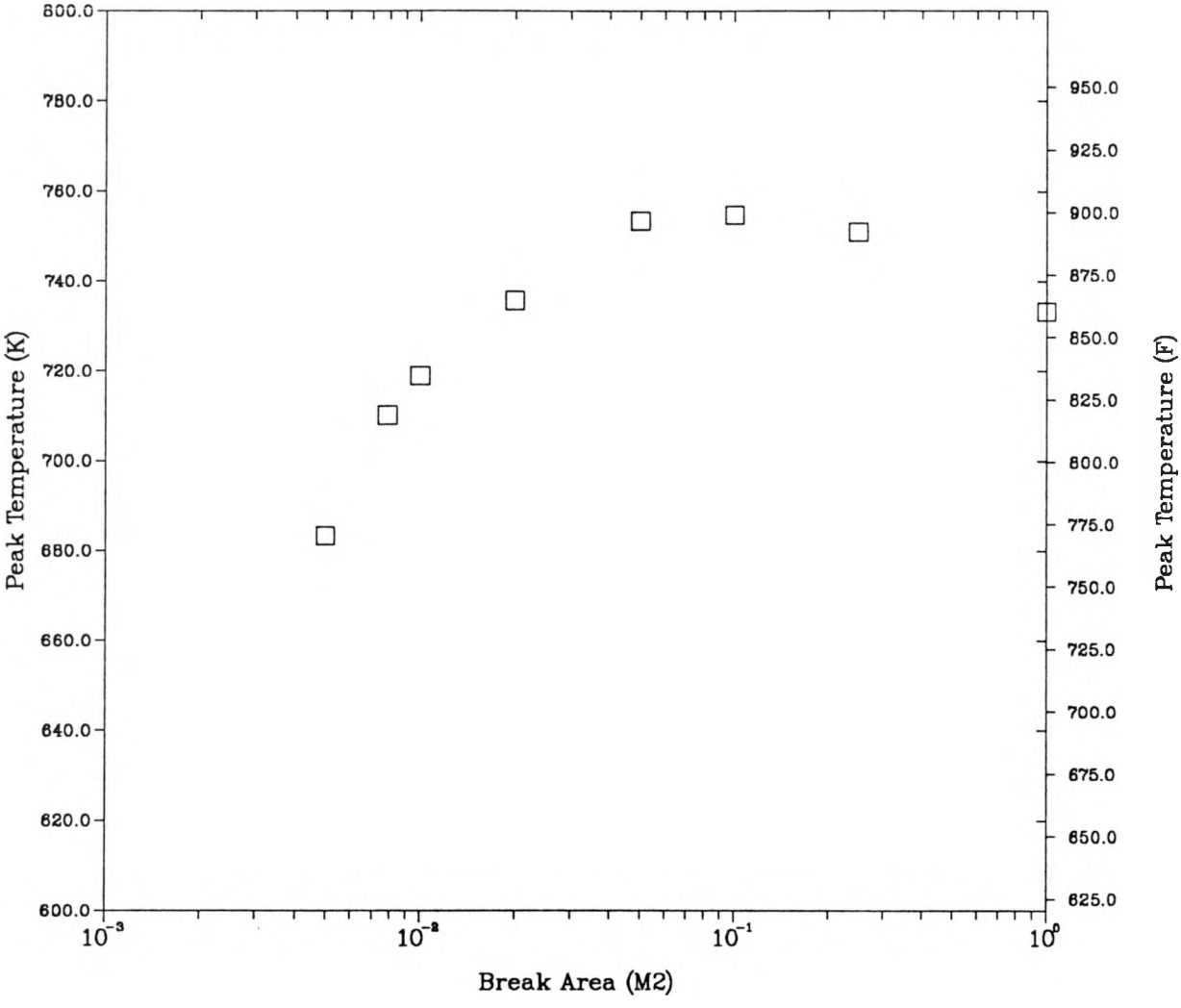

Figure 3-10. Drywell Peak Temperature Sensitivity to Breach Area

The sensitivity of the timing of key events during the depressurization to the break area is shown in Figure 3-11. In this figure, the vent clearing time, the time of peak pressure, the vent closure time, and the approximate end time of reactor vessel depressurization are shown as a function break area. The vent downcomers reflooded with water after the peak pressures are reached, but before the end of the depressurization.

3.4.5 Reactor Vessel Gas Temperature Sensitivity Study

A sensitivity study was performed in which the volume averaged in-vessel gas temperature at the time of vessel head failure was decreased by 200 K and 400 K and increased by 200 K, 400 K, and 600 K relative to the base case values. The drywell pressure and temperature for these calculations are compared in Figures 3-12 and 3-13. The peak pressures and temperatures are shown as a function of the change in the in-vessel gas temperature in Figures 3-14 and 3-15. The peak pressures and temperatures for a study using the 1.0 m^2 break area are also shown.

The peak pressures were not strongly dependent upon the in-vessel gas temperature. In these cases, the reactor vessel pressure at lower head failure was a constant. This means that the mass of gases in-vessel decreased as the in-vessel gas temperatures were increased. The smaller mass counteracted the higher in-vessel gas temperature so that the drywell peak pressures remained relatively constant.

The peak drywell temperatures on the other hand were strongly dependent upon the in-vessel gas temperatures as shown in Figure 3-15. The large break cases showed a stronger dependence than did the small break cases. The slope of the curves at the base case value (0 K change in RPV gas temperature) varies between 0.3 and 0.4 K-Drywell/K-In-Vessel for the small and large break cases.

3.4.6 Suppression Pool Temperature Sensitivity Study

The capability of the suppression pool to condense steam, and hence, suppress containment pressure is dependent upon the temperature of the pool. The temperature of the suppression pool at the time of lower head failure was varied to determine the sensitivity of the containment response to this temperature. The pool temperature in the base case was 399 K at the time of lower head failure. In the sensitivity study, it was varied from 310 to 410 K where it was approaching the saturation temperature.

The drywell pressures for these cases are shown in Figure 3-16. The peak drywell pressures and temperatures are shown as a function of the suppression pool temperature in Figures 3-17 and 3-18. The sensitivities of the drywell peak pressure and peak temperature to the suppression pool temperature at the base case suppression pool temperature are 3690 Pa/K and 0.42 K/K, respectively. Variations in the suppression pool temperature could be important in calculations where the pressure is close to the containment failure pressure.

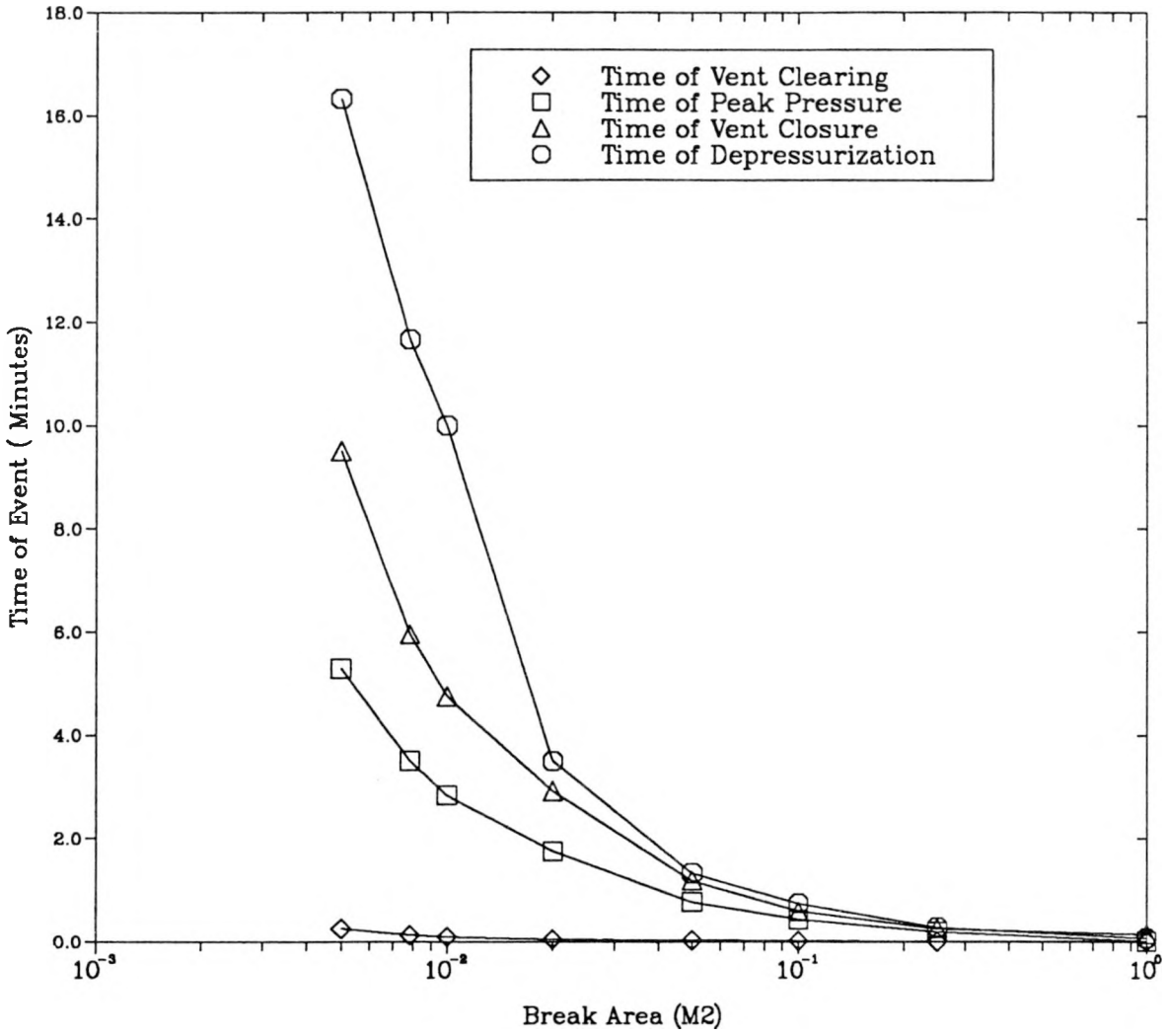

Figure 3-11. Event Timing Sensitivity to Breach Area

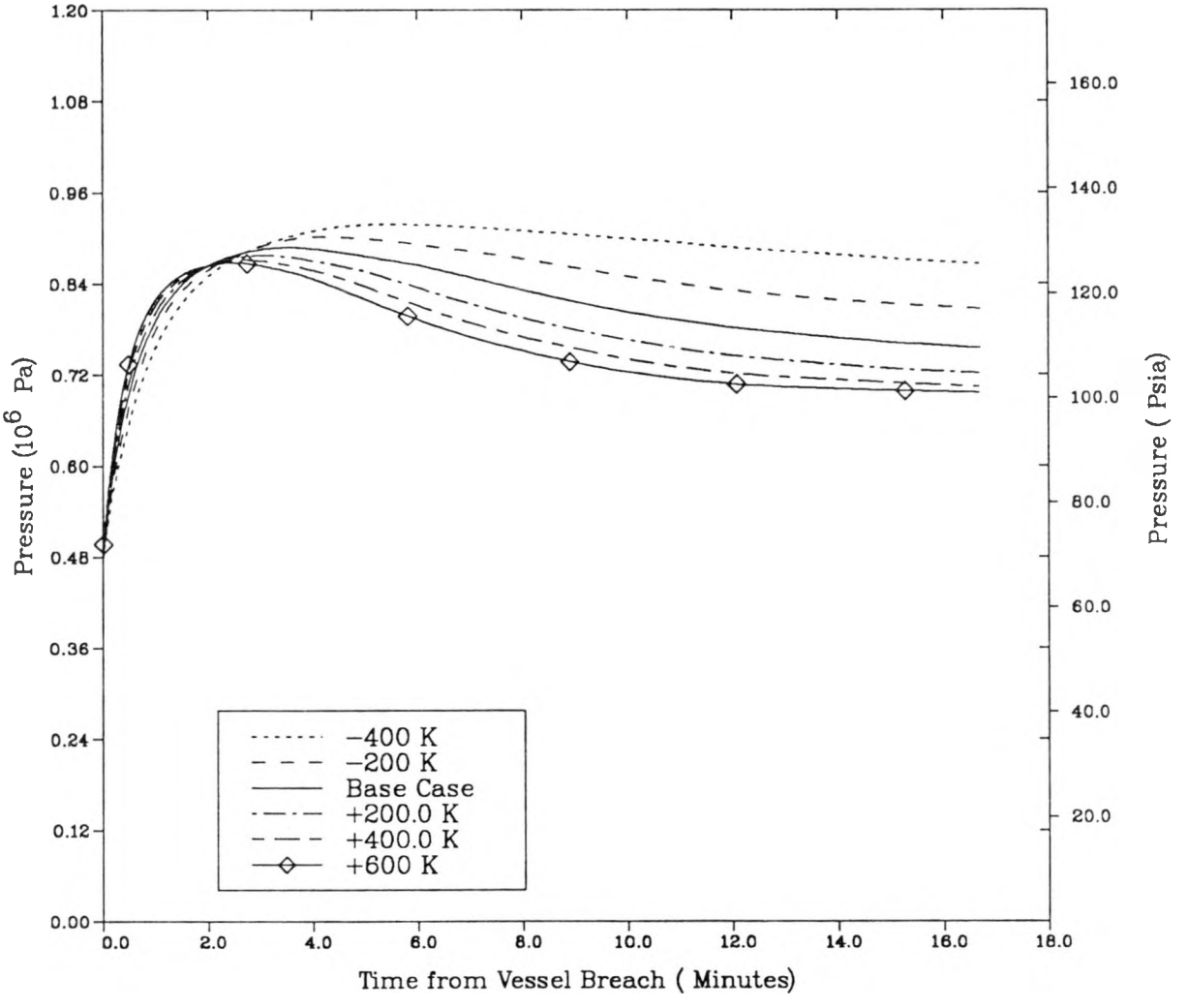

Figure 3-12. Drywell Pressure Sensitivity to RV Gas Temperature

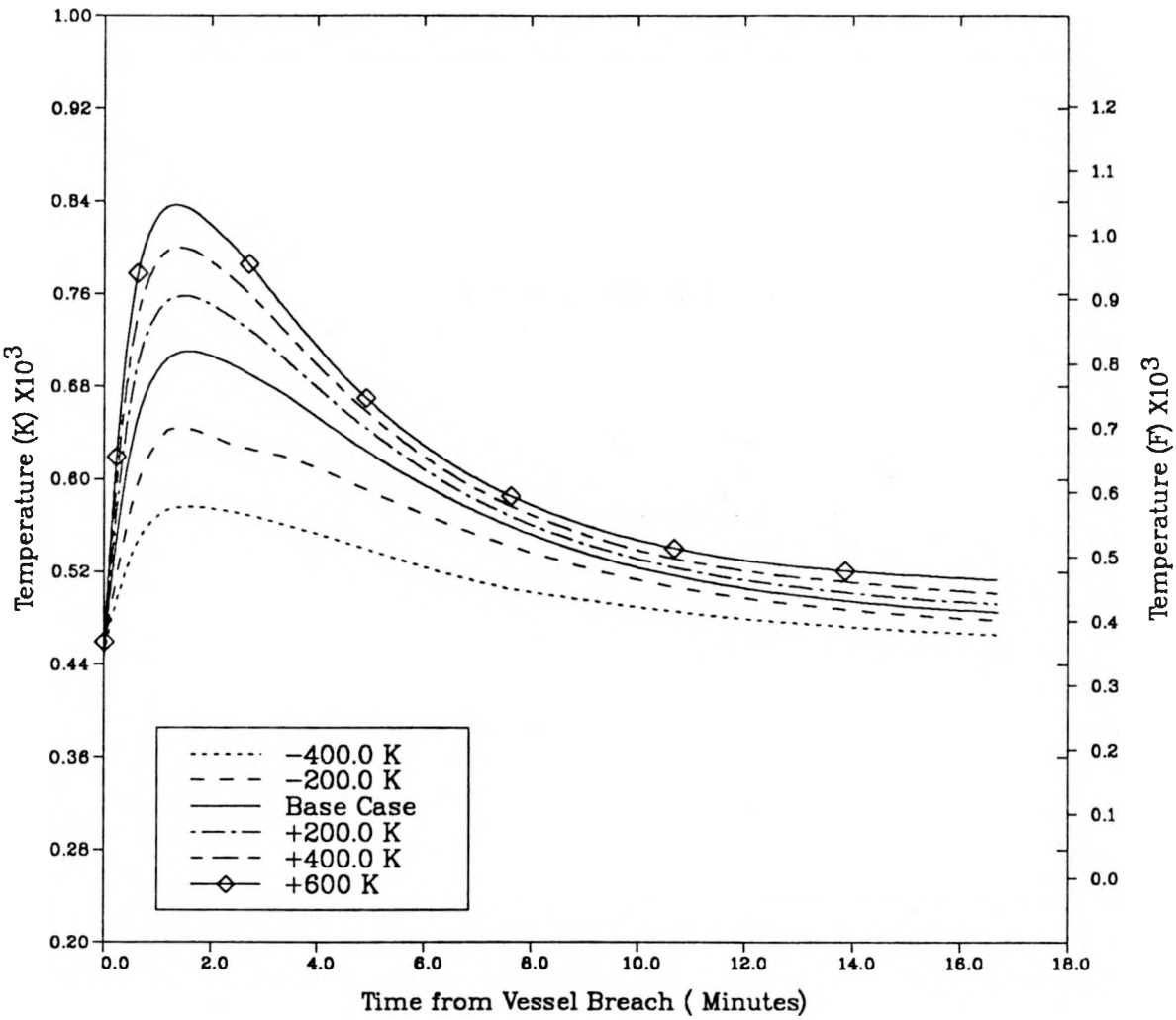

Figure 3-13. Drywell Temperature Sensitivity to RV Gas Temperature

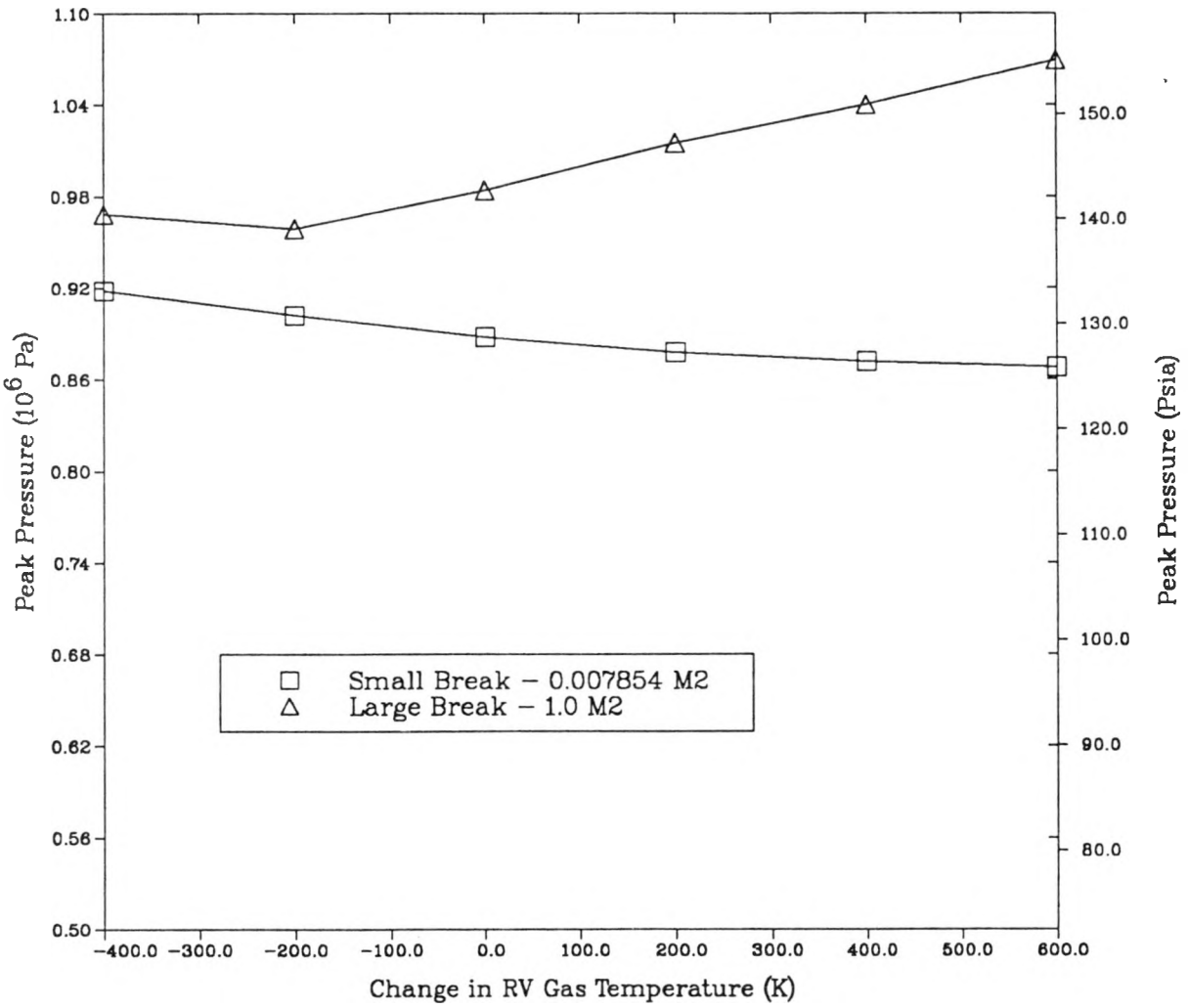

Figure 3-14. Drywell Peak Pressure Sensitivity to RV Gas Temperature

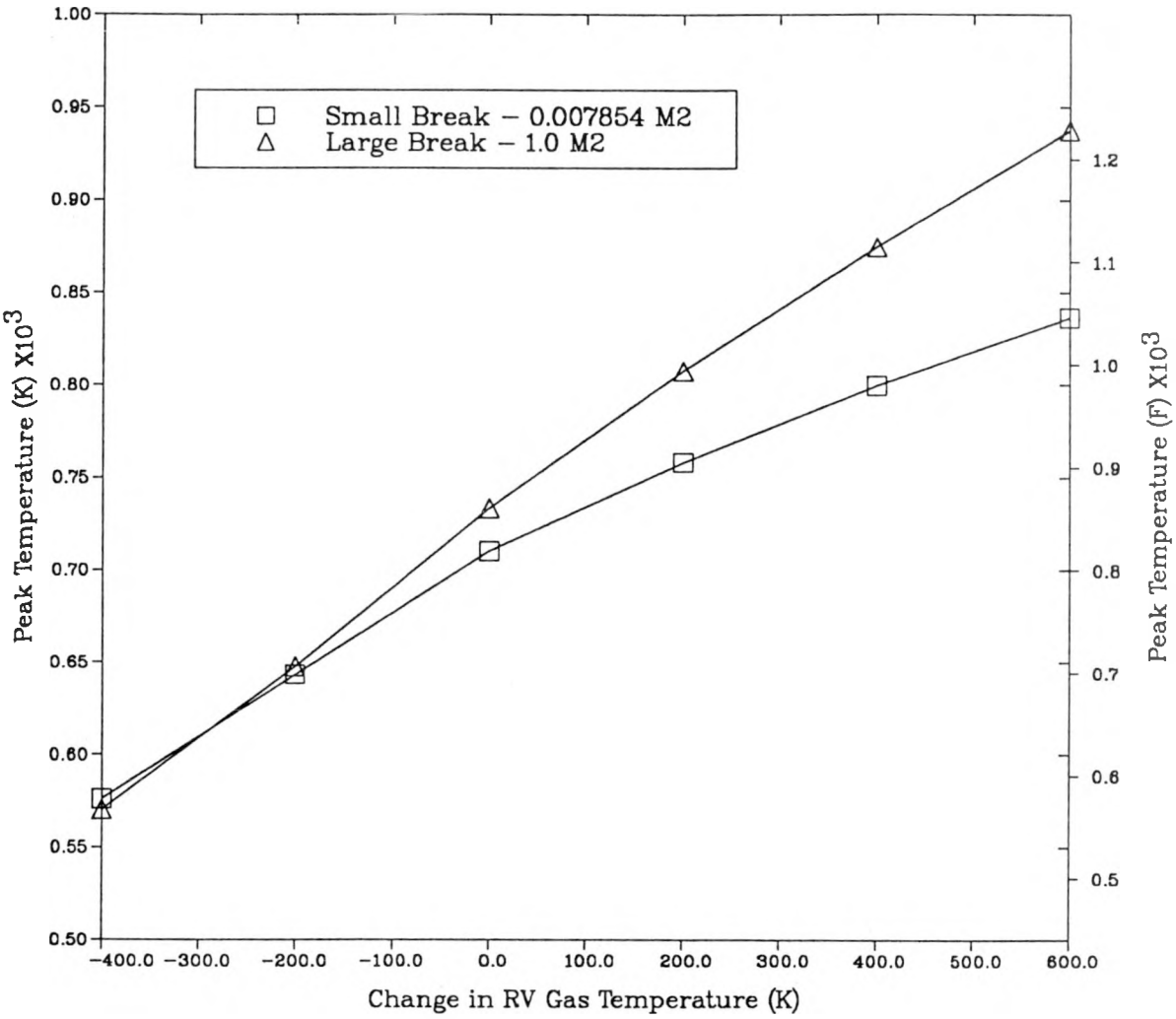

Figure 3-15. Drywell Peak Temperature Sensitivity to RV Gas Temperature

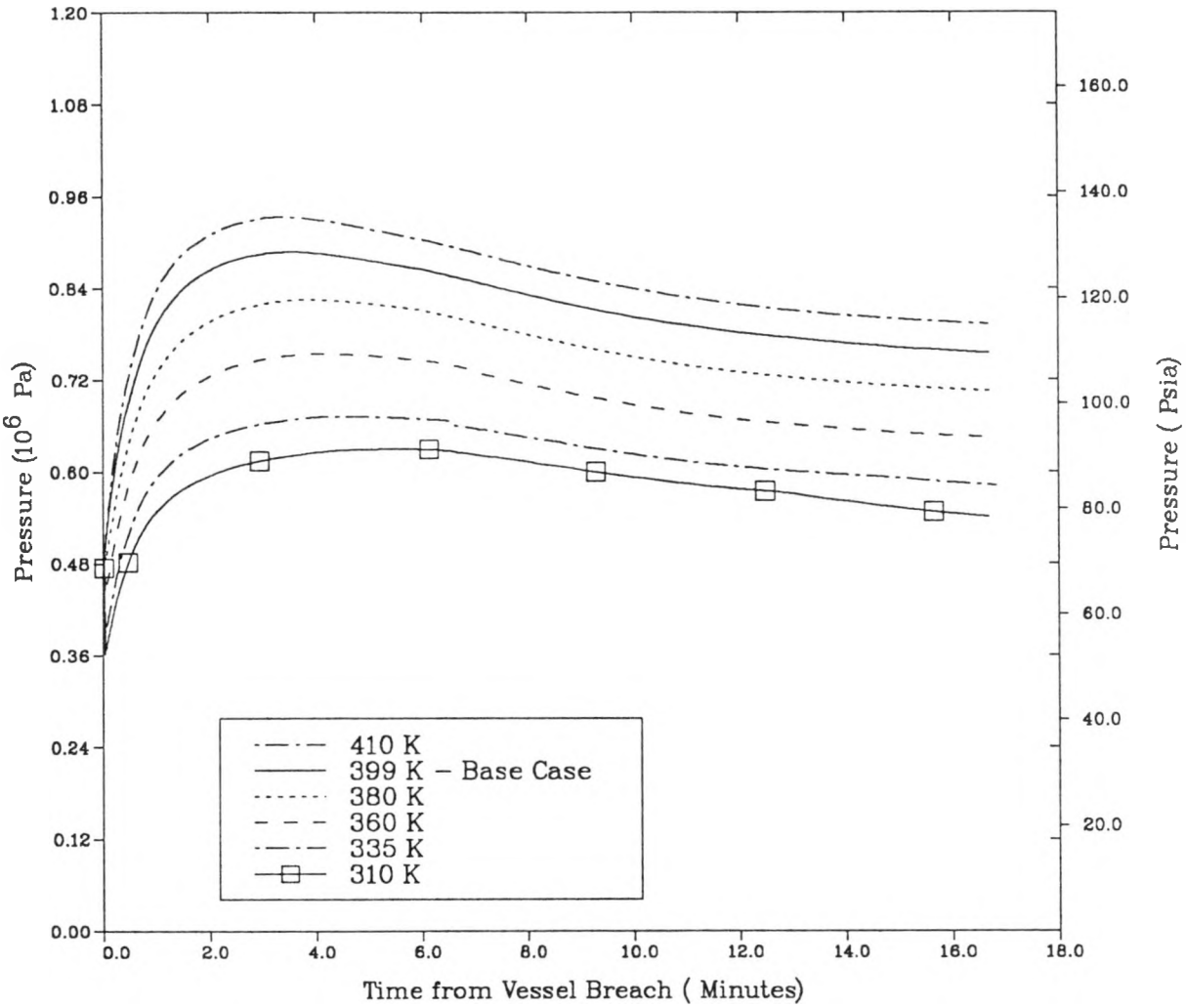

Figure 3-16. Drywell Pressure Sensitivity to Suppression Pool Temperature

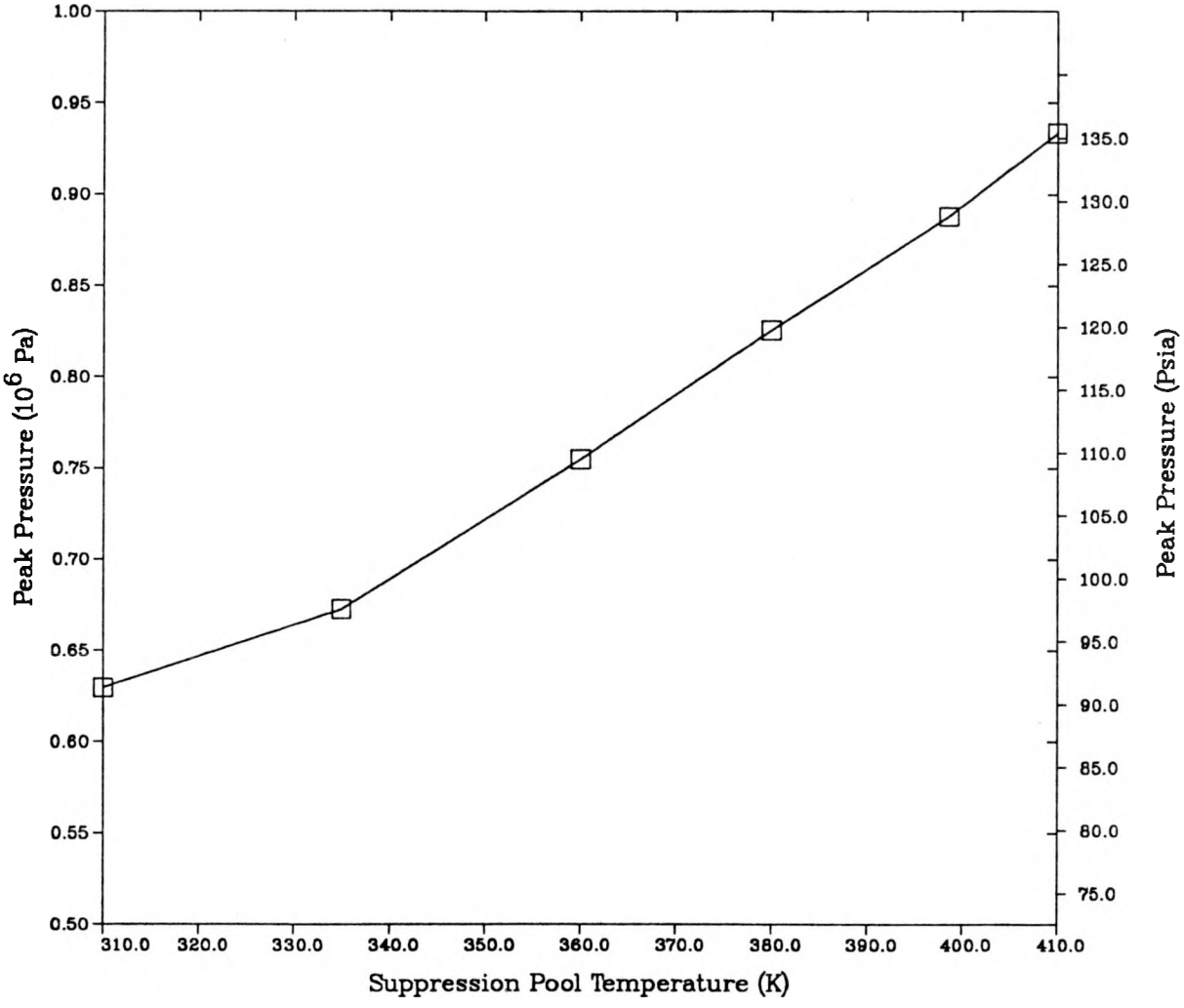

Figure 3-17. Drywell Peak Pressure Sensitivity to Pool Temperature

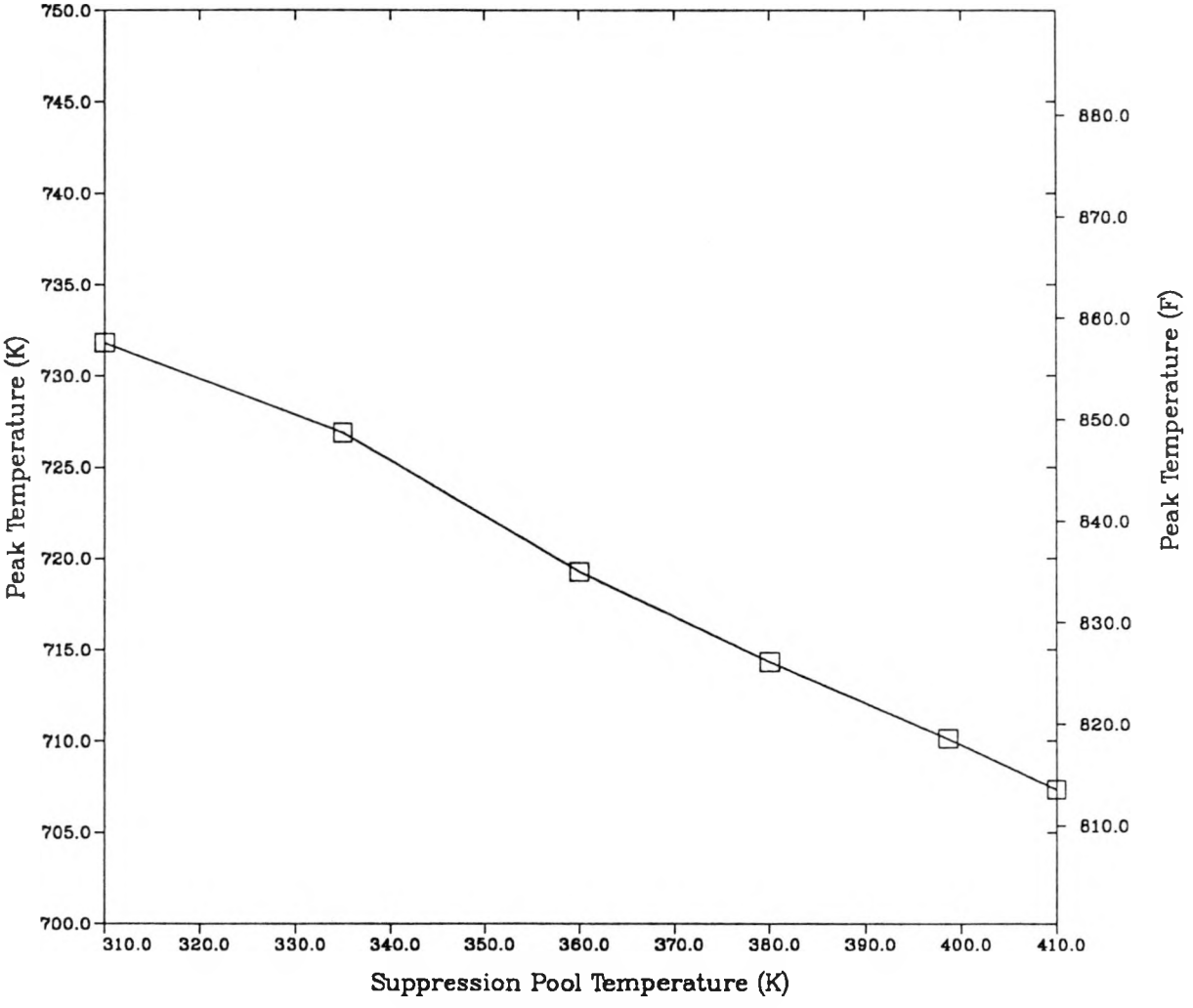

Figure 3-18. Drywell Peak Temperature Sensitivity to Pool Temperature

3.4.7 Bubble Relative Humidity Sensitivity Study

The MELCOR model for the interactions of bubbles rising in a pool allows the user to specify the relative humidity of vapor within the bubbles as the bubbles leave the pool. This parameter directly affects the amount of steam condensed by the pool. Since the gases are being cooled by the pool and steam is condensing, the actual humidity would be expected to be near saturation. Consequently, the MELCOR default value for the relative humidity is 99%. In many previous calculations with other codes (e.g., Refs. 4, 5), it was assumed that the steam within the bubbles was completely condensed and only dry noncondensible gases would be added to the wetwell atmosphere. Hence, in view of the importance of this parameter, the sensitivity of the containment response to variations in the bubble relative humidity was investigated.

The peak drywell pressures are shown as a function of the relative humidity in Figure 3-19. The base case used a relative humidity of 99% and a suppression pool temperature of 399 K. The relative humidity was varied from 0 to 99%. The assumption that the steam was completely condensed (0% relative humidity) resulted in a lower prediction of the peak pressure by 6.4% The peak temperature was relatively insensitive to the humidity.

The sensitivity of the containment response was also investigated at a lower suppression pool temperature of 310 K. As expected, the sensitivity to the relative humidity was much less significant for the colder pool temperature because the colder pool was more effective in condensing steam, giving lower pressure rises even with a higher relative humidity. The peak pressure change was only 0.5%.

3.4.8 Suppression Pool Bypass Sensitivity Study

The effectiveness of the suppression pool in reducing the pressure spike at vessel failure was investigated by using an option in MELCOR that prevents any interaction between the bubbles and the pool, effectively resulting in a complete bypass of the pool. The base case with a break area of 0.0079 m^2 and the case with a 1.0 m^2 break area were studied.

The peak drywell pressure for the 0.0079 m^2 break area calculation increased 14% from 0.89 to 1.02 MPa. The peak pressure for the calculation with the 1.0 m^2 area increased 20% from 0.98 to 1.18 MPa. The 1.0 m^2 break area pressures are compared in Figure 3-20. If a partial bypass were to occur, the result should be bounded by these two calculations.

3.4.9 In-Vessel Hydrogen Content Sensitivity Study

The effect of the in-vessel hydrogen content on the reactor vessel depressurization and containment response was studied using a calculation with no in-vessel hydrogen and one with 22 kg, which is double the base

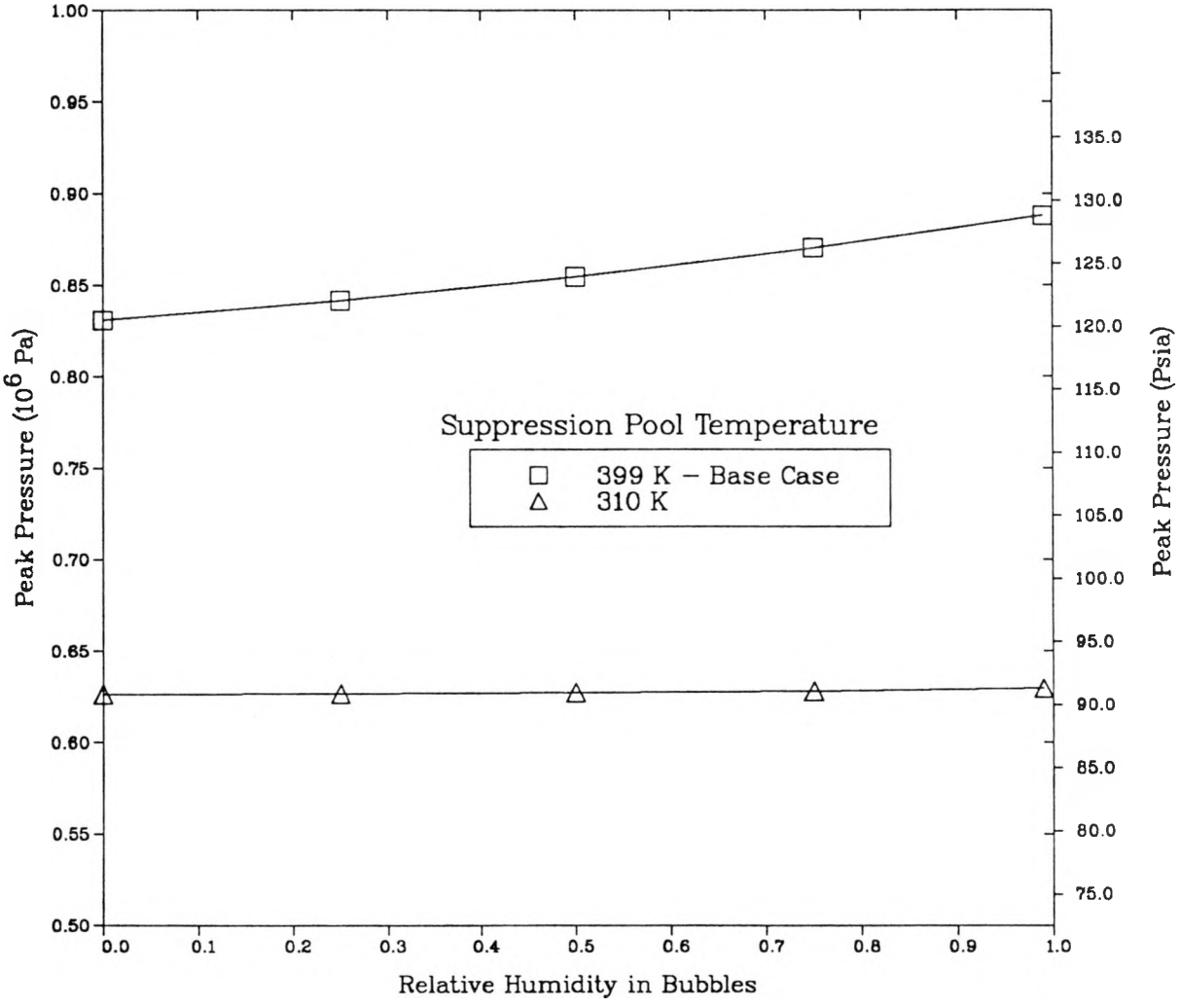

Figure 3-19. Drywell Peak Pressure Sensitivity to Bubble Relative Humidity

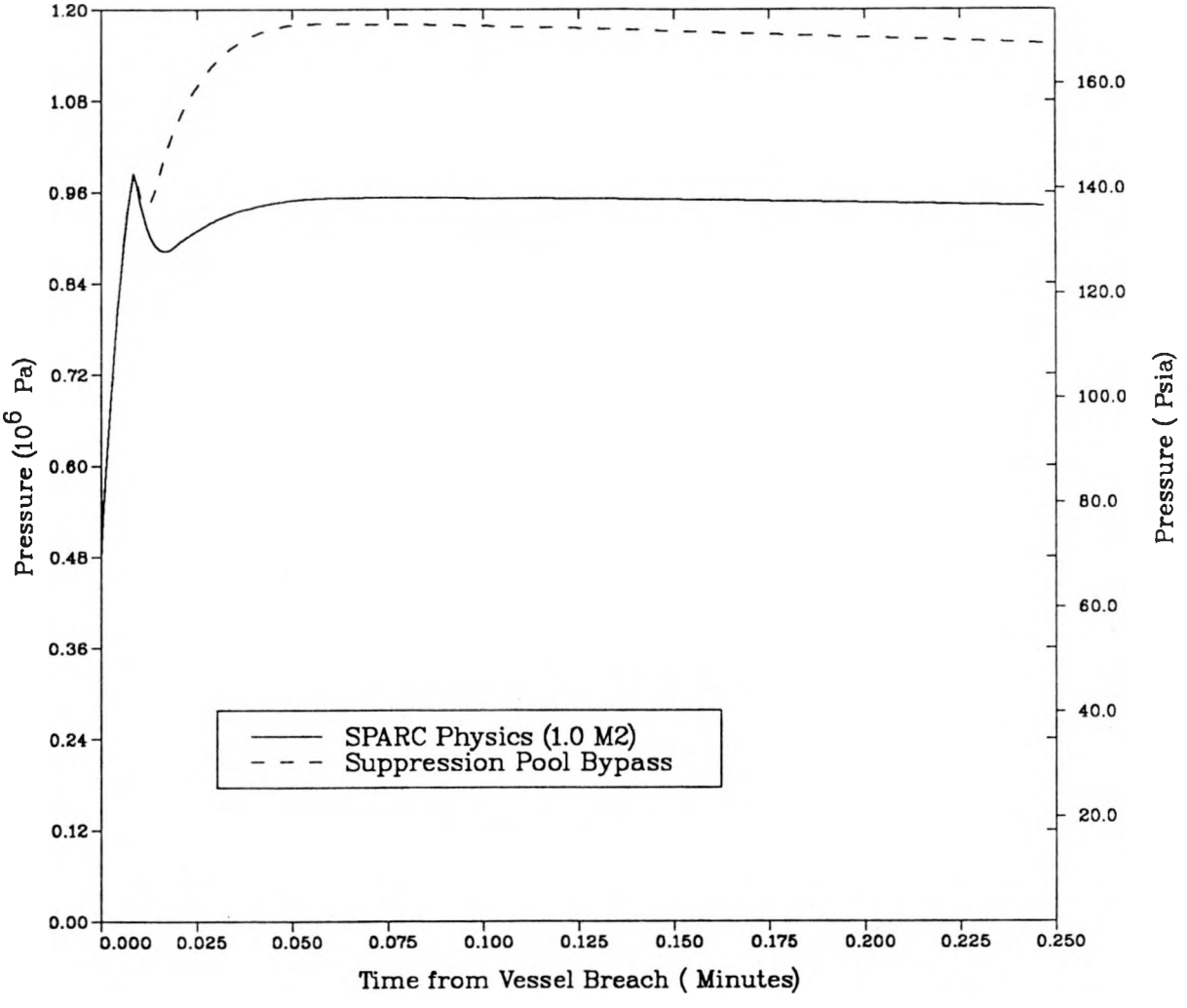

Figure 3-20. Drywell Pressure Sensitivity to Suppression Pool Bypass

calculation hydrogen. The peak pressures of the zero and double hydrogen cases differed by only 2810 Pa and the peak temperatures by only 0.07 K. The hydrogen content had very little effect. At the time of lower head failure, the base calculation had predicted 569 kg, but only 11 kg of this remained in the vessel because the hydrogen was generated much earlier than the time of vessel failure.

3.4.10 Melt Progression Sensitivity Study

The containment response is very dependent upon the core oxidation, melting, and relocation processes. These processes determine the amount of hydrogen produced, the in-vessel gas temperatures, and the conditions within the containment before lower head failure. Currently there are significant uncertainties in the core melt progression processes. Since the models are complex and not easily changed by means of user input, an exhaustive sensitivity study is not practical at this time. Only a limited sensitivity study was performed for the short-term station blackout scenario.

The sensitivity calculation differed from the base short-term station blackout calculation in that the melting temperature for the zircaloy cladding and structures was increased from the default value of 2098 K to 2700 K. (The zircaloy equation of state was adjusted accordingly.) These changes effectively maintained the core in intact geometry for a longer period of time and thereby increased the quantity of hydrogen produced.

The drywell pressure and temperature for this calculation are compared to those of the base calculation in Figures 3-21 and 3-22. The hydrogen produced in this calculation was 1092 kg compared to the base calculation of 609 kg which increased the containment pressure at lower head failure from 0.30 to 0.41 MPa. The peak pressure was 0.75 MPa compared to 0.59 MPa for the base calculation.

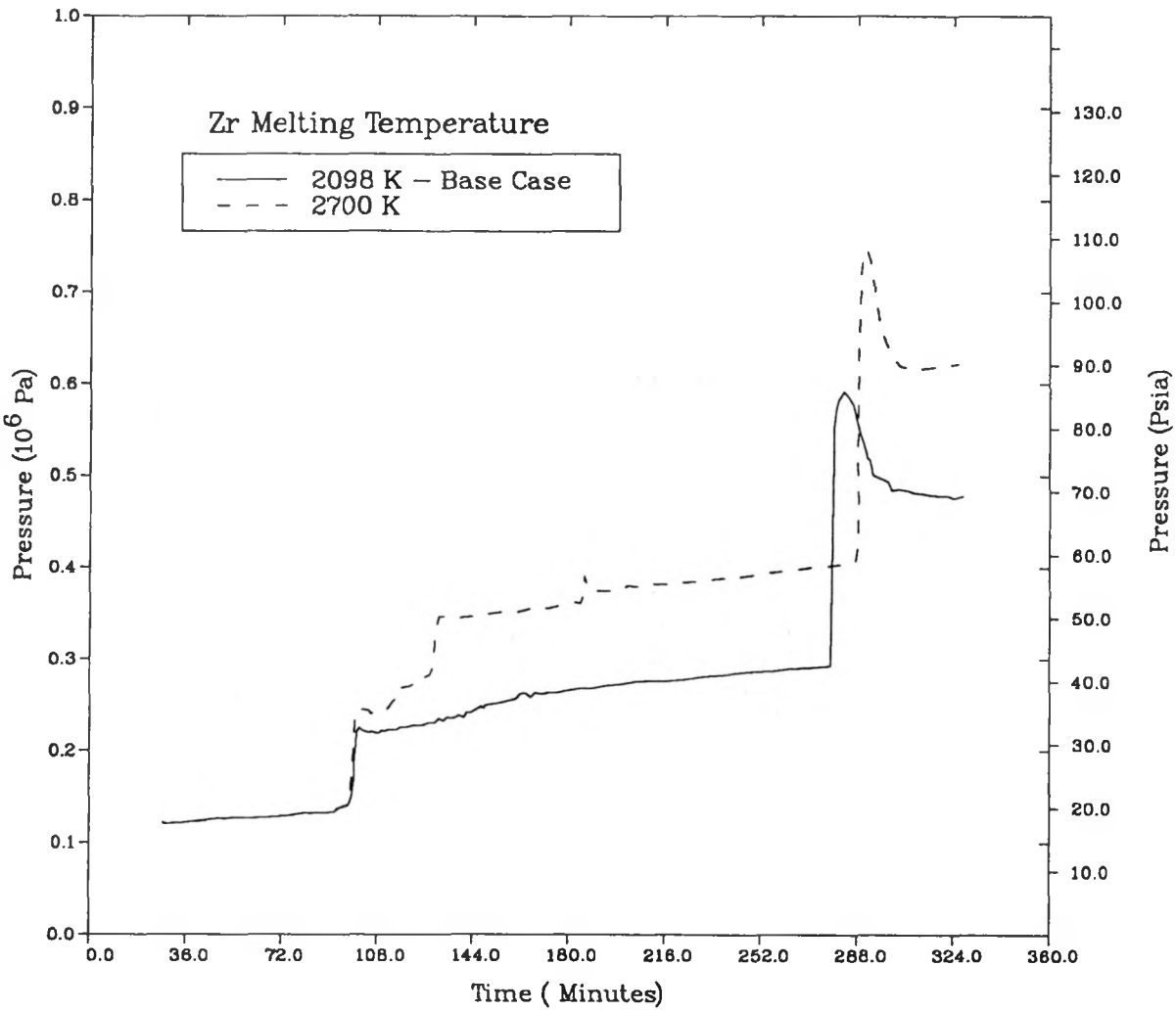

Figure 3-21. Short Term Drywell Pressure Sensitivity to Core Melt Models

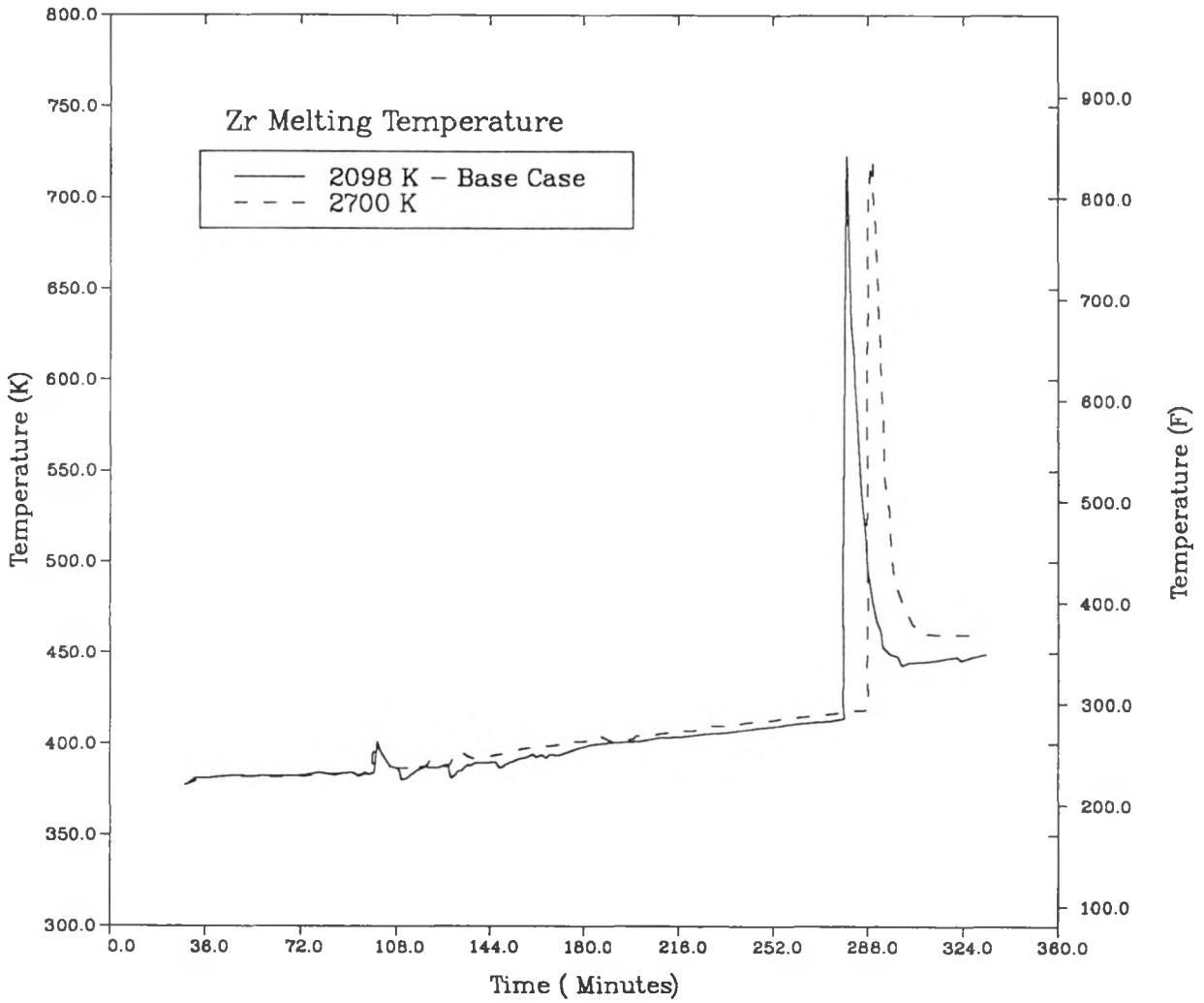

Figure 3-22. Short Term Drywell Temperature Sensitivity to Core Melt Models

4. LaSALLE ANALYSES

The thermal environment in the LaSalle reactor building resulting from steam blowdown from the containment was determined to assess the likelihood of equipment surviving during venting or following containment failure. In addition, scoping calculations of a station blackout scenario were performed to provide guidance for future LaSalle calculations and for other modeling.

4.1 Brief LaSalle Description

LaSalle is a BWR/4 reactor with a Mark II containment. The LaSalle containment, shown in Figure 4-1, consists of a drywell region surrounding the RPV and a wetwell region that is directly below the drywell. The wetwell region contains a suppression pool designed to limit containment pressurization by condensing steam from RPV releases. RPV releases that pass through the SRVs exhaust directly to the suppression pool. Releases through RPV breaks enter the drywell first, then pass through vertical downcomers in the drywell floor, and finally exhaust into the suppression pool. Vacuum breakers allow gas flow from the wetwell to the drywell to relieve any pressure differential that may develop.

The pedestal geometries for the existing Mark II containments are all quite different and these differences can have a significant impact on the accident progression after vessel breach. All of the Mark II containments have an upper pedestal region in the drywell that is separated from a lower pedestal region in the wetwell by the drywell floor. In the LaSalle plant, there are drain lines in the floor of the upper pedestal that pass through the lower pedestal to carry water collected in sumps in the upper pedestal during normal operation out of containment for reprocessing. As will be discussed in Section 4.3, these drain lines are an important consideration for the accident progression analysis at LaSalle because they allow molten debris to be relocated from the upper pedestal to the lower pedestal shortly after the debris is ejected onto the drywell pedestal floor.

A schematic of the LaSalle reactor building and associated regions is shown in Figure 4-2. The upper levels of the reactor building are relatively open, but the lower levels are divided into smaller rooms. The two basement levels of the reactor building house most of the safety-related equipment. Each basement level consists of an annular raceway region surrounding the wetwell and four corner rooms separated from the raceway by normally-closed doors and smaller openings. One of the corner rooms houses the high pressure core spray (HPCS) and control rod drive (CRD) systems, a second corner room houses the low pressure core spray (LPCS) and reactor core isolation cooling (RCIC) systems, and the remaining two rooms house the low pressure coolant injection (LPCI) system. HVAC systems are provided for all four corner rooms.

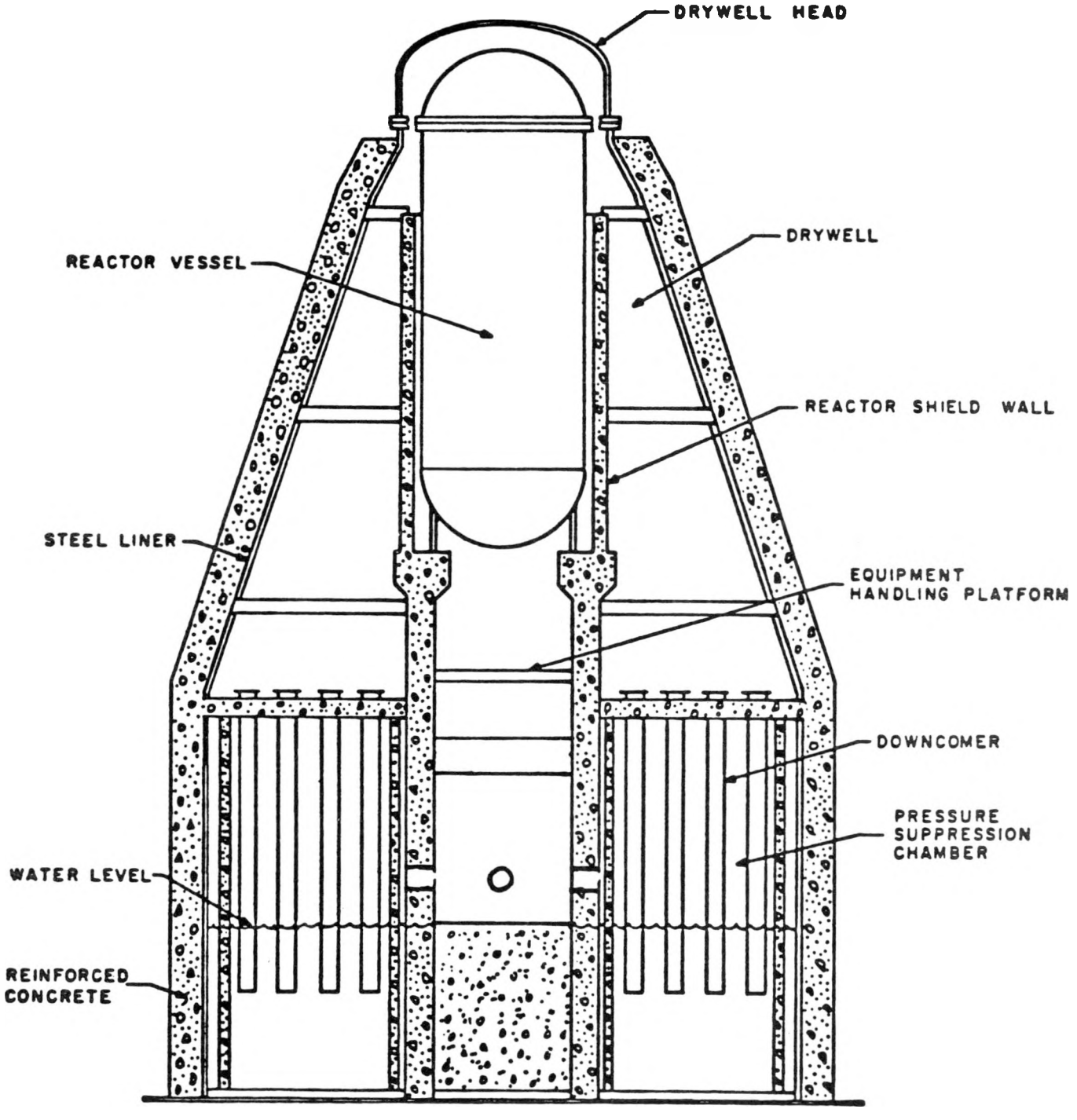

Figure 4-1. LaSalle Containment Schematic

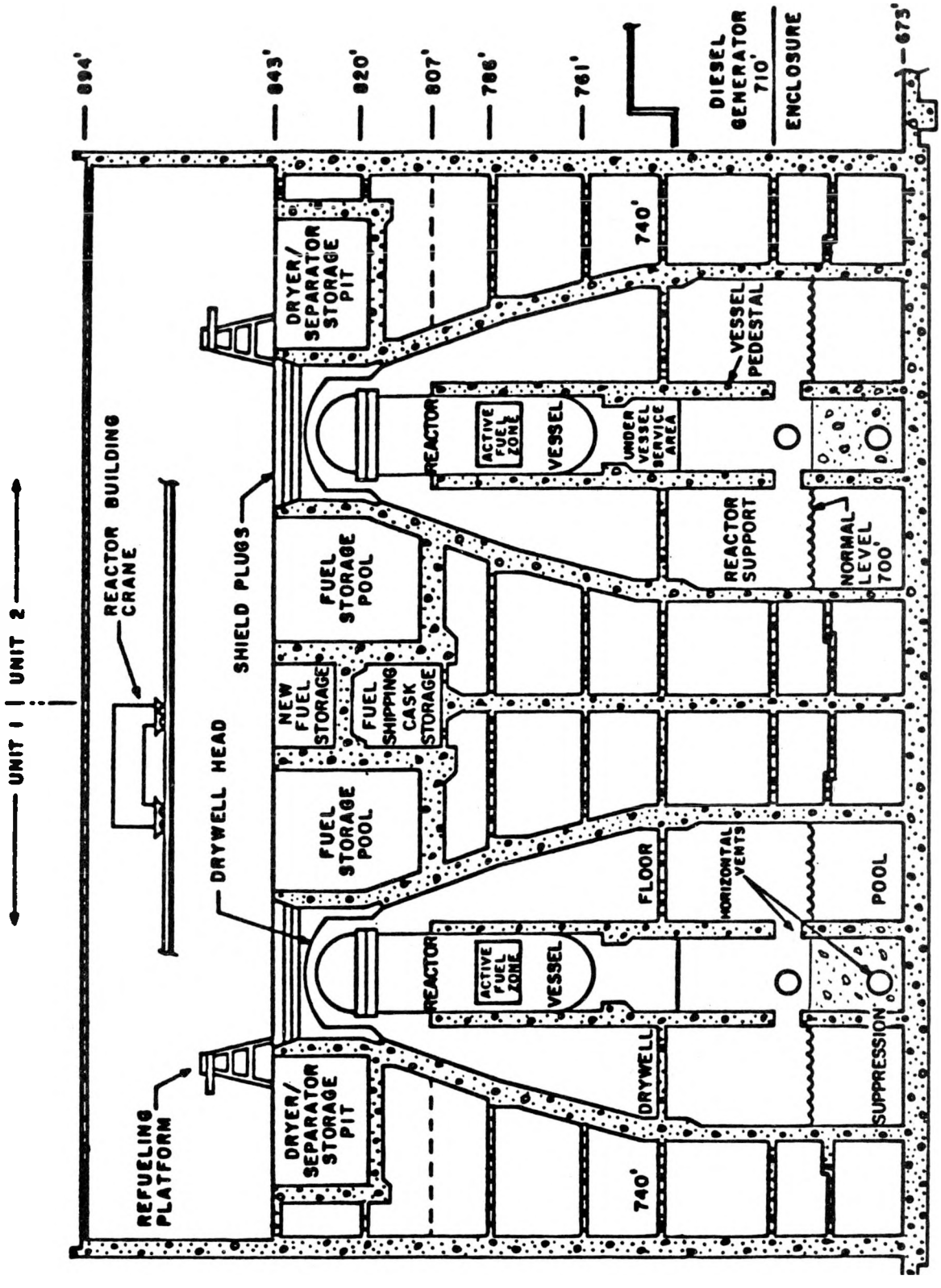

Figure 4-2. LaSalle Reactor Building Schematic

The raceway vents to a steam tunnel through check valves on the upper basement level. The steam tunnel extends up the full height of the auxiliary building and exhausts to the environment through a blowout panel located on top of the auxiliary building roof.

The two LPCI corner basement rooms are separated from the upper reactor building levels by doors, while the other two corner rooms have open stairwells up to the ground level floor. The raceway is only connected to the upper levels through relatively small openings, and as mentioned previously, the corner rooms and raceway are connected by normally-closed doors and small openings. If all of these doors remained intact during a blowdown to the reactor building, the basement rooms would be fairly well isolated from the upper regions, with some flow entering the dead-ended corner rooms with open stairwells. If enough doors open to allow circulation through a corner room, to the raceway, and out to the steam tunnel, a much more severe environment could occur in that region.

The upper levels of the reactor building are fairly open, with the exception of various dead-ended rooms at each level. Most of the flow between the levels occurs through stairways and equipment hatches located at two opposite corners of the reactor building.

The reactor building is separated from the refueling floor above it by a covered equipment hatch and a normally-closed door. The reactor building connects to the reactor building of the second unit at LaSalle through normally-closed doors at almost all of the upper reactor building levels. The refueling floor extends across both reactor buildings.

The LaSalle containment can be vented through either 2 inch or 18 inch diameter lines from either the drywell or wetwell. However, only the 18 inch lines are sufficiently large to relieve containment pressurization in scenarios with loss of containment heat removal. The 18 inch lines from the drywell and wetwell combine into a single 18 inch diameter line which then exhausts into the standby gas treatment system (SGTS). However, connections between the venting system piping and SGTS fan would not be expected to withstand this venting load, so the vented flow would be discharged into the upper region of the reactor building.

4.2 Steam Flooding of Reactor Building

Steam flooding of the reactor building is of concern in several types of sequences that have been identified for LaSalle. In some of the accident progressions, core cooling is initially available but containment heat removal has failed. For these scenarios, the containment pressurizes because of decay heat until either the operator vents the containment (at 515 kPa (75 psia)) or the containment fails from over-pressure (currently predicted at about 1450 kPa (210 psia)). Because of the weaknesses in the venting system discussed in Section 4.1, vented steam would be released into the top floor of the reactor building, just under the refueling floor. Containment failure in the wetwell or drywell would

also release steam to any of a number of locations in the reactor building. Because many of the components of the core cooling systems are located in the lower levels of the reactor building, the systems might fail because of the severe environments, and core damage ensue.

A detailed MELCOR model was constructed for the reactor building for analyzing the thermal-hydraulic conditions during steam blowdown. A description of the model is included in Appendix A and the nodalization is shown in Figure 4-3. Sufficiently-detailed nodalization was used to capture the characteristics of the building that will determine the flow patterns for areas where important equipment is located. Also, adequate representation of doors and blowout panels was necessary because the flow patterns can be greatly affected if normally-closed flow paths are opened during the transient. Slight differences in opening pressure differentials will determine the exact configuration of flow paths for the various scenarios analyzed.

Venting containment through a .46 m (18") line from the wetwell to the top of the reactor building and through 2 sizes of drywell breaks (.10 m (4") diameter and .65 m^2 (7 ft^2)) were studied. Modeling sensitivities were studied with four variations of the venting calculation: (1) with 5 times the nominal equipment mass, (2) with twice the rated heat removal rate for the room coolers, (3) with the vent area reduced to half its base value, and (4) with a blowout panel modeled from the refueling floor to the environment.

The reactor building pressure for the .10 m (4") drywell break is shown in Figure 4-4. The early pressurization opened one of the doors to Unit 1 and the door to the refueling floor, but the blowdown was not large enough to open paths to the environment by either failing the walls of the refueling floor or opening the blowout panel at the top of the steam tunnel. The pressurization was relieved through leakage paths, the SGTS, and condensation on structures. Since the flow was not being forced through the steam tunnel, little steam was drawn down into the ECCS rooms in the basement. The reactor building heatup was relatively gradual as shown by the temperatures plotted in Figure 4-5 and listed in Table 4-1.

Because of the larger blowdown, the pressurization was much more severe for the .65 m^2 (7 ft^2) drywell break than for the 0.10 m break, as shown in Figure 4-6. All doors and blowout panels were forced open except for three of the doors between the raceway and corner rooms in the basement. With the refueling floor failed, most of the blowdown was carried upward through the reactor building rather than being pushed down through the basement and out through the steam tunnel. However, there was sufficient flow down into the basement rooms to cause considerable heatup as shown in Figure 4-7 and Table 4-1.

For the .46 m (18") wetwell vent case, the steam entered near the top of the reactor building at the failure point in the SGTS. Since the release

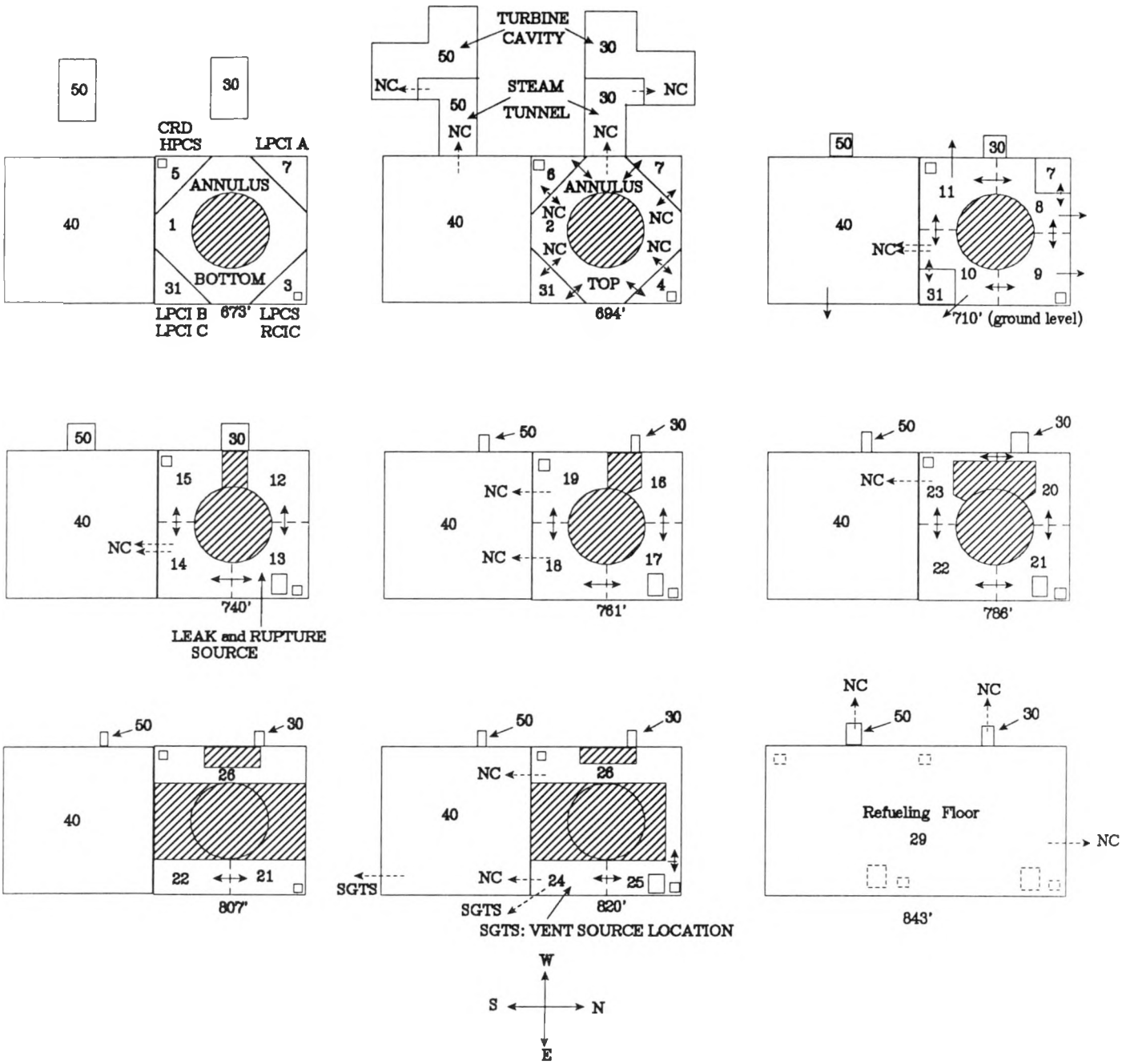

Figure 4-3. MELCOR Nodalization for LaSalle Reactor Building

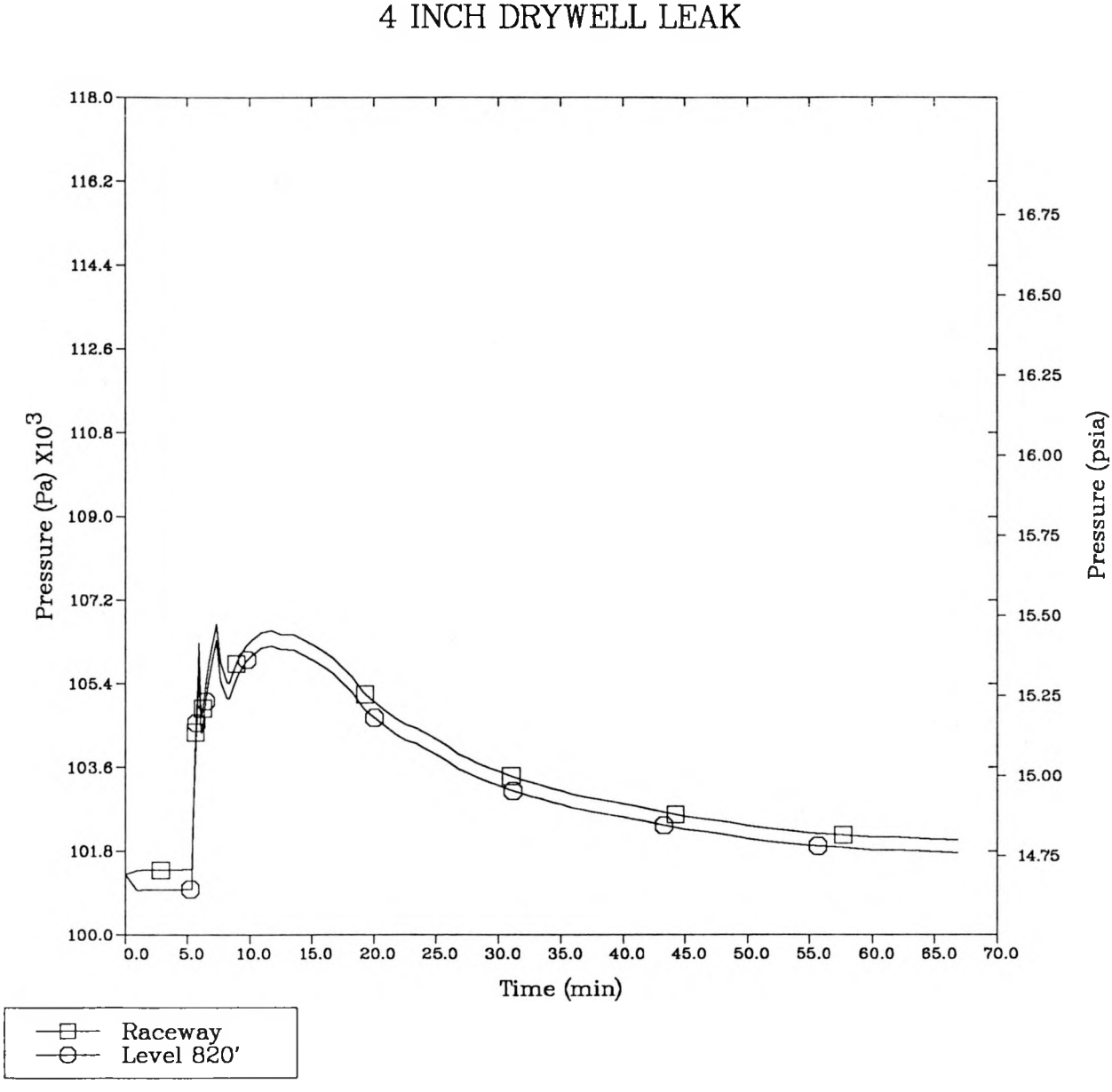

Figure 4-4. Reactor Building Pressures for 4" Drywell Leak

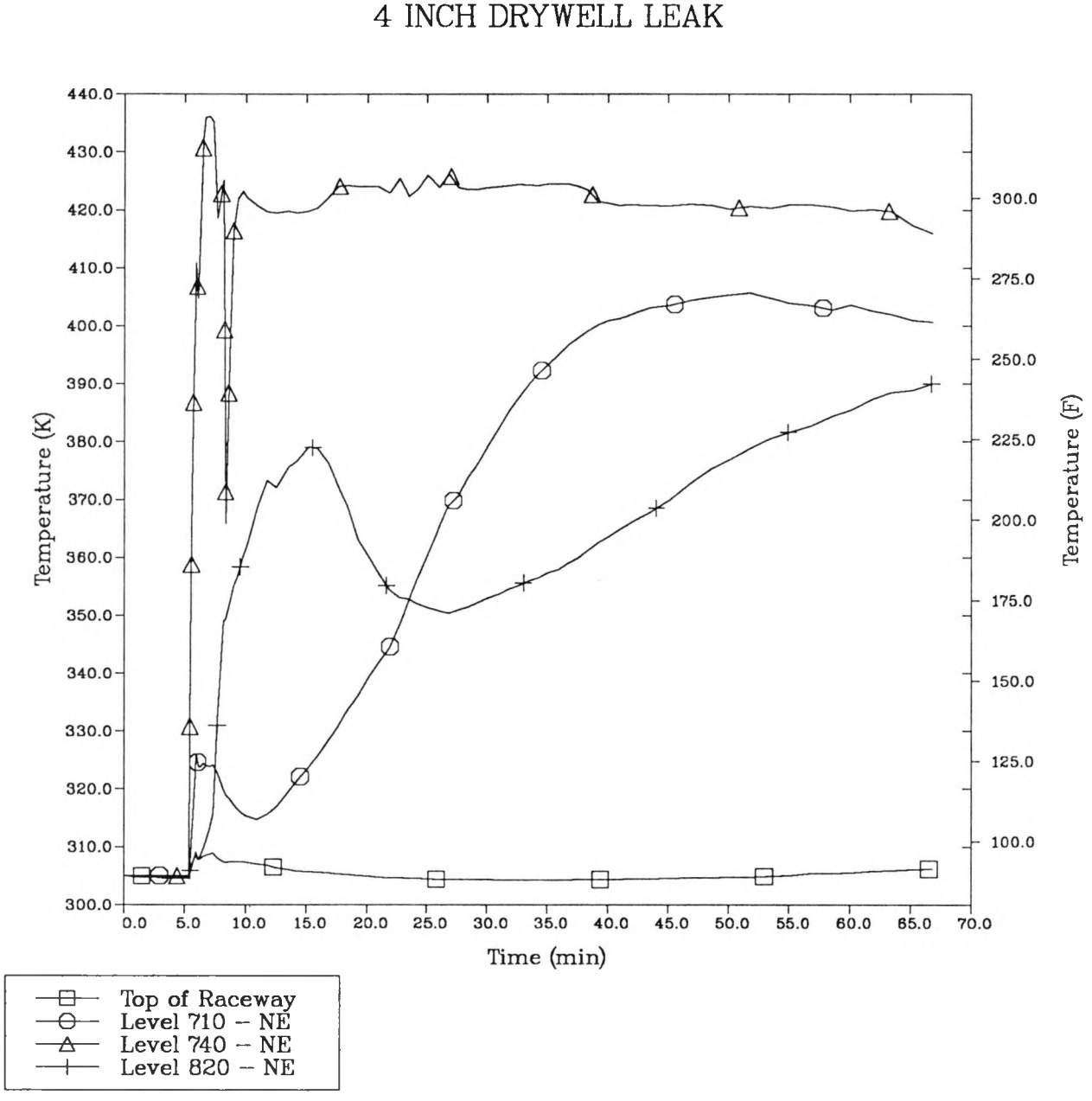

Figure 4-5. Reactor Building Temperatures for 4" Drywell Leak

Table 4-1

Reactor Building Temperatures

Base Cases Temperatures (K)

Control Volume	.10 m (4") Leak		.46 m (18") Vent		.65 m^2 (7 ft^2) Rupture	
	Peak	Average	Peak	Average	Peak	Average
301	309	309	310	305	320	305
302	309	305	390	390	415	415
303	320	315	375	380	355	345
304	330	325	395	390	380	375
305	309	309	315	308	325	308
306	313	310	390	390	420	420
307	305	297	400	390	373	373
308	365	365	415	390	430	415
309	405	400	420	390	430	415
310	365	365	395	390	430	415
311	395	390	390	390	430	415
313	435	420	410	395	435	410
317	420	415	410	395	435	410
321	400	390	410	395	410	410
324	345	340	415	395	410	410
325	390	390	420	395	400	400
331	305	299	390	390	420	420

Sensitivity Cases Temperatures (K)

Control Volume	5 * Steel Mass		2 * Rated Fan Cooler Q		.5 * Vent Area		Refuel Floor Blowout	
	Peak	Avg	Peak	Avg	Peak	Avg	Peak	Avg
301	310	305	310	305	310	305	310	305
302	390	390	390	390	385	385	385	385
303	375	375	370	370	355	355	370	370
304	395	395	380	380	375	375	390	390
305	310	310	310	300	310	310	310	310
306	385	385	380	380	380	380	360	360
307	400	395	390	385	310	300	310	300
308	420	390	415	395	350	350	395	395
309	420	390	420	395	390	390	410	395
310	390	390	395	395	380	380	375	375
311	385	385	385	385	380	380	365	365
313	415	395	415	400	400	400	405	400
317	410	395	410	400	415	400	400	400
321	410	395	410	400	415	400	400	400
324	420	395	415	400	415	400	415	400
325	425	395	420	400	425	400	420	400
331	385	385	385	385	310	300	310	300

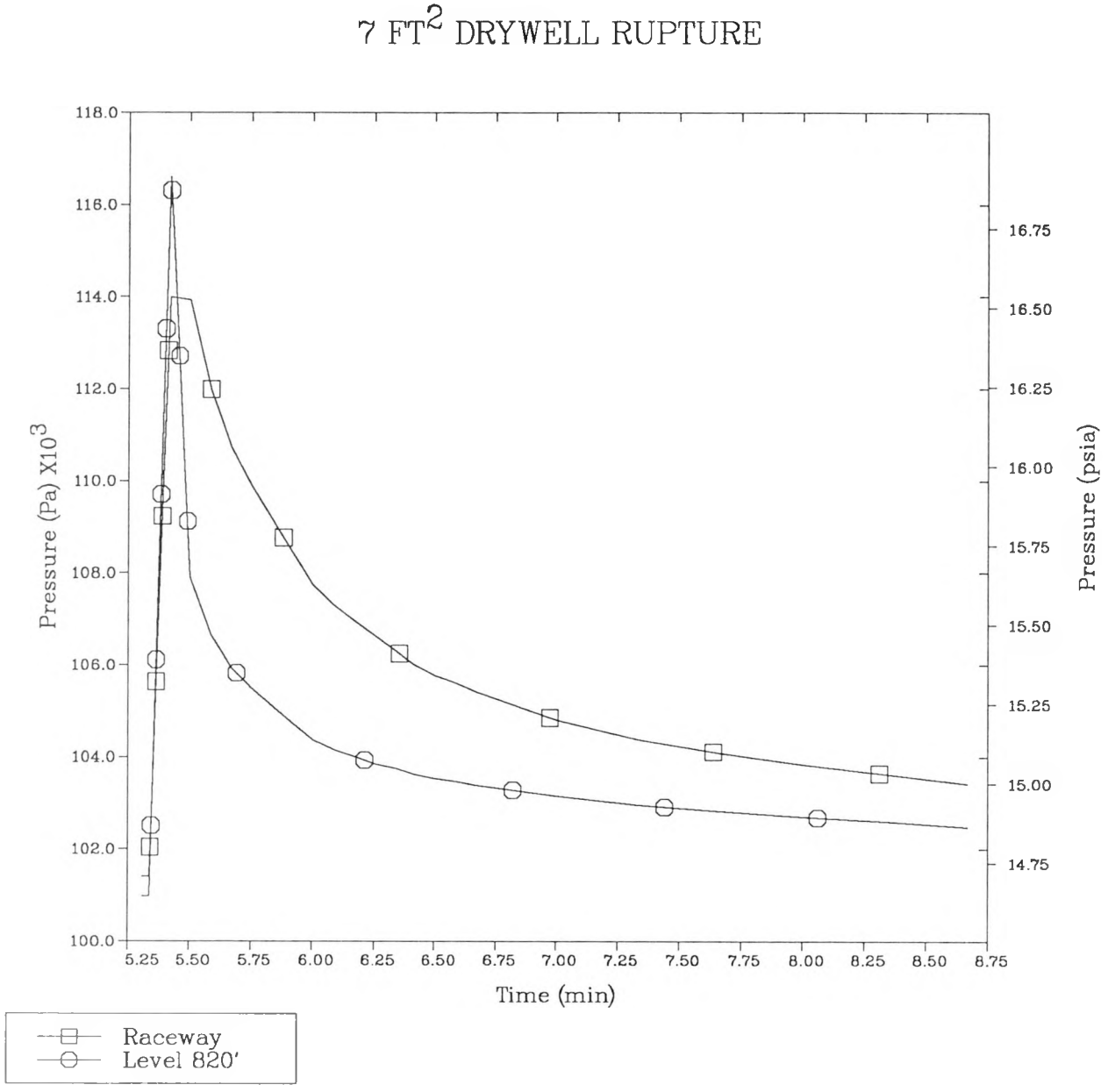

Figure 4-6. Reactor Building Pressures for 7 ft² Drywell Rupture

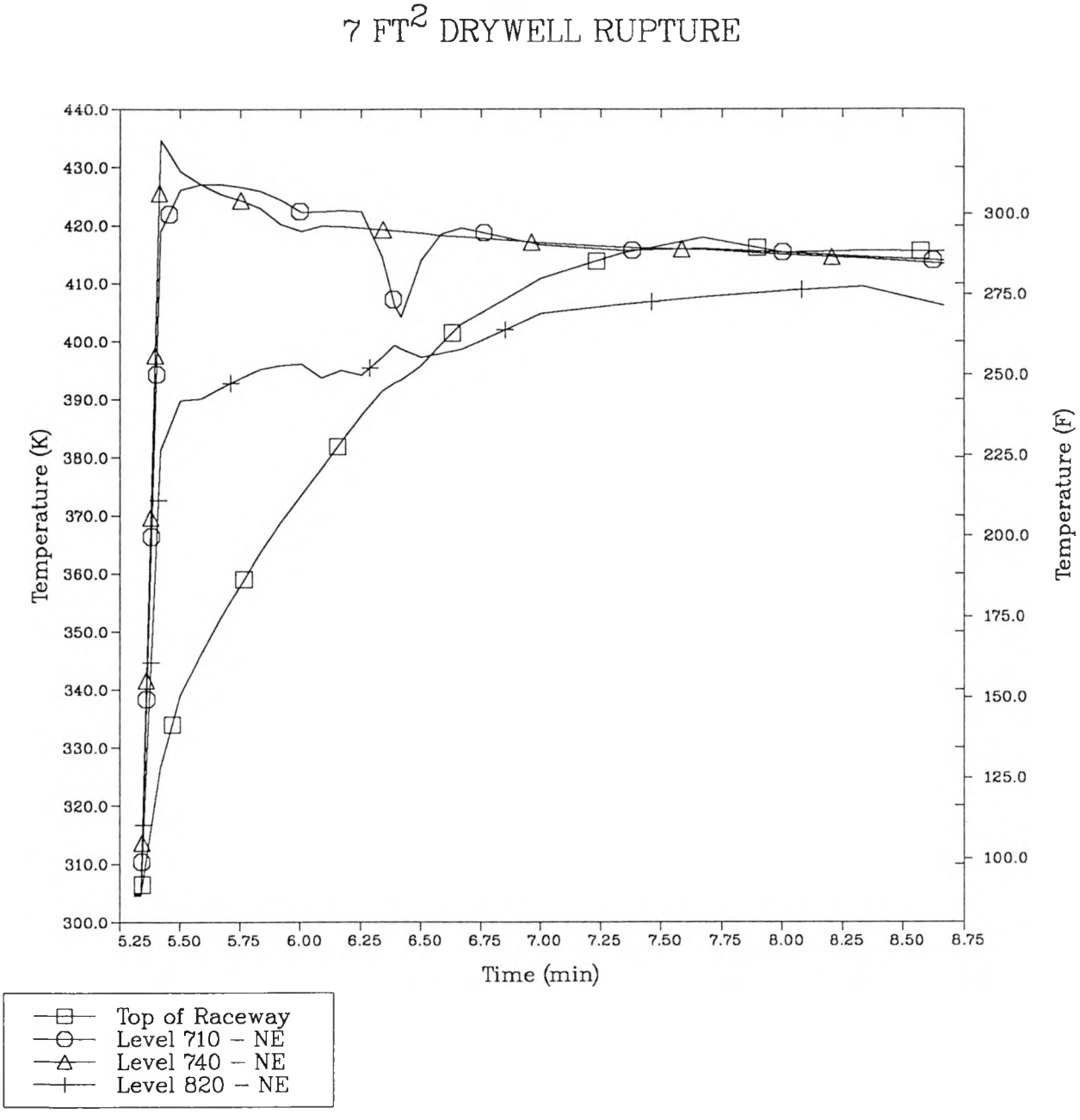

Figure 4-7. Reactor Building Temperatures for 7 ft² Drywell Rupture

point was higher than in the cases with drywell breaks, the potential existed for a less severe environment in the lower reactor building levels which house most of the safety-related equipment. The pressurization from the blowdown opened three of the upper doors to Unit 1, the door to the refueling floor, and the steam tunnel blowout panel, but the walls of the refueling floor were not predicted to fail. Thus, the majority of the steam was drawn down through the basement, then into the steam tunnel before exhausting to the environment. As a result relatively high temperatures were predicted in the basement rooms, as shown in Figure 4-8 and Table 4-1, even though the steam release point was high in the reactor building.

Only minor differences from the base case results were calculated for two variations of the .46 m (18") vent case. A variation with increased steel surface area was virtually identical to the base case, with pressures and temperatures being only slightly reduced. Using twice the rated heat removal for the room coolers also had negligible effect on the pressures and on the temperatures in all rooms except those directly connected to the room coolers. As seen in Table 4-1, the peak and average temperatures in those rooms were reduced on the order of 5-10 K.

For the case using half the blowdown rate, the peak pressure was reduced by about 5 kPa (3/4 psig) at the top of the reactor building and decreased back to atmospheric pressure at about twice the rate of the base case. The smaller blowdown caused a much slower heatup of most of the reactor building, but by the end of the calculation, the temperatures were approaching the same level as in the base case. The largest differences were seen in the LPCI room response. With the lower blowdown rate, the doors to this room did not blow open, giving a more restricted path for steam flow into the room. Therefore, the temperatures remained nominal in the room.

In another sensitivity case, the blowout panel from the refueling floor to the environment opened almost immediately. This additional opening relieved the pressure more quickly than in the base case, resulting in about a 5 kPa (3/4 psig) reduction in peak pressure and a more rapid return to atmospheric pressure. About 2/3 of the steam went out through the refueling floor level, reducing the amount of steam being drawn down to lower levels and out the steam tunnel. Therefore, the response in the lower portions of the building resembled the response for the case with reduced vent flow area. However, the venting of steam through the refueling floor opening resulted in a change in the flow patterns such that flow was mainly directed down through the equipment hatch with less circulation around each level. This can be observed by examining the room temperatures in Table 4-1.

For all of the cases examined, the upper regions of the reactor building were relatively well-mixed. For the .10 m (4") drywell leak case, the blowout panel in the steam tunnel did not open, so the basement rooms were buffered from the blowdown and remained relatively cool. For the

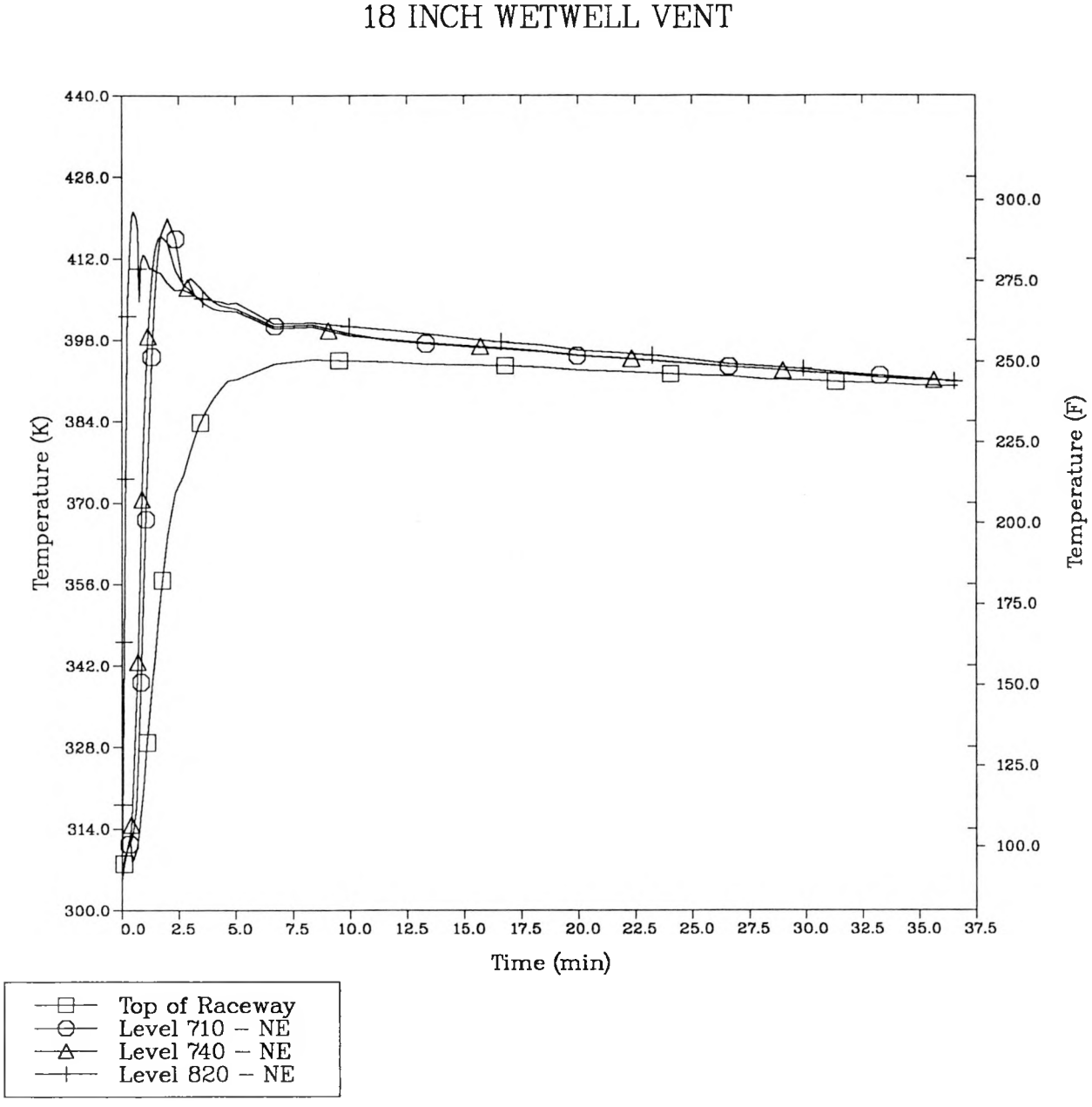

Figure 4-8. Reactor Building Temperatures for 18" Wetwell Vent Case

.46 m (18") vent case, the steam tunnel blowout panel opened, but the walls of the refueling floor did not fail. As a result, steam was drawn down into the basement rooms, giving higher temperatures. For the .65 m^2 (7 ft^2) rupture case, the steam tunnel blowout panel was opened and the walls of the refueling floor failed. Although this allowed some of the steam to flow up through the reactor building, a substantial amount was still drawn down into the basement rooms, resulting in relatively high temperatures. Sensitivity calculations for the .46 m (18") vent case showed that heat transfer uncertainties were much less significant than uncertainties regarding possible flow path configurations.

4.3 Preliminary Station Blackout Analysis

A station blackout calculation was performed to give preliminary estimates of the core melt progression and to examine various modeling options. The model used for the calculation and the modeling insights gained from it are discussed in this section. A detailed description of the deck is included in Appendix A; a brief description is given here.

4.3.1 Nodalization

The nodalization for the LaSalle station blackout calculation is shown in Figure 4-9. The RPV was modeled in detail for both the core and thermal-hydraulic calculations to represent axial and radial variations within the core region that were expected to significantly affect core heat transfer, blockage, and oxidation. The core region was divided into twelve control volumes, consisting of six channel and six bypass volumes. Four additional control volumes were used to model the rest of the RPV. The core itself was modeled by six radial rings and thirteen axial levels. Fine axial divisions were used near the core plate for modeling core inlet blockage and core plate response. Separate nodes were used for the non-fueled regions above and below the active fuel region.

The containment was modeled using 5 control volumes: drywell, upper pedestal, lower pedestal, downcomers, and wetwell. The reactor building model used for the calculations discussed in Section 4.2 was collapsed down because the results of those calculations showed that the upper regions of the reactor building were well-mixed, justifying a simpler nodalization. Six volumes were used: Unit 2 upper reactor building, Unit 2 basement rooms, Unit 2 steam tunnel, Unit 1 reactor building, Unit 1 steam tunnel, and refueling floor.

The modeling related to core-concrete attack was quite different from previous analyses performed for other plants because of the unusual geometry at LaSalle. For this plant, the core debris would initially fall onto the drywell pedestal floor following vessel breach. However, the molten debris could flow into the sump drain lines, and shortly thereafter the melt could fail the lines, flowing out onto the wetwell pedestal floor. This would move the location of the core-concrete attack

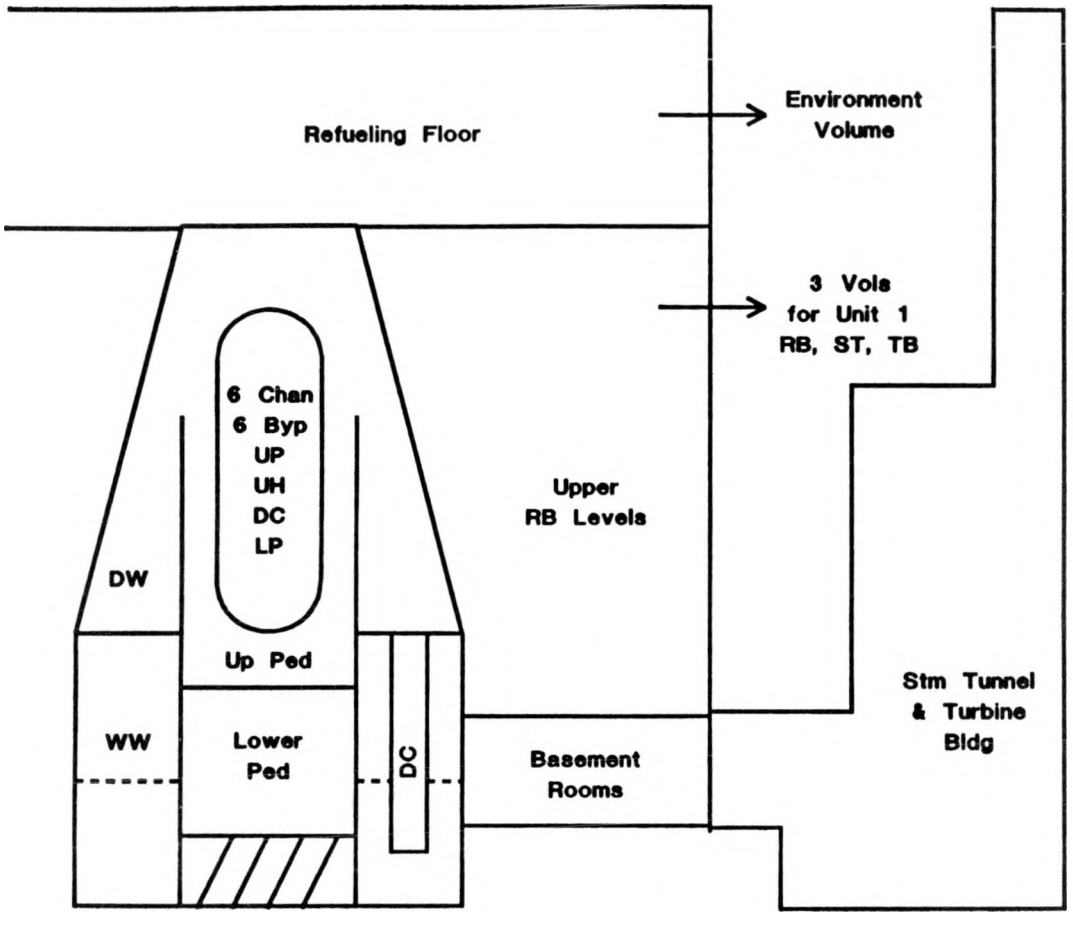

Figure 4-9. MELCOR Nodalization for LaSalle Integral Calculation

and would open a direct path between the drywell and wetwell. Because of the short time expected before failure of the drain lines (20 minutes or less), the initial core-concrete attack in the drywell pedestal was neglected and the corium was moved directly into the wetwell pedestal cavity. Flow path input was selected to direct the gases generated by core-concrete attack to the drywell during this period, however. The area of the flow path between the lower and upper pedestals was set to the full cross-sectional area and the area of the flow path between the lower pedestal and the wetwell was set to 0. At 20 minutes, when the drain lines were expected to fail, the flow area between the lower and upper pedestals was reduced to represent 2 failed drain lines and the flow area between the lower pedestal and wetwell was set to the area of the opening in the pedestal.

An additional cavity modeling concern arose because initial LaSalle calculations predicted temperatures above melting for the drywell pedestal steel liner. This steel, as well as the steel in the sump tank and gratings would be expected to melt, flow down to the cavity, and mix with the debris attacking the concrete. The additional steel would affect the progression of the core-concrete attack. Since MELCOR does not include modeling for melting heat structures, the effect was approximated by including all of this steel in the wetwell pedestal cavity, in the core-concrete attack modeling, from the beginning of the calculation.

4.3.2 In-Vessel Response

Table 4-2 summarizes the predicted timing of key events for the LaSalle station blackout calculation. The calculation began with the water level at TAF using initial conditions from an existing calculation that had been performed with the LTAS code to obtain timing information for the LaSalle core damage frequency analysis for RMIEP. About 35 minutes later, core material consisting mainly of zircaloy and steel began melting and relocating down to lower elevations. Most of the material was predicted to refreeze on structures above the core plate, reducing the inlet flow areas for the core channel control volumes. The inlet to the inner channel became completely blocked at about 62 minutes, and by about 128 minutes, the inlets to the four inner channels were all completely blocked.

The LaSalle nodalization allowed a fairly detailed calculation of core inlet flow blockage caused by refrozen metals that candled down from above. This blockage has the effect of limiting the steam supply for zirconium oxidation of the fuel rod cladding and the canister inner surfaces and of reducing convective heat transfer inside the fuel rod bundles. Although flow blockage was calculated in individual channels, the oxidation process was not completely stopped for the affected channels because steam entered the core region from the upper plenum as the pressure relief valves opened and closed.

Table 4-2

Event Summary for LaSalle Station Blackout Calculation

Event	Time after Uncovering (min)*
Gap Release from Ring 1	37
Gap Release from Ring 2	37
Gap Release from Ring 3	40
Gap Release from Ring 4	50
Channel 1 Blocked	62
Channel 2 Blocked	70
Gap Release from Ring 5	71
Gap Release from Ring 6	83
Channel 3 Blocked	105
Channel 4 Blocked	128
Core Support Plate Failure in Ring 1	245
Core Support Plate Failure in Ring 2	245
Core Support Plate Failure in Ring 3	245
Lower Head Penetration Failure in Ring 2	392
Lower Head Penetration Failure in Ring 3	399
Lower Head Penetration Failure in Ring 1	401
Core-Concrete Interactions Begin	417
Core Support Plate Failure in Ring 4	419
Lower Head Penetration Failure in Ring 4	420
Core Support Plate Failure in Ring 5	445
Core Support Plate Failure in Ring 6	446
Lower Head Penetration Failure in Ring 5	447
Lower Head Penetration Failure in Ring 6	851

* Core uncovering was predicted at 36 minutes after accident initiation by the LTAS code.

Following clad relocation from the nodes, the fuel collapsed and settled downward, forming a debris bed above the blockages formed by refrozen material on the core plate. Since the blockages were mainly steel and zircaloy, there was little decay heat in them. In addition, MELCOR 1.7.1 did not model conduction heat transfer between debris and intact components. As a result, the core plate temperature was calculated to remain low enough that it could continue to support the debris resting on it. Although the possibility that the core plate could continue to support core debris could not be discounted, the core plate was artificially failed at 245 minutes for this calculation so that later phases of the accident could be investigated.

The nodalization used for the core region allowed natural circulation to be calculated. However, the effect of this natural circulation is not fully included in the core modeling for axial fluid temperature variation. Thus, it is recommended that future calculations use a

simplified model with a single volume for the channel region and a single volume for the bypass region until the MELCOR treatment of in-vessel natural circulation is improved.

The relatively long in-vessel debris holdup yielded a higher hydrogen production before vessel breach and higher in-vessel structure temperatures than had been seen in previous calculations (Ref. 21). In Figure 4-10, the hydrogen production for this calculation is compared to the results from a previous analysis for the same sequence which used a simpler nodalization and an earlier version of MELCOR. Shroud and vessel wall temperatures are plotted in Figure 4-11. The high temperatures indicate that failure of vessel structures may need to be included in future modeling.

A large portion of the water in the lower head was predicted to be boiled away as the debris fell through the core plate and quenched in the water pool. The remaining water was boiled away within the next 100 minutes, and about 45 minutes thereafter, lower head penetrations were predicted to heat sufficiently to fail. The lower head debris began melting and pouring out onto the pedestal floor about 25 minutes after lower head failure.

4.3.3 Ex-Vessel Response

The containment pressure is shown in Figure 4-12. Before vessel breach, the pressures increased steadily because of steam and hydrogen addition from RPV releases as well as degassing from the hot concrete structures in the containment. The pressure rise that was calculated at vessel breach is relatively small for the LaSalle containment, which is predicted to fail at 1.4 MPa. After vessel breach the containment pressure continued to climb because of gases generated from core-concrete attack and from continued degassing of the concrete structures. When the calculation was stopped at 1170 min, the containment pressure was still below the failure point.

Degassing of the concrete in containment had a significant impact on this calculation. Figure 4-13 shows the total amount of water and carbon dioxide generated by degassing compared to the amounts generated by core-concrete attack. This large amount of degassing added considerably to the containment pressurization. Since the LaSalle containment failure pressure is relatively high, containment failure was not predicted.

4.3.4 Summary of Insights

The MELCOR results for the LaSalle station blackout sequence indicate that modeling of non-fueled core cells, in-core natural circulation, and core plate heat transfer and failure can be very important. In particular, the results raise the possibility that the core plate may not fail by the normally assumed and modeled mechanism, that the transport of debris to the lower plenum could occur considerably later in time, and that heat transfer to (and possible failure of) the in-vessel heat structures and the reactor vessel could be important.

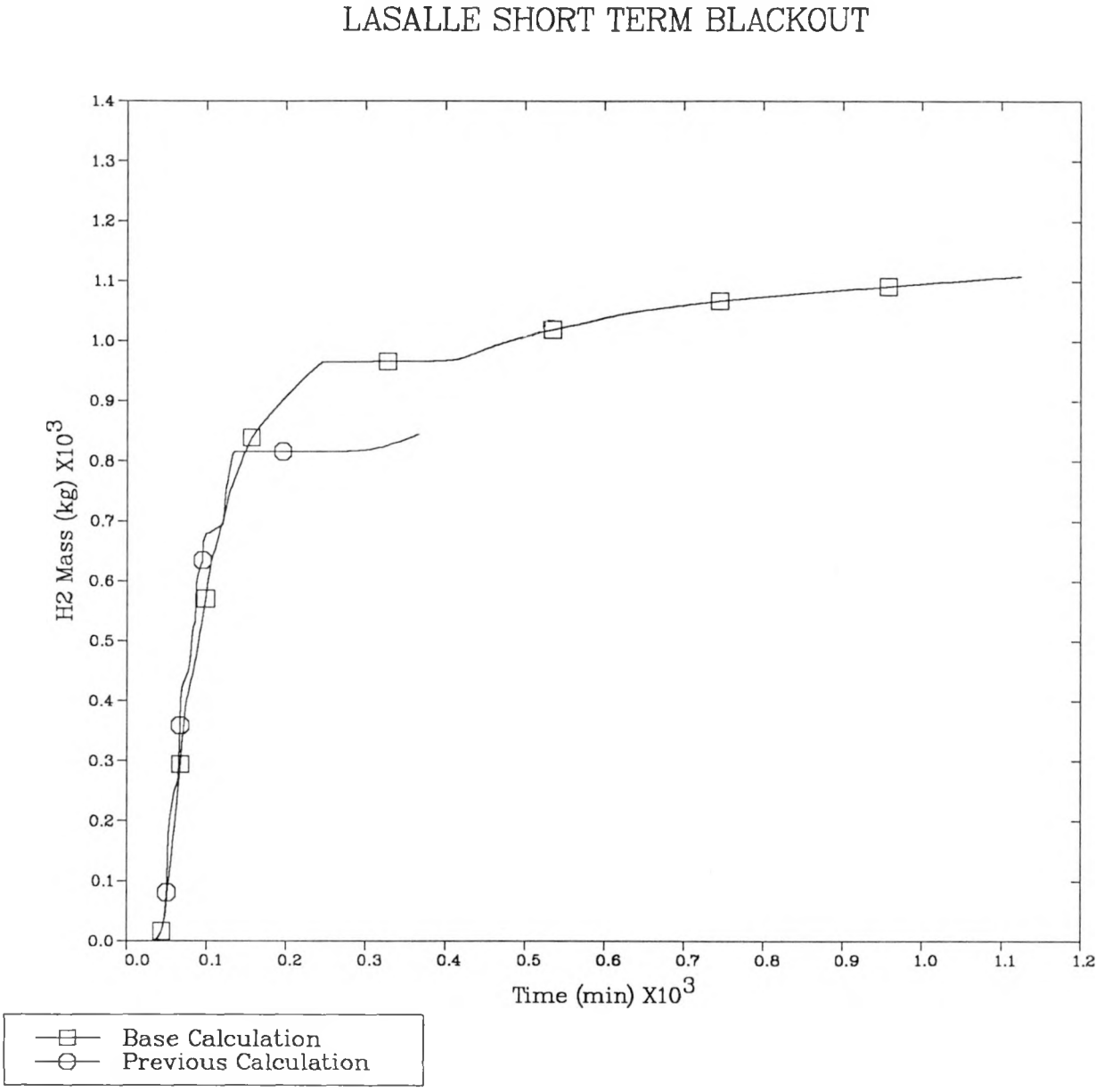

Figure 4-10. Comparison of Hydrogen Production from MELCOR Calculations

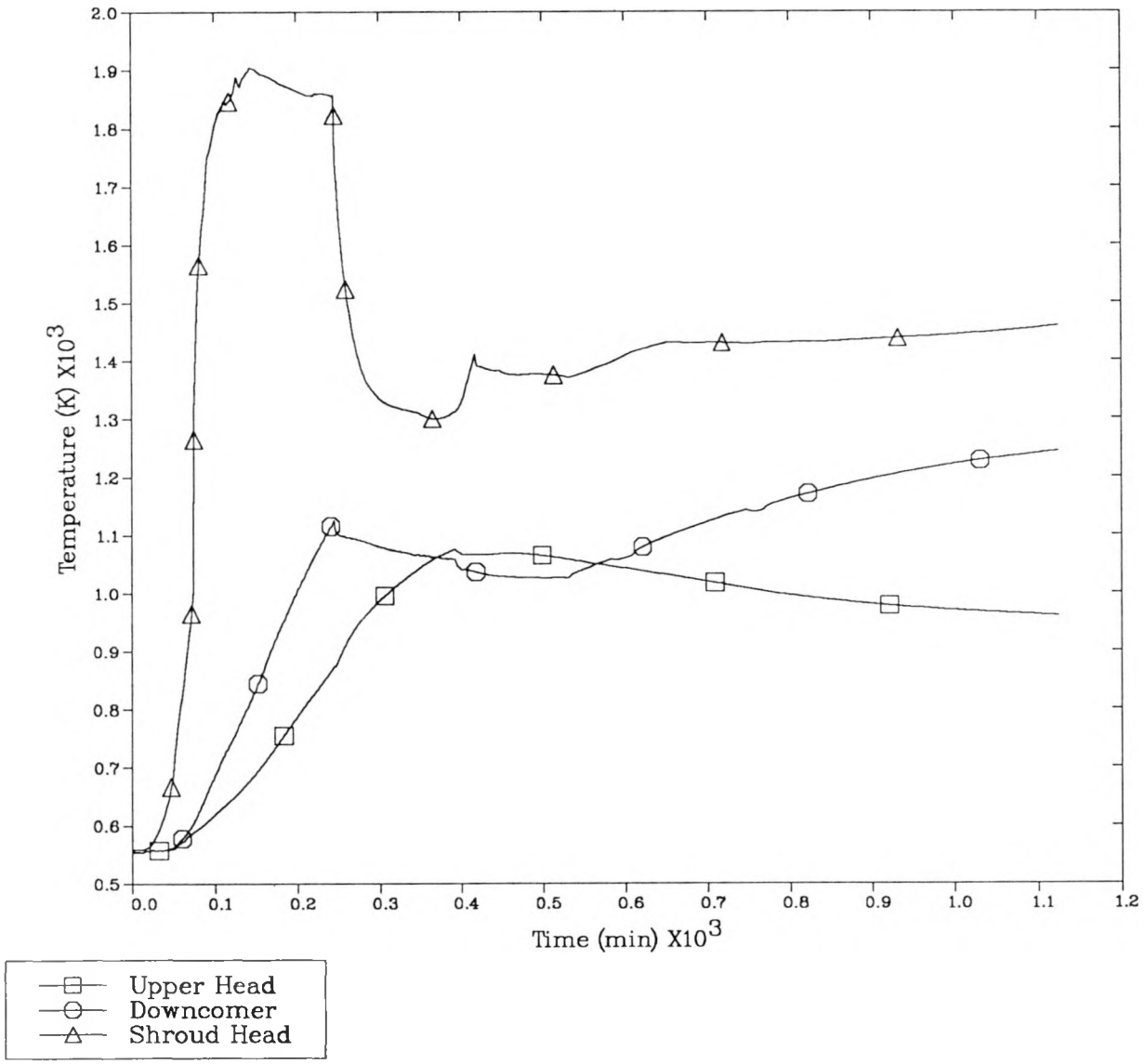

Figure 4-11. Vessel Structure Temperatures for Station Blackout

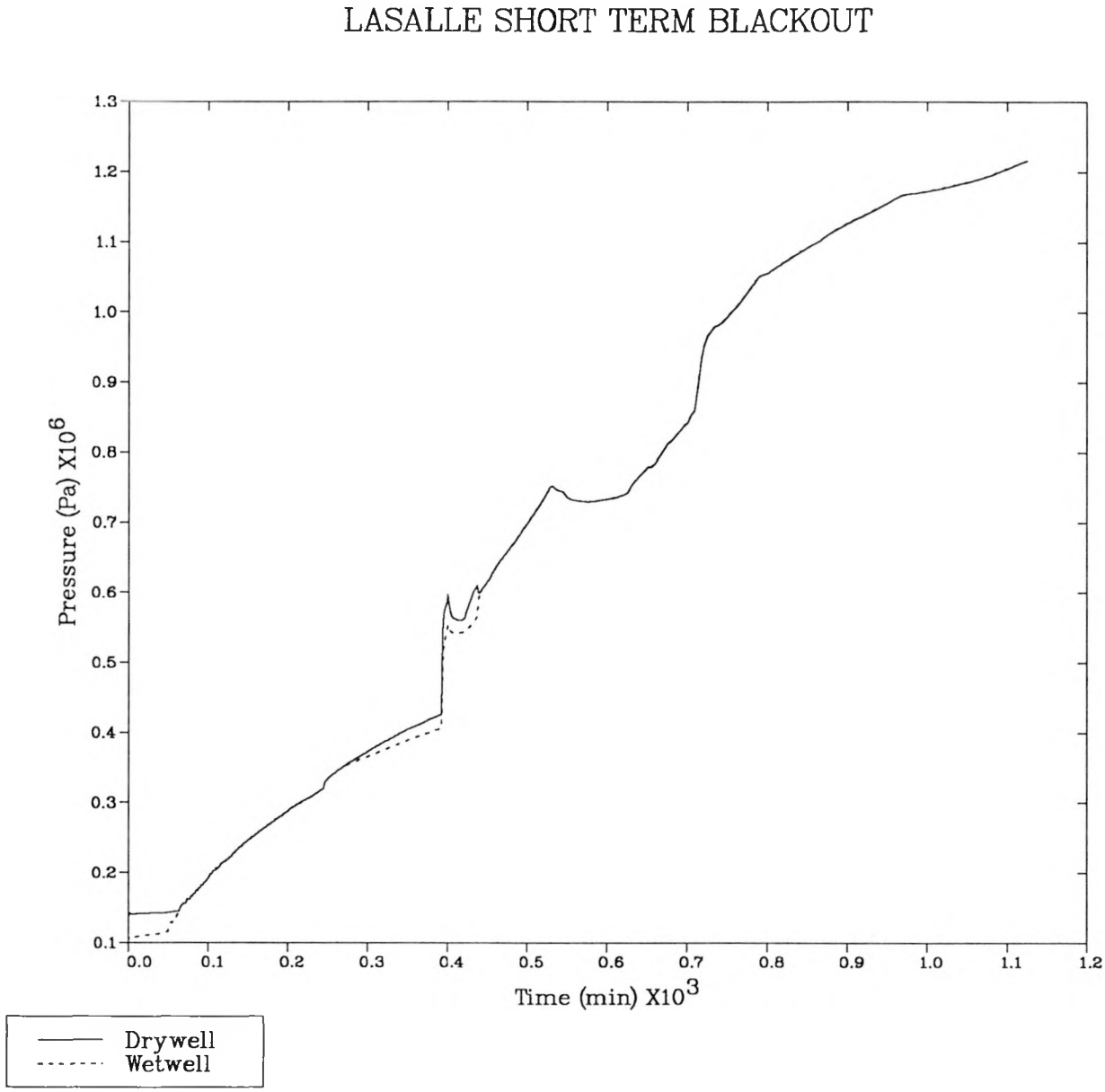

Figure 4-12. Containment Pressures for Station Blackout

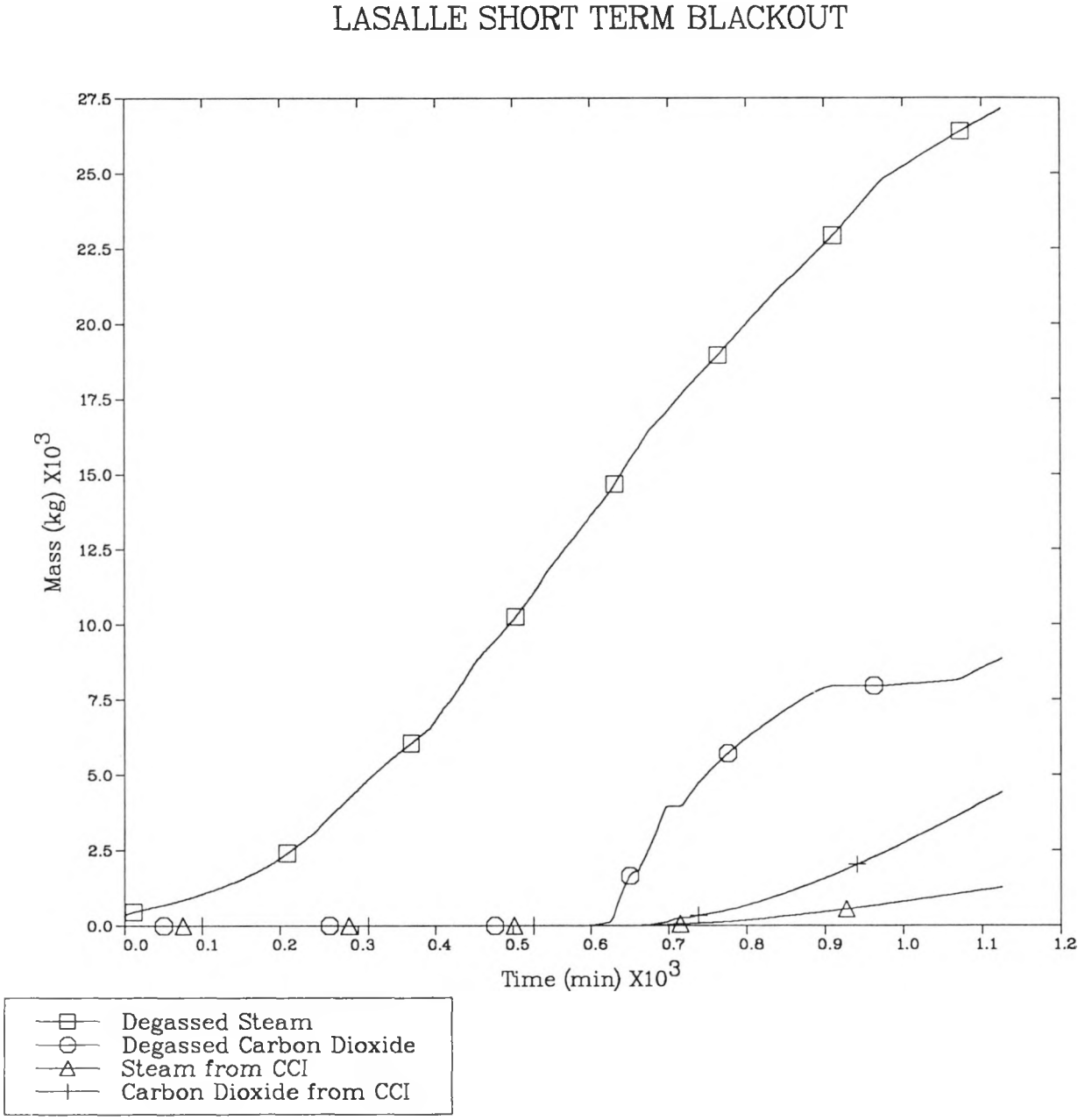

Figure 4-13. Steam and Carbon Dioxide Generation from Degassing and Core-Concrete Attack

5. SEQUOYAH ANALYSES

A scoping calculation was performed to determine the time needed to boil away the water in the reactor cavity when it is flooded with water and the extent of ice condenser bypass following a detonation that damages the ice condenser. The features of Sequoyah relevant for these issues are briefly discussed in the following section. The results of the MELCOR and HECTR calculations are described in the subsequent sections.

5.1 Brief Sequoyah Description

Sequoyah is a pressurized water reactor with a four-loop Westinghouse nuclear steam supply system rated at 3423 MW_t and an ice-condenser containment. A schematic of the Sequoyah containment is shown in Figure 5-1. The containment consists of three main regions: the lower compartment, upper compartment, and ice condenser. The reactor coolant system (RCS) is located in the lower compartment. During an accident the RCS will blow down into the lower compartment, then flow through the ice condenser, before entering the upper compartment. The heat transfer and condensation occurring in the ice condenser greatly reduce the containment pressurization. Water from melting ice in the ice condenser will drain back down into the lower compartment, and this water will spill over into the reactor cavity after sufficient inventory has accumulated.

The ice condenser is located in a 300 degree arc along the outer containment wall. It is approximately 24 m high, and contains perforated metal baskets filled with ice. Because of this geometry, development of asymmetries within the ice condenser during an accident is of concern.

5.2 Sump Boiloff Timing

MELCOR was used to estimate the time needed to boil away the water from an initially coolable debris bed in the Sequoyah reactor cavity when completely flooded with water. This timing information was needed to establish initial conditions for a separate analysis investigating the potential for a delayed core-concrete attack and its consequences.

A two-volume MELCOR deck was used for the analysis. One control volume was used for the reactor cavity and lower compartment, and it exhausted into a second, very large control volume modeling the remainder of containment and the environment. The lower compartment control volume contained 1125 m^3 of water, which is the amount which would overflow from the lower compartment into the reactor cavity if the inventory of the primary system, accumulators, refueling water storage tank, and the water from melting all ice from the ice condensers were added to the lower compartment. The pool was assumed to be saturated, which provides a lower bound on the time needed to boil the inventory. Decay heat for the entire core was added to this water as an energy source, assuming the

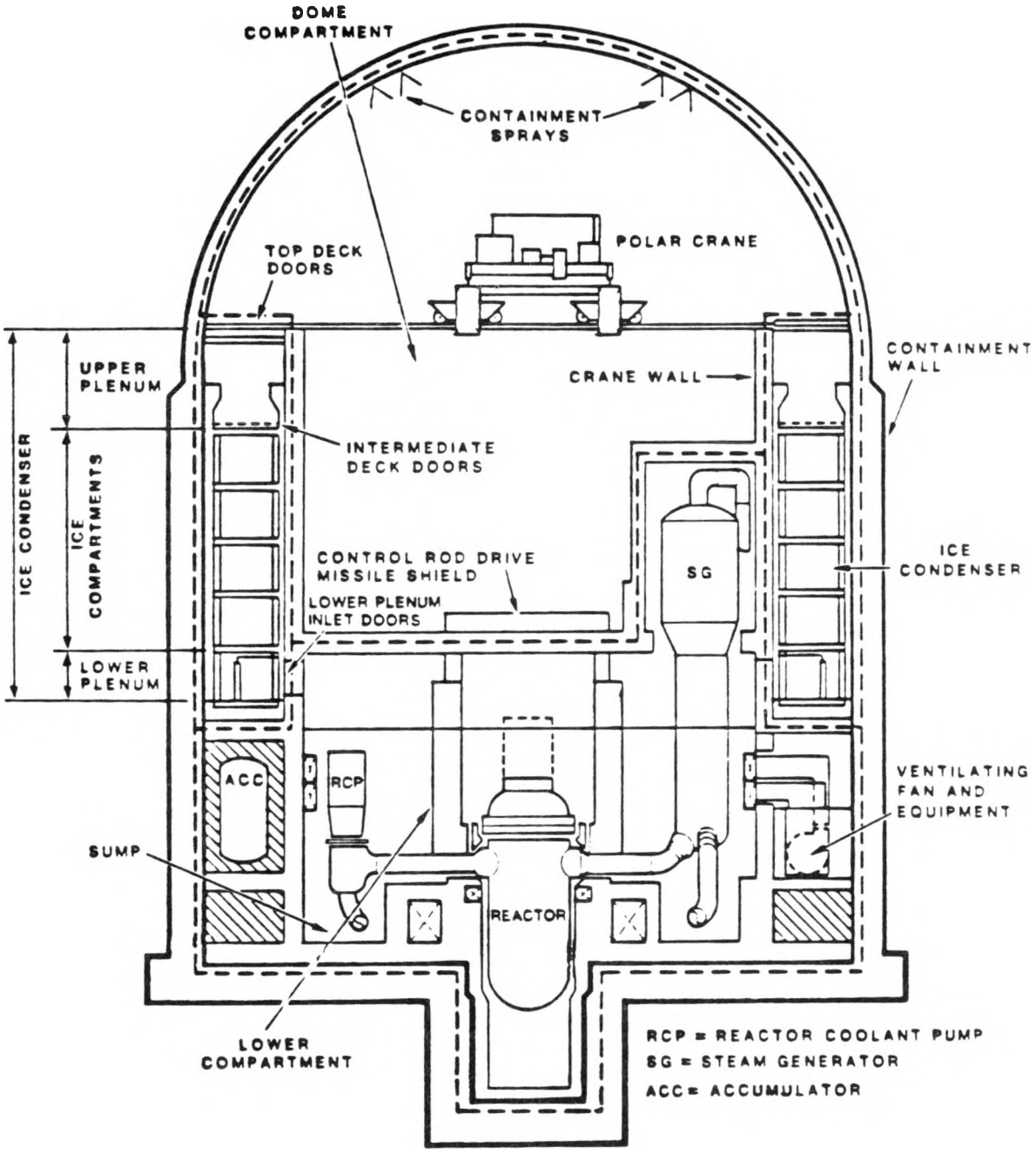

5-1. Schematic of Sequoyah Containment

entire core had been ejected from the vessel, and assuming that vessel breach occurred 410 minutes after scram. MELCOR calculated that it would take 2340 minutes to boil off the water.

5.3 Ice Condenser Bypass Following Detonation

Calculations were performed to examine the response in the ice condenser at vessel breach, assuming a detonation had occurred previously. The detonation was postulated to fail the ice baskets in a region of the ice condenser, leaving no ice in that region. The calculations were performed to estimate the amount of steam that could bypass the ice condenser through the voided region.

MELCOR did not have an ice-condenser model at the time these calculations were performed, so HECTR was used to perform the calculations. HECTR is a lumped-volume containment analysis computer program, whose main purpose is to analyze nuclear reactor accidents involving the transport and combustion of hydrogen. HECTR includes an ice-condenser model which can be divided into vertical and azimuthal sub-regions; thus, the effects of ice basket failure could be examined with it. However, HECTR had to be modified because it automatically divides the ice condenser circumferentially into stacks of ice volumes, but divides them equally. There is no option to override this feature. For this analysis, a case in which only a small fraction of the ice baskets were damaged by a detonation was being examined. Existing HECTR limitations would have forced the ice bed to be divided into 50 or 100 stacks of ice, with 4 volumes in each column. This would not have been reasonable, so the code was modified to allow asymmetric input for geometry and initial conditions.

Two ice-condenser nodalizations were examined. In the first, the ice bed was divided circumferentially into 4 equal-sized stacks of compartments, with 4 compartments per stack (16 total). In the second, the relative sizes of the stacks were adjusted such that one stack modeled about 2% of the ice columns and the remaining 3 stacks represented the other 98%. The steam and hydrogen blowdown sources that were used with both nodalizations approximated those that had been calculated with MARCON for the TMLB' sequence for the Containment Loads Working Group (Ref. 22). Compartment conditions and ice masses at vessel breach were obtained from previous HECTR calculations that were performed using the MARCON sources (calculations to examine detonability in the ice bed and upper plenum) (Ref. 23). The input deck used in Reference 23 was used for these calculations, but with changes to the ice bed to examine five cases:

Cases using nodalization 1:

1) a base case with ice remaining in all 4 columns,

2) ice removed from 1 of the 4 columns, and cross flow allowed between columns,

3) ice removed from 1 of the 4 columns, with no cross flow allowed, the upper doors assumed to be blown off for that column, and all upward flow loss coefficients set to very small values,

4) ice removed from all 4 columns.

Case using nodalization 2:

5) ice removed from the small ice stack, with no cross flow allowed, the upper doors assumed to be blown off for that stack, all upward flow loss coefficients set to very small values, and a 1 ft^2 breach to the environment modeled in the small ice stack.

The pressure rises for cases 1 through 4, respectively were 145, 200, 270, and 465 kPa. These results indicate that even with 1/4th of the ice bed modeled as ineffective, there is still considerable pressure suppression relative to the case with no ice present.

In case 5, the fraction of the ice bed assumed to be destroyed by the detonation was changed from 25% to 2%. This change resulted in a much longer run time, so the calculation was stopped before the vessel breach blowdown was complete. It was continued long enough to indicate that only about 7% of the total steam blowdown entered the voided region of the ice bed. This further supports the previous results indicating that there would not be excessive ice condenser bypass following a detonation in the ice bed.

6. REFERENCES

1. Severe Accident Risks: An Assessment for Five U.S. Nuclear Power Plants, NUREG-1150, U. S. Nuclear Regulatory Commission, June 1989.

2. Summers, R. M., et al., MELCOR 1.8.0: A Computer Code for Severe Nuclear Reactor Accident Source Term and Risk Assessment Analyses, NUREG/CR-5531, SAND90-0364, Sandia National Laboratories, Albuquerque, NM, January 1991.

3. Dingman, S. E., A. L. Camp, and M. J. Wester, "Capabilities of HECTR in Predicting Containment Responses during Hydrogen Combustion," Designing for Hydrogen in Nuclear Power Plants, pp. 65-71, Joint ASME/ANS Nuclear Engineering Conference, Portland, Oregon, August 1984.

4. Gieseke, J. A., et al., Radionuclide Release Under Specific LWR Accident Conditions, Volume III, BWR, Mark III Design, BMI-2104, Battelle Columbus Laboratories, Columbus, Ohio, July 1984.

5. Denning, R. S., et al., Radionuclide Release Calculations for Selected Severe Accident Scenarios, Vol. 4, BWR, Mark III Design, NUREG/CR-4624, BMI-2139, Battelle Columbus Laboratories, Columbus, Ohio, July 1986.

6. Harrington, R. M. and L. C. Fuller, BWR-LTAS: A Boiling Water Reactor Long-Term Accident Simulation Code, NUREG/CR-3764, ORNL/TM-9163, Oak Ridge National Laboratory, February 1985.

7. Murata, K. K. and D. L. Y. Louie, "Parametric CONTAIN Calculations of the Containment Response of the Grand Gulf Plant due to Reactor Pressure Vessel Failure at High Pressure," Proceedings of Fourth Workshop on Containment Integrity, NUREG/CP-0095, SAND88-1836, June 1988.

8. Dingman, S. E., A. L. Camp, and C. C. Wong, HECTR Version 1.5 User's Manual, NUREG/CR-4507, SAND86-0101, Sandia National Laboratories, Albuquerque, NM, April 1986.

9. Benedick, W. B., J. C. Cummings, and P. G. Prassinos, Combustion of Hydrogen:Air Mixtures in the VGES Cylindrical Tank, NUREG/CR-3273, SAND83-1022, Sandia National Laboratories, Albuquerque, NM, May 1984.

10. Marshall, B. W., Hydrogen:Air:Steam Flammability Limits and Combustion Characteristics in the FITS Vessel, NUREG/CR-3468, SAND84-0383, Sandia National Laboratories, Albuquerque, NM, December 1986.

11. Ratzel, A. C., Data Analyses for Nevada Test Site (NTS) Premixed Combustion Tests, NUREG/CR-4138, SAND85-0135, Sandia National Laboratories, Albuquerque, NM, May 1985.

12. Ural, E. A. and F. Tamanini, "Thermal Analysis of Hydrogen Combustion in a 1/4-Scale Boiling Water Reactor Containment Building," Journal of Heat Transfer, Vol. 112, pp. 201-206, February 1990.

13. Cook, D. L., et al., Station Blackout at Browns Ferry Unit One - Accident Sequence Analysis, NUREG/CR-2182, Vol. 1, 1981.

14. Wichner, R. P., et al., Station Blackout at Browns Ferry Unit One - Iodine and Noble Distribution and Release, NUREG/CR-2182, Vol. 2, 1981.

15. Ott, L. J., C. F. Weber, C. R. Hyman, "Station Blackout Calculations for Browns Ferry," Proceedings of the Thirteenth Water Reactor Safety Research Information Meeting, Gaithersburg, MD, October 1985.

16. Hodge, S. A., "Station Blackout Calculations for Peach Bottom," Proceedings of the Thirteenth Water Reactor Safety Research Information Meeting, Gaithersburg, MD, October 1985.

17. U.S. Nuclear Regulatory Commission Containment Loads Working Group, Estimates of Early Containment Loads from Core Melt Accidents, NUREG-1079, December 1985.

18. Denning, R. S., et al., Radionuclide Release Calculations for Selected Severe Accident Scenarios, BWR, Mark I Design, BMI-2139, NUREG/CR-4624, Vol. 1, July 1986.

19. Dingman, S. E., et al., "Analysis of Peach Bottom Station Blackout with MELCOR," Proceedings of the Fourteenth Water Reactor Safety Research Information Meeting, Gaithersburg, MD, October 1986.

20. Ahl, T. J., et al., "Analysis of a Mark I Containment Vessel For Severe Accident Conditions," Proceedings of the Fourth Workshop on Containment Integrity, Arlington, VA, NUREG/CP-0095, June 1988.

21. Summers, R. M., et al., "MELCOR In-Vessel Modeling," Transactions of the Fifteenth Water Reactor Safety Research Information Meeting, Gaithersburg, MD, October 1987.

22. Haskin, F. E., V. L. Behr, and A. L. Camp, "HECTR Results for Ice-Condenser Containment Standard Problem," Proceedings Second Workshop on Containment Integrity, Sandia National Laboratories, June 1984.

23. Dingman, S. E., and A. L. Camp, "Pressure-Temperature Response in an Ice-Condenser Containment for Selected Accidents", Transactions of the Thirteenth Water Reactor Safety Research Information Meeting, NUREG/CP-0071, October 22-25, 1985.

APPENDIX A

MELCOR NODALIZATIONS

CONTENTS

A.1 LaSalle Nodalizations....A-3
A.1.1 LaSalle Reactor Building Model....A-3
A.1.2 Integral LaSalle Model....A-14

A.2 Grand Gulf Nodalizations....A-24
A.2.1 Containment-Only Model....A-24
A.2.2 Integral Grand Gulf Model....A-28

A.3 Peach Bottom Nodalization....A-31

A.4 References....A-36

LIST OF FIGURES

A-1 Nodalization for LaSalle Reactor Building....A-4
A-2 Nodalization for LaSalle Integral Calculation....A-15
A-3 Nodalization for Grand Gulf Containment-Only Calculations....A-25
A-4 Nodalization for Grand Gulf Integral Calculations....A-29
A-5 Nodalization for Peach Bottom Calculations....A-32

LIST OF TABLES

A-1 LaSalle Reactor Building Model Control Volume Input....A-6
A-2 LaSalle Reactor Building Model Flow Path Input....A-7
A-3 LaSalle Reactor Building Model Heat Structure Input....A-9
A-4 LaSalle Reactor Building Model Heat Loads and Fan Cooler Input.A-14
A-5 LaSalle Integral Calculation Control Volume Input....A-17
A-6 LaSalle Integral Calculation Flow Path Input....A-18
A-7 LaSalle Integral Calculation Heat Structure Input....A-20
A-8 LaSalle Integral Calculation Core Input....A-22
A-9 LaSalle Integral Calculation Cavity Input....A-23
A-10 Grand Gulf Containment Model Control Volume Input....A-26
A-11 Grand Gulf Containment Model Flow Path Input....A-26
A-12 Grand Gulf Containment Model Heat Structure Input....A-27
A-13 Grand Gulf Containment Model Spray Input....A-28
A-14 Grand Gulf Integral Calculation Core Input....A-30
A-15 Peach Bottom Control Volume Input....A-33
A-16 Peach Bottom Flow Path Input....A-34
A-17 Peach Bottom Heat Structure Input....A-35

The MELCOR input decks used for the LaSalle, Grand Gulf and Peach Bottom analyses reported in this document are described in this appendix. Decks for calculating full accident scenarios were constructed for both the LaSalle and Grand Gulf plants, and included input for the thermal-hydraulics of the reactor pressure vessel (RPV) and containment, core melting and relocation phenomena, radionuclide behavior, and core-concrete attack. In addition, separate decks were constructed to analyze specific phenomena in more detail. For Grand Gulf, a containment-only deck was generated from the integral deck to allow more efficient calculation of numerous sensitivity cases. For LaSalle, a detailed deck was constructed to examine the thermal response during steam blowdown to the reactor building. For Peach Bottom a deck was constructed to calculate the thermal-hydraulic response during vessel blowdown.

A.1 LaSalle Nodalizations

A detailed deck for the reactor building was used to study steam flooding. An integral deck was used to study a station blackout.

A.1.1 LaSalle Reactor Building Model

The LaSalle reactor building model was used to analyze the thermal response in regions housing important equipment for scenarios that involved steam release to the reactor building from either containment venting or containment failure. A relatively detailed deck was constructed because large variations in conditions would be expected for the various regions of the reactor building.

The model was constructed using information from the plant drawings, the Final Safety Analysis Report (Ref. A-1), and two models developed by the Architect Engineer for LaSalle, Sargent and Lundy. One of the Sargent and Lundy models had been used to calculate gas flow between rooms and provided detailed calculations of flow path areas and resistances. The other model had been used for room environment calculations after high energy line breaks and provided detailed calculations of room volumes and surface areas. Neither model provided calculations of equipment masses or surface areas; reasonable estimates were made using information provided by the Risk Methods Integration and Evaluation Program (RMIEP)*. This information consisted of an identification of the equipment present in each room of the reactor building.

The reactor building was divided into 27 volumes as shown in Figure A-1. The main concern being addressed with the model was equipment survival in the lower levels of the reactor building, so more detailed noding was used in these regions. The raceway, HPCS and LPCS rooms were each divided into two volumes to represent the upper and lower levels. The LPCI rooms were modeled with single volumes because room coolers circulate air between the upper and lower levels, resulting in well-mixed

---

* Payne, A. C., et al., Analysis of the LaSalle Unit 2 Nuclear Power Plant: Risk Methods Integration and Evaluation Program (RMIEP), NUREG/CR-4832, SAND87-7157, October 1990 (unpublished).

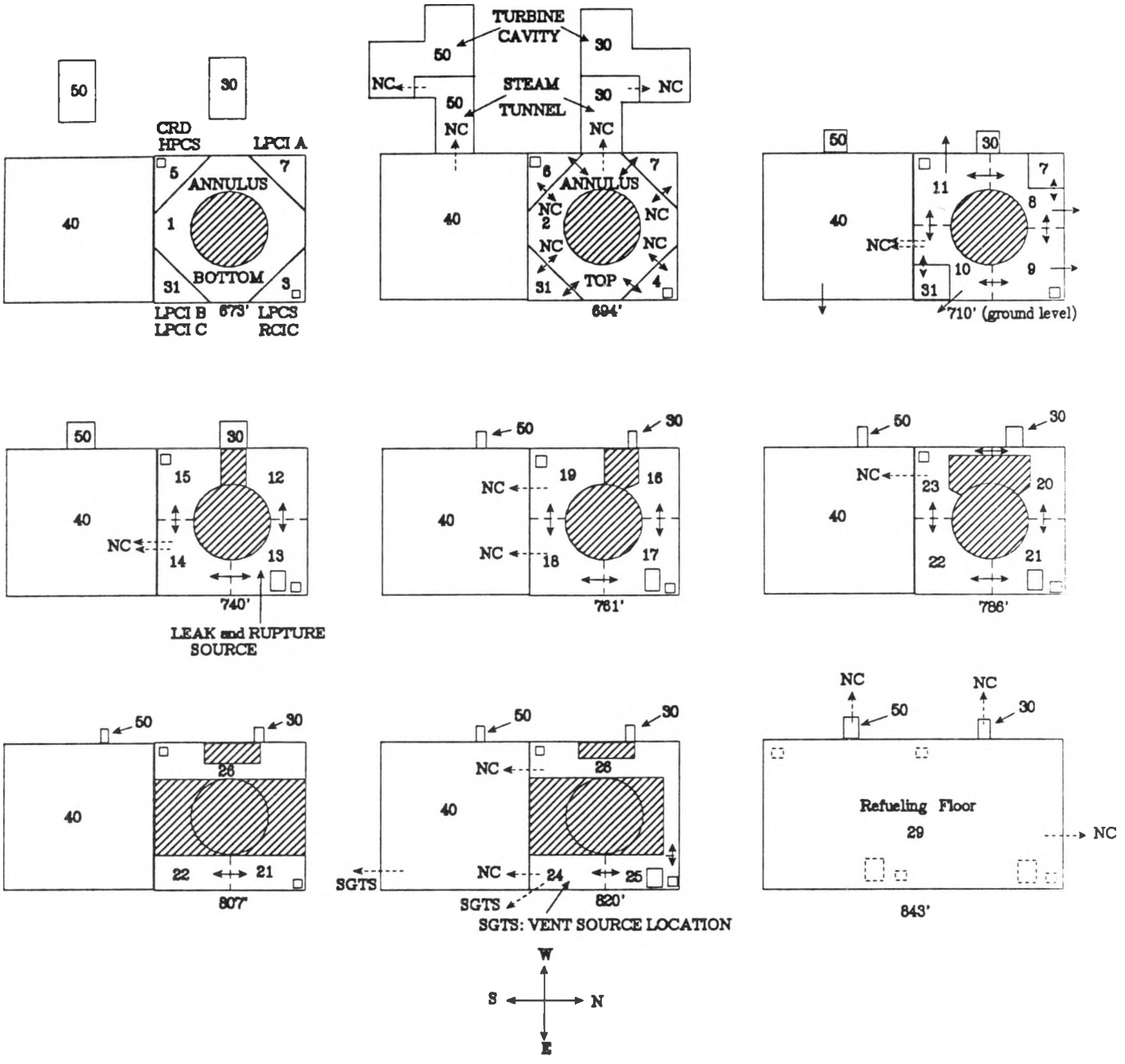

Figure A-1. Nodalization for LaSalle Reactor Building

regions. Levels 710, 740, 761 and 786.5 were each divided into four quadrants to allow the main circulation paths to be calculated. The East portions of levels 807 and 820 were each divided into two volumes and the more dead-ended regions at the West end of the two levels were lumped into a single volume. Single volumes were used to model the steam tunnel, refueling floor, and the unit 1 reactor building. A summary of the MELCOR input for the geometry of the control volumes is provided in Table A-1.

Before describing the MELCOR flow paths, the dominant flow patterns in the reactor building will be summarized. Normally, the corner rooms in the basement of the reactor building are fairly isolated from the other regions, but circulation is increased if doors are blown open during a transient. Unlike the basement where the levels are subdivided into rooms that restrict flow, the floors are essentially wide open at levels 710' and above. Also, there are reasonably large flow areas between the upper levels through stairways and an equipment hatch. Initially, the reactor building is isolated from the refueling floor, but paths can be opened if a door is blown open or concrete slabs are lifted from over the equipment hatch. The reactor building can also vent to the unit 1 reactor building if pressure increases sufficiently to blow open the doors between the two units. In addition, the reactor building can vent from the upper level of the raceway into the steam tunnel if a very small pressure differential is exceeded. The flow is then exhausted to the environment through a blowout panel at the top of the steam tunnel.

The flow paths for the MELCOR model are shown in Figure A-1 and described in Table A-2. All of the major flow paths described in the preceding paragraph are included. Doors and blowout panels are modeled to be closed initially but are opened if sufficient pressure differential builds during the transient. In addition, the walls of the refueling floor level are assumed to fail at 14 kPa (2 psig), opening a 7 m (23 ft) diameter hole to the environment. All leakage/infiltration paths between the reactor building and environment are lumped into flow paths at the 710 level. Flow paths were included for gas flow from the reactor buildings to the environment through the standby gas treatment system. A constant flow rate of 2000 cfm was used for each unit. Failure of the fans because of the harsh environment was not considered.

Heat structures are included in all reactor building volumes to model heat transfer to walls, ceilings, floors, and equipment. The MELCOR heat structure input is summarized in Table A-3. Heat loads from pumps and heat removal by the room coolers in the basement corner rooms were also modeled, using the parameters listed in Table A-4.

A simplified nodalization for the containment and RPV is used to provide blowdown sources to this detailed reactor building model. The RPV is modeled by a single volume, and 3 volumes are used for containment. The containment gases are exhausted to the reactor building at level 820' (volume 324) for cases examining venting, and to level 740' (volume 313) for cases examining containment failure. The control volume, flow path, and heat structure input for the RPV and containment is summarized in Tables A-1, A-2, and A-3, respectively.

Table A-1

LaSalle Reactor Building Model Control Volume Input

Control Volume	Brief Description	Bottom Elevation (m)	Top Elevation (m)	Volume (m^3)
100	Reactor Vessel	0.	21.9	603.2
200	Wetwell	-25.5	-7.2	8264.
201	Downcomers	-21.1	-6.1	412.1
205	Drywell	-9.1	23.8	5778.3
301	Bottom of Raceway	-25.7	-19.2	2413.
302	Top of Raceway	-19.2	-14.4	2119.
303	NE Basement Room	-25.7	-19.2	917.6
304	NE Basement Room	-19.2	-14.4	478.5
305	SW Basement Room	-25.7	-19.2	578.9
306	SW Basement Room	-19.2	-14.4	438.1
307	NW Basement Room	-25.7	-5.4	1525.4
331	SE Basement Room	-25.7	-5.4	1598.6
308	NW Quadrant - 710	-14.4	-5.4	1395.9
309	NE Quadrant - 710	-14.4	-5.4	1820.5
310	SE Quadrant - 710	-14.4	-5.4	1332.7
311	SW Quadrant - 710	-14.4	-5.4	1820.5
312	NW Quadrant - 740	-5.4	1.0	1032.0
313	NE Quadrant - 740	-5.4	1.0	1313.0
314	SE Quadrant - 740	-5.4	1.0	1032.0
315	SW Quadrant - 740	-5.4	1.0	1313.0
316	NW Quadrant - 761	1.0	8.8	1794.1
317	NE Quadrant - 761	1.0	8.8	1931.3
318	SE Quadrant - 761	1.0	8.8	1931.3
319	SW Quadrant - 761	1.0	8.8	1931.3
320	NW Quadrant - 786	8.8	15.0	918.5
321	NE Quadrant - 786	8.8	19.2	2920.5
322	SE Quadrant - 786	8.8	19.2	2920.5
323	SW Quadrant - 786	8.8	15.0	918.5
324	SE Quadrant - 820	19.2	26.2	1496.2
325	NE Quadrant - 820	19.2	26.2	1496.2
326	West Half - 807	15.0	26.2	2092.0
329	Refueling Floor	14.1	41.6	58770.0
330	Steam Tunnel + Turb Bldg	-21.5	29.3	7267.2
340	Unit 1	-25.7	29.3	41489.

Table A-2

LaSalle Reactor Building Model Flow Path Input

Flow Path	From CV	From Elev (m)	To CV	To Elev (m)	Area (m^2)	Loss Coeff	Further Details
21	100	16.5	200	-24.9	1.1	3.5	SRV Path
24	205	-6.1	201	-6.1	27.4	5.2	
25	201	-21.1	200	-21.1	27.4	1.	
26	200	-7.2	205	-6.2	1.	1.	WW-DW VB
401	200	-8.	324	22.7	.16	1.	WW Vent
402	205	-4.	313	-4.	.65	1.	DW Failure
301	301	-19.3	302	-19.3	146.5	1.65	
302	302	-14.4	309	-14.4	1.78	6.58	
303	303	-19.3	304	-19.3	7.24	3.3	
304	304	-14.4	309	-14.4	5.92	2.9	
305	305	-19.3	306	-19.3	2.0	3.89	
306	306	-14.4	311	-14.4	4.47	5.49	
307	307	-13.3	308	-13.3	2.02	5.57	Door
308	331	-13.3	310	-13.3	1.9	5.29	Door
309	302	-18.2	304	-18.2	2.1	2.73	Door
310	302	-18.2	306	-18.2	2.1	2.73	Door
311	302	-18.2	307	-18.2	2.1	3.33	Door
319	302	-18.2	331	-18.2	2.1	4.34	Door
366	302	-18.2	304	-18.2	.581	1.5	
367	302	-18.2	331	-18.2	.581	1.5	
368	302	-18.2	306	-18.2	1.548	1.5	
369	302	-18.2	307	-18.2	.581	1.5	
312	308	-9.9	309	-9.9	74.	1.	
313	309	-9.9	310	-9.9	42.	1.	
314	310	-9.9	311	-9.9	74.	1.	
315	311	-9.9	308	-9.9	42.	1.	
316	309	-13.3	313	-4.3	1.78	8.2	
317	309	-5.4	313	-5.4	18.5	3.36	Equip Hatch
318	311	-5.4	315	-5.4	5.91	5.8	Stair
320	312	-2.2	313	-2.2	51.	1.	
321	313	-2.2	314	-2.2	29.	1.	
322	314	-2.2	315	-2.2	51.	1.	
323	313	1.0	317	1.0	38.0	4.26	Equip Hatch
324	315	1.0	319	1.0	4.63	4.1	Stair
325	316	4.9	317	4.9	63.	1.	
326	317	4.9	318	4.9	36.	1.	
327	318	4.9	319	4.9	63.	1.	
328	317	8.8	321	8.8	37.1	3.35	Equip Hatch
329	319	8.8	323	8.8	5.47	5.8	Stair
330	320	11.9	321	11.9	48.5	1.	

Table A-2 (cont.)

Flow Path	From CV	From Elev (m)	To CV	To Elev (m)	Area (m^2)	Loss Coeff	Further Details
331	321	11.9	322	11.9	49.	1.	
332	322	11.9	323	11.9	48.5	1.	
338	323	11.9	320	11.9	3.95	3.3	
333	321	19.2	325	19.2	37.5	3.64	Equip Hatch
334	324	22.7	325	22.7	77.	1.	
335	325	20.3	326	20.3	2.34	5.	
336	323	15.0	326	15.0	3.6	4.	
337	320	15.0	326	15.0	4.5	4.	
341	325	26.2	329	26.2	33.1	1.	Covered Equip Hatch
342	325	26.2	329	26.2	3.08	2.9	Door at Stair
343	302	-18.4	330	-18.4	3.01	2.8	Check Valve
344	323	9.9	340	9.9	2.1	1.	Door
345	318	2.1	340	2.1	2.1	1.	Door
346	319	2.1	340	2.1	2.1	1.	Door
347	314	-4.3	340	-4.3	4.2	1.	Door
348	310	-13.3	340	-13.3	4.2	1.	Door
349	324	21.3	340	21.3	2.1	1.	Door
350	326	21.3	340	21.3	2.1	1.	Door
352	330	28.8	400	28.8	3.53	1.	Blowout Panel
353	329	33.9	400	33.9	40.	1.	Refuel Fail
361	400	-9.9	308	-9.9	.023	1.	Infiltration
362	400	-9.9	309	-9.9	.023	1.	Infiltration
363	400	-9.9	310	-9.9	.023	1.	Infiltration
364	400	-9.9	311	-9.9	.023	1.	Infiltration
365	400	-9.9	340	-9.9	.092	1.	Infiltration
371	324	22.7	400	22.7	.164	1.	SGTS
372	340	22.7	400	22.7	.164	1.	SGTS

Table A-3

LaSalle Reactor Building Model Heat Structure Input

Heat Structure	Left CV	Right CV	Surface Area (m^2)	Material	Thickness (m)	Description
10001	100	205	33.14	Steel	.118	Lower Head
10306	100	205	48.14	Steel	.179	Vessel Top
10402	100	205	50.59	Steel	.108	Upper Head
10502	100	205	48.65	Steel	.197	Vessel Wall
20001	200	Ins.	1525.	Stl/Conc	.610	Wetwell Wall
20002	200	Ins.	482.7	Stl/Conc	7.006	Base Slab
20003	200	Ins.	62.31	Stl/Conc	.540	Support Cols
20004	200	Ins.	682.4	Stl/Conc	.743	WW Pedestal
20005	200	Ins.	24.71	Stainless	.019	WW Steel
20006	200	Ins.	31.19	Stainless	.019	SP Steel
20101	201	200	28.17	Stainless	.308	Downcomers
20401	205	Ins.	110.3	Concrete	1.473	Cav Pedestal
20501	200	205	83.8	Stl/Conc	.921	DW Floor
20502	205	205	365.0	Stl/Conc	.568	Reac Shield
20503	205	Ins.	2100.	Stl/Conc	1.219	DW Wall
20505	200	205	29.92	Stl/Conc	1.149	Cav Floor
20506	205	Ins.	181.0	Stl/Air/ Conc	4.439	DW Head
20507	205	Ins.	31.96	Steel	.008	DW Steel
20508	205	Ins.	31.96	Steel	.008	DW Steel
30101	301	Ins.	560.9	Concrete	2.438	673 Floor
30102	301	302	560.9	Concrete	.610	673 Ceiling
30103	301	Ins.	585.3	Concrete	.610	673 Wall
30104	301	330	51.19	Concrete	.914	673 Wall
30105	301	400	51.19	Concrete	.914	673 Wall
30106	301	307	118.7	Concrete	.396	673 Wall
30107	301	303	199.9	Concrete	.396	673 Wall
30108	301	Ins.	102.4	Concrete	2.438	673 Wall
30109	301	340	48.2	Concrete	.914	673 Wall
30110	301	305	148.6	Concrete	.396	673 Wall
30111	301	301	2.79	Steel	.006	673 Equip
30112	301	331	118.7	Concrete	.396	673 Wall
30201	303	302	86.54	Concrete	.610	694 Wall
30202	302	308	161.9	Concrete	.610	694 Ceiling
30203	302	309	161.9	Concrete	.610	694 Ceiling
30204	302	310	161.9	Concrete	.610	694 Ceiling
30205	302	311	161.9	Concrete	.610	694 Ceiling
30206	302	Ins.	386.5	Concrete	.610	694 Wall
30207	303	330	67.63	Concrete	.914	694 Wall
30208	302	307	49.10	Concrete	.396	694 Wall

Table A-3 (cont.)

Heat Structure	Left CV	Right CV	Surface Area (m^2)	Material	Thickness (m)	Description
30209	302	Ins.	99.50	Concrete	2.438	694 Wall
30210	302	304	98.20	Concrete	.396	694 Wall
30211	302	340	31.87	Concrete	.914	694 Wall
30212	302	306	98.20	Concrete	.396	694 Wall
30213	302	302	2.79	Steel	.006	694 Equip
30214	302	331	49.10	Concrete	.396	694 Wall
30301	303	Ins.	218.3	Concrete	2.438	673 Floor
30302	303	304	131.7	Concrete	.619	673 Ceiling
30303	303	307	60.11	Concrete	.396	673 Wall
30304	303	Ins.	258.4	Concrete	2.438	673 Wall
30305	303	303	121.1	Concrete	.396	673 Wall
30306	303	303	28.99	Steel	.340	673 Equip
30401	304	309	131.7	Concrete	.610	694 Ceiling
30402	304	Ins.	138.7	Concrete	2.438	694 Wall
30501	305	Ins.	131.7	Concrete	2.438	673 Floor
30502	305	306	131.7	Concrete	.610	673 Ceiling
30503	305	400	99.50	Concrete	.610	673 Wall
30504	305	340	110.7	Concrete	.610	673 Wall
30505	305	305	47.29	Concrete	.396	673 Wall
30506	305	305	28.99	Steel	.400	673 Equip
30601	306	311	131.7	Concrete	.610	694 Ceiling
30602	306	400	65.68	Concrete	.610	694 Wall
30603	306	340	73.02	Concrete	.610	694 Wall
30701	307	Ins.	65.87	Concrete	2.438	673 Floor
30702	307	400	369.6	Concrete	.610	673 Wall
30703	307	Ins.	138.8	Concrete	2.438	673 Wall
30706	307	312	69.49	Concrete	.610	673 Ceiling
30708	307	308	62.24	Concrete	.610	673 Ceiling
30709	307	308	139.7	Concrete	.396	673 Wall
30712	307	307	201.3	Concrete	.610	673 Floor
30713	307	307	14.5	Steel	.400	673 Equip
33101	331	Ins.	65.87	Concrete	2.438	673 Floor
33103	331	Ins.	174.5	Concrete	2.438	673 Wall
33104	331	340	274.6	Concrete	.610	673 Wall
33105	331	400	61.32	Concrete	.610	673 Wall
33107	331	314	70.23	Concrete	.610	673 Ceiling
33110	331	310	61.50	Concrete	.610	673 Ceiling
33111	331	310	141.8	Concrete	.396	673 Wall
33112	331	310	403.	Concrete	.610	673 Floor
33113	331	331	14.5	Steel	.400	673 Equip
30801	308	312	186.7	Concrete	.610	710 Ceiling
30802	308	330	37.44	Concrete	1.219	710 Ceiling
30803	308	Ins.	189.8	Concrete	.610	710 Wall

Table A-3 (cont.)

Heat Structure	Left CV	Right CV	Surface Area (m^2)	Material	Thickness (m)	Description
30804	308	330	46.82	Concrete	.914	710 Wall
30805	308	400	137.2	Concrete	.610	710 Wall
30806	308	400	35.77	Concrete	.396	710 Wall
30807	308	308	2.32	Steel	.014	710 Equip
30901	309	313	293.7	Concrete	.610	710 Ceiling
30902	309	Ins.	189.8	Concrete	.610	710 Wall
30903	309	400	359.6	Concrete	.396	710 Wall
30904	309	309	2.32	Steel	.014	710 Equip
31001	310	314	223.4	Concrete	.610	710 Ceiling
31002	310	Ins.	189.8	Concrete	.610	710 Wall
31003	310	400	133.5	Concrete	.396	710 Wall
31004	310	340	84.36	Concrete	.610	710 Wall
31005	310	310	2.32	Steel	.014	710 Equip
31101	311	315	256.2	Concrete	.610	710 Ceiling
31102	311	330	37.44	Concrete	1.219	710 Ceiling
31103	311	Ins.	147.6	Concrete	.610	710 Wall
31104	311	340	164.8	Concrete	.610	710 Wall
31105	311	400	148.0	Concrete	.610	710 Wall
31106	311	330	46.82	Concrete	.914	710 Wall
31107	311	Ins.	160.8	Concrete	.396	710 Wall
31108	311	311	2.32	Steel	.014	710 Equip
31201	312	316	182.3	Concrete	.610	740 Ceiling
31202	312	Ins.	100.3	Concrete	.610	740 Ceiling
31203	312	400	102.2	Concrete	.610	740 Wall
31204	312	400	113.9	Concrete	.396	740 Wall
31205	312	Ins.	103.5	Concrete	.610	740 Wall
31206	312	330	38.8	Concrete	1.219	740 Wall
31207	312	312	2.32	Steel	.014	740 Equip
31301	313	317	320.1	Concrete	.610	740 Ceiling
31302	313	Ins.	143.4	Concrete	.610	740 Wall
31303	313	400	248.4	Concrete	.396	740 Wall
31304	313	313	152.9	Concrete	.610	740 Wall
31305	313	313	2.32	Steel	.014	740 Equip
31401	314	318	286.6	Concrete	.610	740 Ceiling
31402	314	Ins.	111.5	Concrete	.610	740 Wall
31403	314	400	134.6	Concrete	.396	740 Wall
31404	314	340	113.9	Concrete	.610	740 Wall
31405	314	Ins.	67.08	Concrete	.610	740 Wall
31406	314	314	2.32	Steel	.014	740 Equip
31501	315	319	238.4	Concrete	.610	740 Ceiling
31502	315	Ins.	87.61	Concrete	.610	740 Wall
31503	315	400	102.2	Concrete	.610	740 Wall
31504	315	330	38.83	Concrete	1.219	740 Wall

Table A-3 (cont.)

Heat Structure	Left CV	Right CV	Surface Area (m^2)	Material	Thickness (m)	Description
31505	315	340	113.9	Concrete	.610	740 Wall
31506	315	Ins.	113.0	Concrete	.610	740 Wall
31507	315	315	2.32	Steel	.014	740 Equip
31601	316	320	217.6	Concrete	.610	761 Ceiling
31602	316	Ins.	85.56	Concrete	.610	761 Wall
31603	316	400	64.01	Concrete	.610	761 Wall
31604	316	400	152.8	Concrete	.396	761 Wall
31605	316	Ins.	123.2	Concrete	.610	761 Wall
31606	316	316	2.32	Steel	.014	761 Equip
31701	317	321	355.4	Concrete	.610	761 Ceiling
31702	317	Ins.	154.1	Concrete	.610	761 Wall
31703	317	400	333.4	Concrete	.396	761 Wall
31704	317	317	2.32	Steel	.014	761 Equip
31801	318	322	355.4	Concrete	.610	761 Ceiling
31802	318	Ins.	154.1	Concrete	.610	761 Wall
31803	318	400	180.0	Concrete	.396	761 Wall
31804	318	340	152.8	Concrete	.610	761 Wall
31805	318	318	2.32	Steel	.014	761 Equip
31901	319	330	74.97	Concrete	1.218	761 Floor
31902	319	323	260.0	Concrete	.610	761 Ceiling
31903	319	Ins.	132.8	Concrete	.610	761 Ceiling
31904	319	Ins.	205.4	Concrete	.610	761 Wall
31905	319	340	152.8	Concrete	.610	761 Wall
31906	319	400	224.1	Concrete	.914	761 Wall
31907	319	319	2.32	Steel	.014	761 Equip
32001	320	326	146.6	Concrete	.610	786 Ceiling
32002	320	Ins.	53.60	Concrete	.610	786 Wall
32003	320	400	145.2	Concrete	.610	786 Wall
32004	320	400	122.8	Concrete	.396	786 Wall
32005	320	Ins.	231.4	Concrete	.396	786 Wall
32006	320	320	2.32	Steel	.014	786 Equip
32101	321	325	338.7	Concrete	.610	786 Ceiling
32102	321	329	172.1	Concrete	1.219	786 Ceiling
32103	321	Ins.	160.8	Concrete	.610	786 Wall
32104	321	400	467.7	Concrete	.396	786 Wall
32105	321	321	2.32	Steel	.014	786 Equip
32201	322	324	255.0	Concrete	.610	786 Ceiling
32202	322	329	234.1	Concrete	1.829	786 Ceiling
32203	322	Ins.	107.2	Concrete	.610	786 Wall
32204	322	400	237.3	Concrete	.396	786 Wall
32205	322	340	166.3	Concrete	.610	786 Wall
32206	322	322	2.32	Steel	.014	786 Equip
32301	323	326	135.8	Concrete	.610	786 Ceiling

Table A-3 (cont.)

Heat Structure	Left CV	Right CV	Surface Area (m^2)	Material	Thickness (m)	Description
32302	323	329	144.7	Concrete	1.829	786 Ceiling
32303	323	Ins.	53.60	Concrete	.610	786 Wall
32304	323	340	122.8	Concrete	.610	786 Wall
32305	323	400	173.5	Concrete	.610	786 Wall
32306	323	Ins.	213.0	Concrete	.610	786 Wall
32307	323	323	2.32	Steel	.014	786 Equip
32401	324	329	255.0	Concrete	.610	820 Ceiling
32402	324	329	163.0	Concrete	1.829	820 Wall
32403	324	400	163.0	Concrete	.396	820 Wall
32404	324	340	76.92	Concrete	.610	820 Wall
32405	324	324	2.32	Steel	.014	820 Equip
32501	325	329	321.1	Concrete	.610	820 Ceiling
32502	325	329	184.3	Concrete	1.829	820 Wall
32503	325	400	300.7	Concrete	.396	820 Wall
32504	325	325	2.32	Steel	.014	820 Equip
32601	326	Ins.	126.0	Concrete	.610	807 Floor
32602	326	329	321.8	Concrete	.610	807 Ceiling
32603	326	400	240.8	Concrete	.610	807 Wall
32604	326	400	122.1	Concrete	.396	807 Wall
32605	326	329	517.1	Concrete	1.829	807 Wall
32606	326	340	122.1	Concrete	.610	807 Wall
32607	326	Ins.	1133.	Concrete	.396	807 Wall
32608	326	326	2.32	Steel	.014	807 Equip
32901	329	Ins.	490.2	Concrete	.610	843 Floor
32902	329	340	1828.	Concrete	.610	843 Floor
32903	329	400	3656.	Steel	.003	843 Ceiling
32904	329	400	4016.	Steel	.003	843 Wall
32905	329	329	2.32	Steel	.014	843 Equip
33001	330	Ins.	83.70	Concrete	.610	687 Wall
33002	330	400	412.7	Concrete	1.829	687 Floor
33003	330	400	412.7	Concrete	1.829	687 Ceiling
33004	330	400	1154.	Concrete	1.829	687 Wall

Table A-4

LaSalle Reactor Building Model Heat Loads and Fan Cooler Input

Heat Loads

Control Volume	Heat Load (MW)
305	.188
303	.115
307	.0417
331	.0833

Fan Cooler Parameters

	From CV	To CV	Rated Heat Removal Rate (MW)	Rated Temp (K)	Flow Rate (kg/s)	Secondary Inlet Temp (K)
HPCS	305	305	.2194	337.6	8.5	288.7
LPCS	304	303	.3487	337.6	13.5	288.7
LPCI	307	307	.2194	337.6	8.5	288.7
LPCI	331	331	.3223	337.6	12.5	288.7

A.1.2 Integral LaSalle Model

The integral LaSalle model was developed by collapsing the reactor building model described in Section A.1.1 and adding a more-detailed model for the RPV and containment. The reactor building was collapsed because the results of the steam flooding calculations indicated that the upper levels would be well-mixed. The RPV and containment input was developed using values from an existing RELAP5 deck that had been used for analyses in the RMIEP program, the LaSalle Final Safety Analysis Report (Ref. A-1), and miscellaneous information provided by the Commonwealth Edison contact.

The nodalization for the LaSalle deck is shown in Figure A-2. The RPV had many nodes for both the core and thermal-hydraulic calculations to represent axial and radial variations within the core region that were expected to significantly affect core heat transfer, blockage, and oxidation. The core region was divided into twelve control volumes, six for the channel and six for the bypass. Four additional control volumes were used to model the upper plenum/steam separator region, dryer/steam dome region, downcomer, and lower plenum. The containment was modeled using 5 control volumes: drywell, upper pedestal, lower pedestal, downcomers, and wetwell. The reactor building model described in Section

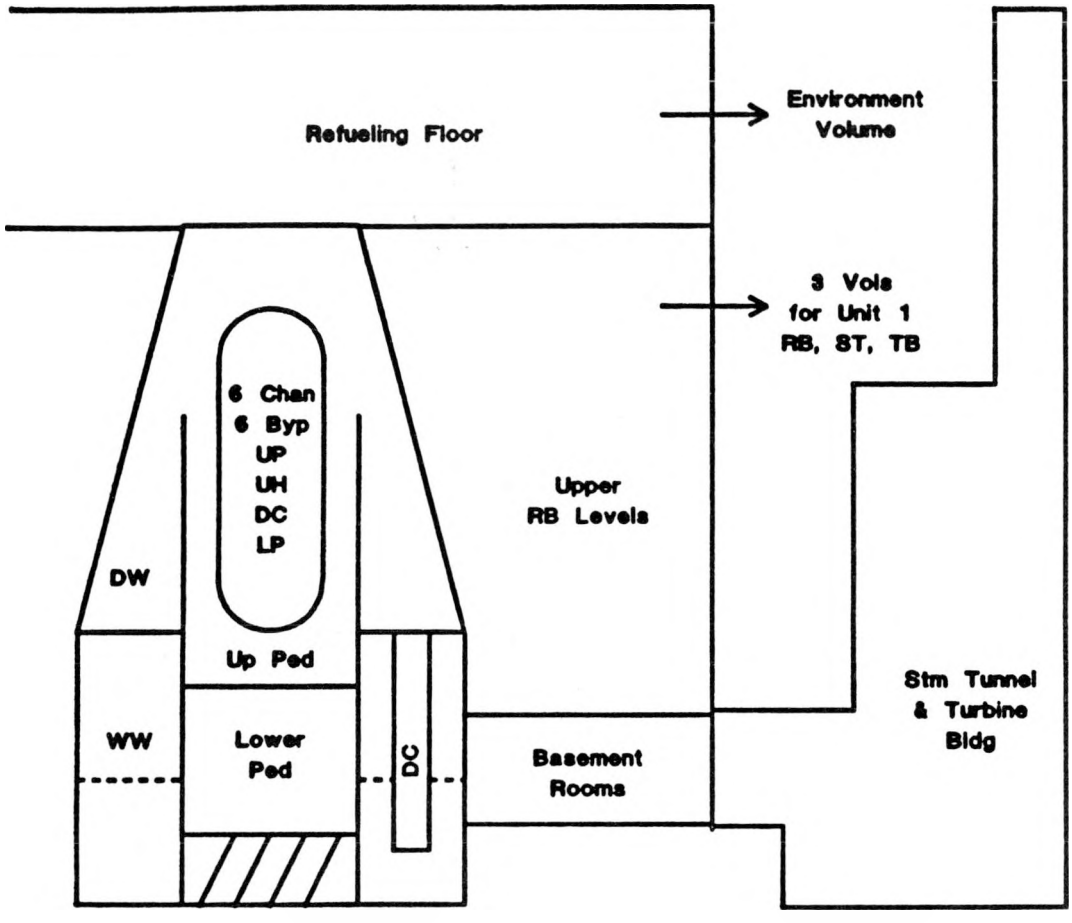

Figure A-2. Nodalization for LaSalle Integral Calculation

A.1.1 was collapsed to six volumes: unit 2 upper reactor building, unit 2 basement rooms, unit 2 steam tunnel, unit 1 reactor building, unit 1 steam tunnel, and refueling floor. The control volume input is summarized in Table A-5.

The locations of the flow paths between control volumes are indicated in Figure A-2, and the characteristics of each are listed in Table A-6. Most of the flow paths are maintained at a constant area throughout the transient. However, flow paths with variable area are included for vacuum breakers and check valves, as well as for paths modeling structural failure.

The heat structures used to model structures and equipment are summarized in Table A-7. Included are RPV walls and internals, containment walls and equipment, and reactor building walls and equipment.

The core was modeled by six radial rings and thirteen axial levels. Fine axial divisions were used near the core plate for modeling core inlet blockage and core plate response. Separate nodes were used for the non-fueled regions above and below the active fuel region. The core input is summarized in Table A-8.

The cavity modeling for calculating core-concrete attack was different from previous analyses of other plants because of the unusual geometry at LaSalle. The core debris would initially fall onto the drywell pedestal floor following vessel breach at LaSalle. However, the molten debris could flow into the sump drain lines. Shortly thereafter, melt could fail the lines, and flow out onto the wetwell pedestal floor. This would move the location of the core-concrete attack and would open a direct path between the drywell and wetwell. Because of the short time expected before failure of the drain lines, the initial core-concrete attack in the drywell pedestal was neglected and the corium was moved directly into the wetwell pedestal cavity. A flow path between the wetwell and drywell through the pedestal floor was also opened for gas flow through the failed drain line. An additional cavity modeling concern arose because initial LaSalle calculations predicted temperatures above melting for the drywell pedestal steel liner. This steel would then be expected to melt and flow down to the cavity. The additional steel would affect the progression of the core-concrete attack. Since MELCOR does not include modeling for melting heat structures, the effect was approximated by including the steel in the wetwell pedestal cavity from the beginning of the calculation instead of modeling it as a heat structure. The input for the MELCOR cavity package is summarized in Table A-9.

Table A-5

LaSalle Integral Calculation Control Volume Input

Control Volume	Brief Description	Bottom Elevation (m)	Top Elevation (m)	Volume (m^3)
100	Lower Plenum	0.	5.28	100.13
103	Upper Plen / Separators	9.66	15.43	65.10
104	Dryers / Steam Dome	15.43	22.23	191.44
105	Downcomer	3.34	15.43	228.16
111	Channel	5.28	9.66	2.60
112	Channel	5.28	9.66	10.64
113	Channel	5.28	9.66	9.84
114	Channel	5.28	9.66	6.20
115	Channel	5.28	9.66	4.40
116	Channel	5.28	9.66	4.59
121	Bypass	5.28	9.66	0.78
122	Bypass	5.28	9.66	3.19
123	Bypass	5.28	9.66	2.95
124	Bypass	5.28	9.66	1.86
125	Bypass	5.28	9.66	1.32
126	Bypass	5.28	9.66	15.22
200	Wetwell	-25.53	-7.15	8049.5
201	Downcomers	-21.11	-6.08	412.06
203	Lower Reactor Cavity	-17.45	-10.29	214.34
204	Upper Reactor Cavity	-9.15	2.5	255.66
205	Drywell	-6.24	23.84	5933.2
401	Lower Unit 2 Rctr Bldg	-19.25	-14.37	3035.6
402	Upper Unit 2 Rctr Bldg	-25.53	26.17	31410.
403	Refueling Floor	14.13	41.56	58770.
404	Unit 2 Stm Tun + Turb Bldg	-21.5	29.3	7267.2
405	Unit 1 Reactor Building	-19.25	26.17	34445.6
406	Unit 1 Stm Tun + Turb Bldg	-21.5	29.3	7267.2

Table A-6

LaSalle Integral Calculation Flow Path Input

Flow Path	From CV	To CV	Elev (m)	Area (m^2)	Loss Coeff	Additional Information
51	100	111	5.28	.53	12./15.	Can Block by Core Melt
52	100	112	5.28	2.19	12./15.	Can Block by Core Melt
53	100	113	5.28	2.02	12./15.	Can Block by Core Melt
54	100	114	5.28	1.27	12./15.	Can Block by Core Melt
55	100	115	5.28	0.90	12./15.	Can Block by Core Melt
56	100	116	5.28	0.94	12./15.	Can Block by Core Melt
61	100	121	5.28	0.16	102./128.	Can Block by Core Melt
62	100	122	5.28	0.66	102./128.	Can Block by Core Melt
63	100	123	5.28	0.61	102./128.	Can Block by Core Melt
64	100	124	5.28	0.38	102./128.	Can Block by Core Melt
65	100	125	5.28	0.27	102./128.	Can Block by Core Melt
66	100	126	5.28	3.44	102./128.	Can Block by Core Melt
71	111	103	9.66	0.53	12./15.	
72	112	103	9.66	2.19	12./15.	
73	113	103	9.66	2.02	12./15.	
74	114	103	9.66	1.27	12./15.	
75	115	103	9.66	0.90	12./15.	
76	116	103	9.66	0.94	12./15.	
81	121	103	9.66	0.16	102./128.	
82	122	103	9.66	0.66	102./128.	
83	123	103	9.66	0.61	102./128.	
84	124	103	9.66	0.38	102./128.	
85	125	103	9.66	0.27	102./128.	
86	126	103	9.66	3.44	102./128.	
57	121	122	7.47	1.86	42.	
58	122	123	7.47	4.18	33.	
59	123	124	7.47	5.34	24.	
60	124	125	7.47	6.27	12.	
67	125	126	7.47	6.73	12.	
15	103	104	15.43	4.19	9.1/2.8	
16	104	105	15.43	13.9	.11	
18	105	100	8.25/3.26	.33	.16/18.	Jet Pump Suction
21	104	200	16.46/-24.85	1.11	3.5	SRVs
370	105	205	6.84	3.E-6	1.	Pump Leakage
371	100	204	.1	3.E-6	1.	CRD Leakage
31	100	204	0.	.1	1.	Vessel Breach
24	205	201	-6.08	27.42	5.2	

** Vent & Leak paths from Containment were included in the deck, but not shown here since they were never opened.

Table A-6 (cont.)

Flow Path	From CV	To CV	Elev (m)	Area (m^2)	Loss Coeff	Additional Information
25	201	200	-21.11	27.42	1.	
26	200	205	-7.15	1.	1.	Vacuum Breakers
27	204	205	-4.5	2.46	2.	
28	205	204	-6.24	.065	2.5	Drywell Drain Lines
29	205	200	14.9/	.001	8.	N2 Line
40	203	204	-10.3	29.9	1.	Pedestal Drain Lines
41	203	200	-15.1	4.57	1.	
401	402	401	-14.2	12.2	4.	
402	402	403	26.2	33.1	1.	Blowout to Refuel Floor
403	402	403	26.2	3.08	2.9	Blowout to Refuel Floor
404	401	404	-18.4	3.01	2.8	Dampers to Stm Tunnel
405	402	405	4.	18.9	1.	Doors between Units 1 & 2
406	404	Env	28.8	3.53	1.	Blowout at Stm Tunnel Top
407	403	Env	33.9	40.	1.	Failure at Refuel Floor
408	402	Env	-9.88	.092	1.	Infiltration
409	405	Env	-9.88	.092	1.	Infiltration
410	402	Env	22.7	.164	1.	SGTS
411	405	Env	22.7	.164	1.	SGTS
412	405	403	26.2	33.1	1.	Blowout to Refuel Floor
413	405	403	26.2	3.08	2.9	Blowout to Refuel Floor
414	405	406	-18.4	3.01	2.8	Dampers to Stm Tunnel
415	406	Env	28.8	3.53	1.	Blowout at Stm Tunnel Top
416	403	Env	14.1	.01	10.	Minor Leakage Paths
417	404	Env	-14.3	.01	10.	Minor Leakage Paths
418	406	Env	-14.3	.01	10.	Minor Leakage Paths

Table A-7

LaSalle Integral Calculation Heat Structure Input

Heat Structure	Left CV	Right CV	Inside Surface Area	Material	Thickness (m)
10402	104	205	63.8	Steel	.178
10403	104	205	72.2	Steel	.178
10501	105	205	242.	Steel	.178
10401	104	104	697.	Stainless	.0066
10303	103	105	520.	Stainless	.0158
10302	103	105	21.6	Stainless	.0508
10301	103	105	14.	Stainless	.0508
10304	103	Ins.	114.	Stainless	.0058
12613	126	105	5.82	Stainless	.0508
12612	126	105	10.3	Stainless	.0508
12611	126	105	10.3	Stainless	.0508
12610	126	105	10.3	Stainless	.0508
12609	126	105	10.3	Stainless	.0508
12608	126	105	10.3	Stainless	.0508
12607	126	105	10.2	Stainless	.0508
12606	126	105	3.39	Stainless	.0508
10005	100	105	1.13	Stainless	.0508
10004	100	105	0.25	Stainless	.0508
10014	100	105	30.1	Stainless	.0508
10003	100	205	28.2	Steel	.0778
10002	100	205	8.71	Steel	.0778
10001	100	205	8.71	Steel	.0778
20001	200	402	1525.	Stainless/Conc	1.219
20002	200	Ins.	483.	Stainless/Conc	7.01
20003	200	Ins.	62.3	Stainless/Conc	.540
20004	200	204	58.6	Stainless/Conc	1.48
20005	200	203	160.8	Stainless/Conc	1.49
20006	200	Ins.	215.4	Stainless/Conc	1.48
20007	200	Ins.	24.7	Stainless	.0190
20008	200	Ins.	31.2	Stainless	.0190
20101	201	200	28.2	Stainless	.308
20301	203	204	29.9	Concrete	1.143
20501	200	205	83.8	Stainless/Conc	.921
20502	205	205	365.	Steel/Conc	4.56
20503	205	402	2100.	Steel/Conc	1.83
20504	205	204	147.6	Concrete	1.47
20505	205	Ins.	181.	Steel/Air/Conc	7.66
20506	205	Ins.	74.55	Steel	.0058
20507	205	Ins.	74.55	Steel	.0058

Table A-7 (cont.)

Heat Structure	Left CV	Right CV	Inside Surface Area	Material	Thickness (m)
40101	401	Ins.	227.7	Concrete	.406
40102	401	Ins.	22.3	Concrete	.523
40103	401	402	151.8	Concrete	.610
40104	401	404	67.6	Concrete	.914
40105	401	405	17.5	Concrete	.702
40106	401	Ins.	2.79	Steel	.0031
40201	402	Ins.	174.5	Concrete	.320
40202	402	Ins.	52.6	Concrete	.501
40203	402	Ins.	2.32	Steel	.0071
40204	402	403	289.7	Concrete	1.0
40205	402	403	86.4	Concrete	1.83
40206	402	404	50.0	Concrete	1.22
40207	402	404	42.8	Concrete	1.05
40208	402	405	63.5	Concrete	.610
40209	402	Env.	63.5	Concrete	.476
40301	403	Ins.	490.2	Concrete	.610
40302	403	Ins.	2.32	Steel	.0071
40303	403	Ins.	3656.	Steel	.0032
40304	403	Env	4016.	Steel	.0032
40401	404	Ins.	33.7	Concrete	.610
40402	404	Env	391.6	Concrete	1.83
40403	404	Env	412.7	Concrete	1.83
40501	405	Ins.	286.5	Concrete	.325
40502	405	Ins.	37.8	Concrete	.506
40503	405	Ins.	2.34	Steel	.0069
40504	405	403	289.7	Concrete	1.0
40505	405	403	86.4	Concrete	1.83
40506	405	406	50.0	Concrete	1.22
40507	405	406	39.8	Concrete	1.01
40508	405	Env	63.5	Concrete	.476
40601	406	Ins.	33.7	Concrete	.61
40602	406	Env	391.6	Concrete	1.83
40603	406	Env	412.7	Concrete	1.83

Table A-8

LaSalle Integral Calculation Core Input

Number of Radial Rings = 6
Number of Axial Levels = 13 (5 in lower plenum)

Level	Bottom Elev (m)
1	0.
2	.64
3	1.28
4	5.20
5	5.21
6	5.28
7	5.49
8	6.13
9	6.76
10	7.40
11	8.03
12	8.67
13	9.30

Ring	X-C Area (m^2)
1	1.208
2	4.923
3	4.552
4	2.880
5	2.044
6	2.137

Total of All 6 Ring Masses for Level

Level	UO2	Zr-Clad	St Steel	B4C	Zr-Can
13	0.	3445.	1389.	0.	2429.
12	26453.	6282.	1646.	146.	4294.
11	26453.	6282.	1646.	146.	4294.
10	26453.	6282.	1646.	146.	4294.
9	26453.	6282.	1646.	146.	4294.
8	26453.	6282.	1646.	146.	4294.
7	26453.	6282.	1646.	146.	4294.
6	0.	863.	6248.	0.	551.
5	0.	0.	10659.	0.	0.
4	0.	0.	2394.	0.	0.
3	0.	0.	22194.	0.	0.
2	0.	0.	2923.	0.	0.
1	0.	0.	3949.	0.	0.

Table A-8 (cont.)

Level	Total of All 6 Ring Surface Areas for Level UO2	Zr-Clad	St Steel	Zr-Can
13	0.	537.7	61.65	147.
12	984.	1420.	115.	260.
11	984.	1420.	115.	260.
10	984.	1420.	115.	260.
9	984.	1420.	115.	260.
8	984.	1420.	115.	260.
7	984.	1420.	115.	260.
6	0.	27.9	131.	5.2
5	0.	0.	9.72	0.
4	0.	0.	6.97	0.
3	0.	0.	603.	0.
2	0.	0.	54.2	0.
1	0.	0.	55.9	0.

Table A-9

LaSalle Integral Calculation Cavity Input

Initially, 15452 kg of stainless steel added to account for sump tank, gratings, liners, pipes, and supports that would be melted by corium

Concrete Composition:

Material	Fraction
SIO2	.368
MNO	5.E-5
CAO	.2226
K2O	.0015
AL2O3	.0090
CO2	.2017
TIO2	1.3E-4
MGO	.0921
NA2O	5.9E-4
FE2O3	.0021
CR2O3	2.E-5
H2OEVAP	.0255
FE	.0560
H2OCHEM	.0189

Other Input
Cavity Radius = 3.086 m
Concrete Density = 2340.
Solidus Temperature = 1420.
Liquidus Temperature = 1670.
Ablation Temperature = 1503.

A.2 Grand Gulf Nodalizations

Two MELCOR input decks were used for the Grand Gulf analyses, a deck modeling only the containment for addressing specific issues regarding containment phenomena and loading, and an integral deck for the station blackout calculation.

A.2.1 Containment-Only Model

The MELCOR model of the Grand Gulf containment was based on an existing HECTR deck that had been used to examine hydrogen mixing and igniter performance [A-2]. Most of the HECTR input was translated directly to MELCOR input, but some modifications were needed because of differences in modeling approaches in the two codes and to include input for phenomena not addressed in the HECTR analyses.

The MELCOR nodalization for the containment-only deck is shown in Figure A-3. Five control volumes were used to model the outer containment: dome, wetwell, equipment hatch, and the upper and lower portions of the remaining region between the wetwell and dome. Three control volumes were used for the drywell. The drywell pedestal and weir annulus were modeled as separate control volumes and the remainder of the drywell was modeled by the third control volume. The weir annulus was modeled as a separate control volume to properly track the motion of the suppression pool surface. The control volume input is summarized in Table A-10.

The flow paths between the containment control volumes are listed in Table A-11. Note that leakage between the drywell and outer containment is included and that flow through the suppression pool vents is modeled using three separate flow paths for the three vent row elevations.

The heat structure input is summarized in Table A-12. The radiative heat transfer input for the outer containment surfaces was only used in calculations analyzing burns in the outer containment.

The spray input used to analyze de-inerting a steam-filled containment is summarized in Table A-13. The spray model was not used in any of the other analyses. The input corresponds to a single spray train operating in the recirculation mode with water being drawn from a saturated suppression pool.

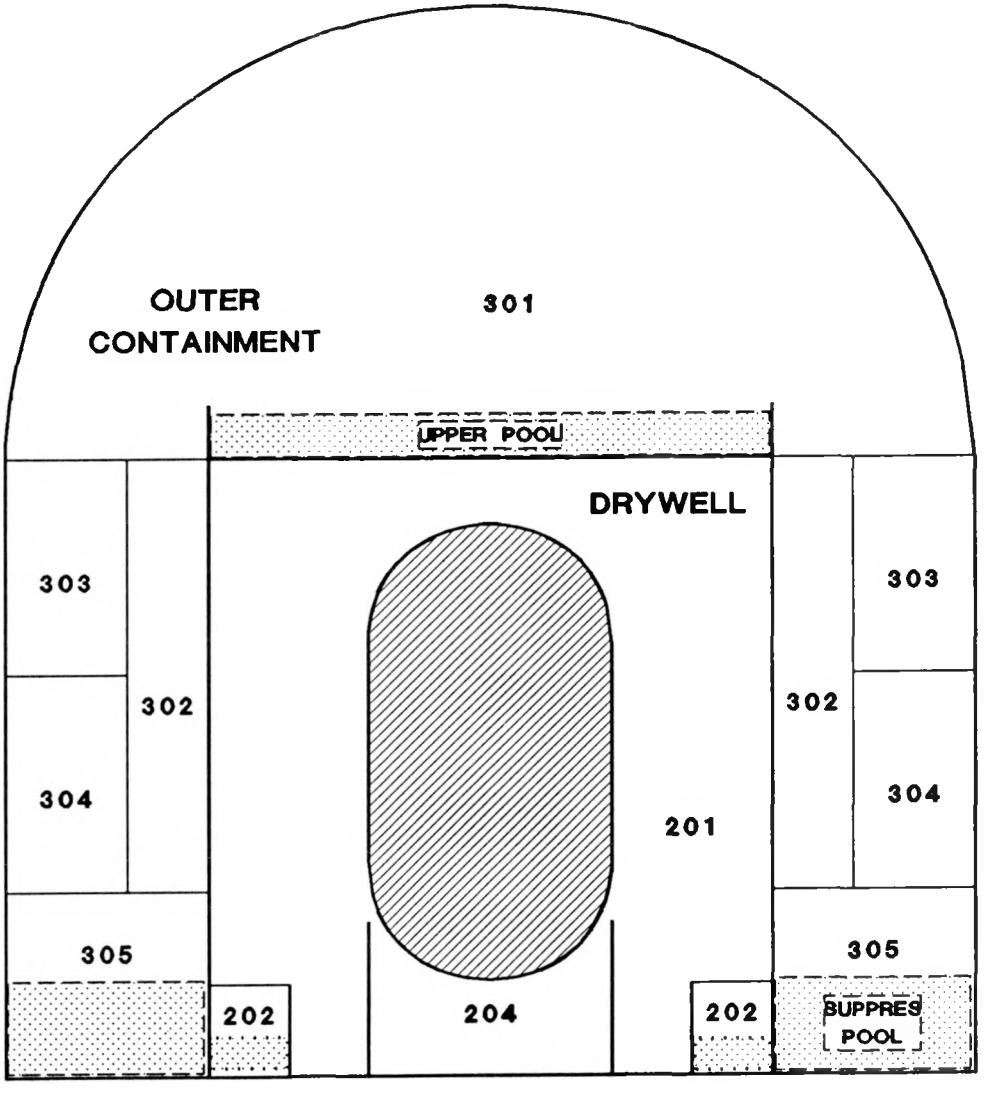

Figure A-3. Nodalization for Grand Gulf Containment-Only Calculations

Table A-10

Grand Gulf Containment Model Control Volume Input

Control Volume	Brief Description	Bottom Elevation (m)	Top Elevation (m)	Volume (m^3)
201	Drywell	-6.73	24.36	6554.
202	Weir Annulus	-9.09	12.56	1462.5
204	Reactor Pedestal	-8.64	3.34	244.5
301	Dome	13.61	53.92	25463.
302	Equipment Hatch	3.71	26.26	1654.
303	Upper Annular Region	11.63	26.26	4480.
304	Lower Annular Region	3.71	11.63	3278.
305	Wetwell / Suppres Pool	-9.09	3.71	7783.

Table A-11

Grand Gulf Containment Model Flow Path Input

Flow Path	From CV	To CV	Elev (m)	Area (m^2)	Loss Coeff	Variable Open Fraction
202	302	201	7.56	.0929	1.	Leak - Fraction Varied
203	201	202	-1.68	51.4	.1	
204	201	202	8.32	51.4	.5	
205	201	204	-4.65	1.95	1.	
206	201	204	-6.73	5.	.5	
211	202	305	-5.64	17.9	4.	
212	202	305	-6.91	17.9	4.	
213	202	305	-8.18	17.9	4.	
301	301	302	26.26	74.3	.75	
302	301	303	26.26	152.1	1.5	
303	302	303	18.95	135.64	1.5	
304	302	304	7.67	157.	1.5	
305	302	305	3.71	62.4	.75	
306	303	304	11.63	228.8	1.5	
307	304	305	3.71	144.4	1.5	
100	301	400	40.	10.	1.	Cont Fail - Only Opened when Fails

Table A-12

Grand Gulf Containment Model Heat Structure Input

Heat Structure	Left CV	Right CV	Surface Area (m^2)	Material	Thickness (m)	Description
30101	301	Ins.	297.3	Concrete	.1534	Floor
30102	301	Ins.	555.	Stainless	.0085	Up Pool Walls
30103	301	Ins.	1188.	Stainless	.216	Crane
30104	301	Ins.	3291.	SS/Conc	1.70	Cont Wall
30201	302	Ins.	393.4	SS/Conc	1.70	Cont Wall
30301	303	Ins.	950.0	SS/Conc	1.70	Cont Wall
30302	303	Ins.	202.0	Concrete	.763	DW Wall
30303	303	Ins.	2103.	Concrete	.1534	Walls/Floors
30304	303	303	1980.	Stainless	.018	Equipment
30401	304	Ins.	702.	SS/Conc	1.70	Cont Wall
30402	304	Ins.	487.	Concrete	.763	DW Wall
30403	304	Ins.	396.	Concrete	.1534	Walls/Floors
30404	304	304	1040.	Stainless	.0238	Equipment
30501	305	Ins.	832.0	SS/Conc	1.70	Cont Wall
30502	305	Ins.	557.	Concrete	.763	DW Wall
30503	305	Ins.	308.	Concrete	.1534	Walls/Floors
30504	305	305	1127.	Stainless	.0103	Equipment
20101	201	Ins.	465.	SS/Conc	.317	Shield Wall
20102	201	Ins.	589.	Concrete	.229	Weir Wall
20103	201	201	2154.	Stainless	.0092	Equipment
20104	201	Ins.	235.0	Concrete	.9144	DW Floor
20105	201	Ins.	235.0	SS/Conc	.9144	DW Wall & Top
20401	204	201	166.3	Conc/SS	1.771	Pedestal

Table A-13

Grand Gulf Containment Model Spray Input

Flow Rate = .356 m^3/s
Injection Temperature = 330 K

Drop Size Distribution:

Fraction	Diameter (m)
.95	3.09E-4
.05	8.10E-4

Carryover Between Compartments:

From CV	To CV	Carryover Fraction
301	302	.1
301	303	.2

A.2.2 Integral Grand Gulf Model

The integral Grand Gulf deck is a combination of the MELCOR containment-only deck that was described in Section A.2.1 and vessel input that was derived from the MELCOR LaSalle deck which was described in Section A.1.2. A nodalization of the Grand Gulf integral model is shown in Figure A-4.

Based on a thorough review of results calculated for the LaSalle station blackout, the vessel model was heavily modified for Grand Gulf. The twelve volumes used to model the channel and bypass were collapsed to two volumes because we felt that the potential for natural circulation needed to be examined more thoroughly before running with such detailed noding. In addition, a valve was added to close the jet pump flow path when the RPV level fell below the bottom of the shroud. This was done to halt natural circulation, which appeared to be contributing to the effects that were excessively cooling the core in the LaSalle station blackout calculation.

The three center radial rings in the core model were collapsed to a single ring because the power profile is reasonably flat in that region. The noding near the core plate was also modified, based on experience gained through the LaSalle analysis. Those results indicated that the

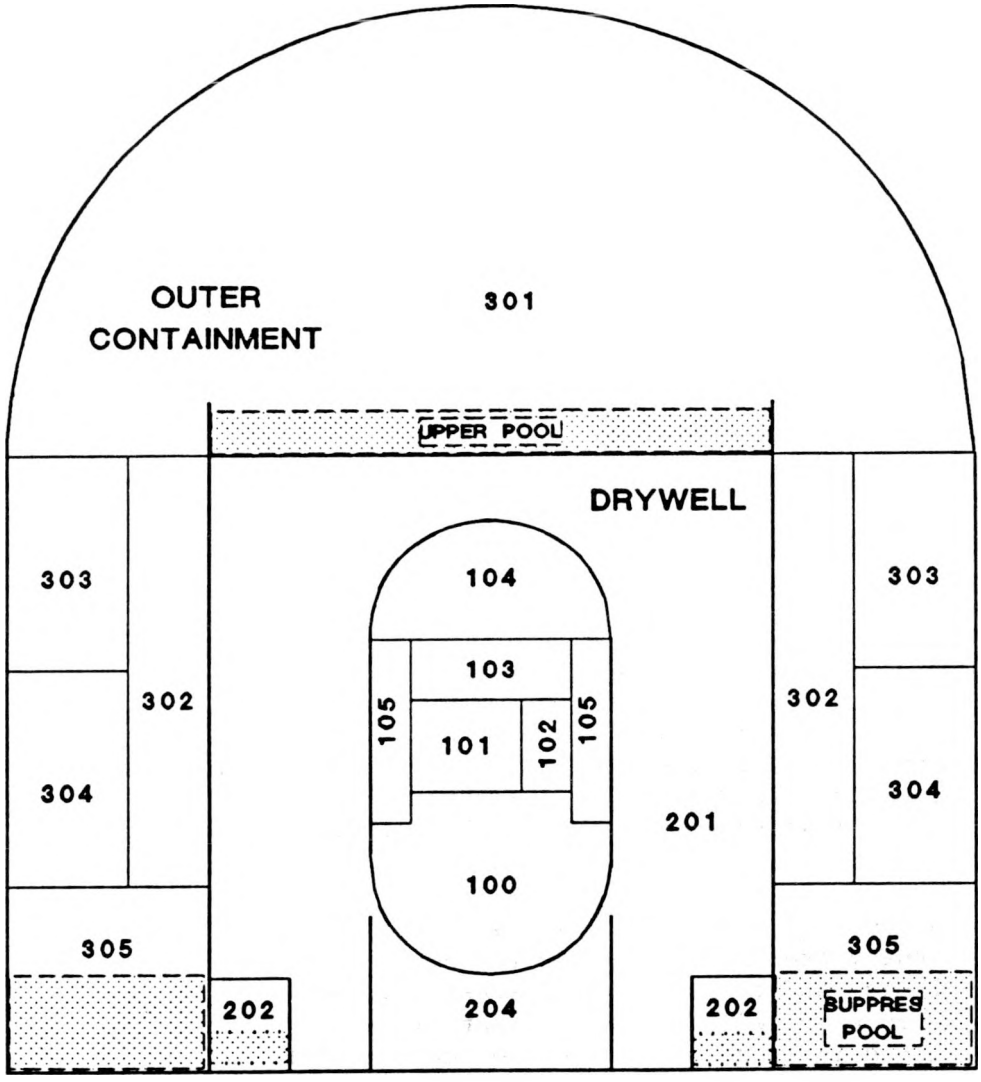

Figure A-4. Nodalization for Grand Gulf Integral Calculations

combined use of a small axial node below the core plate and a large node below it were causing excessive axial conduction through the support structures in the lower plenum. Therefore, for the Grand Gulf model, the small axial node was extended downward to include a larger portion of the lower plenum. The LaSalle results also predicted that the upper core support, which had been modeled as a heat structure, would reach melting temperatures. Therefore, for the Grand Gulf model, the upper core support was included as part of the structure modeled in the core package, rather than a heat structure. Several other minor changes were made to correct errors. The core masses and surface areas were then increased to account for the larger number of fuel assemblies in Grand Gulf relative to LaSalle. Table A-14 summarizes these revisions to the core input for the Grand Gulf integral model.

Table A-14

Grand Gulf Integral Calculation Core Input

Number of Radial Rings = 4
Number of Axial Levels = 13 (5 in lower plenum)

Level	Bottom Elev (m)
1	0.
2	.64
3	1.28
4	4.58
5	5.21
6	5.28
7	5.49
8	6.13
9	6.76
10	7.40
11	8.03
12	8.67
13	9.30

Ring	X-C Area (m^2)
1	10.683
2	2.880
3	2.044
4	2.137

Table A-14 (cont.)

Total of All 4 Ring Masses for Level

Level	UO2	Zr-Clad	St Steel	B4C	Zr-Can
13	0.	3607.	6985.	0.	2543.
12	27700.	6578.	1724.	153.	4497.
11	27700.	6578.	1724.	153.	4497.
10	27700.	6578.	1724.	153.	4497.
9	27700.	6578.	1724.	153.	4497.
8	27700.	6578.	1724.	153.	4497.
7	27700.	6578.	1724.	153.	4497.
6	0.	903.	6542.	0.	577.
5	0.	0.	11162.	0.	0.
4	0.	0.	6287.	0.	0.
3	0.	0.	19460.	0.	0.
2	0.	0.	3061.	0.	0.
1	0.	0.	4135.	0.	0.

Total of All 4 Ring Surface Areas for Level

Level	UO2	Zr-Clad	St Steel	Zr-Can
13	0.	563.	184.	154.
12	1030.	1487.	120.	272.
11	1030.	1487.	120.	272.
10	1030.	1487.	120.	272.
9	1030.	1487.	120.	272.
8	1030.	1487.	120.	272.
7	1030.	1487.	120.	272.
6	0.	29.2	137.	5.4
5	0.	0.	102.	0.
4	0.	0.	110.	0.
3	0.	0.	529.	0.
2	0.	0.	56.7	0.
1	0.	0.	58.5	0.

A.3 Peach Bottom Nodalization

The MELCOR nodalization for the Peach Bottom plant is shown in Figure A-5. The reactor vessel was modeled with six control volumes representing the lower plenum, the core fuel rod flow channels, the core bypass flow channels, the downcomer annulus, the shroud dome, and steam dome. The containment was modeled with three control volumes representing the drywell, the vent downcomers, and the wetwell. The control volume input is summarized in Table A-15 and the flow paths between the control volumes are listed in Table A-16.

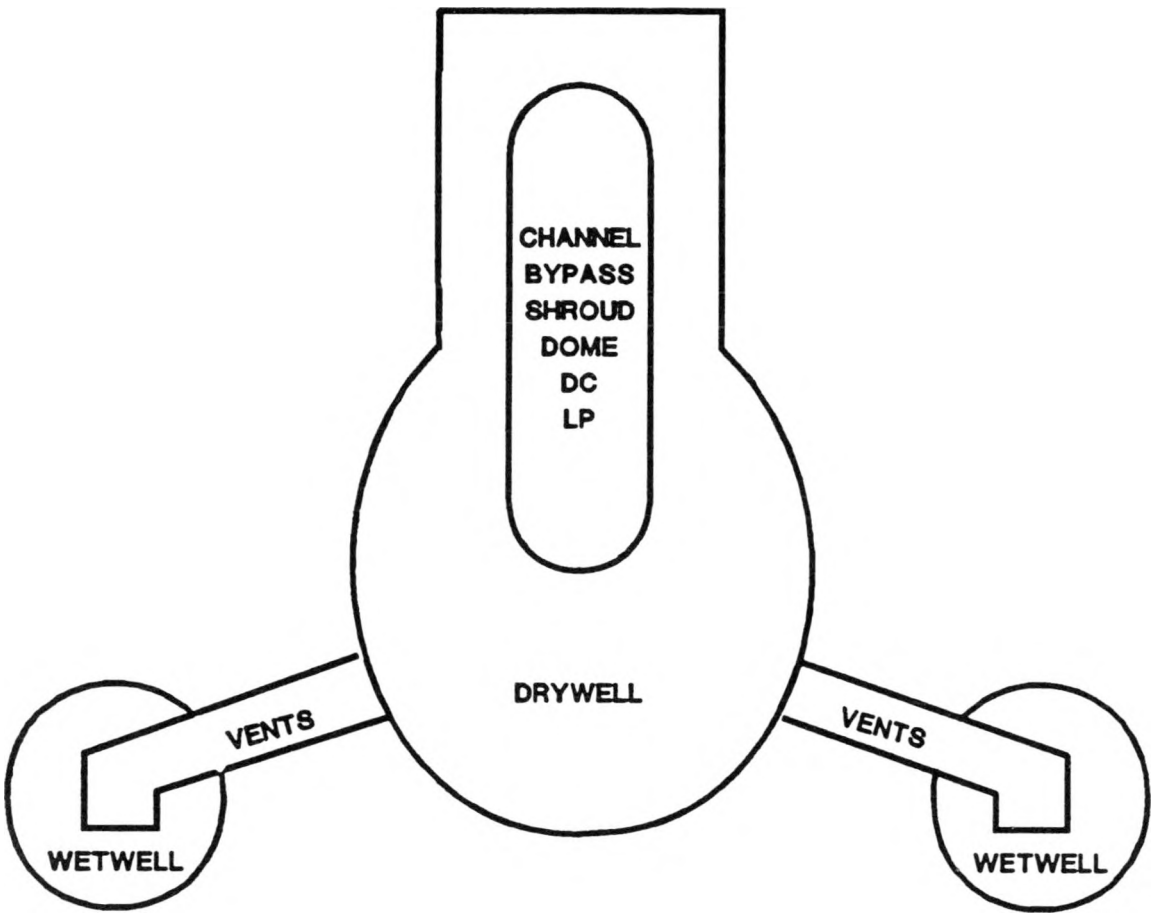

Figure A-5. Nodalization for Peach Bottom Calculations

The heat structure input is summarized in Table A-17. Seven heat structures were used to model structures and equipment in the containment and 13 structures were used to model structures and equipment in the RPV.

Table A-15

Peach Bottom Control Volume Input

Control Volume	Brief Description	Bottom Elevation (m)	Height (m)	Volume (m^3)
100	Drywell	-9.1	32.6	4315.
150	Vent/Downcomer	-13.8	7.2	565.
200	Wetwell	-16.4	9.6	7027.
310	RPV Downcomer	3.1	12.3	183.8
320	RPV Lower Plenum	0.	5.5	98.6
330	Core Bypass	5.5	4.2	25.6
340	Core Channel	5.5	4.2	37.5
350	Shroud Dome	9.7	5.7	44.9
360	Steam Dome	15.4	6.8	218.6

Table A-16

Peach Bottom Flow Path Input

Flow Path	From CV	To CV	Elev (m)	Area (m^2)	Loss Coeff	Variable Open Fraction
DC Inlet	100	150	-7.3	26.6	6.7	
DC Exit	150	200	-13.8	26.6	1.	
Vessel Breach	320	100	0./ -.23	.00785	1.	Opened at time of vessel breach
WW-DW Vacuum Breakers	200	100	-10.1/ -6.6	1.86	1.	Closed until Wetwell P exceeds Drywell pressure
DC to LP	310	320	8.08/ 3.09	.678	.079/ 17.	
Bypass In	320	330	5.49	6..15	.52/ 5.0	Open Fraction = .013
Channel In	320	340	5.49	7.94	10.2/ 13.3	Open Fraction = .617
Channel Out	340	350	9.67	6.15	50./ .5	
Bypass Out	330	350	9.67	7.94	5.7	Open Fraction = .676
Shroud - Dome	350	360	15.43	4.78	12.6/ 5.	
Dome - DC	360	310	15.43	26.1	.11	

Table A-17

Peach Bottom Heat Structure Input

Left CV	Right CV	Surface Area (m^2)	Material	Thickness (m)	Description
100	Ins.	1736.	Steel	.029	Drywell Liner
100	Ins.	132.	Concrete	1.44	Drywell Floor
100	Ins.	767.	Concrete	.349	Upper Reactor Pedestal
100	Ins.	337.	Concrete	.533	Lower Reactor Pedestal
100	Ins.	801.	Steel	.017	Drywell Steel
200	Ins.	1584.	Steel	.016	Wetwell Liner
200	Ins.	4189.	Steel	.017	Wetwell Steel
310	100	317.	Steel	.156	RPV Walls
320	100	33.1	Steel	.119	RPV Lower Head
350	310	472.	Stainless	.019	Separators
360	Ins.	2945.	Stainless	.0018	Dryers
360	100	63.8	Steel	.102	RPV Upper Head
320	310	18.6	Stainless	.02	Lower Plenum Shroud
320	310	15.9	Stainless	.02	Lower Plenum Shroud
320	310	4.5	Stainless	.02	Lower Plenum Shroud
330	310	12.4	Stainless	.02	Core Shroud
330	310	12.4	Stainless	.02	Core Shroud
330	310	12.4	Stainless	.02	Core Shroud
330	310	12.4	Stainless	.02	Core Shroud
330	310	12.4	Stainless	.02	Core Shroud

A.4 References

A-1 LaSalle County Station Final Safety Analysis Report, Commonwealth Edison Company, 1983.

A-2 Cummings, J. C., et al., Review of the Grand Gulf Hydrogen Igniter System, NUREG/CR-2530, SAND82-0218, Sandia National Laboratories, Albuquerque, NM, March 1983.

DISTRIBUTION:

1 ANATECH Research Corp.
Attn: Joe Rashid
3344 N. Torrey Pines Ct.
Suite 1320
La Jolla, CA 90237

1 ANSTO Research Establishment
Attn: E. R. Corran
Nuclear Technology Division
Lucas Heights Research Laboratories
Private Mail Bag 7
Menai, NSW 2234
AUSTRALIA

1 American Nuclear Society
Attn: Lois Webster
555 N. Kensington Avenue
La Grange Park, IL 60525

3 Argonne National Laboratories
Attn: Louis Baker, Bldg 207
S. Y. Chen
Leo LeSage, Bldg 208
9700 South Cass Avenue
Argonne, IL 60439

1 Arizona State University
Attn: Jon Helton
Dept. of Mathematics
Tempe, AZ 85287

2 Atomic Energy Council, Nuclear Safety
Attn: Shih-Kuei Cheng
Der Yu Hsia
67, Lane 144, Keelung Rd. Sec. 4
Taipei, Taiwan
REPUBLIC OF CHINA

1 Atomic Energy Council
Attn: Lainsu Kao, Associate Scientist
Institute of Nuclear Energy Research
P.O. Box 303
Lung-Tan, 32500
Taiwan
REPUBLIC OF CHINA

4 Atomic Energy of Canada Limited
Attn: Samir S. Girgis
E. Kohn, Candu Operations
V. I. Nath, Safety Branch
H. Shapiro, Licensing & Risk Branch
Sheridan Park Research Community
Mississauga, Ontario
CANADA, L5K1B2

2 Atomic Energy of Canada Limited
Attn: David R. Torgerson
D. J. Wren
Whiteshell Nuclear Research Establishment
Pinawa, Manitoba, ROE 1LO
CANADA

1 Australian Nuclear Science and Technology Organisation
Attn: D. J. Higson
Nuclear Safety Bureau
P.O. Box 153
Rosebery, NSW 2018
AUSTRALIA

1 BGA/ISH/ZDB
Attn: Anton Bayer
Postfach 1108
D-8042 Neuherberg
FEDERAL REPUBLIC OF GERMANY

1 Barthold & Associates, Inc.
Attn: W. P. Barthold
132 Seven Oaks Drive
Knoxville, TN 37922

5 Battelle Columbus Laboratories
Attn: Peter Cybulskis
Richard S. Denning
Raymond DiSalvo
Jim Gieseke
Stephen D. Unwin
505 King Avenue
Columbus, OH 43201

1 Battelle Institute EV
Attn: Dr. Lothar Wolf
AM Romerhof 35
D-6000
Frankfurt/Main90
WEST GERMANY

1 Bechtel Power Corporation
Attn: Donald H. Ashton
P.O. Box 2166
Houston, TX 77252-2166

1 Bechtel Power Corporation
Attn: Subir Sen
15740 Shady Grove Road
Location 1A-7
Gaithersburg, MD 20877

2 Bechtel Western Power Co.
Attn: Milton Levenson
Jorge Schulz
50 Beale St.
P.O. Box 3965
San Francisco, CA 94119

2 Belgonucleaire S A
Attn: H. Bairiot
J. Basselier
Rue de Champ de Mars 25
B-1050 Brussels
BELGIUM

1 Jack R. Benjamin & Assoc, Inc.
Attn: John W. Reed
444 Castro St., Suite 501
Mountain View, CA 94041

3 Bettis Atomic Power Laboratory
Attn: J. T. Lobritz
H. W. Ryals
David Teolis, ZAP 34N
P.O. Box 79
West Mifflin, PA 15122

1 Boston Edison Company
Attn: James W. Ashkar
800 Boylston Street
Boston, MA 02199

1 British Embassy
Attn: John Gaunt
3100 Massachusetts Ave, NW
Washington, DC 20008

13 Brookhaven National Laboratory
Attn: R. A. Bari, Bldg 130
E. Cazzoli, Bldg 130
T. Ginsburg, Bldg 820
G. Greene, Bldg 820M
C. Grimshaw, Bldg 130
Walter Kato
H. J. C. Kouts, Bldg 179C
W. J. Luckas, Bldg 130
H. Ludewig, Bldg 130
I. K. Madni, Bldg 130
C. K. Park, Bldg 130
W. T. Pratt, Bldg 130
A. Tingle, Bldg 130
Upton, NY 11973

1 CBI Na-Con Inc.
Attn: Kam Mohktarian
800 Jorie Blvd.
Oak Brook, IL 60521

1 Cabinete de Proteccao e Seguranca Nuclear
Attn: J. de Assuncao
Secretario de Estado de Energia
Ministerio da Industria
av. da Republica, 45-6
1000 Lisbon
PORTUGAL

1 Carolina Power and Light Co.
Attn: Richard C. Anoba
Corp. Nuclear Safety
P. O. Box 1151
Raleigh, NC 27602

1 Case Western Reserve University
Attn: Simon Ostrach
418 Glenman Bldg.
Cleveland, OH 44106

1 Cekmece Nuclear Research and Training Center
Attn: Ulvi Adalioglu
Nuclear Engineering Division
P.K.1, Havaalani
Istanbul
TURKEY

2 Central Electricity Generating Board
Attn: Simon Board
J. P. Longworth
Berkeley Nuclear Laboratory
Berkeley Gloucestershire, GL139PB
UNITED KINGDOM

1 Central Electricity Generating Board
Attn: Nigel E. Buttery
Booths Hall
Chelford Road, Knutsford
Cheshire, WA168QG
UNITED KINGDOM

2 Chalk River Nuclear Laboratories
Attn: Paul J. Fehrenbach
David B. Rhodes
Chalk River, Ontario
CANADA KOJ 1P0

1 Combustion Engineering
Attn: Charles Brinkman
7910 Woodmont Avenue
Bethesda, MD 20814

1 Combustion Engineering, Inc.
Attn: R. E. Jaquith
1000 Prospect Hill Road
M/C 9490-2405
Windsor, CT 06095

2 Commission European Comm.
Attn: Giuseppe Mancini
G. Volta
CEC-JRC Eratom
Ispra Varese
ITALY

1 Commission of the European Communities
Attn: Brian J. R. Tolley
DG/XII/D/1
Rue de la Loi, 200
B-1049, Brussels
BELGIUM

1 Commonwealth Edison Co.
Attn: J. Alman
LaSalle County Station
RR1, Box 220
2601 North 21st Rd.
Marsielles, IL 61341

1 Commonwealth Edison Co.
Attn: George Klopp, Room 35W
Wayne Stiede
P.O. Box 767
Chicago, IL 60690

3 Consejo de Seguridad Nuclear
Attn: Juan Bagues
Jose I. Calvo Molins, Probabilistic Safety Analysis Group
J. I, Villadoniga Tallon, Div. of Analysis and Assessment
Sor Angela de la Cruz 3, Pl. 6
28020 Madrid
SPAIN

1 Consejo de Seguridad Nuclear
Attn: Jose E. DeCarlos
Sor Angela de la Cruz 3, Pl. 8
28016 Madrid
SPAIN

1 C. Allin Cornell
110 Coquito Way
Portola Valley, CA 94025

1 George R. Crane
1570 E. Hobble Creek Dr.
Springville, UT 84663

1 James J. Curry
7135 Salem Park Circle
Mechanicsburg, PA 17055

1 Department de la Surete
Nucleaire
Attn: P. Govaerts
Association Vincotte
avenue du Roi 157
B-1060 Bruxelles
BELGIUM

1 Department de Surete Nucleaire
Attn: J. Pelce
IPSN
Centre d'Estudes Nucleaires du
CEA
B.P. no. 6, Cedex
F-92260 Fontenay-aux-Roses
FRANCE

2 Department Technologie
Attn: N. Marc Decreton
M. Siebertz
CEN/SCK
Boeretang 200
B-2400 Mol
BELGIUM

1 Duke Power Company
Attn: Kenneth S. Canady
422 S. Church Street
Charlotte, NC 28217

10 EG&G Idaho
Attn: Doyle J. Batt
John H. Bickel
A. Brown
R. Jack Dallman
R. D. Fowler
D. W. Golden
Richard Hobbins
Phillip E. MacDonald
Paul North
Marty Sattison
P.O. Box 1625
Idaho Falls, ID 83415

1 EI International
Attn: D. Jones
P.O. Box 50736
Idaho Falls, ID 83405

2 EI Services
Attn: Sharon Brown
Timothy J. Leahy
1851 So. Central Place, Suite 201
Kent, WA 98031

1 ENEA DISP TX612167 ENEUR
Attn: T. Cianciolo
BWR Assistant Director
Rome
ITALY

4 ENEA
Attn: Giovanni Saponaro
G. Petrangeli
A. Valeri
C. Zaffiro
Via Vitaliano Brancati, 48
I-00144 Rome
ITALY

2 ENEA Cre Casaccia
Attn: G. Caropreso, Dept. for
Envir. Protect. & Health
P. Ficara, Dept. for
Thermal Reactors
Via Anguillarese, 301
00100 Roma
ITALY

1 ERC Environmental Services Co.
Attn: Chao-Chin Tung
c/o H. B. Bengelsdorf
P.O. Box 10130
Fairfax, VA 22030

1 ERC International
Attn: G. Bruce Varnado
1717 Louisiana Blvd. NE
Suite 202
Albuquerque, NM 87110

1 Ebasco Services, Inc.
Attn: Edward P. O'Donnell
2 World Trade Center, 89th Floor
New York, NY 10048

1 Ecole Polytechnique de Lausanne
Attn: H. Bargmann
Dept. de Mecanique
Inst. de Machines Hydrauliques
et de Mecaniques des Fluides
CH-1003 Lausanne
M.E. (ECUBLENS)
CH. 1015 Lausanne
SWITZERLAND

6 Electric Power Research Inst.
Attn: R. J. Breen
R. Ritzman
G. D. Sauter
B. R. Sehgal
J. Taylor
I. B. Wall
3412 Hillview Ave
Palo Alto, CA 94303

5 Electric Power Research Inst.
Attn: E. Fuller
W. Lowenstein
R. N. Oehlberg
Technical Library
Richard Vogel
P. O. Box 10412
Palo Alto, CA 94303

1 Electricite de France
Attn: Annick Carnino
32 Rue de Monceau 8EME
Paris, F5008
FRANCE

1 Energy People, Inc.
Attn: Faith Young
Dixou Springs, TN 37057

1 Energy Research Inc.
Attn: M. Khatib-Rahbar
P.O. Box 2034
Rockville, MD 20852

1 Ente Nazionale per l'Energia
Electtrica (ENEL)
Attn: S. Serra
via G. B. Martini 3
Rome
ITALY

1 Exxon Nuclear Company
Attn: S. E. Jensen
2101 Horn Rapids Road
Richland, WA 99352

1 F. R. Farmer
The Long Wood, Lyons Lane
Appleton, Warrington
WA4 5ND
UNITED KINGDOM

3 Fauske & Associates
Attn: Mike Epstein
Robert E. Henry
Marty Plys
16W070 West 83rd Street
P.O. Box 1625
Burr Ridge, IL 60521

1 Federal Ministry for the
Environment, Preservation of
Nature and Reactor Safety
Attn: P. M. Herttrich
Husarenstrasse 30
Postfach 120629
D-5300 Bonn 1
FEDERAL REPUBLIC OF GERMANY

1 Finnish Center Radiation & Nucl.
Safety, Dept. of Nuclear Safety
Attn: Jorma V. Sandberg
P.O. Box 268
SF-00101 Helsinki
FINLAND

1 Finnish Centre Radiation & Nucl.
Safety, Dept. of Nuclear Safety
Attn: R. Virolainen
P.O. Box 268
Kumpulantie 7
SF-00520 Helsinki
FINLAND

1 Florida Power Corporation
Attn: Mark Averett
P.O. Box 14042
St. Petersburg, FL 33733

1 Future Resources Associates
Attn: Robert J. Budnitz
734 Alameda
Berkeley, CA 94707

1 GPU Nuclear Corporation
Attn: Nick Trikouros
One Upper Pond Road
Parsippany, NJ 07054

4 General Electric Company
Attn: J. A. Bast
G. H. Epstein
E. Love
K. J. McDonough
Knolls Atomic Power Laboratory
Bldg. F3, Room 8
P.O. Box 1072
Schenectady, NY 12301-1072

2 General Electric Company
Attn: W. P. Sullivan
S. Visweswaran
175 Curtner Avenue
San Jose, CA 95125

1 General Electric, Inc.
Attn: Mark I. Temme
P.O. Box 3508
Sunnyvale, CA 94088

1 Gabor, Kenton & Associates
Attn: M. A. Kenton
770 Pasquinelli Drive
Suite 426
Westmont, IL 60559

2 Gesellschaft fur
Reaktorsicherheit
Attn: Ulrich Erven
F. Heuser
Schwerthergasse 1
D-5000 Cologne 1
WEST GERMANY

8 Gesellschaft fur
Reaktorsicherheit
Forschungsgelande
Attn: Werner Bastl
Adolf Birkhofer
E. F. Hicken
Edward Hofer
Peter Kafka
Klaus Koberlein
Klaus Trambauer
Wolfgang Werner
D-8046 Garching
FEDERAL REPUBLIC OF GERMANY

1 Greek Atomic Energy Commission
Attn: X. Zikidis
Agia Paraskevi, Attiki
Athens
GREECE

1 Gulf States Utilities
Attn: Joseph Miller
P.O. Box 220
St. Francisville, LA 70775

3 IAEA A-1400
Attn: Lennart Carlsson
Michael C. Cullingford
Lars Hoeghort
Wagramerstrasse 5
P.O. Box 100
Vienna, 22
AUSTRIA

1 IMPELL
Attn: Don Wesley
1651 East 4th Street
Suite 210
Santa Ana, CA 92701

2 Illinois Dept. of Nuclear Safety
Attn: James Blackburn
Michael C. Parker
1035 Outer Park Drive
Springfield, IL 62704

1 Imatran Voima Oy
Attn: Jussi K. Vaurio
Loviisa NPS
SF-07900 Loviisa
FINLAND

1 Inst. for Nuclear Power Operations
Attn: Roger Wyrick
1100 Circle 75 Parkway
Suite 1500
Atlanta, GA 30339

1 Institute for Resource and Security Studies
Attn: Gordon Thompson
27 Ellworth Avenue
Cambridge, MA 02139

1 Institut fur Nukleare Sicherheitsforschung
Attn: W. Kroger
Kernforschungsanlage Julich GmbH
Postfach 1913
D-5170 Julich 1
FEDERAL REPUBLIC OF GERMANY

1 Institute of Nuclear Energy Research
Attn: Sen-I Chang
P.O. Box 3
Lungtan, 325
TAIWAN

1 International Energy Assoc., Ltd.
Attn: J. Mark Elliot
600 New Hampshire Ave, NW
Suite 600
Washington, DC 20037

1 JBF Associates, Inc.
Attn: J. B. Fussell
1630 Downtown West Boulevard
Knoxville, TN 37919

3 Japan Atomic Energy Research Inst.
Attn: Kiyoharu Abe, Dept. of Reactor Safety Research
Michio Ichikawa, Dept. of Fuel Safety Research
Kunihisa Soda, Chemical Engineering Safety
Tokai-mura, Naga-gun
Ibaraki-ken,
JAPAN

1 Japan Institute of Nuclear Safety
Attn: Dr. Susumi Suguri, Director General
Fujita Kankou Toranoman Bldg. 7F
3-17-1, Toranoman
Minato-Ku, Tokyo, 105
JAPAN

1 Japan Institute of Nuclear Safety
Attn: Takeo Uga
Nuclear Power Engineering Test Center
3-6-2, Toranomon
Minato-Ku, Tokyo, 108
JAPAN

1 JAYCOR
Attn: Rick Sherry
P.O. Box 85154
San Diego, CA 92138

1 KMC, Inc.
Attn: Thomas C. Houghton
1747 Pennsylvania Ave, NW
Washington, DC 20006

1 Ralph. L. Keeney
101 Lombard Street
Suite 704W
San Francisco, CA 94111

5 Kernforschungszentrum, Karlsruhe
Attn: Joachim Ehrhardt
A. Fiege
Sigfried Hagen
Peter Hofmann
Bernhard Kuczera
P.O. Box 3640
D-7500 Karlsruhe 1
WEST GERMANY

3 Korea Advanced Energy Research Inst.
Attn: H. R. Jun
Soo-Pong Suk
Kung-Joong Yoo
P.O. Box 7, Daeduk Danji
Chungnam 300-31
KOREA

1 Kyunghee University
Attn: Won-Guk Hwang
Yongin-Kun
Kyunggi-Do 170-23
KOREA

3 Lawrence Livermore Laboratory
Attn: Garth Cummings, L-91
Sergio Guarro
Garry Thomas, L-499
P.O. Box 808
Livermore, CA 94526

1 League of Women Voters
Attn: Grant Thompson
1730 M. Street, NW
Washington, DC 20036

5 Los Alamos National Laboratory
Attn: B. E. Boyack, K-551
D. R. Liles, K-553
M. Meyer, F-600
J. Richardson, K-555
H. Stumpf, K-555
Los Alamos, NM 87545

1 Louisiana Power and Light
Attn: Krishna R. Iyengar
200 A Huey P. Long Ave
Gretna, LA 70053

1 R. Lynette and Associates
Attn: Jonathan Young
15042 Northeast 40th St.
Suite 206
Redmond, WA 98052

1 MHB Technical Associates
Attn: Steven C. Sholly
1723 Hamilton Avenue, Suite K
San Jose, CA 95125

2 Massachusetts Institute of Technology
Attn: M. S. Kazimi, 24-219
Norman C. Rasmussen
77 Massachusetts Ave
Cambridge, MA 02139

1 Charles Miller
8 Hastings Rd.
Momsey, NY 10952

1 James Moody
P.O. Box 641
Rye, NH 03870

1 Walter B. Murfin
P.O. Box 550
Mesquite, NM 88048

1 NASA, Code QS
Attn: Ben Buchbinder
600 Maryland Ave. SW
Washington, DC 20546

2 NUS Corporation
Attn: Robert C. Bertucio
Jeffery Julius
1301 S. Central Ave, Suite 202
Kent, WA 98032

1 NUS Corporation
Attn: Larry Conradi
16835 W. Bernardo Drive
Suite 202
San Diego, CA 92127

2 NUS Corporation
Attn: James Fulford
Gareth Parry
910 Clopper Road
Gaithersburg, MD 20878

1 National Commission on Nuclear Safety & Safeguards (CNSNS)
Attn: Alejandro Huerta-Bahena
Insurgentes Sur N. 1776
Col. Florida
C. P. 04230 Mexico, D.F.
MEXICO

1 Nat. Resources Defense Council
Attn: Thomas Cochran
1350 New York Ave NW, Suite 300
Washington, D.C. 20005

1 Nebraska Public Power District
Attn: B. Raychaudhuri
PRA & Engineering Review Group
P.O. Box 499
Columbus, NE 68601

3 Netherlands Energy Research Foundation
Attn: Karel J. Brinkmann
M. Bustraan
H. J. Van Grol
P.O. Box 1
1755 ZG Petten NH
THE NETHERLANDS

1 New York Power Authority
Attn: Herschel Spector
123 Main Street
White Plains, NY 10601

1 Susan J. Niemczyk
1545 18th St. NW, #112
Washington, DC 20036

2 Northeast Utilities
Attn: Raymond O. Bagley
Mario V. Bonace
P.O. Box 270
Hartford, CT 06141-0270

1 Nuclear Installations Inspectorate
Attn: J. F. Campbell
Balliol Road, Bootle
Merseyside, L20 3L2
UNITED KINGDOM

1 NUMAEC
Attn: William Raisin
1726 M St. NW
Suite 904
Washington, DC 20036

2 NUMARC
Attn: Librarian
John Siegal
7101 Wisconsin Ave
Bethesda, MD 20814

1 Nutech
Attn: R. H. Buchholz
6835 Via Del Oro
San Jose, CA 95119

1 NUTECH
Attn: N. W. Edwards
145 Martinvale Lane
San Jose, CA 95119

2 OECD Nuclear Energy Agency
Attn: S. Mori
Klaus B. Stadie
38 Blvd. Suchet
75016 Paris
FRANCE

8 Oak Ridge National Laboratory
Attn: S. R. Greene, MS-8057
T. L. Heatherly, MS-8057
S. A. Hodge, MS-8057
C. R. Hyman, MS-8057
B. W. Patton, MS-8087
D. B. Simpson, MS-8057
R. P. Taleyarkhan, MS-8057
M. L. Tobias, MS-8088
P.O. Box 2009
Oak Ridge, TN 37831-8057

3 Oak Ridge National Laboratory
Attn: George F. Flanagan
Thomas Kress
A. P. Malinauskas
P.O. Box Y
Oak Ridge, TN 37831

3 Ontario Hydro
Attn: Oguz Akalin
Allan R. Brown
Frank King, Bldg H11 G5
700 University Avenue
Toronto, Ontario
CANADA M5G 1X6

1 PNC
Attn: Kiyoto Aizawa
Safety Research Group
Reactor Research and Development Project
9-13m 1-Chome Akasaka
Minatu-Ku
Tokyo
JAPAN

1 PRD Consulting
Attn: Peter R. Davis
1935 Sabin Drive
Idaho Falls, ID 83401

2 Pacific Northwest Laboratory
Attn: Raymond H. V. Galucci
V. V. Truong
Battelle Blvd.
P.O. Box 999
Richland, WA 99352

1 Philadelphia Electric Co.
Attn: R. A. Diederich
2301 Market St.
Philadelphia, PA 19101

3 Philadelphia Electric Co.
Attn: Greg Krueger
955-65 Chesterbrook Blvd.
62A-7
Wayne, PA 19187

5 Pickard, Lowe & Garrick, Inc.
Attn: Dennis C. Bley
Karl N. Fleming
John Garrick
D. H. Johnson
John Stetkar
2260 University Drive
Newport Beach, Ca 92660

1 Pickard, Lowe & Garrick, Inc.
Attn: Alfred F. Torri
191 Calle Magdalena, Suite 290
Encinitas, CA 92024

1 Public Service Company
Attn: Bruce B. Beckley
P.O. Box 330
Manchester, NH 03105

1 Purdue University
Attn: Raymond Viskanta
Heat Transfer Laboratory
School of Mechanical Engineering
West Lafayette, IN 47907

1 RPI
Attn: Mike Podowski
Dept. of Nuclear Engineering and Engineering Physics
Troy, NY 12180-3590

1 Risk Management Association
Peter P. Bieniarz
2309 Dietz Farm Road NW
Albuquerque, NM 87107

2 Riso National Laboratory
Attn: H. Larsen
Ingvard Rasmussen
Postbox 49
DK-4000 Roskilde
DENMARK

1 Rocky Flats Plant
Attn: Terry Foppe
P.O. Box 464, Bldg T886A
Golden, CO 80402-0464

1 Frank Rowsome
9532 Fern Hollow Way
Gaithersburg, MD 20879

1 Royal Institute of Technology
Attn: A. Hedgran
Nuclear Safety Department
Bunellvagen 60
10044 Stockholm
SWEDEN

5 SERI
Attn: John G. Cesare
Mat Crawford
Kenneth Hughey
Wayne Russell
Gary Smith
5360 I-55 North
Jackson, MS 39211

1 Safety and Reliability
Optimization Services
Attn: Gary J. Boyd
9724 Kingston Pike, Suite 102
Knoxville, TN 37922

2 Sargent and Lundy Engineers
Attn: Adolf Walser
Norman Weber
55 E. Monroe Street
Chicago, IL 60603

5 Savannah River Laboratory
Attn: Mike Hitchler
J. K. Norkus
D. Paddleford
L. A. Wooten
Dave Sharp, Bldg 773-41A
Westinghouse Savannah River Co.
Aiken, SC 29808-0001

5 Science & Engineering Associates
Attn: Clint J. Shaffer
P.O. Box 3722
Albuquerque, NM 87190

2 Science Applications Intl. Corp.
Attn: David Aldrich
Geoffrey D. Kaiser
1710 Goodridge Drive
McLean, VA 22102

9 Science Applications Intl. Corp.
Attn: Christopher N. Amos
Mary T. Drouin
Earl Dombrowski
Alan M. Kolaczkowski
Jeffrey L. LaChance
Mark T. Leonard
Lanny N. Smith
K. C. Wagner
K. A. Williams
2109 Air Park Rd, SE
Albuquerque, NM 87106

1 Science Applications Intl. Corp.
Attn: Roger Blond
20030 Century Blvd., Suite 201
Germantown, MD 20874

1 Science Applications Intl. Corp.
Attn: Vernon Denny
5150 El Camino Real, Suite 3
Los Altos, CA 94303

1 Science Applications Intl. Corp.
Attn: Joseph R. Fragola
247 Madison Avenue
New York, NY 10016

1 Science Applications Intl. Corp.
Attn: Bonnie J. Shapiro
360 Bay Street
Suite 200
Augusta, GA 30901

2 Science Applications Intl. Corp.
Attn: William E. Vesely
John Wreathall
2929 Kenny Road, Suite 245
Columbus, OH 43221

1 SCIENTECH, Inc.
Attn: Roger J. Mattson
11821 Parklawn Dr.
Suite 208
Rockville, MD 20852

1 S. California Edison Company
Attn: Kenneth S. Baskin
P.O. Box 800
Rosemead, CA 91770

4 Stone & Webster Engineering Corp.
Attn: Frank Elia
Andrzej Drozd
Jim Metcalf
Edward Warman
P.O. Box 2325
Boston, MA 02107

1 Stone & Webster
Attn: Michael Hazzan
3 Executive Campus
Cherry Hill, NJ 08034

1 Stratton & Associates
Attn: William Stratton
2 Acoma Lane
Los Alamos, NM 87544

1 Studsvik Energiteknik AB
Attn: Kjell Johannson
S-611 82, Nykoping
SWEDEN

4 Swedish Nuclear Power Inspectorate
Attn: L. Hammar
Lars Hoegberg
Wiktor Frid
Bo Liwnang
Box 27106
S-102 52 Stockholm
SWEDEN

3 Swiss Federal Nuclear Safety Inspectorate
Attn: S. Chakraborty
H. Hirschmann
J. Peter Hoseman
CH-5303 Wurenlingen
SWITZERLAND

1 Taiwan Power Company
Attn: Eng Lin
242, Roosevelt Rd., Sec. 3
Taipei
TAIWAN

1 Technical Analysis Corp.
Attn: Stephen Hanauer
6723 Whittier Ave
Suite 202
McLean, VA 22101

1 Technical Research Centre of Finland
Attn: Lasse Mattila
Nuclear Engineering Laboratory
P.O. Box 169
00181 Helsinki
FINLAND

1 Technical Research Centre of Finland
Attn: Urho Fulkkinen
Electrical Engineering Laboratory
Otakaari 7 B
SF-02150 Espoo 15
FINLAND

1 TENERA L.P.
Attn: Robert G. Brown
1340 Saratoga-Sunnyvale Rd.
Suite 206
San Jose, CA 95129

3 TENERA L.P.
Attn: James C. Carter, III
William Parkinson
Paul Wood
308 North Peters Road
Suite 280
Knoxville, TN 37922

1 Tennessee Environmental Council
Attn: John Sherman
1719 West End Avenue, Suite 227
Nashville, TN 37203

4 Tennessee Valley Authority
Attn: Robert F. Christie
Wang L. Lau
William Mims
Robert L. Olson
400 W. Summit Hill Ave
Knoxville, TN 37902

1 Tennessee Valley Authority
Attn: Oliver D. Kingsley, Jr.
1101 Market Street
GN-38A Lookout Place
Chattanooga, TN 37402

1 TERA Corporation
Attn: Michael B. Aycock
7101 Wisconsin Ave
Bethesda, MD 20814

1 TRACTEBEL
Attn: M. Preat
Chef du Service Surete Nucleaire
et Assurance Qualite
Bd. du Regent 8
B-100 Bruxells
BELGIUM

1 TUV-Norddeutschland
Attn: H-P. Balfanz
Grosse Bahnstrasse 31,
2000 Hamburg 54
FEDERAL REPUBLIC OF GERMANY

1 Union of Concerned Scientists
Attn: Henry Kendall
Executive Director
Cambridge, MA

1 Union of Concerned Scientists
Attn: Robert D. Pollard
1616 P Street, NW, Suite 310
Washington, DC 20036

2 United Engineers & Construction
Attn: M. Sarran
Rich Toland, MS 4V7
P.O. Box 8223
30 S 17th Street
Philadelphia, PA 19101

3 United Kingdom Atomic Energy
Agency
Attn: T. Haste
Stephen R. Kinnersly
R. Potter
Reactor Safety Studies Dept.
Winfrith Technology Center
Winfrith, Dorchester, Dorset
United Kingdom, DT2 8DH
UNITED KINGDOM

7 United Kingdom Atomic Energy
Authority
Attn: Frank Abbey
Peter Cooper
N. J. Hollaway
M. I. Robertson
Tony Taig
Harry Teague
C. Wheatley
Wigshaw Lane, Culcheth,
Warrington
Cheshire, WA3 4NE
ENGLAND

1 United Kingdom Atomic Energy
Authority
Attn: Michael Haynes
Oxfordshire
Didcot, Oxon., OX11 ORA
ENGLAND

1 United Kingdom Atomic Energy
Authority
Attn: Brian D. Turland
Culham Laboratory
Abingdon, Oxon OX14 3DB
ENGLAND

2 USDOE - Office of Nuclear Safety
Attn: P. K. Niyogi
D. Pyatt, EH-332
Washington, DC 20545

48 U.S. Nuclear Regulatory Commission
Attn: S. Acharya, NLS-372
B. Agrawal, NLN-344
P. Baranowsky, 11E-22
R. Barrett, 10A-2
E. S. Beckjord, NLS-007
W. Beckner, NLS-324
R. M. Bernero, 6A-4
G. R. Burdick, NLS-007
A. J. Buslik, NLS-372
Y. S. Chen, NLN-344
F. Coffman, NLN-316
J. Costello, NLS-217A
M. A. Cunningham, NLS-372
A. A. El-Bassioni, 10A-2
F. Eltawila, NLN-344
M. L. Ernst, RGN II
J. Flack, NLS-169
R. B. Foulds, NLN-344
F. P. Gillespie, 12G-18
J. C. Glynn, NLS-372
B. Hardin, NLS-169
D. Houston, ACRS, P-315
S. Israel, MNBB-2104
J. E. Jackson, NLS-007
L. E. Lancaster, NLS-372
N. Lauben, NLN-353
T. Lee, NLN-353
D. McPherson, 12G-18
R. O. Meyer, NLS-007
J. A. Mitchell, NLS-314
J. A. Murphy, NLS-007
R. L. Palla, Jr., 10A-2
D. M. Rasmuson, NLS-372
J. N. Ridgely, NLS-324
R. Robinson, NLS-372
J. E. Rosenthal, MNBB-2104
D. F. Ross, NLS-007
C. P. Ryder, NLS-372
B. Sheron, NLS-007
M. Silberberg, NLS-260
T. P. Speis, NLS-007
L. Soffer, NLS-324
L. M. Shotkin, NLN-353
A. C. Thadani, 7E-4
C. G. Tinkler, NLN-344
H. VanderMolen, NLS-372
P. Worthington, NLN-344
R. W. Wright, NLN-344
Washington, DC 20555

1 Universidad Politecnica de Madrid
Attn: Prof. Augustin Alonzo Santos
E.T.S. Ingenieros Industriales
Jose Gutierrez Abascal, 2
28006 Madrid
SPAIN

1 Universite Libre de Bruxelles
Attn: J. Devooger
Faculte des Sciences Appliques
av. Franklin Roosevelt
B-1050 Bruxelles
BELGIUM

2 University of California
Attn: W. H. Amarasooriya
T. G. Theofanous
ERC-CRSS
Santa Barbara, CA 93106

4 University of California
Attn: George Apostolakis
V. K. Dhir
William Kastenberg
David Okrent
Boelter Hall, Room 5532
Los Angeles, CA 90024

1 University of California
Attn: Daniel Hirsch
A. Stevenson Program on Nuclear Policy
Santa Cruz, CA 95064

1 University of Hawaii at Hilo
Attn: Stephen C. Hora
Division of Business Administration and Economics
College of Arts and Sciences
Hilo, HI 96720-4091

1 The University of Michigan
Attn: John C. Lee
Dept. of Nuclear Engineering
Cooley Building, North Campus
College of Engineering
Ann Arbor, MI 48109-2104

1 University of Minnesota
Attn: Y. H. (Ben) Liu
Dept. of Mechanical Engineering
Minneapolis, MN 55455

1 University of Missouri-Rolla
Attn: Nicholas Tsoulfanidis
Nuclear Engineering Dept.
Rolla, MO 65401-0249

2 University of New Mexico
Attn: F. Eric Haskin
Sharif Heger
Deptartment of Chemical &
Nuclear Engineering
Albuquerque, NM 87131

2 University of Southern California
Attn: Ward Edwards, Social
Sciences Research Inst.
Detlof von Winterfeldt,
Inst. of Safety & Systems
Management
Los Angeles, CA 90089

1 University of Southern California
Attn: Richard John
SSM, Room 102
927 W. 35th Place
Los Angeles, CA 90089-0021

2 University of Tokyo
Attn: Ryohel Kiyose
S. Kondo
Dept. of Nuclear Engineering
7-3-1 Hongo Bunkyo
Tokyo 113
JAPAN

1 University of Virginia
Attn: W. Reed Johnson
Department of Nuclear Engineering
Charlottesville, VA 22901

2 University of Wisconsin
Attn: M. L. Corradini
G. A. Moses
Dept of Nuclear Engineering
Engineering Research Bldg.
1500 Johnson Drive
Madison, WI 53706

1 William F. Vinck
Kapellestract 25
1980
Tervuren
BELGIUM

5 Virginia Electric Power Co.
Attn: Ronald Bayer
Ronald Berryman
R. J. Hardwich, Jr.
Doug Richeard
David Sommers
P.O. Box 26666
Richmond, VA 23261

1 Washington Public Power Supply
System
Attn: George F. Bailey
P.O. Box 968
Richland, WA 99352

3 Westinghouse Electric Corp.
Attn: N. J. Liparulo
Robert J. Lutz, Jr.
Dennis Richardon
P.O. Box 355
Pittsburgh, PA 15230

4 Westinghouse Hanford Co.
Attn: D. Ogden
Gary L. Smith
O. Wang
Mike Zentner
P.O. Box 1970
Richland, WA 99352

1 World Resources Institute
Attn: Jim Mackenzie
1735 New York Ave NW
Washington, DC 20006

1 Yankee Atomic Electric Co.
Attn: J. R. Chapman
1671 Worcester Road
Framingham, MA 01701

5	3141	S. A. Landenberger
1	3151	G. L. Esch
1	6344	E. D. Gorham
1	6400	D. J. McCloskey
1	6401	J. E. Kelly
1	6410	D. A. Dahlgren
1	6411	D. D. Carlson
1	6412	A. L. Camp
1	6412	S. L. Daniel
1	6412	S. E. Dingman
1	6412	T. M. Hake
1	6412	L. A. Miller
1	6412	D. B. Mitchell
1	6412	A. C. Payne, Jr.
1	6412	B. D. Staple
1	6412	T. T. Sype
1	6412	D. W. Whitehead
1	6412	G. D. Wyss
1	6413	T. D. Brown
1	6413	G. S. Rightley
1	6413	F. T. Harper
1	6415	W. R. Cramond
1	6418	E. A. Boucheron
1	6418	M. K. Carmel
1	6418	R. K. Cole, Jr.
1	6418	A. A. Elsbernd
1	6418	R. J. Gross
1	6418	L. N. Kmetyk
1	6418	R. S. Longenbaugh
1	6418	K. J. Maloney
1	6418	G. M. Martinez
1	6418	R. J. Pryor
1	6418	D. S. Stuart
1	6418	R. M. Summers
1	6418	S. L. Thompson
1	6420	W. B. Gauster
1	6422	D. A. Powers
1	6423	K. O. Reil
1	6424	K. D. Bergeron
1	6424	J. J. Gregory
1	6429	K. E. Washington
1	6460	J. V. Walker
1	6463	M. Berman
1	6471	L. D. Bustard
1	6573	W. A. von Riesemann
1	8524	J. A. Wackerly